

# **The allosteric core region of the M<sub>2</sub> muscarinic acetylcholine receptor: role for ligand selectivity and action**

Dissertation

zur

Erlangung des Doktorgrades (Dr. rer. nat.)

der

Mathematisch-Naturwissenschaftlichen Fakultät

der

Rheinischen Friedrich-Wilhelms-Universität Bonn

vorgelegt von

**Brian Chirinda**

aus

Harare

Bonn 2015

Angefertigt mit Genehmigung der Mathematisch-Naturwissenschaftlichen Fakultät der  
Rheinischen Friedrich-Wilhelms-Universität Bonn

1. Gutachter                      Prof. Dr. K. Mohr

2. Gutachter                      Prof. Dr. I. von Kügelgen

Tag der Promotion:              17 July 2015

Erscheinungsjahr:

Die vorliegende Arbeit wurde in der Zeit von März 2012 bis März 2015 in der Abteilung Pharmakologie und Toxikologie des Pharmazeutischen Institutes der Rheinischen Friedrich-Wilhelms-Universität Bonn unter der Leitung von Herrn Prof. Dr. K. Mohr angefertigt.

# Table of contents

<b>1. Introduction</b> .....	1
1.1 Muscarinic acetylcholine receptors .....	1
1.2 Allosteric modulation.....	3
1.3 Dualsteric compounds.....	4
1.4 The core region of M <sub>2</sub> allosteric binding site - basis of the M <sub>2</sub> triple mutation.....	6
1.5 Biogenic amines .....	8
1.6 Aim of study.....	13
<b>2. Materials and Methods</b> .....	14
2.1 Compounds.....	14
2.1.1 Radioligands .....	14
2.1.2 Muscarinic orthosteric and allosteric ligands .....	14
2.1.3 Muscarinic dualsteric ligands and their allosteric moieties.....	16
2.1.4 Biogenic amines .....	17
2.2 Materials.....	19
2.2.1 Reagents .....	19
2.2.2 Solutions and buffers .....	20
2.2.3 Disposables.....	23
2.2.4 Equipment.....	24
2.2.5 Manufacturers.....	25
2.2.6 Software.....	27
2.3 Cell culture .....	28
2.3.1 Thawing, passaging and freezing CHO cells.....	28
2.3.2 Cell membrane preparation .....	29
2.3.3 LOWRY protein assay.....	29
2.4 Radioligand binding assays .....	30
2.4.1 Law of mass action.....	30
2.4.2 [ <sup>3</sup> H]NMS dissociation binding .....	31

2.4.2.1 Complete dissociation .....	31
2.4.2.2 Allosteric interaction .....	31
2.4.2.3 Experimental procedure .....	33
2.4.3 Equilibrium binding assays .....	35
2.4.3.1 Homologous competition .....	35
2.4.3.2 Heterologous competition .....	36
2.4.3.3 [ <sup>3</sup> H]NMS equilibrium binding with dualsteric ligands .....	37
2.4.3.4 Experimental procedure .....	39
2.5 Functional assays.....	41
2.5.1 [ <sup>35</sup> S]GTP $\gamma$ S binding assay .....	41
2.5.1.1 Operational model of agonism .....	42
2.5.1.2 Experimental procedure .....	42
2.5.2 cAMP assay .....	43
2.5.2.1 Experimental procedure .....	44
2.5.3 Dynamic mass redistribution assay (DMR).....	44
2.5.3.1 Experimental procedure .....	45
2.6 Statistics .....	46
2.6.1 Mean value .....	46
2.6.2 Standard deviation and standard error of the mean (SEM) .....	46
2.6.3 One-way ANOVA .....	47
2.6.3.1 One-way ANOVA with Turkey's Multiple Comparison Test.....	47
2.6.3.2 One-way ANOVA with Dunnett's test .....	48
2.6.4 F-test .....	48
2.6.5 T-test.....	49
<b>3. Results</b> .....	<b>50</b>
3.1 Characterisation of allosteric binding at the M <sub>2</sub> triple mutant .....	50
3.1.1 W84 loses allosteric potency and efficacy to retard [ <sup>3</sup> H]NMS at the M <sub>2</sub> triple mutant.....	50
3.1.2 W84 loses equilibrium binding affinity at the M <sub>2</sub> triple mutant.....	53

3.2 Characterisation of the M <sub>2</sub> triple mutant with muscarinic orthosteric ligands.....	56
3.2.1 Radioligand binding studies .....	56
3.2.1.1 [ <sup>3</sup> H]NMS dissociation binding .....	56
3.2.1.2 [ <sup>3</sup> H]NMS Equilibrium binding .....	57
3.2.1.2.1 Muscarinic inverse and partial agonists .....	57
3.2.1.2.2 Muscarinic agonists .....	60
3.2.2 Receptor activation .....	64
3.2.2.1 [ <sup>35</sup> S]GTPγS binding.....	67
3.2.2.2 Dynamic mass redistribution (DMR) .....	67
3.2.2.2.1 G <sub>i/o</sub> signaling .....	67
3.2.2.2.1 G <sub>s</sub> signaling .....	68
3.2.2.3 cAMP accumulation -G <sub>s</sub> signaling .....	70
3.3 The allosteric core region of the M <sub>2</sub> receptor: a ‘gate-keeper’ against the biogenic amine ligands? .....	73
3.3.1 Epinephrine appears to bind and activate the muscarinic M <sub>2</sub> triple mutant receptor .	73
3.3.2 Epinephrine partially activates [ <sup>35</sup> S]GTPγS binding .....	75
3.3.3 Epinephrine failed to activate DMR through the M <sub>2</sub> triple mutant receptor .....	81
3.3.4 Epinephrine is unable to bind to the allosteric binding site of the inactive M <sub>2</sub> wt and triple mutant receptor .....	83
3.3.5 Other biogenic amines.....	86
3.3.5.1 [ <sup>35</sup> S]GTPγS binding .....	86
3.3.5.2 Dynamic Mass redistribution (DMR) .....	88
3.3.5.3 [ <sup>3</sup> H]NMS equilibrium binding studies against dopamine and histamine .....	92
3.3.5.4 [ <sup>3</sup> H]Iperoxo equilibrium binding studies against norepinephrine .....	93
3.3.5.5 Serotonin and histamine are unable to retard [ <sup>3</sup> H]NMS dissociation .....	94
3.4 Role of the M <sub>2</sub> receptor allosteric core region for orthosteric/allosteric binding cooperativity.....	96
3.4.1 Allosteric moiety ligands.....	96
3.4.2 Dualsteric ligands .....	98
3.4.2.1 [ <sup>3</sup> H]NMS Equilibrium binding.....	99
3.4.2.2 [ <sup>3</sup> H]NMS dissociation binding.....	109
3.4.2.3 Supplementary figures .....	113

<b>4. Discussion</b> .....	117
4.1 Pronounced loss of allosteric function at the M <sub>2</sub> triple mutant .....	117
4.2 The M <sub>2</sub> core allosteric binding site confers some selectivity to chemically distinct muscarinic full agonists orthosteric ligand binding .....	120
4.3 The core region of the allosteric binding site regulates M <sub>2</sub> receptor orthosteric activation .....	121
4.4 The M <sub>2</sub> core allosteric binding site as a selectivity filter against non-muscarinic biogenic amine ligands?.....	126
4.5 The M <sub>2</sub> triple mutant increases the fraction of active receptor populations.....	129
<b>5. Summary</b> .....	136
<b>6. Outlook</b> .....	139
<b>7. Abbreviations</b> .....	141
<b>8. References</b> .....	143
<b>9. Publications</b> .....	156
<b>10. Curriculum vitae</b> .....	157
<b>11. Acknowledgements</b> .....	158

# 1 Introduction

## 1.1 Muscarinic acetylcholine receptors

G-protein coupled receptors (GPCRs) are seven transmembrane domain proteins which can be divided into five families, the Rhodopsin, Secretin, Adhesion, Glutamate and Frizzled/Taste2 (Fredriksson *et al.*, 2003; Cherezov *et al.*, 2007). The muscarinic acetylcholine receptors (mAChRs) belong to the  $\alpha$ -group of the Rhodopsin receptor family (class A), which forms the largest family of GPCRs (Lagerström and Schiöth, 2008). mAChRs are embedded in the lipidic layers of the membrane bilayer (Haga *et al.*, 2012) and are made up of a single chain of approximately 400-500 amino acids. The amino acid chain consists of seven  $\alpha$ -helical transmembrane domains, three extracellular and three intracellular loops. The amino terminal and the carboxy terminal are located at the extracellular and intracellular sides of the cell, respectively (Hulme *et al.*, 1990; Caulfield and Birdsall, 1998). The binding site of the mAChRs endogenous ligand acetylcholine (ACh) and other conventional muscarinic agonists, antagonists and inverse agonists is located within a pocket formed by the seven transmembrane domains (Wess, 1993). mAChRs also possess the “common allosteric binding site” which is located directly above the orthosteric binding site in the extracellular region (Ellis *et al.*, 1993; Mohr *et al.*, 2010).

### Receptor subtypes

The muscarinic actions of ACh are mediated by 5 different receptor subtypes ( $M_1$ - $M_5$ ) which were found to be encoded by genes lacking introns in their coding sequence (Hammer *et al.*, 1980; Bonner *et al.*, 1987). mAChRs are widely distributed throughout the body periphery and in the central nervous system (CNS) (Hulme, 1990; Caulfield, 1993; Levey, 1993). The  $M_1$  subtype is mainly located in the brain, particularly in the hippocampus, cerebral cortex and the striatum (Levey *et al.*, 1991). The  $M_2$  receptor can be located in the body periphery mainly in the heart and smooth muscle tissue, and is also widely distributed in the CNS. The  $M_2$  receptor is important in the regulation of the human heart rate and the contractile force of cardiomyocytes (Miao *et al.*, 2013). The main effect of the  $M_2$  receptor activation mediated by ion channels is the activation of inwardly rectifying acetylcholine sensitive potassium channels ( $K_{ACh}$ ). This results in an increased  $K^+$  permeability leading to hyperpolarization and negative inotropy in the atria. Hence, this results in decreased heart rate and decreased force of atrial contraction (Myslivecek and Trojan, 2003).



The M<sub>3</sub> receptor is widely expressed in the brain (Levey *et al.*, 1994) and in the periphery where it is thought to be involved in regulating salivary secretion and smooth muscle contractility (Caulfield, 1993; Eglén *et al.*, 1996). The M<sub>4</sub> receptor is predominantly found in the CNS particularly in the forebrain. Most of the important effects stimulated by the M<sub>4</sub> receptors have been observed in the striatum. The M<sub>5</sub> receptor is expressed in low amounts in the central nervous system with main functions in striatum and cerebral arteries (Vilaro *et al.*, 1990; Weiner *et al.*, 1990). As the mAChR subtypes are found in different tissues and body regions, this enables them to mediate different effects as shown by **Figure 1.1** adapted from Wess, 2004. The M<sub>2</sub> and M<sub>4</sub> preferentially couple to the G<sub>i/o</sub>α subtype of heterotrimeric guanine nucleotide-binding proteins (G-proteins) whilst M<sub>1</sub>, M<sub>3</sub> and M<sub>5</sub> preferentially couple to G<sub>q/11</sub>α proteins in order to bring about effects depicted in **Figure 1.1**.

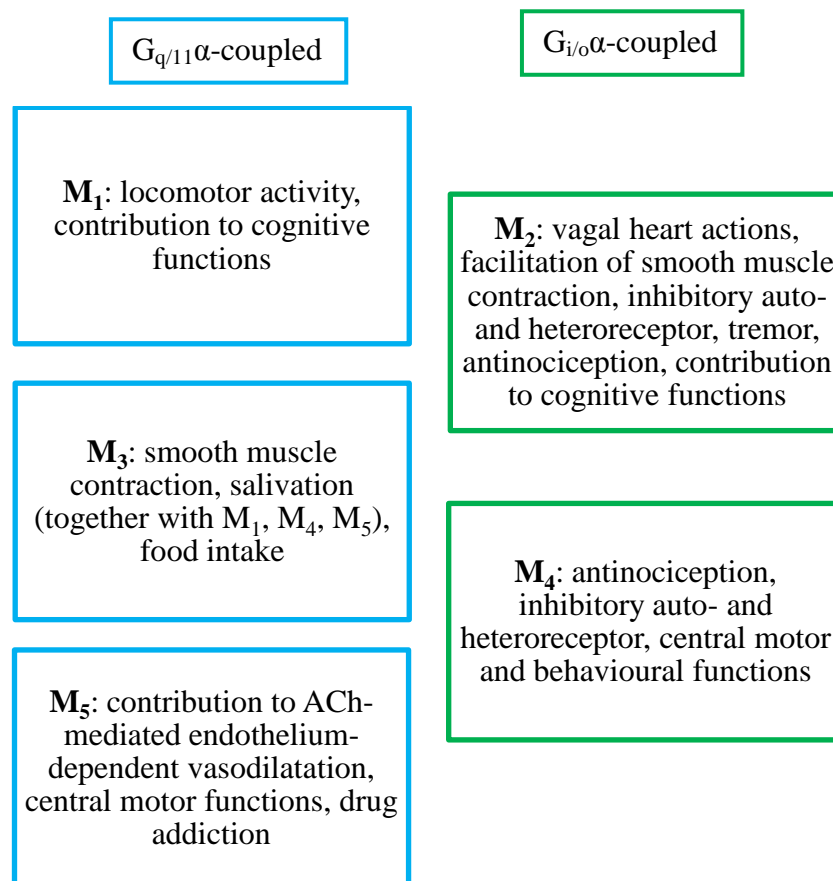


**Figure 1.1 mAChRs physiological functions.** mAChRs are divided into 5 subtypes which can be grouped by their G-protein coupling preferences. M<sub>1,3,5</sub> preferentially couple to G<sub>q/11</sub>α and M<sub>2,4</sub> to G<sub>i/o</sub>α. Adapted from Wess, 2004.

## Receptor activation and signalling

When mAChRs become activated they experience a change in receptor conformation which results in receptor-G-protein interaction. G-proteins are heterotrimeric consisting of a  $\beta\gamma$  and an  $\alpha$  subunit. The  $G_\alpha$  subunit family can be subdivided into four subfamilies ( $G_{i/o}\alpha$ ,  $G_s\alpha$ ,  $G_{q/11}\alpha$  and  $G_{12/13}\alpha$ ) (Milligan and Kostenis, 2006). The receptor-G-protein interaction upon receptor activation induces the exchange of GDP for GTP at the  $G_\alpha$  subunit.  $\beta\gamma$  then dissociates from the  $G_\alpha$ -GTP subunit and both subunits can go on to independently activate downstream signalling pathways (Simon *et al.*, 1991; Oldham and Hamm, 2008).  $G_s\alpha$  stimulates adenylyl cyclase activation which in turn catalyses the increase in cyclic adenosine monophosphate (cAMP). cAMP then goes on to activate further downstream effectors such as protein kinase A (PKA) (Ross and Gilman, 1980). On the other hand,  $G_{i/o}\alpha$  inhibits adenylyl cyclase activity leading to a decrease in intracellular cAMP accumulation (Bokoch *et al.*, 1984). The  $\beta\gamma$  subunit which dissociates from the  $G_{i/o}\alpha$  can proceed to activate G-protein activated inwardly-rectifying potassium (GIRK) channels (Woehler and Ponimaskin, 2009).  $G_{q/11}\alpha$  activates phospholipase C $\beta$  (PLC $\beta$ ) which catalyses the hydrolysis of phosphatidylinositol(4,5)bisphosphate (PIP2) into inositol(1,4,5)triphosphate (IP3) and diacylglycerol (DAG). IP3 goes on to induce an increase in intracellular  $Ca^{2+}$  by interacting with IP3 receptors at the smooth endoplasmic reticulum (ER) whilst DAG activates Protein Kinase C (PKC) (Kostenis *et al.*, 2005).  $G_\alpha$ -GTP possesses intrinsic GTPase capabilities whereby it hydrolyses the GTP terminal phosphate to produce GDP. GTP hydrolysis can be enhanced by regulators of G-protein signalling (RGS) which interact with  $G_\alpha$  subunit. The re-binding of GDP to the nucleotide binding pocket of the  $G_\alpha$  protein enables the reassociation of  $G_\alpha$  and  $\beta\gamma$  subunits. In turn, this completes the activation cycle and prepares the G-protein for the next activation cycle (Snow *et al.*, 1998).

### 1.2 Allosteric modulation

The mAChR five subtypes are susceptible to allosteric modulation and the allosteric binding site is situated directly at the entrance to the orthosteric binding site. Allosteric modulators can bind to a receptor simultaneously with the orthosteric ligands in a cooperative interaction (Christopolous and Kenakin, 2002). The allosteric modulator can therefore affect the binding affinity and properties of an orthosteric ligand by affecting the latter's association and dissociation from the receptor (Tränkle *et al.*, 1998; Zahn *et al.*, 2002). The nature of interaction between the two ligands (A and B) binding concomitantly to topographically

distinct binding sites can be described and quantified by a mechanism termed the allosteric ternary complex model (ATCM) (Ehlert, 1988). The ATCM includes the free, orthosteric-bound, allosteric-bound and the fourth receptor state whereby both the allosteric and orthosteric ligands are bound to the receptor forming a ternary complex.

The cooperativity factor ( $\alpha$ ) measures the magnitude at which the ligands A and B reciprocally affect each other's binding affinities when both are bound in a ternary complex with the receptor. Therefore, an allosteric modulator can promote or inhibit orthosteric ligand binding, termed positive and negative cooperativity, respectively. Neutral cooperativity is when the presence of the allosteric ligand has no effect on the affinity of the orthosteric ligand (Christopoulos *et al.*, 1998; May *et al.*, 2007). The effects of allosteric modulators on the orthosteric ligand binding are saturable. This means that even at high concentrations, the allosteric modulator is unable to completely displace the orthosteric ligand from its binding site. Therefore, the allosteric ligand does not abolish the binding of ligands to the orthosteric site (Lazareno and Birdsall, 1995; Christopoulos, 2014). Some allosteric modulators are capable of directly activating GPCRs in the absence of an orthosteric ligand. This is termed allosteric agonism (Langmead and Christopoulos, 2006).

### 1.3 Dualsteric compounds

The dualsteric ligands are composed of the orthosteric moieties covalently linked to the allosteric moieties (Disingrini *et al.*, 2006; Schmitz *et al.*, 2014). Hence, these ligands can also be termed bipharmacophoric. In Antony *et al.*, 2009 dualsteric ligands were used to gain both subtype selectivity of receptor binding and signalling pathway activation. Dualsteric ligands can bind in a dualsteric binding mode whereby both the orthosteric and the allosteric moieties interact with their respective binding sites simultaneously, in a bitopic manner (Steinfeld *et al.*, 2007; Bock and Mohr, 2013). The binding orientation of a dualsteric ligand is determined by the binding affinities of the building blocks to their respective binding sites (Bock *et al.*, 2014a).

Hence the dualsteric ligands composed of an orthosteric activator moiety and an allosteric moiety without intrinsic efficacy, are able to stabilise active receptor states when bound in a bitopic orientation whilst the purely allosteric binding pose stabilises the inactive receptor states (**Figure 1.2**). This is termed dynamic ligand binding. The combination of inactive and active receptor states in a system results in an overall partial agonism (Bock *et al.*, 2014a,b).

The dynamic binding of the dualsteric (active) and allosteric (inactive) pose can be described by the equilibrium binding constants  $K_A$  and  $K_B$ , respectively. The ratio of  $K_A$  and  $K_B$  yields the orientation ratio  $R_{pose}$  which describes the equilibrium position between the active and inactive receptor populations. This means that if the binding affinity of the dualsteric active pose ( $K_A$ ) is higher than of the inactive pose ( $K_B$ ), the majority (> 50%) of the ligand bound receptors will be in the active state, and vice versa. The degree of partial agonism is also co-determined by the efficacy ( $\epsilon$ ) of the dualsteric ligand in activating signalling pathways. If a dualsteric ligand displays similar efficacy to a full agonist, the extent of receptor activation is then predominantly determined by the orientation ratio. However, when the dualsteric ligand exhibits lower efficacy than a full agonists, the active receptor fraction will result in partial agonism, even at full receptor occupancy (Bock *et al*, 2014b).

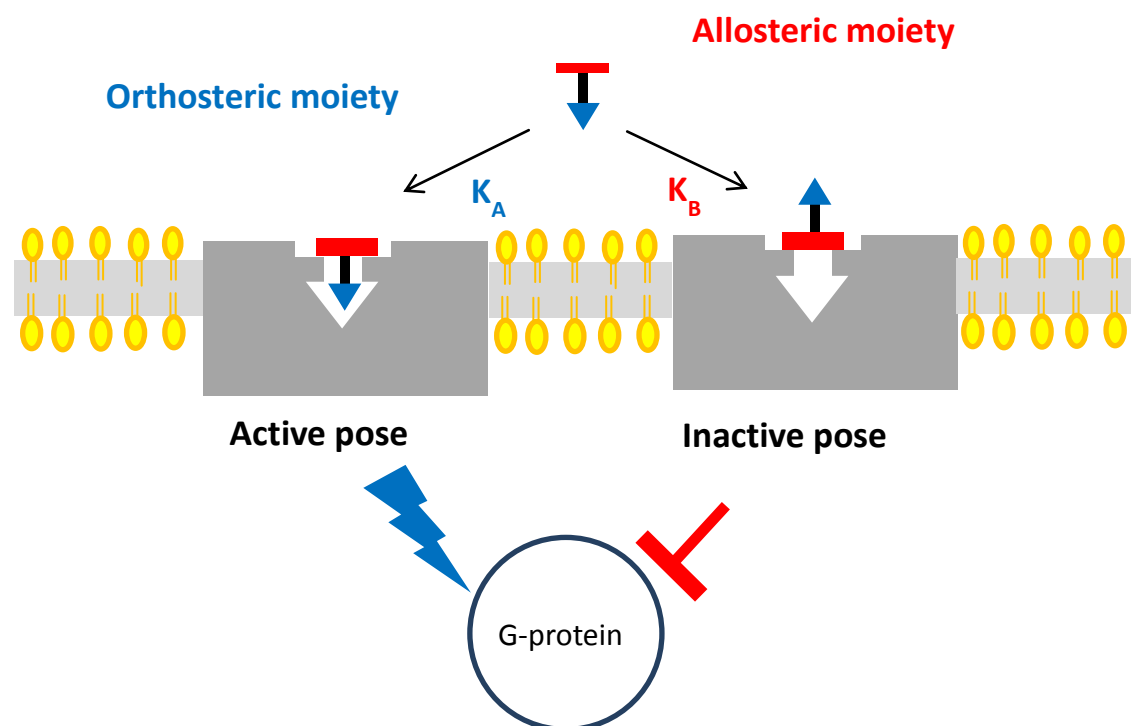


**Figure 1.2 Schematic diagram showing the active and inactive binding orientations of the dualsteric ligands in dynamic ligand binding.** A dualsteric ligand consists of an allosteric moiety (red), carbon chain linker (black) and the orthosteric moiety (blue).  $K_A$  and  $K_B$  are equilibrium dissociation constants for the active and inactive binding poses. Adapted from Bock *et al*, 2014a

## 1.4 The core region of M<sub>2</sub> allosteric binding site - basis of the M<sub>2</sub> triple mutation

The orthosteric binding site was observed to be highly conserved among the five subtypes of the muscarinic receptors (Hulme *et al.*, 1990; Wess, 1993). On the other hand, the allosteric binding site appears to be less conserved than the orthosteric site, thereby presenting an opportunity for development of compounds with greater subtype selectivity (Ellis *et al.*, 1993; Leppik *et al.*, 1994; Tucek and Proska, 1995). A number of studies have been conducted using the M<sub>2</sub> receptor as a model to get a deeper insight into the function of the allosteric binding site of muscarinic receptors. Receptor mutagenesis studies such as the use of M<sub>2</sub>/M<sub>5</sub> chimeric receptors (Gnagey *et al.*, 1999; Ellis and Seidenberg, 2000), development of allosteric modulators with greater selectivity and affinity for M<sub>2</sub> receptors (Holzgrabe *et al.*, 2006) and the use of docking simulations (Prilla *et al.*, 2006) has shed greater light on the important epitopes and domains involved in the binding of allosteric modulators.

The M<sub>2</sub> muscarinic receptor is the most sensitive for allosteric modulators compared to the other muscarinic receptor subtypes. M<sub>2</sub> amino acids Y177<sup>ECL2</sup> and T423<sup>7.36</sup> located in the extracellular loop 2 (E2) and at the top of TM7 respectively, account entirely for the 100-fold M<sub>2</sub>/M<sub>5</sub> selectivity of a wide range of structurally diverse allosteric modulators (Voigtländer *et al.*, 2003). The numbering of amino acid residues (e.g. Y177<sup>ECL2</sup>) in this thesis is based on the Ballesteros and Weinstein method (1995) which gives the most conserved residue in a transmembrane the index number 50. Hence the other amino acids are then indexed in reference to this position. These two residues Y177<sup>ECL2</sup> and T423<sup>7.36</sup> are also independently involved in determining the binding affinity of allosteric modulators at both the free and orthosterically-occupied M<sub>2</sub> receptor (Buller *et al.*, 2002; Voigtländer *et al.*, 2003). M<sub>2</sub> W422<sup>7.35</sup> has been found to be important for baseline affinity, subtype selectivity and cooperativity depending on the allosteric modulator (Prilla *et al.*, 2006).

Three-dimensional simulations provided an M<sub>2</sub> model which showed that Y177<sup>ECL2</sup>, W422<sup>7.35</sup> and T423<sup>7.36</sup> are spatially closely related and form a pivotal docking point complex for allosteric modulators. The 3D simulations also revealed that these three allosteric epitopes are located at the bottom of the allosteric binding cavity and thereby concurrently forming part of the entrance to the orthosteric binding pocket (**Figure 1.3**) (Prilla *et al.*, 2006). In support of the M<sub>2</sub> model findings, M<sub>2</sub> W422<sup>7.35</sup> has been observed to influence the binding of orthosteric ligands. M<sub>2</sub> W422<sup>7.35</sup> conserved among all muscarinic subtypes (Matsui *et al.*, 1995) is essential in the binding of M<sub>2</sub> receptor agonists and for receptor activation in the absence of an allosteric modulator (Jäger *et al.*, 2007). A homology model of the M<sub>2</sub> mAChR showed

that the E2 loop which contains Y177<sup>ECL2</sup>, points in over the orthosteric binding site crevice in the non-bound receptor state. This showed that the E2 loop directly contributes to the orthosteric binding site (Avlani *et al.*, 2007). Recently, the M<sub>2</sub> active state crystal structure revealed that the aromatic rings of the allosteric modulator LY2119620 were situated between the Y177<sup>ECL2</sup> and the W422<sup>7.35</sup> located just directly above the orthosteric binding pocket. The interaction of LY2119620 with these two epitopes resulted in the formation of a three-layered aromatic stack (Kruse *et al.*, 2013).

Therefore, combining all this information it was shown that the three amino acids Y177<sup>ECL2</sup>, W422<sup>7.35</sup> and T423<sup>7.36</sup> were an important part of the M<sub>2</sub> allosteric/orthosteric transition zone. Hence, for this study these amino acids were mutated to Alanine (Ala) creating an M<sub>2</sub> triple mutant.

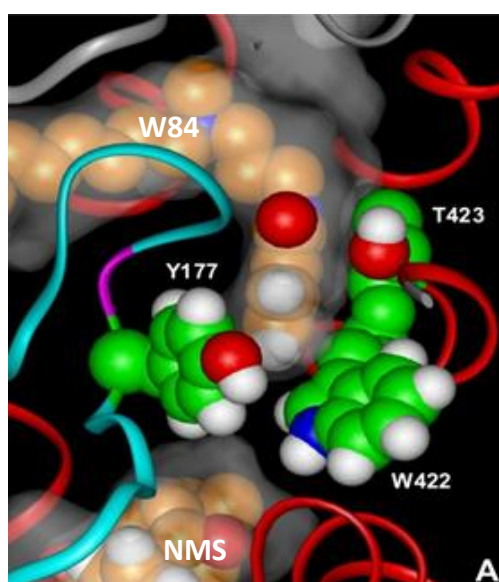


**Figure 1.3** The three M<sub>2</sub> amino acids Y177<sup>ECL2</sup>, W422<sup>7.35</sup> and T423<sup>7.36</sup> are spatially closely related and form a core docking point of allosteric ligands. A top view into the receptor with the allosteric ligand W84 and the orthosteric inverse agonist NMS docked in the allosteric and orthosteric pockets, respectively. (Modified from Prilla *et al.*, 2006).

## 1.5 Biogenic amines

There are five known biogenic amine ligands epinephrine (adrenaline), norepinephrine (noradrenaline), dopamine, histamine and serotonin. The first three biogenic amines can be classified as catecholamines because they possess a catechol moiety and are all synthesized from a common precursor which is the amino acid tyrosine (**Figure 1.4**). Similar to the mAChRs, the biogenic amine receptors also belong to the  $\alpha$ -group of class A receptor family. This amine-binding cluster of receptors forms the largest group of receptors which bind similar types of ligands (Lagerström and Schiöth, 2008).

Epinephrine and norepinephrine signal through  $\alpha$  and  $\beta$  adrenoceptor subtypes. The  $\alpha$  subtype is divided into  $\alpha_{1A,B,D}$  and  $\alpha_{2A,B,C}$  whilst the  $\beta$  subtype constitutes  $\beta_1$ - $\beta_3$  (Bylund, 1988; Chen and Minneman, 2005; Gyires *et al.*, 2009). Epinephrine and norepinephrine are important in the regulation of blood pressure, airway reactivity and the contractile rate of cardiomyocytes (Bylund *et al.*, 1994). Adrenoceptors are located in the CNS and almost in all peripheral tissues. In the CNS norepinephrine is involved in the regulation of sleep, wakefulness and attention. The brain stem nucleus called locus coeruleus which projects into several parts of the forebrain, also uses norepinephrine as a neurotransmitter. Norepinephrine exhibits differences with epinephrine by possessing a higher affinity for  $\alpha$ -receptors and low affinity for  $\beta_2$  receptors.  $\alpha_1$ -receptors signal through the  $G_{q/11}\alpha$  leading to the activation of phospholipase C (PLC $\beta$ 1). This results in increased DAG and subsequent activation of protein kinase C (Jensen *et al.*, 2011).  $\alpha_2$ -receptors preferentially activates the inhibitory  $G_{i/o}\alpha$  whereby the  $\beta\gamma$  subunit can activate phospholipase C leading effects such as contraction of smooth muscle cell contraction. All  $\beta$  subtypes  $\beta_1$ - $\beta_3$  appear to stimulate  $G_s\alpha$  activation increasing intracellular cAMP accumulation (Evans *et al.*, 2010).

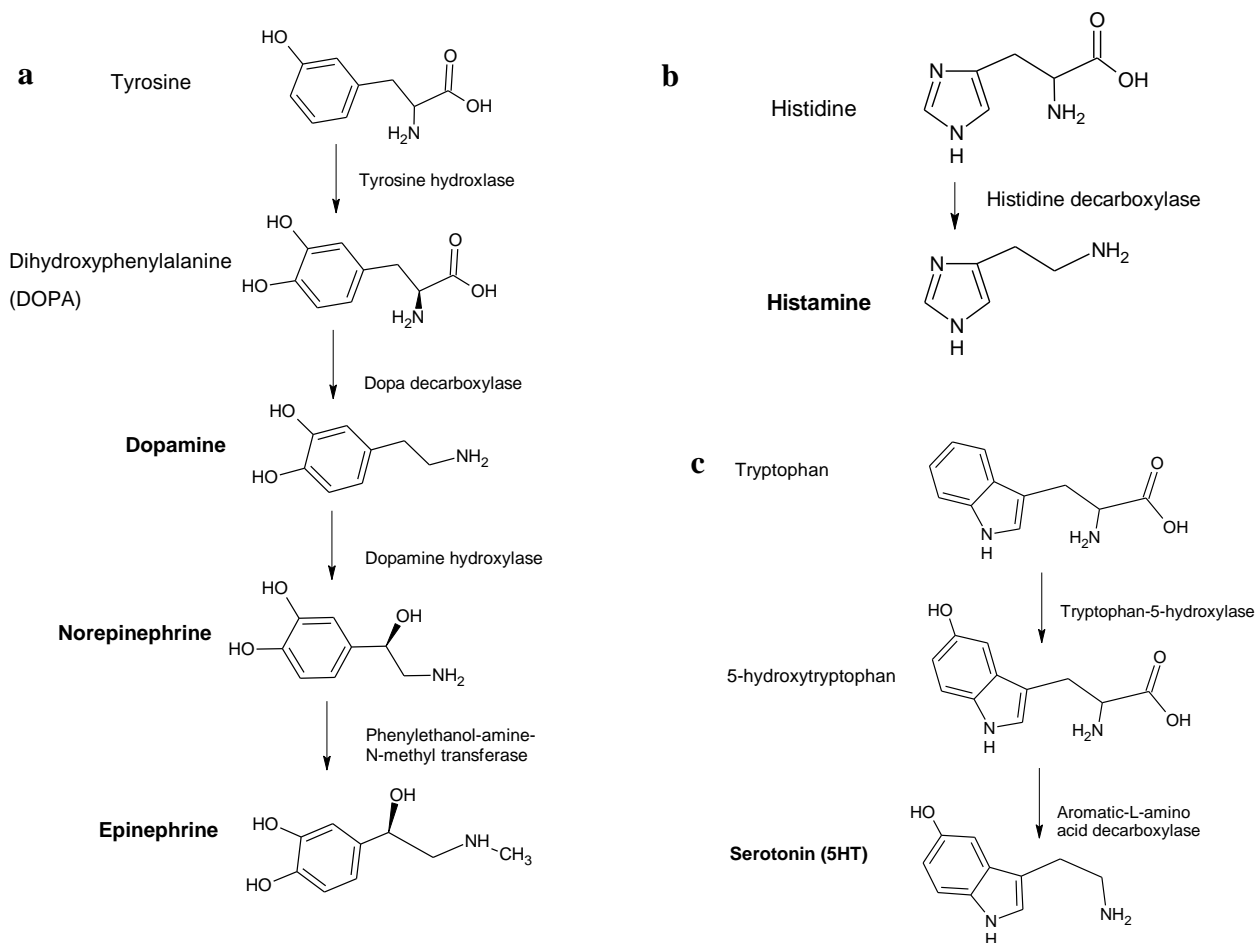


**Figure 1.4 Synthesis of the biogenic amines from their precursor amino acids. (a)** Synthesis of the catecholamines dopamine, norepinephrine and epinephrine from tyrosine. **(b)** Histamine is synthesised from histidine by removing  $\text{CO}_2$ . **(c)** Serotonin (5HT) synthesis by a two-step process involving tryptophan-5-hydroxylase and a decarboxylase.

Dopamine acts as a neuromodulator in the CNS and can also stimulate different functions in the periphery. Dopamine is an important neurotransmitter in the physiological function of the brain where it is distributed in several areas, mainly in the striatum (Porritt *et al.*, 2006; Huot and Parent, 2007). In the periphery, dopamine receptors have been observed in varying concentrations in locations such as the kidneys, heart, blood vessels and adrenal glands. Dopamine signals through the dopaminergic receptors which can be classified into 5 subtypes  $\text{D}_1$ - $\text{D}_5$ . The 5 subtypes can be subdivided into the  $\text{D}_1$ -like ( $\text{D}_1$  and  $\text{D}_5$ ) and the  $\text{D}_2$ -like ( $\text{D}_2$ ,  $\text{D}_3$  and  $\text{D}_5$ ) subfamilies. These 7TM receptors mediate all of the physiological functions of dopamine such as hypertension, voluntary movement, reward and hormonal regulation (Seeman and Van Tol, 1994; Bealieu and Gainetdinov, 2011; Lane *et al.*, 2014). The  $\text{D}_1$ -like class couples to the  $\text{G}_{s/olf}\alpha$  family of G-proteins to activate cAMP production. The  $\text{D}_2$ -like class activates the  $\text{G}_{i/o}\alpha$  leading to the inhibition of adenylyl cyclase and reduction in cAMP (Neve *et al.*, 2004).



Histamine is synthesised from the amino acid histidine by the enzyme histamine decarboxylase (**Figure 1.4b**). Histamine signals through four subtypes H<sub>1</sub>-H<sub>4</sub> which are expressed in both the CNS and periphery. In the brain, histamine has been observed to mediate functions such as arousal, cognition, attention and feeding rhythms (Passani and Blandina, 2011). In the periphery histamine mediates effects including smooth muscle contraction and relaxation, stimulation of nitric oxide (NO) release from the endothelium and stimulates immunoglobulin E (IgE)-mediated allergic reactions (Hill *et al.*, 1997). The H<sub>1</sub> receptors preferentially couple to the G<sub>q/11</sub>α family of G-proteins leading to the activation of phospholipase C (Leurs *et al.*, 1995). H<sub>1</sub> receptors have been detected in a variety of tissues including the heart, smooth muscle, endothelial cells, adrenal medulla and the CNS. H<sub>2</sub> receptors activate the G<sub>s</sub>α protein (Tubio *et al.*, 2010) and the effects of cAMP accumulation have been observed in the tissues including the brain, cardiac myocytes, vascular smooth muscle and fat cells (Reinhardt and Ritter, 1979; Al-Gadi and Hill, 1985). High histamine concentrations have been observed in the cardiac tissues in which they can induce positive inotropic and chronotropic effects on atrial and ventricular tissues by stimulating the H<sub>2</sub> receptors. The H<sub>3</sub> receptor is involved in inhibition of neurotransmitter release. The H<sub>4</sub> receptor play a regulatory role in the immune system by modulating eosinophil migration, recruiting mast cells, dendritic cell activation and T-cell differentiation (Zampeli and Tiligada, 2009) Both H<sub>3</sub> and H<sub>4</sub> have been observed to couple to the G<sub>i/o</sub>α proteins (Feliszek *et al.*, 2015).

Serotonin (5-hydroxytryptamine 5HT) is synthesised from the amino acid tryptophan in a two-step process (**Figure 1.4c**). Serotonin receptors can be found in both the central and peripheral nervous system. Serotonin is involved in the regulation of a wide range of human behavioural processes such as anger, reward, mood attention and memory (Barnes and Sharp, 1999; Berger *et al.*, 2009). Outside the CNS, serotonin receptors are expressed in tissues such as the gut and cardiovascular system whereby serotonin regulates effects including cardiovascular and pulmonary physiology, endocrine function and food intake (Hannon and Hoyer, 2008). Apart from 5HT<sub>3</sub> which belongs to the ion channel family, the serotonin receptors belong to the family of GPCRs divided into seven subtypes (5HT<sub>1</sub>-5HT<sub>7</sub>) (Hoyer *et al.*, 1994). The serotonin receptor family consists of at least 14 known receptors making it one of the most complex families of neurotransmitter receptors. The 5HT<sub>1</sub> subtype preferentially couple to the G<sub>i/o</sub>α family of G-proteins, 5HT<sub>2</sub> to G<sub>q/11</sub>α and 5HT<sub>4,6,7</sub> to G<sub>s</sub>α. For the subtype 5HT<sub>5</sub>, only 5HT<sub>5A</sub> has been shown to couple to G<sub>i/o</sub>α (Hoyer *et al.*, 2002).

### 1.5.1 The ligand binding site of aminergic receptors

The amino acid composition, shape and size of GPCR ligand binding pockets explain the ability of GPCRs to recognize and discriminate between distinct chemical entities (Rosenbaum *et al.*, 2007; Granier and Kobilka, 2012). Different ligands dock into their respective receptor binding sites in different binding orientations. Nonetheless, most of the ligand-aminergic GPCR interactions appear to involve similar positions in these ligand binding sites. This results in the Asp<sup>3.32</sup> (D<sup>3.32</sup>) residue which is completely conserved in aminergic receptors and is located in the extracellular half of the transmembrane domain, making a direct contact with the protonated amine of all aminergic ligands (van Rhee and Jacobson, 1996; Shi and Javitch, 2002).

A positively ionisable group forms a charge-mediated hydrogen bond with the residue D<sup>3.32</sup> which is the key interaction for all biogenic amine-binding GPCRs (Evers *et al.*, 2005). In most of the aminergic receptors, mutation of the conserved D<sup>3.32</sup> results in a loss of ligand binding. Some examples of these D<sup>3.32</sup> mutations are D103E in M<sub>2</sub> receptor (Heitz *et al.*, 1999), D113A in  $\beta_2$ AR (Strader *et al.*, 1987), D115N in serotonin 5HT<sub>2A</sub> receptor (Wang *et al.*, 1993), and D107A in the histamine H<sub>1</sub> receptor (Ohta *et al.*, 1994; Nonaka *et al.*, 1998).

S<sup>3.36</sup> can act as a second interaction site of the protonated amine of serotonin in 5HT<sub>2A</sub> receptors (Almaula *et al.*, 1996). The residues S<sup>5.42</sup> and S<sup>5.46</sup> have been shown to be critical in many aminergic ligand binding. The imidazole nitrogens of histamine interact with both S<sup>5.42</sup> and S<sup>5.46</sup> in H<sub>1</sub> and H<sub>2</sub> receptors (Gantz *et al.*, 1992; Mognilevsky *et al.*, 1995). Catecholamine agonists also form critical interactions with both S<sup>5.42</sup> and S<sup>5.46</sup> whilst the antagonists appear to interact with only S<sup>5.42</sup> (Cavalli *et al.*, 1996; Liapakis *et al.*, 2000; Wilcox *et al.*, 2000). Mutation of S<sup>5.42</sup> in cholinergic receptors has been shown to disrupt the binding of agonists ligands and/or receptor activation (Wess *et al.*, 1991; Allman K *et al.*, 2000). Biogenic amine GPCRs possess a conserved cluster of aromatic residues in TM6 (W<sup>6.48</sup>, F/Y<sup>6.51</sup> and F<sup>6.52</sup>) which plays an important role in the binding of agonists and antagonists (Shin *et al.*, 2002; Bruysters *et al.*, 2004; Kooistra *et al.*, 2013)

### 1.5.2 Class A family receptor activation mechanisms

The mechanism of activation seems to be very similar amongst the class A GPCRs which contain the aminergic receptors. The agonist-bound structure of the  $\beta_2$  adrenergic receptor shows that the TM5 helix shifts inwards resulting in the contraction of the ligand binding pocket (Ring *et al.*, 2013). TM helices 5, 6 and 7 have also been found to move inwards

towards the agonist in the active M<sub>2</sub> receptor (Kruse *et al.*, 2013). The active state crystal structures of both the β<sub>2</sub>AR and the M<sub>2</sub> receptor show the rearrangement of the highly conserved DRY motif in TM3 and the NPXXY motif in TM7. Arg121<sup>3,50</sup> of the DRY motif in the active M<sub>2</sub> displays an extended conformation which is almost identical to that observed in the β<sub>2</sub>AR-Gs complex and in metarhodopsin II (Choe *et al.*, 2011; Ring *et al.*, 2013).

The classification of biogenic amine receptors is conferred mainly by the diversity of their ligand binding pockets within the 7TM regions. The extracellular vestibule is less well conserved amongst the muscarinic receptor subtypes and this is also true for all of the class A GPCRs (Rosenbaum *et al.*, 2007, Kruse *et al.*, 2014). The M<sub>2</sub> receptor has been shown to possess a very small narrow passage at the bottom of the allosteric vestibule which concurrently forms part of the entrance to the orthosteric binding pocket (Kruse *et al.*, 2013). This small narrow passage has been found to also play a key role in M<sub>2</sub> receptor - G-protein coupling. The spatial rearrangement of this allosteric narrow channel is involved in the fine-tuning of signals generated by orthosteric ligands (Bock *et al.*, 2012).

Molecular dynamics simulations using the β<sub>1</sub> and β<sub>2</sub> adrenoceptors have shown that drug entry into the binding site involves a two-step process. The first step is characterized by a substantial dehydration which accompanies the drug entry into the extracellular vestibule. The second step involves structural changes of the receptor's narrow passage whereby the Y308<sup>7,35</sup> and F193<sup>5,32</sup> separates enough allowing the hydrophobic moiety of the drug to pass between them. Also, there is further dehydration at this narrow passage whereby the drug loses most of its hydration shell as it passes from the extracellular vestibule into the orthosteric binding pocket (Dror *et al.*, 2011).

The orthosteric entry point has been implicated in the selective binding of orthosteric ligands within receptor families such as the β adrenoceptors (Rosenbaum *et al.*, 2007). In opioid receptors, the selective binding of the antagonist naltrindole to the δ-opioid receptor is due to a single amino acid difference in the outer part of the binding pocket (Granier *et al.*, 2012). Interestingly, the allosteric binding site in the M<sub>2</sub> muscarinic receptor is structurally very similar to the selective region found in the opioid receptor family (Granier and Kobilka, 2012). M<sub>2</sub> W422<sup>7,35</sup>, a key epitope of the allosteric binding site, is essential in the binding of M<sub>2</sub> receptor agonists and for receptor activation in the absence of an allosteric modulator (Jäger *et al.*, 2007). It has also been reported that constraining flexibility of the extracellular loop 2 (E2) significantly impairs orthosteric ligand access at the M<sub>2</sub> receptor (Avlani *et al.*,

2007). All these findings propose the presence of a selectivity filter just outside the orthosteric binding cavity of GPCRs.

## 1.6 Aim of study

The aim of the thesis was to investigate the gate-keeper function of the core domain of the allosteric binding site of the M<sub>2</sub> receptor. The thesis aimed at investigating the role of the small channel located between the orthosteric and the allosteric site of the M<sub>2</sub> receptor as a selective filter against the biogenic amine ligands epinephrine, noradrenaline, dopamine, histamine and serotonin (5HT). At least to our knowledge nothing is published in the literature regarding the function of this narrow passage in the M<sub>2</sub> receptor as a selective barrier against the binding of biogenic amine ligands.

Therefore in this study, an M<sub>2</sub> triple mutant receptor (Y177<sup>ECL2</sup> →Ala, W422<sup>7.35</sup> →Ala and T423<sup>7.36</sup> →Ala) was made by substituting the three allosteric epitopes with alanine (Ala). The hypothesis was that substitution of these large and spacious aromatic compounds with a small amino acid alanine would result in the broadening of the narrow passage and thereby increasing the free volume between the allosteric and orthosteric binding cavities. The opening of this narrow passage would then allow other non-cholinergic biogenic amine ligands to access the M<sub>2</sub> receptor orthosteric binding site and/or cause receptor activation.

The thesis therefore started by investigating the effects of the M<sub>2</sub> triple mutation on the classical muscarinic ligands-receptor interaction. First, the hypothesis was that the M<sub>2</sub> triple mutation would severely reduce or completely abolish receptor-allosteric ligand interaction. It went on to investigate if the M<sub>2</sub> triple mutation would affect the binding of structurally distinct orthosteric muscarinic orthosteric ligands. Experiments were also carried out to investigate the effects of the M<sub>2</sub> triple mutation at the receptor activation and signalling level induced by the orthosteric muscarinic ligands.

The thesis also focused on the interaction of dualsteric ligands with the M<sub>2</sub> triple mutant. The hypothesis was that substituting the triple amino acids in the allosteric core binding domain would favour the binding of dualsteric ligands in the active dualsteric pose. This would be as a result of a reduction in the binding affinity of the allosteric (inactive) pose due to the disruption of the core docking site of allosteric moieties.

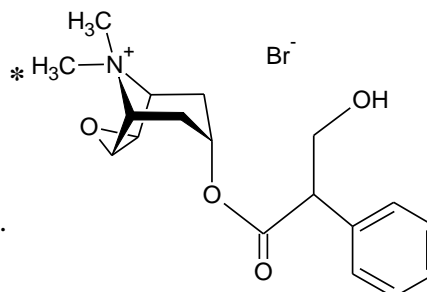
## 2 Material and methods

### 2.1 Compounds

#### 2.1.1 Radioligands

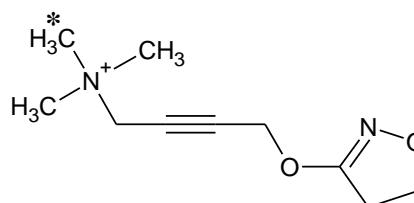
##### [<sup>3</sup>H]N-methylscopolamine

Molecular weight: 398.3 g/mol  
Supplier: Perkin Elmer  
Product number: NET636001MC  
\*: Position of the radioactive label.



##### [<sup>3</sup>H]Iperoxo

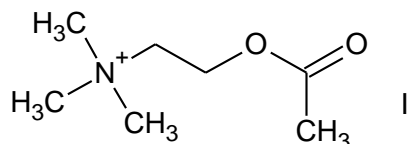
Molecular weight: 324.16 g/mol  
Supplier: Perkin Elmer  
Lot number: 100226  
\*: Position of the radioactive label.



#### 2.1.2 Muscarinic orthosteric and allosteric ligands

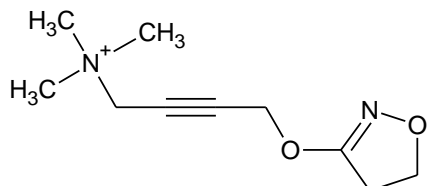
##### Acetylcholine (ACh)

Molecular weight: 273.1 g/mol  
Supplier: Sigma Aldrich  
Product number: A-7000



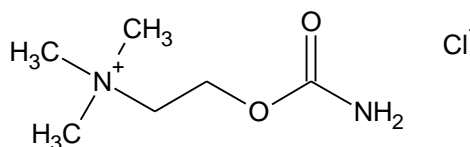
##### Iperoxo

Molecular weight: 342.16 g/mol  
Supplier: Prof Holzgrabe  
University of Würzburg, Germany



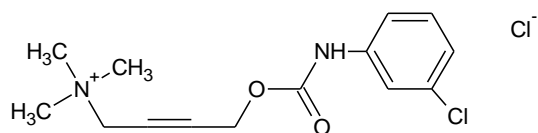
##### Carbamoylchloride chloride (Carbachol)

Molecular weight: 182.65 g/mol  
Supplier: Fluka  
Product number: 1048960

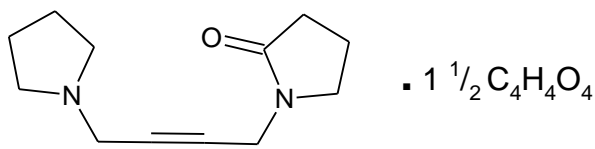


**McN-A-343**

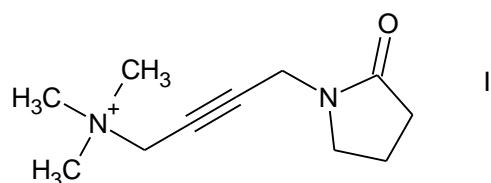
Molecular weight: 317.24g/mol  
 Supplier: Sigma Aldrich  
 Product number: C7041

**Oxotremorine**

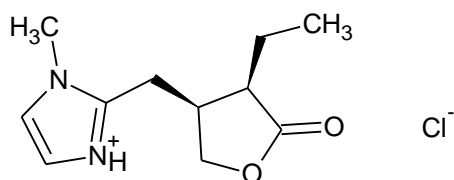
Molecular weight: 380.4 g/mol  
 Supplier: Sigma Aldrich  
 Product number: O9126

**Oxotremorine M**

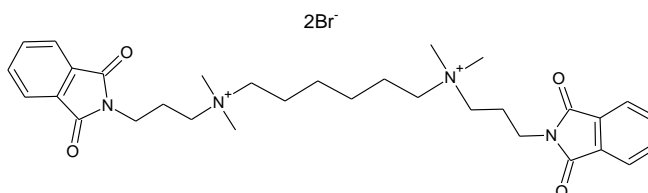
Molecular weight: 322.19 g/mol  
 Supplier: Sigma Aldrich  
 Product number: O100

**Pilocarpine**

Molecular weight: 244.72 g/mol  
 Supplier: Sigma Aldrich  
 Product number: P6503

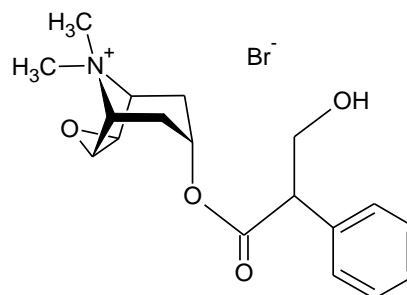
**W84**

Molecular weight: 708.5 g/mol  
 Supplier: Dr Pfeffer  
 University of Kiel, Germany



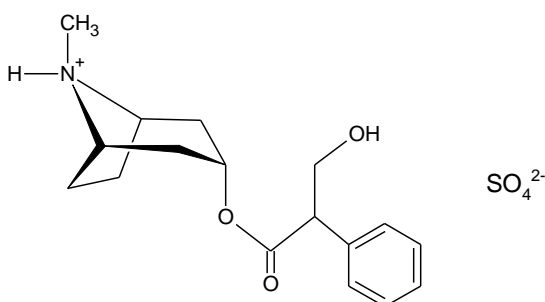
### N-methylscopolamine (NMS)

Molecular weight: 398.3 g/mol  
Supplier: Sigma Aldrich  
Product number: S-8502



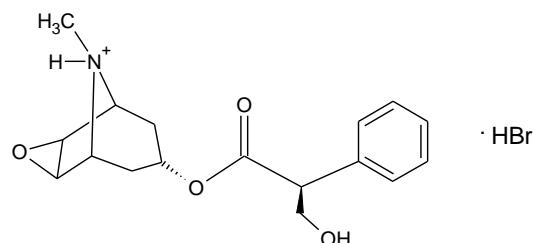
### Atropine (Atr)

Molecular weight: 694.8 g/mol  
Supplier: Sigma Aldrich  
Product number: A0257



### Scopolamine

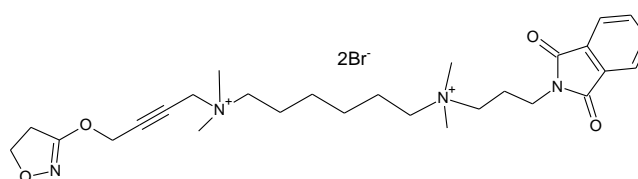
Molecular weight: 384.3 g/mol  
Supplier: Sigma Aldrich  
Product number: S1875



## 2.1.3 Muscarinic dualsteric ligands and their allosteric moieties

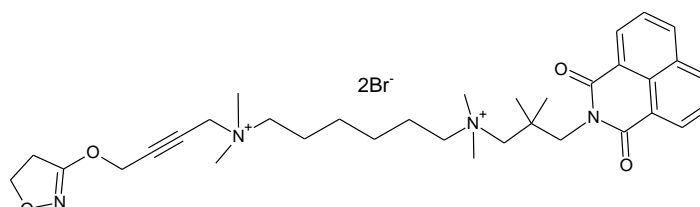
### Iper-6-phth

Molecular weight: 685.5 g/mol  
Supplier: Prof De Amici  
Universita degli Studi di Milano, Italy



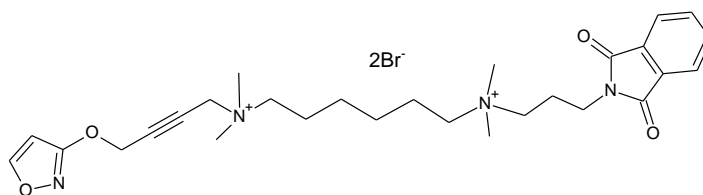
### Iper-6-naph

Molecular weight: 736.6 g/mol  
Supplier: Prof De Amici  
Universita degli Studi di Milano, Italy



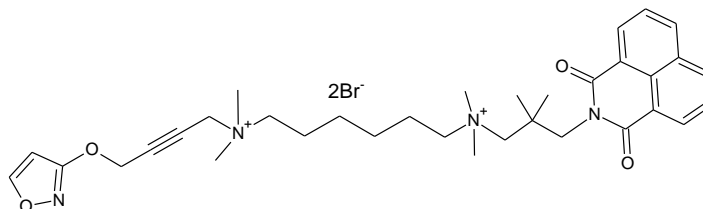
### Isox-6-phth

Molecular weight: 658.5g/mol  
Supplier: Prof Holzgrabe  
University of Würzburg, Germany



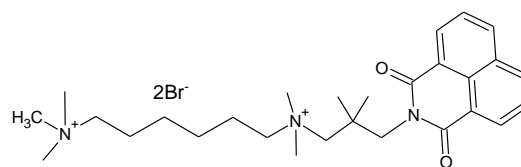
### Isox-6-naph

Molecular weight: 734.6g/mol  
Supplier: Prof Holzgrabe  
University of Würzburg, Germany



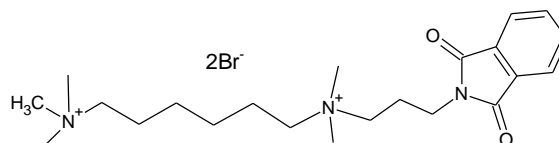
### 6-naph

Molecular weight: 627.4 g/mol  
Supplier: Prof Holzgrabe  
University of Würzburg, Germany



### 6-phth

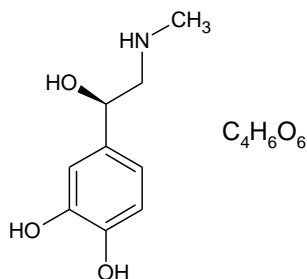
Molecular weight: 549.4 g/mol  
Supplier: Prof Holzgrabe  
University of Würzburg, Germany



## 2.1.4 Biogenic amines

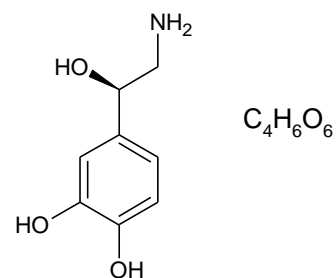
### Epinephrine

Molecular weight: 333.29 g/mol  
Supplier: Sigma  
Product number: E4375



### Norepinephrine

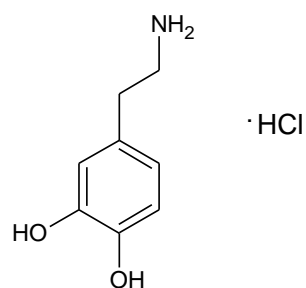
Molecular weight: 319.26 g/mol  
Supplier: Santa Cruz Biotechnology  
Product number: sc-255396



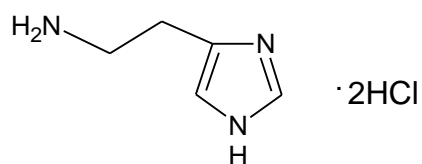


**Dopamine**

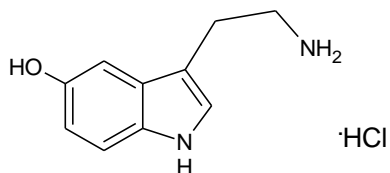
Molecular weight: 189.64 g/mol  
Supplier: Sigma Aldrich  
Product number: H8502

**Histamine**

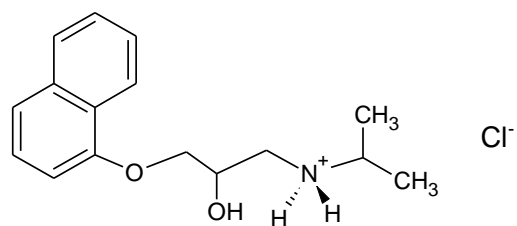
Molecular weight: 184.07 g/mol  
Supplier: Sigma Aldrich  
Product number: H7250

**Serotonin**

Molecular weight: 212.68 g/mol  
Supplier: Sigma  
Product number: H9523

**Adrenergic antagonist****Propranolol**

Molecular weight: 295.8 g/mol  
Supplier: Sigma Aldrich  
Product number: P0884



## 2.2 Materials

### 2.2.1 Reagents

	<b><u>Description</u></b>	<b><u>Article no.</u></b>	<b><u>Manufacturer</u></b>
<b>R1</b>	Copper sulfate penta hydrate ( $\text{CuSO}_4 \times 5\text{H}_2\text{O}$ )	1.027.900.250	Merck
<b>R2</b>	Dimethyl sulfoxide (DMSO; $M_r=78,1 \text{ g mol}^{-1}$ )	D-5879	Sigma
<b>R3</b>	Distilled water (Elix® sytem)		Millipore
<b>R4</b>	Distilled water (Milli Q® sytem)		Millipore
<b>R5</b>	D-PBS (Dulbecco's phosphate buffered salt solution) without magnesium and calcium	1880551	PAN-Bio
<b>R6</b>	Emusifier-Safe™	6013389	Perkin
<b>R7</b>	Ethylenediaminetetraacetic acid disodium salt ( $\text{Na}_2\text{-EDTA}$ ; 100mM)	20271	Grüssing
<b>R8</b>	Fetal bovine serum (FBS)	F-7524	Sigma
<b>R9</b>	Guanosine diphosphate (GDP) sodium salt	G-7127	Sigma
<b>R10</b>	Hanks' balanced salt solution (HBSS) (1.23 mM $\text{CaCl}_2$ , 0.5 mM $\text{MgCl}_2$ , 0.4 mM $\text{MgSO}_4$ , 5.3 mM $\text{KCl}$ , 0.44 mM $\text{KH}_2\text{PO}_4$ , 4.2 mM $\text{NaHCO}_3$ , 137.9 mM $\text{NaCl}$ , 0.34 mM $\text{Na}_2\text{HPO}_4$ , 5.56 mM dextrose)	14025-050	Invitogen
<b>R11</b>	HEPES acid ( $M_r: 260.3 \text{ g mol}^{-1}$ )	H-3375	Sigma
<b>R12</b>	HEPES buffer solution (1 M)	15630-0566	Invitrogen
<b>R13</b>	HEPES salt ( $M_r: 260.3 \text{ g mol}^{-1}$ )	H-7006	Sigma
<b>R14</b>	HTRF®-cAMP-dynamic 2	62AM4PEC	Cisbio
<b>R15</b>	Human serum albumin	A-1653	Sigma
<b>R16</b>	3-Isobutyl-1-methylxanthin (IBMX)	15879	Sigma
<b>R17</b>	L-Glutamine solution (200 mM)	G-7513	Sigma
<b>R18</b>	Magnesium chloride hexahydrate ( $\text{MgCl}_2 \times 6 \text{ H}_2\text{O}$ ) ( $M_r: 302.3 \text{ g/mol}$ )	M-2670	Sigma
<b>R19</b>	Nutrient Mixture F-12 Ham	N-4888	Sigma

<b>R20</b>	Penicillin-streptomycin solution (PenStrep)	P-0781	Sigma
<b>R21</b>	Pertussis toxin (PTX)	BP0372	Biotrend
<b>R22</b>	Polyethylenimine solution (PEI)	P-3143	Sigma
<b>R23</b>	Potassium phosphate	30407	Sigma
<b>R24</b>	Potassium-sodium tartate tetrahydrate (KNaC <sub>4</sub> H <sub>4</sub> O <sub>6</sub> x 4 H <sub>2</sub> O)	379832	Sigma
<b>R25</b>	Ready Protein™ Scintillation reagent	P/N 586604	Beckman C
<b>R26</b>	Sodium butyrate	26319	Acros
<b>R27</b>	Sodium carbonate (Na <sub>2</sub> CO <sub>3</sub> )	1.063.920.500	Merck
<b>R28</b>	Sodium chloride (NaCl)	1064041	Merck
<b>R29</b>	Sodium hydroxide (NaOH) (1 mol/l)	35256	Riedel-deH
<b>R30</b>	Sodium phosphate (Na <sub>2</sub> HPO <sub>4</sub> x 2H <sub>2</sub> O)	S0876	Sigma
<b>R31</b>	Trypsin-EDTA solution (0.5 g/l Trypsin; 0.2 g L <sup>-1</sup> Na <sub>4</sub> EDTA)	T-3924	Sigma

### 2.2.2 Solutions and buffers

#### **S1** Butyrate stock solution (100 mM)

1.101 g sodium butyrate  
100 ml distilled water  
Storage: 2-8 °C.

#### **S2** Copper sulfate solution 1%

1g copper sulfate penta hydrate  
100 ml distilled water  
Storage: room temperature

#### **S3** Centrifugation buffer (20 mM HEPES, 0.1 mM Na<sub>2</sub>-EDTA)

50 ml HEPES stock solution  
0.5 ml Na<sub>2</sub>-EDTA (100 mM)  
Fill with distilled water up to 500 ml  
Storage: 2-8°C

**S4** Folin-Ciocalteu reagent

1 part      folin-ciocalteus phenol reagent  
3parts      distilled water  
Storage: room temperature

**S5** GDP stock solution (10 mM)

4.65 mg    GDP sodium salt  
1 ml        distilled water  
Storage: -20°C in 50 µl aliquots

**S6** HBSS+20 mM HEPES buffer

490 ml     HBSS  
10 ml      Hepes buffer solution  
Storage: 2-8°C

**S7** HEPES buffer (12.5 mM HEPES, 12.5 mM MgCl<sub>2</sub>, 125 mM NaCl)

1.085 g    HEPES salt  
1.986 g    HEPES acid  
2.541 g    magnesium chloride hexahydrate  
7.305 g    sodium chloride  
Solution prepared with distilled water filled up to 1L, pH set to 7.4 using 1 M NaOH  
Storage: 2-8°C

**S8** HEPES stock solution (200 mM, pH 7.4 )

17.353 g   HEPES salt  
31.773 g   HEPES acid  
Solution prepared with distilled water filled up to 1L, pH set to 7.4 using 1 M NaOH  
Storage: 2-8°C

**S9** Homogenisation buffer (20 mM HEPES, 10 mM Na<sub>2</sub>EDTA)

50 ml       HEPES stock solution (200mM)  
50 ml       Na<sub>2</sub>EDTA (100 mM)  
400 ml      distilled water  
Storage:     2-8°C

**S10** Lowry working solution

100 parts    2% Sodium carbonate solution  
1 part        2% Potassium-sodium tartate solution  
1 part        1% Copper sulfate solution  
Storage: room temperature

40 mM NaKPi Buffer (33.3 mM Na<sub>2</sub>HPO<sub>4</sub> and 6.7 KH<sub>2</sub>PO<sub>4</sub>)

**S11** 178.0g  $\text{Na}_2\text{HPO}_4 \times 2\text{H}_2\text{O}$  in 2.0 L distilled  $\text{H}_2\text{O}$  (B1)  
68.0g  $\text{KH}_2\text{PO}_4$  in 1.0 L distilled  $\text{H}_2\text{O}$  (B2)  
Add 300 ml of B1 + 60 ml B2 and fill up to 4.5 L with distilled  $\text{H}_2\text{O}$ .  
Dilute the 40 mM buffer to 5mM with distilled  $\text{H}_2\text{O}$   
Storage: 2-8°C

**S12** Nutrient mixture F12-Ham

500 ml Nutrient mixture F12-Ham  
50 ml fetal bovine serum  
6 ml L-Glutamine solution 200 mM  
5 ml penicillin-streptomycin solution  
Storage: 2-8°C

**S13** Polyethylenimine stock solution (PEI) (1%)

10g PEI-solution 50%  
Add distilled water up to 500 ml  
Storage: 2-8°C

**S14** Polyethylenimine stock solution (PEI) (0.1%)

50 ml Polyethylenimine stock solution (PEI) (1%)  
450 ml distilled water  
Storage: 2-8°C

**S15** Sodium carbonate solution

2 g sodium carbonate ( $\text{Na}_2\text{CO}_3$ )  
100 ml distilled water

### 2.2.3 Disposables

	<b>Description</b>	<b>Article no.</b>	<b>Manufacturer</b>
<b>D1</b>	Cell scraper, sterile, 25 cm	831.830	Starlab
<b>D2</b>	Cellstar® tissue culture flask 75 cm <sup>2</sup>	658175	Greiner
<b>D3</b>	Corning®Epic® 384 well assay microplates	5040	Corning
<b>D4</b>	Corning®Epic® 384 well storage microplates	3657	Corning
<b>D5</b>	Cryogenic vials, 1 mL	50001012	Nalgene
<b>D6</b>	Falcon tube, sterile. 15 mL	188271	Greiner
<b>D7</b>	Falcon tube, sterile. 50 mL	227261	Greiner
<b>D8</b>	Finnpipette® Multistepper pipet tips (0.5 ml, 1.25 ml, 2.5 ml, 5.0 ml, 12.5 ml)		ThermoF
<b>D9</b>	Inject disposable syringe 20 ml		B.Braun
<b>D10</b>	MeltiLex™ A scintillation wax	145-441	Perkin
<b>D11</b>	Microtiter plate (384-well)	784080	Greiner
<b>D12</b>	Microtiter plate, PP (96-well)	AB-0564	Abgene
<b>D13</b>	Parafilm® M laboratory film	PM-996	Bemis
<b>D14</b>	Pasteur pipette (glass, 150 mm)	747715	Brand
<b>D15</b>	Pipette tips 0.5 – 5.0 mL		Brand/Starlab
<b>D16</b>	Polycarbonate-PC-centrifuge tubes with cap, 50 mL	3138-0050	Nalgene
<b>D17</b>	Polypropylene-PP-reaction vessels safe lock, 1.5 mL	30.120.086	Eppendorf AG
<b>D18</b>	Polypropylene-PP-reaction vessels, 1.5 mL	616201	Greiner
<b>D19</b>	Printed Filtermat A (90 x 120 mm)	1450-421	Perkin
<b>D20</b>	Qualilab® Syringe filter units (0.22 µM CM membrane, sterile)	5122110	Merk Labor
<b>D21</b>	Sample bag for MicroBeta® Trilux, 100/PK	1450-432	Perkin
<b>D22</b>	Scintillation vials 27/60	619301	Fish
<b>D23</b>	Screw caps for scintillation vials, white, 27 mm	619080	Fish
<b>D24</b>	Sterile pipette tips (5 ml)	2032E	Sar
<b>D25</b>	Sterile pipette tips (10 ml)	2241E	Sar
<b>D26</b>	Sterile pipette tips (25 ml)	3018E	Sar
<b>D27</b>	Tissue culture plate, sterile 100/20 mm	664160	Greiner
<b>D28</b>	Tissue culture plate, sterile 145/20 mm	639160	Greiner

## 2.2.4 Equipment

	<b>Description</b>	<b>Manufacturer</b>
<b>E1</b>	Accu-Jet® pipette	Brand
<b>E2</b>	Axiovert 25 microscope	Zeiss
<b>E3</b>	Beckman Avanti J-20 XP ultracentrifuge	Beck C
<b>E4</b>	Beckman LS 6000 + LS 6500	BeckInstr
<b>E5</b>	Cuvette 100-QS	Hellma
<b>E6</b>	Dri-Block® DB2A	Techne
<b>E7</b>	Elix® still	Milli
<b>E8</b>	EM Techcolor measuring flask DURAN®, (different sizes)	Hirsch
<b>E9</b>	Epic® microplate reader	Corning
<b>E10</b>	Eppendorf 5417C centrifuge	Eppend
<b>E11</b>	Finnpipette® digital pipettes of different sizes	ThermoF
<b>E12</b>	Finnpipette® multistepper pipette	ThermoF
<b>E13</b>	Freezer -86 °C ULT	Therm
<b>E14</b>	GFL® shaking water bath 1083	GFL
<b>E15</b>	Heraeus 6060 incubator	Kendro
<b>E16</b>	Herasafe® bench HS15, class I	Heraeus
<b>E17</b>	1450-Microbeta® Trilux Liquid Scintillation & Luminescence counter	Wallac
<b>E18</b>	Ice machine, AF 100 AS-E 230/50/1	Brand
<b>E19</b>	Microwave R-611/Energia NN-E25WB	Sharp/Panas
<b>E20</b>	Milli-Q® Biocel A10 ultrapure still	Millipore
<b>E21</b>	Mithras LB 960	Berthold
<b>E22</b>	MS 1 Minishaker	IKA
<b>E23</b>	Mr Frosty 5100 Cyro 1 °C freezing container	Nalgene
<b>E24</b>	Neubauer counting chamber	VWR

<b>Description</b>	<b>Manufacturer</b>
<b>E25</b> Nitrogen tank LS 750	TWH
<b>E26</b> pH 523 pH-meter	WTW
<b>E27</b> Plate cassette for Trilux	Perkin
<b>E28</b> Polytron homogenizer PT 10/35	WTW
<b>E29</b> Scales AG204, B2002-S, PB1502-S, PB403-S	Met
<b>E30</b> Thermoforma series II water jacketed CO <sub>2</sub> -incubator	Thermo
<b>E31</b> Tomtec® Harvester 96® Mach III (product number: 963-589)	Tomtec
<b>E32</b> Tomtec® Harvester 96® Mach III M (product number: 990607010)	Tomtec
<b>E33</b> Ultrospec 3300 pro, UV-Vis spectrometer	Biochrom
<b>E34</b> Vacuum pump RE16/1023-703Q-ER56X	Vacuu/Gast
<b>E35</b> Variomag® heatable magnetic stirrer	H+P
<b>E36</b> Vortex Genie 2®, G-560 E	Scientific
<b>E37</b> Φ 390 pH/Temp/mV/ISE Meter	BeckCoul

### 2.2.5 Manufacturers

<b>Abbreviation</b>	<b>Address</b>
<b>Abgene</b>	Abgene House, Epsom, UK
<b>Acros</b>	Acros Organics, Geel, BEL
<b>BeckCoul</b>	Beckman Coulter GmbH, Krefeld, GER
<b>BeckInstr</b>	Beckman Instruments, Palo Alto, USA
<b>Bemis</b>	Bemis, Flexible Packaging, Neenah, WI 54965, USA
<b>Berthold</b>	BERTHOLD TECHNOLOGIES GmbH & Co. KG, Bad Wildbad, G
<b>Biochrom</b>	Biochrom Ltd., Cambridge, UK
<b>Brand</b>	BRAND GmbH & Co. KG, Wertheim, GER



---

<b>Abbreviation</b>	<b>Address</b>
<b>Corning</b>	Corning Inc. (Corning, NY, USA)
<b>EMD</b>	EMD Chemicals, Inc. San Diego, USA
<b>Eppend</b>	Eppendorf AG, Hamburg, GER
<b>Gast</b>	Gast Manufacturing Inc., Benton Harbour, USA
<b>GFL</b>	Gesellschaft für Labortechnik mbH, Burgwedel, GER
<b>Greiner</b>	Greiner-Bio-One, Solingen, GER
<b>Grüssing</b>	Grüssing GmbH Analytika, Filsum, GER
<b>H+P</b>	H+P Labortechnik AG, Oberschleißheim, G
<b>Hellma</b>	Hellma GmbH & Co. KG, Mühlheim, GER
<b>Heraeus</b>	Heraeus, Hilden, GER
<b>Hirsch</b>	Hirschmann® Laborgeräte GmbH & Co. KG, Eberstadt, GER
<b>IKA</b>	IKA® Werke GmbH & Co. KG, Staufen, G
<b>Invitrogen</b>	Invitrogen Corporation, Carlsbad, California, USA
<b>Kendro</b>	Kendro Laboratory Products GmbH, Langenselbold, GER
<b>Merck</b>	Merck KGaA, Darmstadt, GER
<b>Merck Labor</b>	Merck Labor und Chemie Vertrieb GmbH, Bruchsal, GER
<b>Millipore</b>	Millipore, Schwalbach, GER
<b>Nalgene</b>	Nalgene Company (Sybron Corporation),
<b>Panas</b>	Panasonic Europe GmbH, Hamburg, GER
<b>PAN-Bio</b>	PAN-Biotech GmbH, Aidenbach, GER
<b>Perkin</b>	Perkin Elmer Life Science GmbH, Rodgau-Jügesheim, GER
<b>Riedel-deH</b>	Riedel-deHäen, Laborchemikalien GmbH & Co. KG, Seelze, GER
<b>Sar</b>	Sarstedt AG Co., Nümbrecht, G
<b>Scientific</b>	Scientific Industries Inc., Bohemia, New York, USA
<b>Sharp</b>	Sharp Electronics GmbH, Hamburg, GER

---

---

<b>Abbreviation</b>	<b>Address</b>
<b>Sigma</b>	Sigma-Aldrich Chemie GmbH, Hamburg, GER
<b>Starlab</b>	STARLAB GmbH, Ahrensburg, GER
<b>Techne</b>	Techne AG, Jahnsdorf, GER
<b>Thermo</b>	ThermoFischer Scientific, Marietta, Ohio, USA
<b>ThermoF</b>	ThermoFischer Scientific Oy, Vantaa, FIN
<b>Tomtec</b>	TOMTEC Inc., Hamden, USA
<b>TWH</b>	Taylor Wharton Harsco GmbH. Husum, GER
<b>Vacuu</b>	Vacuubrand GmbH & Co. KG, Wertheim, GER
<b>Wallac</b>	Wallac, Turku, FIN
<b>WTW</b>	Wissenschaftlich-Technische-Werkstätten GmbH, Weilheim, GER
<b>Zeiss</b>	Carl Zeiss AG, Oberkochen, GER

---

### 2.2.6 Software

ChemSketch 2010:	Version 12.01 Advanced Chemistry Development, Inc.
GraphPad Prism5 <sup>®</sup>	Version 5.03 GraphPad <sup>®</sup> Software, San Diego, USA
Microsoft Excel <sup>®</sup> 2010	Microsoft Corporation Redmont, USA
Microsoft PowerPoint <sup>®</sup> 2010	Microsoft Corporation Redmont, USA
Microsoft Word <sup>®</sup> 2010	Microsoft Corporation Redmont, USA

## 2.3 Cell culture

### 2.3.1 Thawing, passaging and freezing CHO cells.

Flp-In-Chinese hamster ovary cells (Flp-In-CHO) stably expressing the hM<sub>2</sub> wild type and the hM<sub>2</sub> triple mutant receptors were thawed from the nitrogen tank where they were stored in 1ml aliquots in cryogenic vials. The CHO cells had already been previously stably transfected with the respective expression vectors using FLP-FRT site directed mutagenesis. Each cell line was thawed quickly and transferred to a 14.5cm culture dish containing 35ml Ham's nutrient mixture F-12 (Ham's F12) supplemented with 10% (v/v) fetal bovine serum (FBS), Streptomycin (100µg/ml), L-glutamine (2mM) and Penicillin (100 U/ml). The cell preparation was done in a sterile laminar flow hood and the cells were grown at 37°C in a 5% CO<sub>2</sub> humidified incubator.

For the CHO M<sub>2</sub> triple mutant cells, the media was changed in four consecutive days in which they were allowed to grow and attach to the bottom of the dish before they were split. The CHO M<sub>2</sub> triple mutant cells were cultured in hygromycin containing nutrient medium after 7 days of growth in normal nutrient medium to select only the cells with the hygromycin resistance gene. CHO cells containing the hygromycin gene expressed the M<sub>2</sub> triple mutant gene. Therefore, cells were transferred to a culture dish containing 10 ml hygromycin-medium (600µg/ml hygromycin) in a 1:100 dilution, respectively. The cells were cultured in the hygromycin-medium for another week before reverting back to the normal nutrient medium.

For subsequent culturing, both CHO M<sub>2</sub> wt and triple mutant cells were grown until they reached 80-90% confluency. The old medium was aspirated and cells were washed with 10 ml PBS to get rid of residual medium and serum which would inhibit the enzyme trypsin function. 3ml trypsin-EDTA was applied for about two minutes to detach the cell monolayer from the culture dish. Remaining attached cells were detached by a gentle knock of the culture dish. 7ml nutrient medium was added to stop trypsinisation and the cells were resuspended by pipetting the cell suspension up and down. Cells were distributed to respective culture dishes mostly at a dilution of 1:10.

In order to have back up cells with a lower passage, cell lines were frozen and stored in liquid nitrogen. To achieve this, cells were collected as mentioned above and the cell suspension centrifuged at 900 rpm (JS 4.3 rotor) at 4°C for 4 minutes. The supernatant was aspirated and the pellet was resuspended in medium containing 10% DMSO. 1ml cell suspension was

aliquoted in labelled cryovials stored in a freezing container (MisterFrosty). This enabled the slow freezing of 1°C per minute until -80 °C before transfer to the nitrogen tank.

### 2.3.2 Cell membrane preparation.

When cells had reached about 80-90% confluency, the nutrient medium was aspirated and replaced by fresh nutrient medium containing 5mM Na-butyrate. The cells were incubated in this medium for 16-18 hours before membrane preparation. Addition of Na-butyrate would enhance protein biosynthesis and thereby increase receptor expression levels (Kruh, 1982). To obtain membranes with a silenced  $G_{i/o}$  pathway, the  $G_{i/o}$ -protein inhibitor pertussis toxin (PTX) (100µg/ml) was added to the cells for about 18hrs prior to membrane preparation. For the membrane preparation, the medium was aspirated and 2.4ml ice-cold homogenisation buffer was added to the cells. The cells were detached off the culture dish using a cell scraper and the cell suspension was transferred to a centrifuge tube. A total of five culture dish suspensions were collected and stored on ice in a single centrifuge tube. 7 ml ice-cold homogenisation buffer was added to the first plate to collect the remaining cells and transferred to the other four plates until all 5 plates were washed, before adding the suspension to the centrifuge tube. Depending on the amount of culture dishes, this step was repeated for all the other culture dishes until all cells were collected in centrifuge tubes. The cells were then shredded twice for 20 seconds at level six using a polytron homogeniser and the resulting cell fragments were centrifuged using the rotor JA25.50 at 40 000g for 10 minutes (2°C). The supernatant was aspirated and the pellet resuspended in 15 ml ice-cold centrifugation buffer before centrifugation in conditions mentioned above. This step was repeated once and the pellets were resuspended in ice-cold HEPES buffer. 1 ml and 0.5 ml aliquots were filled to labelled 1.5 ml eppendorf tubes then quickly frozen and stored at -80°C.

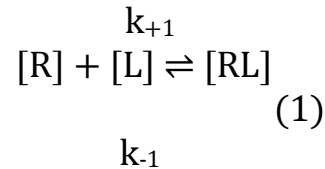
### 2.3.3 LOWRY protein assay

In order to determine the protein content of the cell membrane homogenates obtained, the Lowry (1951) protein assay was used (Lowry *et al.*, 1951). Seven dilution series of the human serum albumin concentrations ranging from 0 – 2mg/ml were used as a measure of calibration. The extinction was measured at 500nm using a UV-Photometer. Values obtained were plotted on a linear calibration curve whereby the protein content was determined.

## 2.4 Radioligand binding assays

### 2.4.1 Law of mass action

A free receptor [R] is able to interact with a free ligand [L] in a reversible manner to form a receptor-ligand complex [RL].



[R] : Free receptor concentration

[L] : Free ligand concentration

[RL] : Ligand receptor complex

$k_{+1}$  and  $k_{-1}$ : Rate constants of association and dissociation of the receptor complex, respectively

The rate of association ( $v_{+1}$ ) is proportional to the ligand and receptor concentrations, with  $k_{+1}$  as a constant of proportionality. The reverse is true for the rate of dissociation ( $v_{-1}$ ) which depends on the ligand-receptor complex and  $k_{-1}$  as proportionality constant.

$$\begin{aligned} v_{+1} &= k_{+1} \cdot [R] \cdot [L] \\ v_{-1} &= k_{-1} \cdot [RL] \end{aligned} \quad (2)$$

When the rate of association ( $v_{+1}$ ) and dissociation ( $v_{-1}$ ) become equal, a state of equilibrium is reached. This results in the law of mass action which directly links the ligand, receptor and ligand-receptor complex concentrations. The ratio of the constants  $k_{-1}/k_{+1}$  therefore produces the equilibrium dissociation constant  $K_D$ .

$$\frac{[R] \cdot [L]}{[RL]} = \frac{k_{-1}}{k_{+1}} = K_D \quad (3)$$

The dissociation constant  $K_D$  functions as a measure of ligand affinity for a receptor which indicates the concentration of the ligand resulting in a half maximal occupancy of the receptors ( $[R] = [RL]$ ). A high  $K_D$  reflects low ligand binding affinity whereby less ligand-receptor complexes are formed. This consequently results in more free ligand and receptor concentrations. The opposite would be true for a low  $K_D$  value.

## 2.4.2 [<sup>3</sup>H]NMS dissociation binding

### 2.4.2.1 Complete dissociation.

[<sup>3</sup>H]NMS dissociation binding experiments were conducted both in the presence and absence of allosteric modulators. Radioligand dissociation in the absence of an allosteric modulator produces the radioligand dissociation constant  $k_{-1}$  and the half-life of dissociation  $t_{1/2}$ . Cell membranes and live cells were pre-labelled with the orthosteric radioligand [<sup>3</sup>H]NMS before an excess of the inverse agonist atropine was added to visualise dissociation. Excess atropine prevents the radioligand from rebinding as atropine has more probability of binding to the orthosteric site due to higher concentrations. Therefore, the reduction in radioligand-receptor complexes follows an exponential decrease assuming that the receptor density is constant. This can be described by a one phase exponential decay.

$$[RL]_t = [RL]_0 \cdot e^{-k_{-1} \cdot t} \quad (4)$$

$[RL]_t$  : Radioligand-receptor complexes at time-point  $t$  after initiation of dissociation

$[RL]_0$  : Radioligand-receptor complexes at time-point  $t = 0$

$k_{-1}$  : Dissociation constant of radioligand-receptor-complexes

$t$  : Time after initiation of dissociation

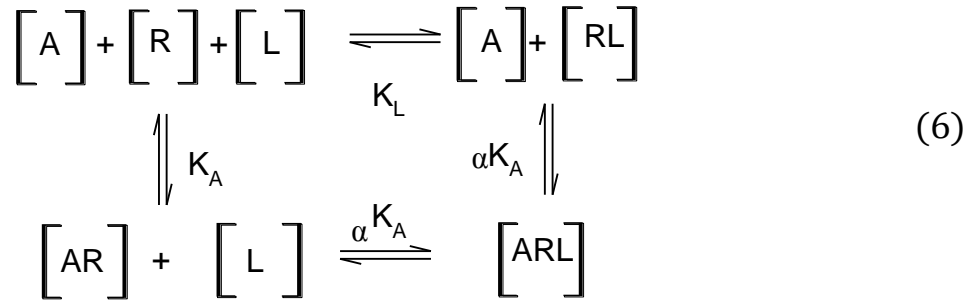
The half-life ( $t_{1/2}$ ) of dissociation is the time needed to reduce the total binding of the radioligand to half its initial value. This value can then be calculated from equation (5).

$$t_{1/2} = \frac{\ln 2}{k_{-1}} \quad (5)$$

$t_{1/2}$  : Half-life time of dissociation

### 2.4.2.2 Allosteric interaction

The dissociation rate constant  $k_{-1}$  of an orthosteric ligand can be influenced by an allosteric modulator in a concentration-dependent manner (Kostenis and Mohr, 1996). Allosteric and orthosteric ligands are able to bind simultaneously to the receptor whereby they reciprocally influence the binding of each other. The mutual influence between the two ligands is termed cooperativity ( $\alpha$ ). The simultaneous interaction of these two ligands with the receptor can be described by the allosteric ternary complex model (ATCM) (Ehlert, 1988).



$\alpha$  : Cooperativity factor

$K_A$  : Dissociation constant of the binding of the allosteric modulator and to the free receptor

$K_L$  : Dissociation constant of the orthosteric ligand and the free receptor

[A] : Concentration of the allosteric modulator

[AR] : Concentration of the allosteric ligand-receptor complex

[ARL] : Concentration of the ternary allosteric-orthosteric ligands-receptor complex

The allosteric modulator can enhance, decrease or leave unaffected the binding affinity of the orthosteric ligand. This can be termed positive, negative and neutral cooperativity, respectively. Values between 0 and 1 reflect positive cooperativity whilst negative cooperativity is shown by values greater than 1.  $\alpha = 1$  reflects neutral cooperativity. In order to describe the allosteric interaction with the ATCM, equation (7) (Ehlert, 1988) is used to obtain the parameters  $K_A$  and  $\alpha$ .

$$B_L([A]) = \frac{B_0 * ([L] + K_L)}{[L] + K_L * \left( \frac{K_A + [A]}{K_A + [A]/\alpha} \right)} \tag{7}$$

$B_L([A])$  : Specific binding of the orthoster L in the presence of an allosteric ligand concentration of [A] ( $B_L([A]) = [RL] + [ARL]$ )

$B_0$  : Specific binding of the orthosteric ligand in the absence of the allosteric ligand

The concentration of an allosteric ligand which causes half maximal retardation of orthosteric radioligand dissociation is called the  $EC_{0.5,diss}$ . Therefore, the  $EC_{0.5,diss}$  functions as a measure of allosteric ligand affinity for the occupied receptors. According to ATCM,  $EC_{0.5,diss} = \alpha K_A$  (Tränkle *et al.*, 1998). The half-life of radioligand dissociation in the presence of an allosteric ligand can be deduced from equation (8) developed by Lazareno and Birdsall in 1995.

$$t_{1/2 \text{ obs}} = t_{1/2 \text{ off}} \cdot \left(1 + \frac{[A]}{EC_{0.5 \text{ diss}}}\right) \quad (8)$$

$t_{1/2 \text{ obs}}$ :	Half-life of radioligand dissociation in presence of allosteric ligand
$t_{1/2 \text{ off}}$ :	Half-life of radioligand dissociation in absence of allosteric ligand
[A] :	Concentration of the allosteric modulator
$EC_{0.5, \text{diss}}$ :	Concentration of the allosteric modulator required to half-maximally retard radioligand dissociation

The incubation time of the allosteric ligand required for equilibrium binding was then estimated by calculating the  $5 \times t_{1/2}$  of the highest ligand concentration.

### 2.4.2.3 Experimental procedure

#### 2.4.2.3.1 Complete dissociation binding

Complete dissociation binding was carried out to determine the dissociation half-life of [<sup>3</sup>H]NMS at the M<sub>2</sub> wt and triple mutant receptors. The assays were performed in a 96 well plate using the pipetting scheme shown in **Table 2.1**. CHO cell membranes were incubated with the radioligand [<sup>3</sup>H]NMS for 30 min in a shaking water bath at 30°C. Experiments were carried out in HEPES buffer or NaKP<sub>i</sub> buffer. Excess atropine was added to determine the unspecific radioligand binding. After 30 min incubation, atropine was added at different time points over a course of 20 min to initiate radioligand dissociation. In the presence of an allosteric modulator, atropine was mixed with the allosteric modulator in a 1:1 ratio to probe the allosteric effects on complete [<sup>3</sup>H]NMS dissociation. 1 minute after the last atropine addition to stop dissociation, incubation was terminated by rapid filtration through glass fibre mats which had been immersed in polyethyleneimine (PEI) solution for 2-5 minutes to reduce unspecific radioligand adsorption. The filtration was performed using the TomTec filtration machine and the filter mats were then washed twice with ice-cold distilled water. The filters were then further dried for 2.5 min in a microwave and covered with melt-on scintillator sheets on a heating block. The filter mats were then transferred into a plastic sample bag and placed into a reading cassette. Finally, a solid scintillation counter was used to quantify the radioactivity on the filter mats.



#### 2.4.2.3.1 [<sup>3</sup>H]NMS dissociation binding (2-point kinetics)

In contrast to the complete dissociation, the method of two-point kinetic dissociation measures radioligand dissociation at only two time points in the presence of increasing concentrations of test compound. The cell membranes were incubated with the radioligand [<sup>3</sup>H]NMS in a falcon tube in a shaking water bath at 30°C for 40 and 45 min. 10 and 5 min of radioligand dissociation, respectively were allowed before the reaction was stopped by a rapid filtration as explained in chapter 2.2.1. The plates were prepared as shown in **Table 2.2**.

	<b>Total binding (μl)</b>	<b>Unspecific binding (μl)</b>	<b>Control (μl)</b>	<b>Allosteric competition (μl)</b>	<b>Final concentration/well</b>
<b>[<sup>3</sup>H]NMS</b>	50	50	50	50	2nM
<b>Ligand</b>	-	-	-	50	variable
<b>Atropine</b>	-	50	50	50	10μM
<b>Cells</b>	100	100	100	100	75 000 cells
<b>HBSS buffer</b>	350	300	300	250	20mM Hepes

**Table 2.1 Pipetting scheme of [<sup>3</sup>H]NMS dissociation binding in live cells.** [<sup>3</sup>H]NMS, atropine and cells were diluted in assay buffer (HBSS buffer + 20mM HEPES).

	<b>Total binding (μl)</b>	<b>Unspecific binding (μl)</b>	<b>Control (μl)</b>	<b>Allosteric competition (μl)</b>	<b>Final concentration/well</b>
<b>[<sup>3</sup>H]NMS</b>	50	50	50	50	2nM
<b>H<sub>2</sub>O</b>	100	50	50	-	-
<b>Ligand</b>	-	-	-	50	variable
<b>Atropine</b>	-	50	50	50	10μM
<b>Membranes</b>	100	100	100	100	15μg
<b>HEPES buffer or NaKPi buffer</b>	250	250	250	250	10mM Hepes 5mM

**Table 2. 2 Pipetting scheme of [<sup>3</sup>H]NMS dissociation binding in cell membranes.**

[<sup>3</sup>H]NMS and test ligands were diluted in distilled water. Membranes and atropine were diluted in assay buffer. variable = depends on the type of experiment (see results section, chapter 3).

### 2.4.3 Equilibrium binding assays

The equilibrium binding assay is used here to investigate the interaction of a test compound with the orthosteric binding site. This can be determined by investigating how a ligand is able to affect the binding of an orthosteric radioligand under equilibrium binding conditions. [<sup>3</sup>H]NMS and [<sup>3</sup>H]Iperoxo were used as radioactive probes in this work. The radioligand is applied at a constant concentration against increasing concentrations of the test compound. The radioligand total binding is determined in the absence of a test compound whilst the unspecific binding is determined in the presence of an excess non radiolabelled orthosteric ligand which saturates all specific binding sites. In this work, the inverse agonist atropine concentration was used to determine unspecific binding. Hence, the test compound can affect the binding of the radioligand either by directly competing with the radioligand for the orthosteric binding site or by binding to the allosteric site and influencing the binding affinity of the radioligand via receptor conformational changes (Birdsall and Lazareno, 2005). Dualsteric ligands are capable of simultaneously binding to both the orthosteric and the allosteric binding sites (Antony *et al.*, 2009).

#### 2.4.3.1 Homologous competition

In competition experiments the test compound acts as a competitive inhibitor of radioligand binding. A concentration-dependent increase of the test compound leads to the complete inhibition of radioligand binding at saturating concentrations. When both the test compound and the radioligand have identical structures this is termed homologous competition. It is assumed that the substitution of a hydrogen atom by tritium does not constitute a structural change. Therefore, the radioligand equilibrium dissociation constant  $K_D$  can be derived from equation (9).

$$K_D = IC_{50} - [L] \quad (9)$$

$K_D$  : Dissociation constant of the radioligand

$IC_{50}$  : Concentration of the inhibitor which reduces radioligand binding by 50%

[L] : Concentration of the radioligand

The total concentration of binding sites can be calculated from equation (10) by substituting  $K_D$  in the law of mass action with equation (9) (DeBlasi *et al.*, 1989).

$$B_{\max} = \frac{B * IC_{50}}{[L]} \quad (10)$$

$B_{\max}$  : Total concentration of binding sites

$B$  : Specific radioligand binding in absence of an inhibitor

#### 2.4.3.2 Heterologous competition

When the radioligand and the test compound are structurally different, the competitive interaction is termed heterologous competition. Here, the dissociation constant of the inhibitor is termed  $K_i$ .  $K_i$  as an independent measure can be calculated from equation (11) according to Cheng and Prusoff (1973).

$$K_i = \frac{IC_{50}}{1 + \frac{[L]}{K_D}} \quad (11)$$

$K_i$  : Dissociation constant of the inhibitor

$IC_{50}$  : Concentration of the inhibitor which reduces radioligand binding by 50 %

$[L]$  : Concentration of free radioligand

$K_D$  : Dissociation constant of the radioligand

Nonlinear regression analysis is used to plot the radioligand binding against the increasing concentrations of the competitor. The analysis is based on the four parameter logistic function (equation 12) which produces a sigmoidal curve (Barlow and Blake, 1989).  $IC_{50}$  reflects the inhibitor concentration which reduces the radioligand concentration by 50% and thereby depicts the affinity of the inhibitor for the receptor. The Hill slope ( $n_H$ ) reflects the steepness of the curve. When  $n_H = -1$  this assumes that ligands compete in a 1:1 ratio and that the receptor population is homogenous with similar affinities towards a particular ligand.

$$B_{\text{tot}}([X]) = \text{Bottom} + \frac{\text{Top}-\text{Bottom}}{1+(IC_{50}/[X])^{n_H}} \quad (12)$$

$B_{\text{tot}}([X])$  : Total binding of the radioligand in the presence of the inhibitor concentration  $[X]$

Bottom : Lower plateau of the curve

Top : Upper plateau of the curve

$IC_{50}$  : Inflection point of the curve (inhibitor concentration reducing ligand binding by 50%)

$[X]$  : Concentration of the inhibitor

$n_H$  : Hill coefficient, Hill slope (steepness of the curve)

### 2.4.3.3 [<sup>3</sup>H]NMS equilibrium binding with dualsteric ligands

As dualsteric ligands occupy the orthosteric and allosteric binding sites simultaneously, this introduced a fifth dimension in the allosteric ternary complex model to cater for dualsteric binding. [<sup>3</sup>H]NMS equilibrium binding data of dynamic ligands was analysed using the extended allosteric ternary complex model (equation 13) (May *et al.*, 2007) according to the model of dualsteric ligand binding to the orthosteric and allosteric site (Antony *et al.*, 2009; Bock *et al.*, 2014a). Equation 13 and 14 were used in the global analysis of two curves (allosteric fragment binding and dualsteric ligand binding).

$$Y = \frac{[L]*R_T}{[L] + K_L * \frac{\left(1 + [AB] * \left(\frac{K_A + K_B}{K_A * K_B}\right)\right)}{1 + \frac{\alpha' * [AB]}{K_B}}} \quad (13)$$

- Y : Specific binding of the radioligand L [<sup>3</sup>H]NMS]  
[L] : Concentration of the radioligand L  
R<sub>T</sub> : Total number of receptors  
K<sub>L</sub> : Equilibrium dissociation constant of the [<sup>3</sup>H]NMS-receptor complex (affinity of radioligand L)  
AB : Concentration of the dynamic ligand  
K<sub>A</sub> and K<sub>B</sub> : Equilibrium dissociation constants of the active and inactive dualsteric ligand-receptor complexes, respectively  
α' : Cooperativity between AB and L

The allosteric fragments equilibrium binding data was analysed according to the allosteric ternary complex model (Tränkle *et al.*, 2003; May *et al.*, 2007; Antony *et al.*, 2009; Bock *et al.*, 2014a) and attributed to the equation 14.

$$Y = B_0 \frac{(1 + K_L * [L]) (1 + \alpha' * (K_B * [B])^{1 + K_B * [B]})^n}{1 + K_B * [B]^n + K_L * [L] (1 + \alpha' * (K_B * [B])^n)} \quad (14)$$

- B<sub>0</sub> : Specific radioligand equilibrium binding in absence of allosteric fragment B  
K<sub>L</sub> : [<sup>3</sup>H]NMS equilibrium dissociation constant  
K<sub>B</sub> : Allosteric fragment equilibrium dissociation constant  
α' : Cooperativity between the allosteric ligand B and radioligand L  
[L] : Radioligand concentration  
n : Slope factor describing the steepness of the curve

The global fit analysis of a set of four curves (dualsteric ligand binding, allosteric moiety binding, dualsteric ligand functional and acetylcholine functional data) was performed using equations 13, 14 and 15. The concentration effect curves (CECs) of the dualsteric ligand together with the reference agonist acetylcholine were fitted with equation 15.

$$E = \frac{E_{\max}}{1 + \frac{([AB] + \frac{K_A * K_B}{K_A + K_B})^{n_{op}}}{[AB]^{n_{op}} * \tau_{dyn}^{n_{op}}}} \quad (15)$$

$E_{\max}$  : Maximum response of the system induced by saturating concentrations of agonist ACh

[AB] : Concentration of dynamic ligand

$\tau_{dyn}$  : Dynamic transduction coefficient of ligand

$K_A$  and  $K_B$  : Affinity of the dualsteric ligand in the active and inactive pose, respectively

$n_{op}$  : Transducer slope

Fractional occupancy data was calculated from the  $K_A$ ,  $K_B$  and  $R_T$  values obtained from either the global analysis of two CECs. Computation was based on the following equations:

Total binding: 
$$Y_{tot} = \frac{[AB] * R_T}{[AB] + K_{obs}} \text{ with } K_{obs} = \frac{K_A * K_B}{K_A + K_B} \quad (16)$$

Fractional occupancy of the active pose: 
$$Y_{RAB} = \frac{f_{RAB} * [AB] * R_T}{[AB] + K_{obs}} \text{ with } f_{RAB} = \frac{K_B}{K_A + K_B} \quad (17)$$

Fractional occupancy of the inactive pose: 
$$Y_{ABR} = \frac{f_{ABR} * [AB] * R_T}{[AB] + K_{obs}} \text{ with } f_{ABR} = \frac{K_A}{K_A + K_B} \quad (18)$$

$R_T$ : Total number of receptors

[AB]: Concentration of the dualsteric ligand

$K_{obs}$ : Observed equilibrium dissociation constant of the dualsteric ligand

$K_A$  and  $K_B$ : Equilibrium dissociation constants of the dualsteric ligand for the active and inactive pose, respectively

$f_{RAB}$  and  $f_{ABR}$ : Maximal fractional occupancies at receptor saturation of the active and inactive pose, respectively

The ratio of the active and inactive receptor populations ( $R_{pose}$ ), was calculated according to equation (19). (Bock *et al.*, 2014a,b; Chen *et al.*, 2015).

$$R_{pose} = -\log\left(\frac{K_A}{K_B}\right) = -\log\left(\frac{K_{active}}{K_{inactive}}\right) \quad (19)$$

#### 2.4.3.4 Experimental procedure

Equilibrium binding assays were performed with both CHO live and membranes of  $M_2$  wt, triple mutant and non-transfected cells. [ $^3H$ ]NMS and [ $^3H$ ]Iperoxo were used as radioligands in this work. For experiments with live cells, the cells were collected from culture dishes as mentioned in chapter 2.1, resuspended in the assay buffer (HBSS+20mM HEPES) and counted using the Neubauer counting chamber. The experiment was performed in triplicates on a 96-well plate as shown in **Table 2.3**. [ $^3H$ ]NMS (0.1 nM and 0.2 nM) concentrations were used for the homologous and heterologous competition, respectively. An excess of atropine (10 $\mu$ M) was used to measure non-specific binding. The plate was incubated for 2 hours to achieve equilibrium in a shaking water bath at 28 $^{\circ}$ C. The reaction was terminated and radioactivity determined as shown in chapter 2.2.1.

In membranes, the experimental setting was as shown in **Table 2.4**. HEPES buffer and the low ionic strength NaKP<sub>i</sub> buffer were used as assay buffers. There was an addition of GDP (100  $\mu$ M) in order to obtain monophasic curves by uncoupling the G-proteins from the receptor. [ $^3H$ ]Iperoxo (1 nM) was used at a higher concentration in the  $M_2$  triple mutant membranes as the agonist lost binding affinity at the mutant receptor. [ $^3H$ ]NMS concentrations were similar to those applied in live cells for both homologous and heterologous equilibrium binding. In contrast to live cells, incubation was conducted at 30 $^{\circ}$ C. The incubation time ranged from 2-18 hours depending with the test compound's equilibration time.

	<b>Total binding (μl)</b>	<b>Unspecific binding (μl)</b>	<b>Competition (μl)</b>	<b>Final concentration /well</b>
<b>[<sup>3</sup>H]NMS</b>	50	50	50	variable
<b>Ligand</b>	-	-	50	variable
<b>Atropine</b>	-	50	-	10μM
<b>Cells</b>	100	100	100	75 000 cells
<b>HBSS buffer</b>	350	300	300	20mM Hepes

**Table 2. 3 Pipetting scheme of equilibrium binding in live cells.** [<sup>3</sup>H]NMS 0.1 nM and 0.2nM concentration were used for homologous and heterologous binding, respectively. Ligand concentrations were applied as shown in results section, chapter 3.

	<b>Total binding (μl)</b>	<b>Unspecific binding (μl)</b>	<b>Competition (μl)</b>	<b>Final concentration/well</b>
<b>Ligand</b>	-	-	50	variable
<b>Atropine</b>	-	50	-	10μM
<b>H<sub>2</sub>O</b>	50	-	-	-
<b>GDP</b>	50	50	50	100μM
<b>Membranes</b>	100	100	100	variable
<b>HEPES buffer or NaKPi buffer</b>	250	250	250	10mM HEPES 5mM
<b>[<sup>3</sup>H]NMS or [<sup>3</sup>H]Iperoxo</b>	50	50	50	variable

**Table 2.4 Pipetting scheme of radioligand equilibrium binding in cell membranes.** Membranes and GDP were diluted in incubation buffer. [<sup>3</sup>H]NMS, [<sup>3</sup>H]Iperoxo and test ligands were diluted in distilled water. variable = depends on the type of experiment, ([<sup>3</sup>H]NMS = 0.1 nM and 0.2 nM for the homologous and heterologous competition, respectively. [<sup>3</sup>H]Iperoxo = 1 nM).

## 2.5 Functional assays

### 2.5.1 [<sup>35</sup>S]GTPγS binding assay

The [<sup>35</sup>S]GTPγS binding assay is a functional assay which measures the direct consequence of receptor activation. The [<sup>35</sup>S]GTPγS binding assay enables for the determination of proximal signaling in membrane preparations (Akam *et al.*, 2001). When an agonist binds to the receptor it induces a change in receptor confirmation causing the receptor to interact with the heterotrimeric G-protein. A G-protein consist of a βγ and a GDP-bound α subunit. An active receptor hence, acts as a guanine nucleotide exchange factor whereby it induces the exchange of GDP for GTP at the Gα subunit. The βγ then dissociates from the Gα-GTP subunit and both subunits can go on to independently activate downstream signalling pathways. The Gα subunit is inactivated by its intrinsic GTPase activity which hydrolyses GTP to GDP. The Gα-GDP subunit reassociates with and thereby inactivates the βγ subunit (Wess, 1997).

In the [<sup>35</sup>S]GTPγS assay, a radioactively labelled guanosine triphosphate with a sulphur atom (<sup>35</sup>S) substituting an oxygen atom in the terminal phosphate group, is added to the reaction mixture. This radioactive probe is a non-hydrolysable analogue of GTP but still able to interact with the Gα subunit. As the relative expression level of G<sub>i/o</sub> proteins is substantially higher than of the other G proteins in the M<sub>2</sub> muscarinic receptors, this assay therefore primarily measures G<sub>i/o</sub> signalling (Milligan, 2003). Hence, upon receptor activation [<sup>35</sup>S]GTPγS accumulates in the membranes and this is measured as a direct consequence of receptor activation. GDP can be added to the reaction in order to inhibit [<sup>35</sup>S]GTPγS binding to inactive G-proteins which have a higher affinity for GDP. The accumulation of the [<sup>35</sup>S]GTPγS as a response of increasing test compound concentration was analysed by the four parameter logistic function (equation 12) to yield the EC<sub>50</sub> and E<sub>max</sub>. EC<sub>50</sub> is the concentration of the test ligand causing half maximal activation whilst E<sub>max</sub> reflects the maximal receptor activation.



### 2.5.1.1 Operational model of agonism

The operational model of agonism (Black and Leff, 1983) was used in this work to determine the signalling efficacy of compounds that is how efficient an agonist binding is transduced into a response. Black and Leff combined two parameters  $K_E$  and  $R_T$  into a ratio to produce the parameter tau ( $\tau$ ) termed the ‘transducer constant’.

$$\tau = \frac{[R_T]}{K_E} \quad (20)$$

$K_E$  : Agonist-receptor complex [AR] concentrations that produces half maximal tissue response

$[R_T]$  : Total receptor density of tissue

Therefore, the mean values of function can be fitted into an operational model (equation 21) which also takes into account the transducer slope.

$$E = \frac{Effect_{max} * \tau^n * [A]^n}{(K_A + [A])^n + \tau^n * [A]^n} \quad (21)$$

E : Response

Effect<sub>max</sub> : Maximal response of the system

[A] : Concentration of the agonist

n : Transducer slope (unequal to the Hill slope  $n_H$ )

$\tau$  : Operational efficacy of the agonist

$K_A$  : Operational agonist equilibration constant

Hence, the operational efficacy ( $\tau$ ) and the operational agonist equilibrium constant  $K_A$  can be derived from the operational model (equation 21).

### 2.5.1.2 Experimental procedure

Test compounds were pipetted into a 96-well microtiter plate as shown in table 2.5. Cell membranes and the radioligand were then added to initiate the reaction. Plates were incubated for 1 hour at 30°C in a shaking water bath. Unspecific binding was determined in the presence of atropine (10  $\mu$ M) and total binding in the presence of distilled water instead of test compound. For agonists-induced activation in the presence of an allosteric compound or an inverse agonist, distilled water was replaced by either of the two in the pipetting scheme. The

glass fibre filter mats were immersed in distilled water for 3 minutes and filtration was conducted as previously described in chapter 2.2.1.

	<b>Agonist-induced binding (µl)</b>	<b>Basal binding (µl)</b>	<b>Final concentration/well</b>
<b>Distilled water</b>	50	100	-
<b>Agonist</b>	50	-	variable
<b>GDP</b>	50	50	10µM
<b>Membrane suspension</b>	100	100	40µg
<b>HEPES buffer</b>	200	200	10 mM Hepes
<b>[<sup>35</sup>S]GTPγS in Incubation buffer</b>	50	50	0.07nM

**Table 2.5 Pipetting scheme of [<sup>35</sup>S]GTPγS binding assay.** [<sup>35</sup>S]GTPγS, GDP and membrane suspension were diluted in HEPES buffer. Agonist concentrations were diluted in distilled water. Total volume/ well = 500 µl. variable = see ligand concentrations in results section, chapter 3.

### 2.5.2 cAMP assay

The cAMP assay is a functional assay which measures the amount of cyclic adenosine monophosphate (cAMP) accumulation or decrease in the cytosol upon receptor activation. This assay can be used to measure the activation of both the G<sub>i/o</sub> and G<sub>s</sub> proteins. M<sub>2</sub> receptors exhibit promiscuous signalling properties whereby they can couple to both G<sub>i/o</sub> and G<sub>s</sub> proteins (Kenakin, 2014). In this work, PTX a G<sub>i/o</sub>-protein inhibitor was applied to inhibit G<sub>i/o</sub> signalling leading to the accumulation of cAMP as a measure of G<sub>s</sub> activation. The cAMP assay was conducted using the HTRF<sup>®</sup> technology. The assay works by a mechanism whereby the endogenous cAMP and d2-labelled cAMP competes for binding to the cryptate-labelled monoclonal anti-cAMP. When d2 and cryptate are close together a FRET signal is generated, which can be detected and measured as a measure of cAMP concentration in the cytosol. When G<sub>s</sub> is activated, more endogenous cAMP is produced to compete with the d2-

labelled cAMP. This results in the decrease in the FRET signal as the cryptate-d2 interactions diminish.

#### 2.5.2.1 Experimental procedure

CHO M<sub>2</sub> wt and triple mutant cells were seeded onto 10 cm culture dishes so as to be nearly confluent the following day. PTX (100ng/ml) was applied to the cells for 16-18hrs before the experiment. On the day of experiment, the test compound dilution series were prepared in the IBMX (1mM) assay buffer. IBMX is a phosphodiesterase inhibitor which prevents the degradation of the endogenous cAMP in the cytosol (Ferrari-Dileo *et al.*, 1992). Cells were then collected by washing with 5ml PBS, trypsinisation by 1.5 ml trypsin-EDTA and addition of 3.5ml nutrient media to stop trypsinisation. Cell suspension was centrifuged (rotor JS 4.3; 900 rpm; 4 min; 4°C) and the pellet resuspended in HBSS+20mM HEPES buffer. Cells were counted using the Neubauer counting chamber to obtain (50 000 cells/well) for the total amount of wells needed. The cell suspension was centrifuged as mentioned above and the pellet resuspended in the IBMX (1mM) assay buffer to obtain a 50 000 cells/5µl. 5µl cell suspension was seeded into each well on a 384 microtiter plate and incubated for 30min at 37°C, 5% CO<sub>2</sub>. 5µl assay buffer was added to the wells of the negative control and basal signal whilst 5µl of test compound was added to respective wells. The plate was incubated again for 30 min at 37 °C, 5% CO<sub>2</sub>. 5µl conjugate and lysis buffer (C+L buffer) was added to the negative control whilst d2-cAMP was added to the rest of the wells. 5µl anti-cAMP cryptate was then added to all wells. The plate was incubated in the dark at room temperature for at least 2 hours before measuring with the Mithras LB 940 multimode microplate reader.

#### 2.5.3 Dynamic mass redistribution assay (DMR)

When a receptor becomes activated it stimulates downstream receptor signalling which in turn can be measured as cellular response. This response can comprise events such as cytoskeletal rearrangement, protein trafficking and receptor internalisation (Kholodenko 2006; Schröder *et al.*, 2010). The global localisation of biomolecules can be detected and measured as dynamic mass redistribution (DMR) using the EPIC<sup>®</sup> corning system. DMR can be observed by passing polarised broadband light through the bottom sensing volume of the cell grown on a 384 well microtiter plate (Fang and Ferrie, 2007; Lee *et al.*, 2008). A resonant waveguide grating (RWG) biosensor is embedded in the bottom part of the microtiter plate. The RWG

forms an optical system by interacting with cell layer on its surface, which propagates and reflects specific wavelength resonance to the system. This generates an evanescent wave which enters the bottom part of the cell up to a depth of 150nm, also known as the sensing volume of the biosensor (Scott and Peters, 2010). The outgoing resonant wavelength is then recorded and normalized to zero. This resonant wavelength depends on optical density of the cell layer. Hence, when a ligand is added to the cells it results in a change in optical density and a shift in outgoing resonant wavelength relative to the baseline read out. If a ligand increases the optical density in the sensing volume, this result in an increased outgoing wavelength measured as a positive  $\Delta\text{pm}$ . A decrease in optical density results in negative  $\Delta\text{pm}$  (**Figure 2.1**) (Schröder *et al.*, 2010 and 2011).

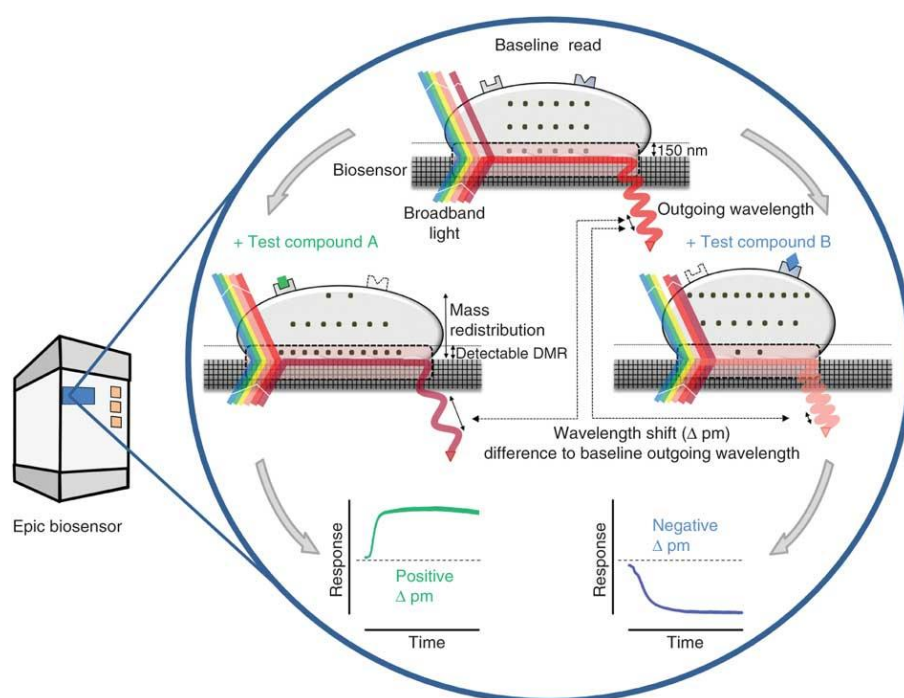


**Figure 2.1 Schematic diagram showing DMR detection using the Epic biosensor.** (Schröder *et al.*, 2011).

### 2.5.3.1 Experimental procedure

CHO M<sub>2</sub> wt, triple mutant and non-transfected CHO cells were seeded into a 384-well microtiter EPIC<sup>®</sup> plate. Cells were collected as explained in chapter 2.1 and seeded at a density of 12 500 cells per well in 40  $\mu\text{l}$  of nutrient medium. The plate was incubated at 37°C, 5% CO<sub>2</sub> for at least 4 hrs for cells to settle before toxins were added. In this work the G<sub>i/o</sub>-protein inhibitor, PTX (100ng/ml) was added per well to monitor G<sub>s</sub> signalling. Cells were

incubated in conditions mentioned above for 18-21 hrs until a confluent single cell monolayer was achieved. The medium was aspirated and cells were washed twice with 50 µl assay buffer (HBSS+20mM HEPES) per well. Cells were covered with 30 µl assay buffer per well and atropine was applied to wells designated for monitoring muscarinic signalling. The plate was then incubated for 1 hour in the EPIC<sup>®</sup> machine at 28°C for the cells to adjust to new temperature conditions. The live changes in cellular DMR were then measured for at least 2 hours.

## 2.6 Statistics

### 2.6.1 Mean value

Multiple data were averaged using the arithmetic mean  $\bar{x}$ . The mean is calculated by dividing the sum of all values by the number (n) of individual values obtained.

$$\bar{x} = \frac{1}{n} \sum_{i=1}^n x_i \quad (22)$$

$\bar{x}$  : Arithmetic mean  
n : Number of individual values  
 $x_i$  : Individual values

### 2.6.2 Standard deviation and standard error of the mean (SEM)

Standard deviation calculates the scatter which represents how much the values differ from each other.

$$s = \sqrt{\frac{1}{n-1} \sum_{i=1}^n (x_i - \bar{x})^2} \quad (23)$$

s : Standard deviation

On the other hand the standard error of the mean (SEM) calculates the true mean value of the population by taking into account both the population size and the standard deviation.

$$SEM = \frac{s}{\sqrt{n}} \quad (24)$$

SEM : Standard error of the mean

s : Standard deviation

SEM was used in this work as by definition the SEM is always smaller than standard deviation. Therefore, with larger population size, the mean obtained is more precise and likely to be closer to the true population mean compared to smaller samples.

### 2.6.3 One-way ANOVA

One-way analysis of variance (ANOVA) is used to compare the means of three or more groups assuming that the populations are Gaussian. According to an F-test, a small p-value ( $p < 0.05$ ) indicates at least two significantly different population means. If the P value is large ( $p > 0.05$ ) reflects that there is insufficient evidence that the population means differ. The test was performed using GraphPad Prism®.

$$MS_{\text{between}} = \frac{SS_{\text{between}}}{df_{\text{between}}} \quad (25)$$

$$MS_{\text{within}} = \frac{SS_{\text{within}}}{df_{\text{within}}} \quad (26)$$

$$F = \frac{MS_{\text{between}}}{MS_{\text{within}}} \quad (27)$$

$SS_{\text{between}}$  : Sum of squares between the groups

$SS_{\text{within}}$  : Sum of squares within one group

$MS_{\text{between}}$  : Mean sum of squares between the groups

$MS_{\text{within}}$  : Mean sum of squares within one group

#### 2.6.3.1 One-way ANOVA with Turkey's Multiple Comparison Test

ANOVA calculations only show that there is a significant difference somewhere among the sample population. The Tukey's Multiple comparison post-hoc test was therefore used to compare all population means against each other and determine the groups which have

significant differences among the sample. This post-hoc test also allows comparison of unequal sample sizes.

$$\text{HSD} = \frac{x_1 - x_2}{\sqrt{\frac{\text{MS}_{\text{within}}}{N}}} \quad (28)$$

HSD : Honestly significant difference

$x_1, x_2$  : Mean values

N : Number of groups

The HSD value indicates the distance between the means and it uses the Studentised Range Statistic which states that as the number of the compared means increases, the difference between the smallest and largest means appears to increase.

#### 2.6.3.2 One-way ANOVA with Dunnett's test

The Dunnett's post-hoc test was also used in this work to compare every to a control mean.

$$t_d = \frac{M_i - M_c}{\sqrt{\frac{2\text{MSE}}{n_h}}} \quad (29)$$

$M_i$  : Mean of the  $i$ th experimental group

$M_c$  : Mean of the control group

MSE: Mean square error as computed from analysis of variance

$n_h$  : Harmonic mean of the sample sizes of experimental group and the control group

#### 2.6.4 F-test

The F-test takes into account the ratio of variances (squares of the standard deviation) (equation 30) of two data sets whereby the null hypothesis states that there is no difference between the variances of the two data sets.

$$F = \frac{S_1^2}{S_2^2} \quad (30)$$

The F-test is used to compare two equations and decide the equation more suitable to fit a given data set in a regression analysis. In order to decide which of the two given equations is more suitable to be used in a regression analysis, equation 31 is used to derive the test statistic

F. Here, the F value can be derived from the sum of squares of the distances and the degrees of freedom of the two hypotheses. The null hypothesis can be rejected if the p-value is less than 0.05 ( $p < 0.05$ ), indicating that the data are better described by the alternative complex hypothesis.

$$F = \frac{(ss_{null} - ss_{alt}) / (df_{null} - df_{alt})}{ss_{alt} / df_{alt}} \quad (31)$$

$ss_{null}$  : Sum of the square of the distances for the simpler equation (null hypothesis)

$ss_{alt}$  : Sum of the square of the distances from the more complex equation (alternative hypothesis)

$df_{null}$  : Number of degrees of freedom of the simpler equation

$df_{alt}$  : Number of degrees of freedom of the more complex equation

### 2.6.5 T-test

The unpaired, two-tailed t-test is conducted to determine if the means of two normally distributed data sets are equal. The t value (equation 32) on its own does not give any conclusions and a p-value which indicates the level of significance has to be determined. When  $p < 0.05$  this indicates a significant difference between the two mean values, whilst  $p > 0.05$  shows an insignificant difference between the means.

$$t = \frac{x_1 - x_2}{\sqrt{\left(\frac{1}{n_1} + \frac{1}{n_2}\right) * \frac{((n_1) - 1) * s_1^2 + ((n_2) - 1) * s_2^2}{n_1 + n_2 - 2}}} \quad (32)$$

$n_1$  : Number of individual values of data set 1

$n_2$  : Number of individual values of data set 1

$x_1$  : Mean of data set 1

$x_2$  : Mean of data set 2

$s_1^2$  : Standard deviation of data set 1

$s_2^2$  : Standard deviation of data set 1



## 3. RESULTS

### 3.1 Characterisation of allosteric binding at the M<sub>2</sub> triple mutant

#### 3.1.1 W84 loses allosteric potency and efficacy to retard [<sup>3</sup>H]NMS at the M<sub>2</sub> triple mutant

Experiments were carried out to investigate the effects of mutating the three critical M<sub>2</sub> allosteric epitopes Y177<sup>ECL2</sup>, W422<sup>7.35</sup> and T423<sup>7.36</sup> to alanine (Ala), on the allosteric properties of the receptor. The aim here was to investigate if the allosteric binding site was still functional or now unable to interact with allosteric ligands. If the allosteric site was still functional, the next step was to determine how severely compromised it was by the triple mutation.

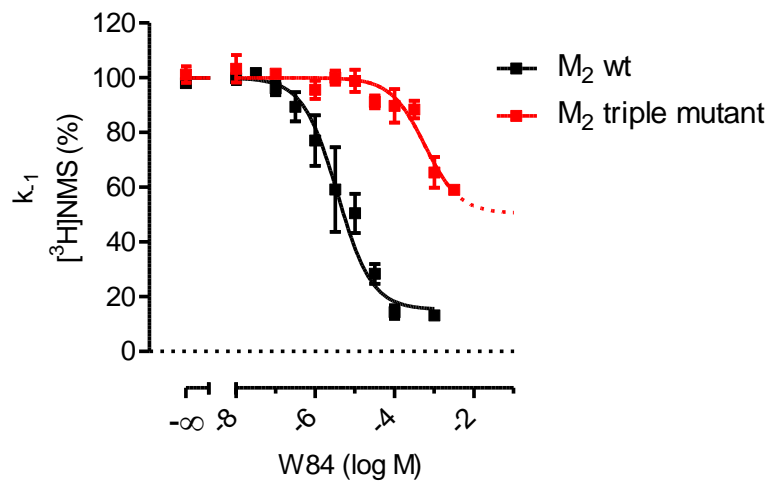


**Figure 3.1 Allosteric potency and efficacy decreases at the M<sub>2</sub> triple mutant in living CHO cells.** Concentration-effect curves for the allosteric delay of the orthosteric radioligand [<sup>3</sup>H]NMS dissociation. CHO-hM<sub>2</sub> cells were pre-labeled with 2nM [<sup>3</sup>H]NMS and the dissociation rate of the labeled ligand was determined in the presence of increasing concentrations of the allosteric modulator W84. Atropine (10μM) was applied to prevent radioligand re-association and, thus, disclose the time-course of [<sup>3</sup>H]NMS dissociation. The dissociation rate constant (k<sub>-1</sub>) was derived from one phase exponential decay analysis of single experiments. The curve fitting is dashed beyond the highest concentration applied at the M<sub>2</sub> triple mutant. Indicated are mean values ± S.E.M of 4 experiments performed in triplicates.

Radioligand dissociation experiments were carried out whereby the receptor orthosteric site was pre-occupied by [<sup>3</sup>H]NMS. A delay in the rate of [<sup>3</sup>H]NMS dissociation from the orthosteric binding site in the presence of a modulator, reveals the allosteric capabilities of that modulator. W84, which is a typical allosteric modulator at the M<sub>2</sub> receptor, was used to characterise the effects of the M<sub>2</sub> triple mutation on the formation of ternary complexes,

which is the main hallmark of allosteric interactions (Prilla *et al.*, 2006). W84 was able to cause a delay of [<sup>3</sup>H]NMS dissociation at both the M<sub>2</sub> wild type (wt) and triple mutant receptor in CHO-M<sub>2</sub> live cells (**Figure 3.1 and Table 3.1**). This shows that the allosteric binding site was still functional, at least for W84 in this case. However, W84 lost a substantial amount of allosteric potency of about 2.61 log units at the M<sub>2</sub> triple mutant compared to the M<sub>2</sub> wt.

The dissociation experiments with CHO-M<sub>2</sub> membranes in the HEPES buffer produced similar pEC<sub>0.5,diss</sub> values as those obtained in the CHO-M<sub>2</sub> live cells at both the M<sub>2</sub> wt and triple mutant receptors (**Figure 3.2 and Table 3.1**). It has been shown from previous studies that the modes of allosteric interactions in [<sup>3</sup>H]NMS occupied M<sub>2</sub> receptors can be influenced by changes in experimental buffer conditions. Also, allosteric modulators were found to be more potent in low ionic strength buffers (Tränkle *et al.*, 1996; Shröter *et al.*, 2000). Therefore, a low ionic strength NaKPi buffer was employed here to investigate whether the M<sub>2</sub> triple mutant would behave differently compared to the high ionic strength HEPES buffer conditions regarding ligand-allosteric interactions.

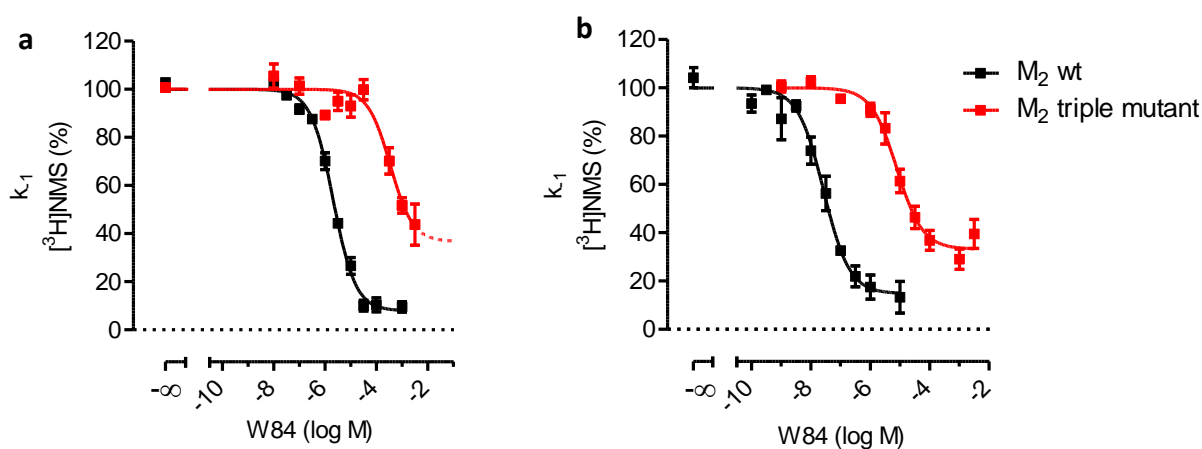


**Figure 3.2 The overall W84 allosteric binding potency to retard [<sup>3</sup>H]NMS dissociation is buffer dependent.** Concentration-effect curves for the allosteric delay of [<sup>3</sup>H]NMS dissociation. Membranes of CHO-hM<sub>2</sub> cells were pre-labeled with 2nM [<sup>3</sup>H]NMS and the dissociation rate of the labeled ligand was determined in the presence of increasing concentrations of the allosteric modulator W84. Experiments were conducted in (a) HEPES buffer and (b) NaKPi buffer, respectively. Atropine (10μM) was applied to prevent radioligand re-association and, thus, disclose [<sup>3</sup>H]NMS dissociation. The dissociation rate constant ( $k_{-1}$ ) was derived from one phase exponential decay analysis of single experiments. (a) The curve fitting is dashed beyond the highest concentration applied at the at the M<sub>2</sub> triple mutant. Indicated are mean values  $\pm$  S.E.M of 4 experiments.

W84 - [ <sup>3</sup> H]NMS dissociation binding			
	M <sub>2</sub> wt	M <sub>2</sub> triple mutant	
		pEC <sub>0.5,diss</sub> (Bottom k <sub>-1</sub> %)	ΔpEC <sub>0.5,diss</sub> (wildtype-mutant)
<b>HBSS+20 mM HEPES buffer</b> (cells)	5.76 ± 0.13 (15 ± 4)	3.15 ± 0.29 (50 ± 6.3)	2.61 ± 0.32
<b>HEPES buffer</b> (membranes)	5.66 ± 0.03 (8 ± 1.5)	3.13 ± 0.16 (37 ± 6.4)	2.53 ± 0.11
<b>NaKPi buffer</b> (membranes)	7.55 ± 0.08 <sup>***</sup> (15 ± 2.8)	5.05 ± 0.12 <sup>***</sup> (34 ± 3.0)	2.50 ± 0.17

**Table 3.1 Dissociation binding of [<sup>3</sup>H]NMS (2nM) in the presence of the allosteric modulator W84.** pEC<sub>0.5,diss</sub> indicates the negative logarithm of the concentration which causes half maximal delay of [<sup>3</sup>H]NMS dissociation. ΔpEC<sub>0.5,diss</sub> is the difference between the pEC<sub>0.5,diss</sub> values of the M<sub>2</sub> wt and triple mutant. Bottom k<sub>-1</sub> (%) reflects the lower plateau of the k<sub>-1</sub> curves. The slope factor (n<sub>H</sub>) for all individual curves was -1. Data shown are means ± S.E.M of 4 experiments.

<sup>\*\*\*</sup>Significantly different from the pEC<sub>0.5,diss</sub> obtained in the HEPES buffer ( <sup>\*\*\*</sup>p < 0.0001 One-way Anova, Tukey's Multiple Comparison Test).

An increase in the allosteric binding affinities of 1.89 and 1.92 log units for W84 at the M<sub>2</sub> wild type and triple mutant, respectively, was observed in the NaKPi buffer compared to the HEPES buffer (**Figure 3.2 and Table 3.1**). There was also a significant difference in allosteric binding affinities between the NaKPi buffer and the HBSS+20mM HEPES buffer at the M<sub>2</sub> wt and the triple mutant, respectively. Hence, decreasing the ionic strength in the phosphate buffer led to increased allosteric binding affinity of W84. Nevertheless, the loss in allosteric binding affinity between the M<sub>2</sub> wt and triple mutant was similar irrespective of the buffer conditions. Also, the decrease in allosteric binding affinity observed at the M<sub>2</sub> triple mutant receptor of about 2.5 log units was not significantly different in both the live cells and cell membranes (**Table 3.1**).

W84 also lost its efficacy to retard [<sup>3</sup>H]NMS dissociation at the M<sub>2</sub> triple mutant receptor. In live cells the minimum rate of [<sup>3</sup>H]NMS dissociation (k<sub>-1</sub>) observed was 50 ± 6.3% at the M<sub>2</sub> triple mutant compared to 15 ± 4% at the M<sub>2</sub> wt, at the maximal concentration of W84 studied. In membranes the minimum [<sup>3</sup>H]NMS off-rate at the triple mutant was significantly

lower compared to that observed in the live cells. The minimum [<sup>3</sup>H]NMS off-rates of  $37 \pm 6.4\%$  and  $34 \pm 3\%$  for the HEPES buffer and NaKPi buffer, respectively were observed at the M<sub>2</sub> triple mutant. These data show that although W84 could still form allosteric ternary complexes with the receptor and radioligand [<sup>3</sup>H]NMS, its ability to retard [<sup>3</sup>H]NMS dissociation was severely compromised (**Figure 3.1, 3.2 and Table 3.1**).

### 3.1.2 W84 loses equilibrium binding affinity at the M<sub>2</sub> triple mutant

To gain insight into the effects of the triple mutation on the binding of an allosteric modulator at an NMS-free receptor, equilibrium binding experiments with [<sup>3</sup>H]NMS were carried out. Experiments were carried out in both the HEPES buffer and the low ionic strength NaKPi buffer. Equilibrium binding experiments also reveal the nature of cooperativity between the allosteric modulator and the orthosteric ligand (Lazareno and Birdsall, 1995).

The affinity values ( $pK_A$ ) of the allosteric modulator W84 and the cooperativity values with [<sup>3</sup>H]NMS ( $\alpha$ ) were obtained from the curve fitting based on the ternary complex model of allosteric interactions (Ehlert, 1988). There was a pronounced decrease in affinity for W84 of 2.47 and 2.24 log units in the HEPES and NaKPi buffers, respectively, at the M<sub>2</sub> triple mutant compared to the M<sub>2</sub> wt. This data show that the loss in the allosteric affinity ( $\Delta pK_A$ ) at the M<sub>2</sub> triple mutant for the unoccupied receptor is independent of the buffer conditions. However, the overall affinity of W84 was increased by about 2.22 (M<sub>2</sub> wt) and 2.45 (M<sub>2</sub> triple mutant) log units in the low ionic strength NaKPi buffer compared to HEPES buffer, respectively (**Figure 3.3a,b and Table 3.2**). The overall increase in W84 binding affinity can also be visually observed by the leftward curve shift of the M<sub>2</sub> wt and triple mutant in the NaKPi (**Figure 3.3b**) buffer relative to the HEPES buffer (**Figure 3.3a**).

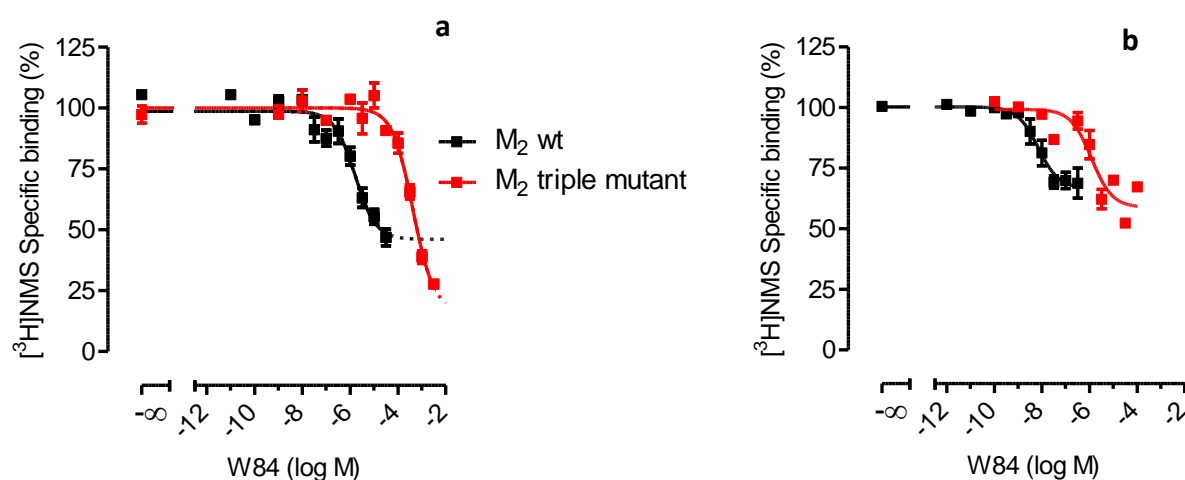


**Figure 3.3 W84 effects on the equilibrium binding of  $[^3\text{H}]\text{NMS}$ .** Equilibrium binding of  $[^3\text{H}]\text{NMS}$  (0.2nM) against the allosteric modulator W84 in the  $\text{M}_2$  wt (black) and triple mutant CHO cell membranes. Non-specific binding was determined by atropine (10 $\mu\text{M}$ ). Experiments were conducted in (a) HEPES buffer and (b) NaKPi buffer. Shown are the mean values  $\pm$  S.E.M 4 experiments performed in triplicates and analysed by the four parameter logistic function with a slope factor of -1.

$[^3\text{H}]\text{NMS}$ equilibrium binding			
	$\text{M}_2$ wt	$\text{M}_2$ triple mutant	$\Delta\text{pK}_A$ (wildtype-mutant)
		$\text{pK}_A$ ( $\alpha$ )	
HEPES buffer	$5.97 \pm 0.11$ ( $2.6 \pm 0.31$ )	$3.50 \pm 0.06$ ( $7.3 \pm 1.27$ ) <sup>**</sup>	2.47
NaKPi buffer	$8.19 \pm 0.12$ <sup>###</sup> ( $1.72 \pm 0.09$ )	$5.95 \pm 0.15$ <sup>ooo</sup> ( $1.96 \pm 0.03$ ) <sup>ns</sup>	2.24

**Table 3.2 Binding parameters for the binding of W84 to unoccupied receptors.**  $\text{pK}_A$  represents the negative logarithm of affinity values for the allosteric compound W84 at the unoccupied  $\text{M}_2$  wt and  $\text{M}_2$  triple mutant receptors.  $\Delta\text{pK}_A$  is the difference between the  $\text{pK}_A$  values of the  $\text{M}_2$  wt and  $\text{M}_2$  triple mutant.  $\alpha$  is a measure of binding cooperativity between the allosteric compound W84 and the radioligand  $[^3\text{H}]\text{NMS}$ . When  $\alpha > 1$ , this shows negative cooperativity between W84 and  $[^3\text{H}]\text{NMS}$ .

<sup>\*\*</sup>Significantly different from the  $\alpha$  value at the  $\text{M}_2$  wt (<sup>\*\*</sup>  $p < 0.05$ )

<sup>ns</sup> Not significantly different from  $\alpha$  value at the  $\text{M}_2$  wt

<sup>###</sup>Significantly different from the  $\text{pK}_A$  at the  $\text{M}_2$  wt in HEPES buffer (<sup>###</sup>  $p < 0.05$ )

<sup>ooo</sup>Significantly different from the  $\text{pK}_A$  at the  $\text{M}_2$  triple mutant in HEPES buffer (<sup>ooo</sup>  $p < 0.05$ )

Statistics performed by the Student's t-test

W84 displayed negative cooperativity ( $\alpha > 1$ ) with [ $^3\text{H}$ ]NMS at both the  $M_2$  wt and triple mutant receptors. This means that W84 could still promote the displacement of the radioligand [ $^3\text{H}$ ]NMS from the orthosteric binding site of the  $M_2$  triple mutant. The negative cooperativity was observed in both the low and high ionic strength buffers. However, there was higher negative cooperativity in experiments conducted in the high ionic strength HEPES buffer of ( $\alpha = 2.6 \pm 0.31$  and  $7.3 \pm 1.27$ ) in comparison to the low ionic strength NaKPi buffer ( $\alpha = 1.72 \pm 0.09$  and  $1.96 \pm 0.03$ ) for  $M_2$  wt and triple mutant, respectively. In the high ionic strength buffer, W84 exhibited nearly a 3-fold increase in negative cooperativity ( $\alpha = 7.3 \pm 1.27$ ) at the  $M_2$  triple mutant compared to the  $M_2$  wt ( $\alpha = 2.6 \pm 0.31$ ). In contrast, a significant increase in negative cooperativity could not be observed at the  $M_2$  triple mutant in the low ionic strength buffer (**Figure 3.3 and Table 3.2**).

## 3.2 Characterisation of the M<sub>2</sub> triple mutant receptor with orthosteric ligands

### 3.2.1 Radioligand binding studies

#### 3.2.1.1 [<sup>3</sup>H]NMS dissociation binding

[<sup>3</sup>H]NMS dissociation binding experiments were performed in the absence of an allosteric modulator to investigate the effects of the allosteric triple mutation on the orthosteric radioligand dissociation kinetics. First, full-time course [<sup>3</sup>H]NMS dissociation studies were conducted to probe the influence of the M<sub>2</sub> triple mutant on the time needed to reduce the total binding of the radioligand [<sup>3</sup>H]NMS to half its initial value ( $t_{1/2}$ ).

The radioantagonist [<sup>3</sup>H]NMS dissociation was measured over a time period of 20min and radioligand reassociation was prevented by applying atropine (10  $\mu$ M) in excess. The radioligand dissociation rate constant ( $k_{-1}$ ) was much about 2.4 fold slower at the triple mutant ( $0.14 \pm 0.01 \text{ min}^{-1}$ ) compared to the M<sub>2</sub> wt ( $0.34 \pm 0.01 \text{ min}^{-1}$ ). Correspondingly, the half-life ( $t_{1/2}$ ) of radioligand dissociation at the M<sub>2</sub> triple mutant ( $4.9 \pm 0.12 \text{ min}$ ) was also about 2.4 fold slower in comparison to the M<sub>2</sub> wt ( $2.04 \pm 0.12 \text{ min}$ ) (**Figure 3.4 and Table 3.3**). These results are in agreement with the published data from Prilla *et al.*, 2006 which also showed an increase in the dissociation half-life ( $t_{1/2}$ ) and decreased apparent dissociation rate constants ( $k_{-1}$ ) for the single mutants W422<sup>7.35</sup>A and T423<sup>7.36</sup>A.

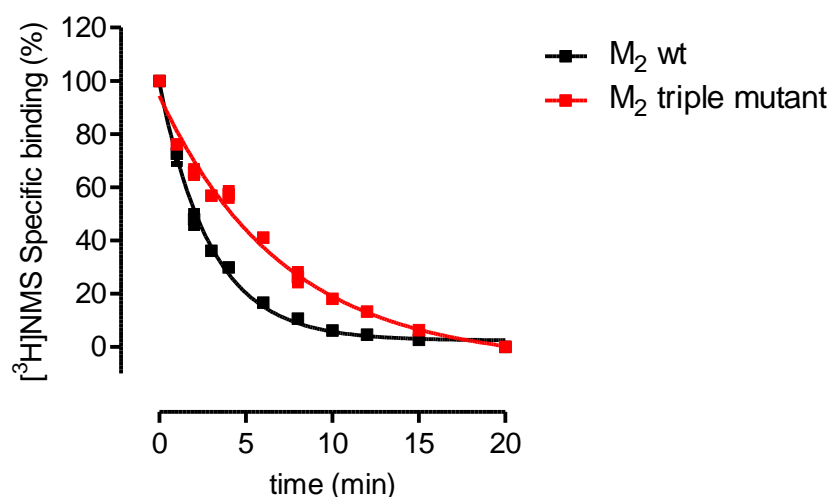


**Figure 3.4** [<sup>3</sup>H]NMS dissociation at the M<sub>2</sub> wt and M<sub>2</sub> triple mutant. [<sup>3</sup>H]NMS binding in % of maximal binding against time of dissociation (min). CHO-hM<sub>2</sub> wt and triple mutant cell membranes were pre-labeled with [<sup>3</sup>H]NMS (2nM). Radioligand re-association was blocked by atropine (10 $\mu$ M). Curve fitting was performed by one phase exponential decay analysis of single experiments. For half-lives and  $k_{-1}$  values see table 3.3. Data shown are mean values  $\pm$  S.E.M of 3 experiments performed in triplicates.

<b>[<sup>3</sup>H]NMS binding</b>					
	<b>pK<sub>D</sub></b>	<b>B<sub>max</sub> (receptors/cell)</b>	<b>B<sub>max</sub> (pmol/mg)</b>	<b>k<sub>-1</sub> (min<sup>-1</sup>)</b>	<b>t<sub>1/2</sub> (min)</b>
M <sub>2</sub> wt	9.79 ± 0.09	122 000 ± 25 608	3.9 ± 0.75	0.34 ± 0.01	2.04 ± 0.12
M <sub>2</sub> triple mutant	9.65 ± 0.06 <sup>ns</sup>	112 000 ± 23 706 <sup>ns</sup>	3.8 ± 0.65 <sup>ns</sup>	0.14 ± 0.01	4.9 ± 0.12

**Table 3.3 Radioligand binding parameters of the M<sub>2</sub> wt and M<sub>2</sub> triple mutant.** pK<sub>D</sub> is the negative logarithm of the equilibrium dissociation constant of the radioligand [<sup>3</sup>H]NMS. B<sub>max</sub> (pmol/mg) indicates the total amount of binding sites per mg membrane protein. B<sub>max</sub> (receptors/cell) indicates the amount of receptor molecules per cell in the CHO-M<sub>2</sub> cell membranes and live cells. B<sub>max</sub> values were determined from homologous equilibrium binding studies. k<sub>-1</sub> and t<sub>1/2</sub> denotes the dissociation rate constant and the half-life of radioligand dissociation, respectively. Data represent mean values ± S.E.M of 3-9 experiments performed in triplicates.

<sup>ns</sup> Not significantly different from the M<sub>2</sub> wt (Student's t-test)

### 3.2.1.2 [<sup>3</sup>H]NMS Equilibrium binding

#### 3.2.1.2.1 Muscarinic inverse and partial agonists

[<sup>3</sup>H]NMS equilibrium binding studies were carried out to probe the effects of the M<sub>2</sub> triple mutation on the binding affinities of the muscarinic inverse agonists, N-methylscopolamine(NMS), scopolamine and atropine and the partial agonist pilocarpine. First, it was important to determine if the receptor expression of both the M<sub>2</sub> wt and the M<sub>2</sub> triple mutant receptors were similar in CHO cells and also in cell membranes which were going to be used throughout the study. Also, it was important to probe if the radiotracer of choice [<sup>3</sup>H]NMS could be able to label the M<sub>2</sub> triple mutant receptors with high affinity.

The homologous competition, which is binding competition between compounds of similar chemical structure in this case [<sup>3</sup>H]NMS and the unlabelled NMS, was used to obtain the binding affinities for NMS and the total amount of receptors (B<sub>max</sub>pmol/mg ± S.E.M ) in the CHO-M<sub>2</sub> cells. The receptor expression measured as the total amount of binding sites per mg membrane protein was always similar between the M<sub>2</sub> wt (3.9 ± 0.75 pmol/mg) and triple mutant (3.8 ± 0.65 pmol/mg) receptors in the membrane preparations of CHO-M<sub>2</sub> cells used in this thesis. In the CHO-M<sub>2</sub> live cells the (B<sub>max</sub>receptors/cell ± S.E.M) measured as the amount of receptor molecules per cell was also not significantly different between the M<sub>2</sub> wt



(122 000 ± 25 608 receptors/cell) and the triple mutant (112 000 ± 23 706 receptors/cell) receptors (**Table 3.3**).

The IC<sub>50</sub> values from the homologous competition of [<sup>3</sup>H]NMS against unlabeled NMS were used to obtain the binding affinities (K<sub>D</sub> values) of the unlabeled ligand. The Cheng-Prusoff correction was used to convert the IC<sub>50</sub> values into the equilibrium dissociation constants K<sub>D</sub> as described in (**chapter 2.4.3.2**). Data obtained from nine experiments performed in triplicates, show that the binding affinity for the radioantagonist [<sup>3</sup>H]NMS was similar at both the M<sub>2</sub> wt (pK<sub>D</sub> = 9.79 ± 0.09) and the M<sub>2</sub> triple mutant (pK<sub>D</sub> = 9.65 ± 0.06) (**Table 3.3**). Heterologous competition [<sup>3</sup>H]NMS equilibrium binding studies were carried out with the inverse agonists scopolamine and atropine to further probe the effects of the triple mutant receptor on inverse agonists binding. Results show that the inverse agonists scopolamine and atropine also do not lose affinity at the M<sub>2</sub> triple mutant compared to the M<sub>2</sub> wt receptor (**Figure 3.5 and Table 3.4**). Therefore, this shows that mutating the core binding site of the allosteric ligands does not affect the equilibrium binding affinity of the inverse agonists to the orthosteric binding pocket of the M<sub>2</sub> receptor. The equilibrium binding affinity of the partial agonist pilocarpine was also insensitive to the allosteric triple mutation at the M<sub>2</sub> receptor (**Figure 3.6 and Table 3.5**).

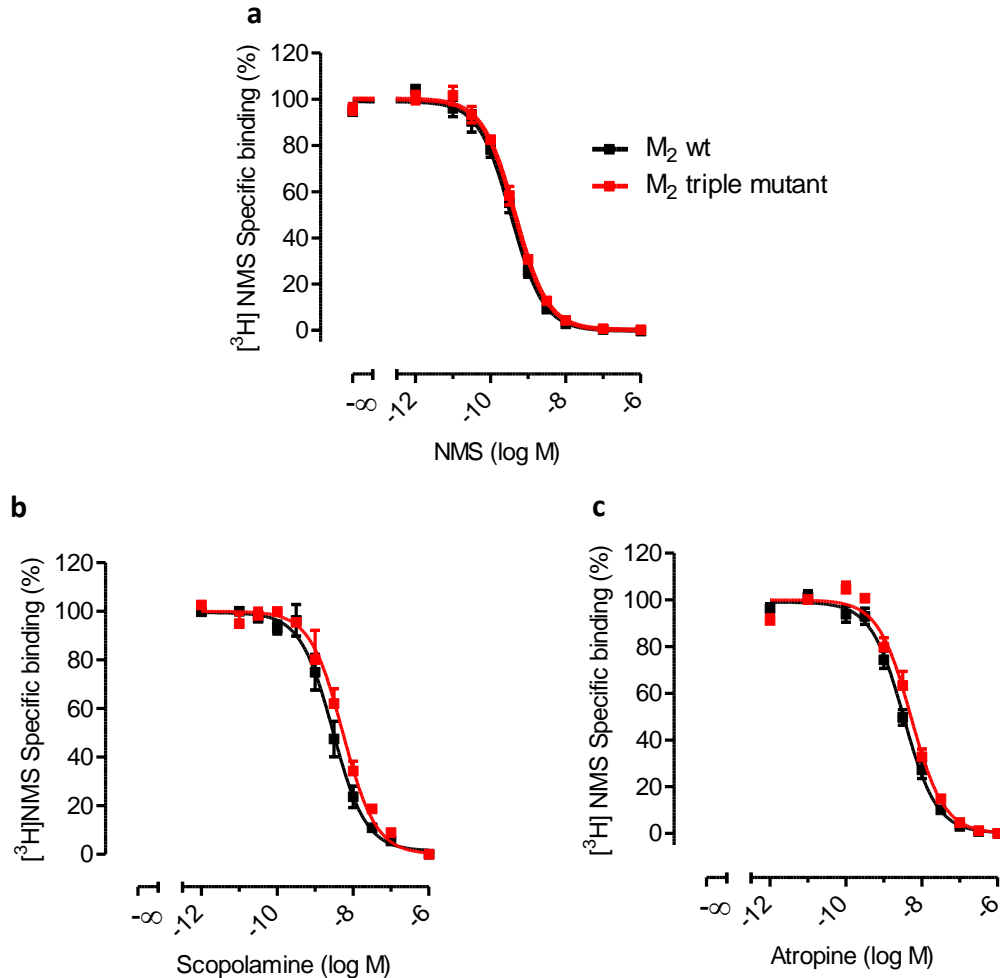


**Figure 3.5 Inverse agonists do not lose affinity at the  $M_2$  triple mutant receptor.** Equilibrium binding of [ $^3\text{H}$ ]NMS against increasing concentrations of inverse agonists N-methylscopolamine (NMS), scopolamine and atropine in CHO-h $M_2$  wild type (black) and triple mutant intact cells (red) (**a-c**). [ $^3\text{H}$ ]NMS (0.1nM) and (0.2nM) were applied for the (**a**) homologous and (**b,c**) heterologous competition, respectively. Non-specific binding was determined by addition of atropine (10 $\mu\text{M}$ ). (**a-c**) There is no significant difference in the specific binding of [ $^3\text{H}$ ]NMS in the presence of investigated inverse agonists between the CHO-h $M_2$  wild type and triple mutant CHO cells (One-way Anova, Tukey's Multiple Comparison Test). Shown are the mean values  $\pm$  S.E.M of 3-9 experiments performed in triplicates and analysed by the four parameter logistic function with a slope factor ( $n_H$ ) of -1.

<b>[<sup>3</sup>H]NMS equilibrium binding</b>				
	<b>M<sub>2</sub> wt</b>	<b>M<sub>2</sub> triple mutant</b>		
		<b>pK<sub>D</sub></b>	<b>ΔpK<sub>D</sub> (Wild type- mutant)</b>	<b>n</b>
NMS	9.79 ± 0.09	9.65 ± 0.06 <sup>ns</sup>	0.14 ± 0.11	9
		<b>pK<sub>i</sub></b>	<b>ΔpK<sub>i</sub> (Wild type- mutant)</b>	
Scopolamine	8.89 ± 0.13	8.59 ± 0.12 <sup>ns</sup>	0.30 ± 0.18	4
Atropine	8.95 ± 0.16	8.57 ± 0.09 <sup>ns</sup>	0.38 ± 0.19	3

**Table 3.4 The binding of inverse agonists is insensitive to the allosteric triple mutation at CHO-hM<sub>2</sub> receptor.** pK<sub>D</sub> and pK<sub>i</sub> are negative logarithms of the equilibrium dissociation constants K<sub>D</sub> and K<sub>i</sub>, respectively. ΔpK<sub>D</sub> and ΔpK<sub>i</sub> represents the difference between the pK<sub>D</sub> and pK<sub>i</sub> values, respectively, of the M<sub>2</sub> wt and triple mutant. n represents the number of experiments. Data points from individual experiments were fitted to a four-parameter logistic function obtaining slope factor n<sub>H</sub> of -1 and subsequently transformed by the Cheng-Prusoff correction to obtain the equilibrium binding constants K<sub>D</sub> and K<sub>i</sub>. Shown are the mean values ± S.E.M of 3-9 experiments performed in triplicates.

<sup>ns</sup>Not significantly different to the pK<sub>D</sub> or the pK<sub>i</sub> of the M<sub>2</sub> wt, respectively (Student's t-test)

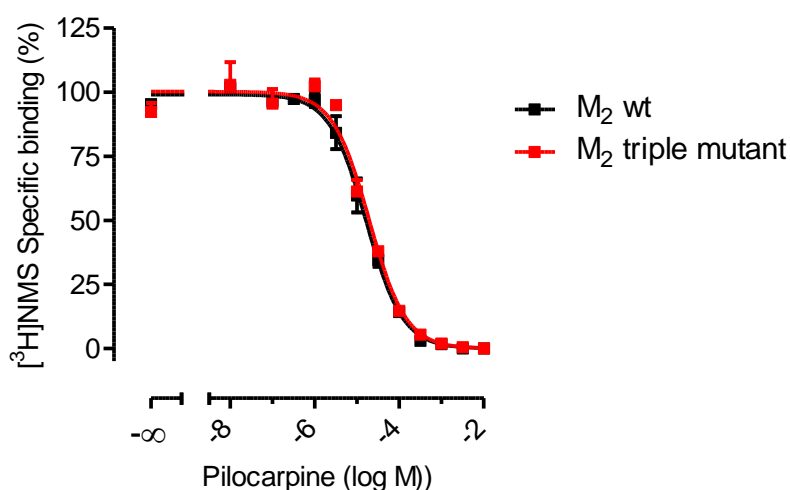


**Figure 3.6 The binding affinity of the partial agonist pilocarpine is insensitive to the M<sub>2</sub> triple mutation.** Equilibrium binding of [<sup>3</sup>H]NMS (0.2nM) against the muscarinic partial agonist pilocarpine in CHO-hM<sub>2</sub> wild type (black) and triple mutant intact cells (red). Non-specific binding was determined by addition of atropine (10μM). There is no significant difference in the specific binding of [<sup>3</sup>H]NMS between the CHO-hM<sub>2</sub> wild type and triple mutant cells (Student' t-test). Shown are the mean values ± S.E.M of four experiments performed in triplicates and analysed by the four parameter logistic function with a slope factor (n<sub>H</sub>) of -1.

### 3.2.1.2.2 Muscarinic agonists

The muscarinic agonists exhibited a different trend in contrast to the inverse and partial agonists in terms of orthosteric binding. The agonists acetylcholine, carbachol, iperoxo, McN-A-343, oxotremorine-M and oxotremorine studied in this investigation all showed a loss of binding affinity at the M<sub>2</sub> triple mutant. The endogenous ligand acetylcholine lost about 2 log units of affinity, which was indeed the biggest loss of affinity amongst all the agonists investigated. Interestingly, the loss in affinity of these agonist ligands was not uniform and appeared to differ for some of the structurally distinct agonists (**Figure 3.7; Table 3.5 and chapter 2.1.2**).

Compounds which displayed similar binding affinity with the endogenous ligand at the M<sub>2</sub> wt type did not show the same binding characteristics as acetylcholine at the M<sub>2</sub> triple mutant (**Table 3.5**). At the M<sub>2</sub> wt, the binding affinity of acetylcholine did not differ significantly from that of oxotremorine and McN-A-343. However, at the M<sub>2</sub> triple mutant the endogenous ligand acetylcholine lost more of its binding affinity ( $\Delta pK_i = 2.08 \pm 0.15$ ) compared to oxotremorine and McN-A-343 ( $\Delta pK_i = 1.00 \pm 0.05$  and  $1.33 \pm 0.11$ ), respectively. The full agonist carbachol and the partial agonist pilocarpine's binding affinities were not significantly different from each other at the M<sub>2</sub> wt ( $pK_i = 5.46 \pm 0.12$  and  $5.17 \pm 0.11$ ), respectively but at M<sub>2</sub> triple mutant ( $pK_i = 3.87 \pm 0.07$  and  $4.98 \pm 0.05$ ), respectively (**Table 3.5**).

The loss in binding affinity of carbachol ( $\Delta pK_i = 1.59 \pm 0.14$ ) was significantly greater than of oxotremorine ( $\Delta pK_i = 1.00 \pm 0.05$ ). Carbachol lost about 1 log unit of binding affinity more than pilocarpine at the M<sub>2</sub> triple mutant. On the other hand, oxotremorine and McN-A-343 exhibited similar affinities with the partial agonist pilocarpine the M<sub>2</sub> triple mutant. This was different at the M<sub>2</sub> wt whereby both oxotremorine and McN-A-343 displayed a higher binding affinity of 1.24 and 1.26 log units of affinity, respectively than pilocarpine. Oxotremorine and McN-A-343, however, bound at the M<sub>2</sub> wt and the M<sub>2</sub> triple mutant with similar affinities (**Figure 3.7; Table 3.5**). This data suggests that the narrow passage located at the entrance to the M<sub>2</sub> orthosteric binding site is able to selectively regulate the binding of chemically distinct muscarinic agonist ligands.

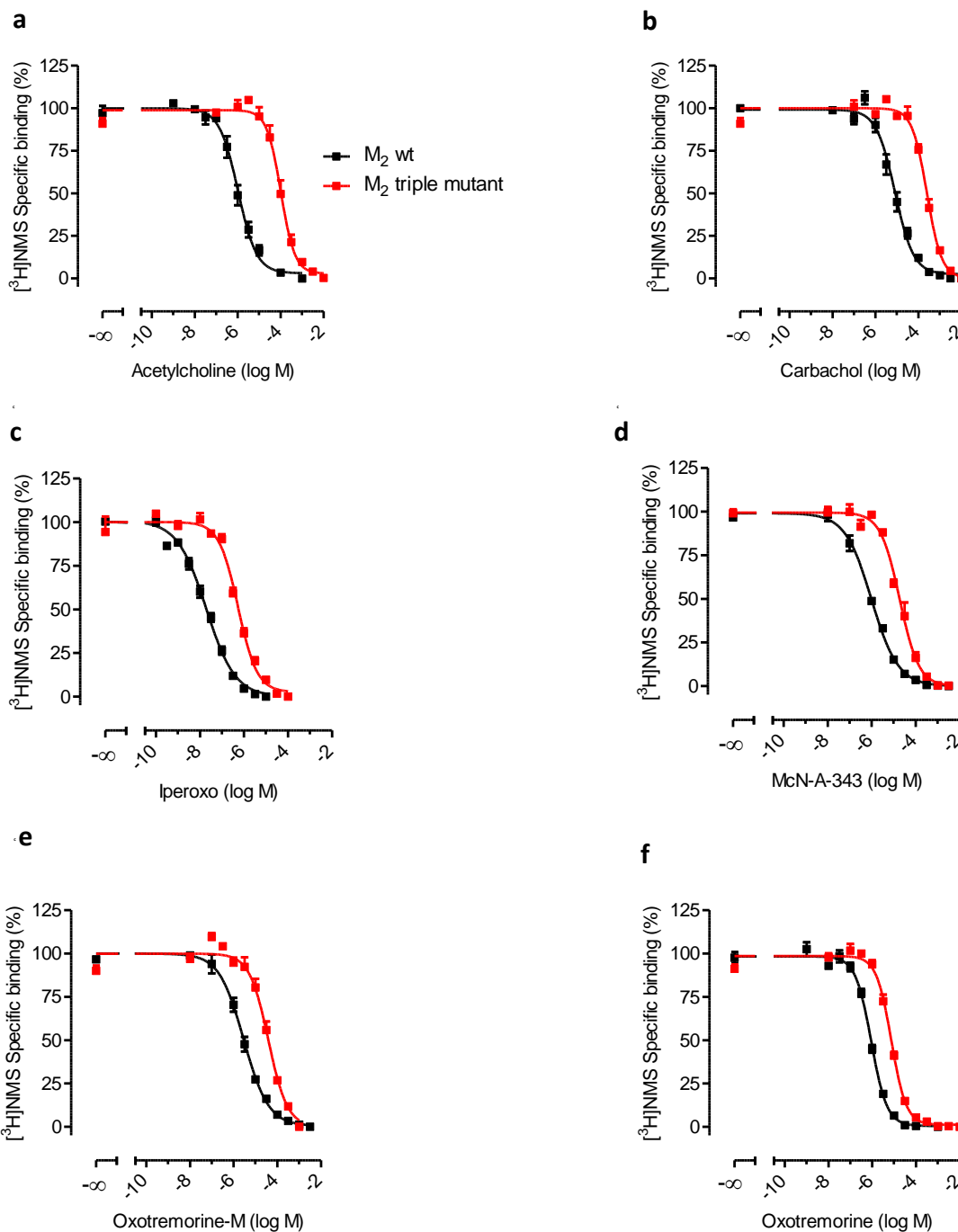


**Figure 3.7 Muscarinic agonists lose affinity at the M<sub>2</sub> triple mutant receptor in a selective-dependent manner.** Equilibrium binding of  $[^3\text{H}]\text{NMS}$  (0.2nM) against increasing concentrations of the muscarinic full agonists in CHO-hM<sub>2</sub> wild type (black) and triple mutant intact cells (red) (a-f). Non-specific binding was determined by addition of atropine (10 $\mu\text{M}$ ). There is a significant difference in the specific binding of  $[^3\text{H}]\text{NMS}$  in the presence of investigated agonists between the CHO-hM<sub>2</sub> wild type and triple mutant cells. There is a decrease in the loss of binding affinity depending on the ligand, when compared to the loss in binding affinity of ACh (One-way Anova, Tukey's Multiple Comparison Test). The slope factors ( $n_{\text{H}}$ ) of each curve varied as shown in **Table 3.5**. Shown are the mean values  $\pm$  S.E.M of 3-4 experiments performed in triplicates and analysed by the four parameter logistic function.

[ <sup>3</sup> H]NMS equilibrium binding				
	M <sub>2</sub> wt	M <sub>2</sub> triple mutant		
		pK <sub>i</sub> (n <sub>H</sub> )	ΔpK <sub>i</sub> (wildtype- mutant)	n
Acetylcholine	6.37 ± 0.11 (-1)	4.29 ± 0.11 (-1.33 ± 0.20)	2.08 ± 0.15	4
Carbachol	5.46 ± 0.12 (-1)	3.87 ± 0.07 (-1.26 ± 0.14)	1.59 ± 0.14 <sup>ns</sup>	4
Iperoxo	8.05 ± 0.05 (-0.66 ± 0.06)	6.55 ± 0.05 (-1)	1.50 ± 0.07*	3
McN-A-343	6.43 ± 0.11 (-0.71 ± 0.05)	5.10 ± 0.03 (-1)	1.33 ± 0.11**	4
Oxotremorine-M	5.93 ± 0.08 (-0.77 ± 0.06)	4.67 ± 0.08 (-1)	1.26 ± 0.11***	4
Oxotremorine	6.41 ± 0.04 (-1.20 ± 0.09)	5.41 ± 0.04 (-1.27 ± 0.10)	1.00 ± 0.05***, <sup>#</sup>	4
Pilocarpine	5.17 ± 0.11 (-1)	4.98 ± 0.05 (-1)	0.19 ± 0.12***, <sup>&amp;</sup>	4

**Table 3.5 Muscarinic agonists display a structure-related, selective loss of binding affinity at the M<sub>2</sub> triple mutant receptor.** pK<sub>i</sub> is the negative logarithm of the equilibrium dissociation constant K<sub>i</sub>. ΔpK<sub>i</sub> represents the difference between the pK<sub>i</sub> values of the M<sub>2</sub> wt and triple mutant. n<sub>H</sub> represents the slope factor. n represents the number of experiments. Data points from individual experiments were fitted to a four-parameter logistic function and subsequently transformed by the Cheng-Prusoff correction to obtain the equilibrium binding constant K<sub>i</sub>. Shown are the mean values ± S.E.M 3-4 independent experiments performed in triplicates.

\*\*\*\*\*Significantly different from the ΔpK<sub>i</sub> of Acetylcholine (\*p < 0.05; \*\*\* p < 0.0001)

<sup>#</sup>Significantly different from the ΔpK<sub>i</sub> of Carbachol (<sup>#</sup>p < 0.05)

<sup>ns</sup>Not significantly different from ΔpK<sub>i</sub> of Acetylcholine

<sup>&</sup> Significantly different from each independent ΔpK<sub>i</sub> value of the full agonists (<sup>&</sup>p < 0,0001)

Statistical analysis was performed by One-way Anova with Tukey's Multiple Comparison Test.

### 3.2.2 Receptor activation

#### 3.2.2.1 [<sup>35</sup>S]GTPγS binding

Muscarinic M<sub>2</sub> receptors predominantly couple to the G<sub>i/o</sub>-proteins to convey downstream signaling. Here, the activation of both the M<sub>2</sub> wt and triple mutant receptors was measured by the [<sup>35</sup>S]GTPγS binding assay. The endogenous agonist acetylcholine, superagonist iperoxo and partial agonist pilocarpine were used to investigate the effects of the allosteric triple mutation on M<sub>2</sub> receptor activation.

The full agonists acetylcholine and iperoxo lost potency but the maximum effect remained the same at the M<sub>2</sub> triple mutant compared to the M<sub>2</sub> wt. However, the partial agonist pilocarpine showed a decrease in maximum activation but not in potency at the M<sub>2</sub> triple mutant (**Figure 3.8**). These findings are in agreement with previously published data which showed that acetylcholine lost potency but not maximum effect at the M<sub>2</sub> single mutation (W422<sup>7.35</sup>A). Also at W422<sup>7.35</sup>A, pilocarpine displayed a decrease in maximum effect but potency remained unchanged (Jäger *et al.*, 2007).

Acetylcholine and iperoxo showed a decrease of 1.6 and 1.5 log units in potency, respectively, at the M<sub>2</sub> triple mutant in comparison to the M<sub>2</sub> wt. However, the acetylcholine curve at the M<sub>2</sub> wt was shallow with a slope factor (n<sub>H</sub> = 0.59 ± 0.09) significantly different from unity. The iperoxo curve at the M<sub>2</sub> triple mutant was also shallow with a slope factor (n<sub>H</sub> = 0.56 ± 0.09) significantly different from unity. On the other hand the partial agonist lost about 43% of its maximum effect at the M<sub>2</sub> triple mutant compared to the M<sub>2</sub> wt. This shows that pilocarpine lost nearly half of its ability to induce receptor activation upon the induction of the allosteric triple mutation at the M<sub>2</sub> receptor (**Figure 3.8 and Table 3.6**).

The potency of iperoxo was 2.5 log units higher than that of the endogenous ligand acetylcholine at the M<sub>2</sub> wt. This reflected the characteristics of iperoxo as a “superpotent” agonist at the M<sub>2</sub> wt receptors. This was in agreement with previously published data which showed that iperoxo had a higher potency than acetylcholine at the M<sub>2</sub> wt (Bock *et al.*, 2012, Schrage *et al.*, 2012). At the M<sub>2</sub> triple mutant iperoxo (pEC<sub>50</sub> = 7.96 ± 0.13) maintained its superpotent features whereby it also displayed 2.5 log units higher potency than acetylcholine (pEC<sub>50</sub> = 5.49 ± 0.07) (**Table 3.6**).

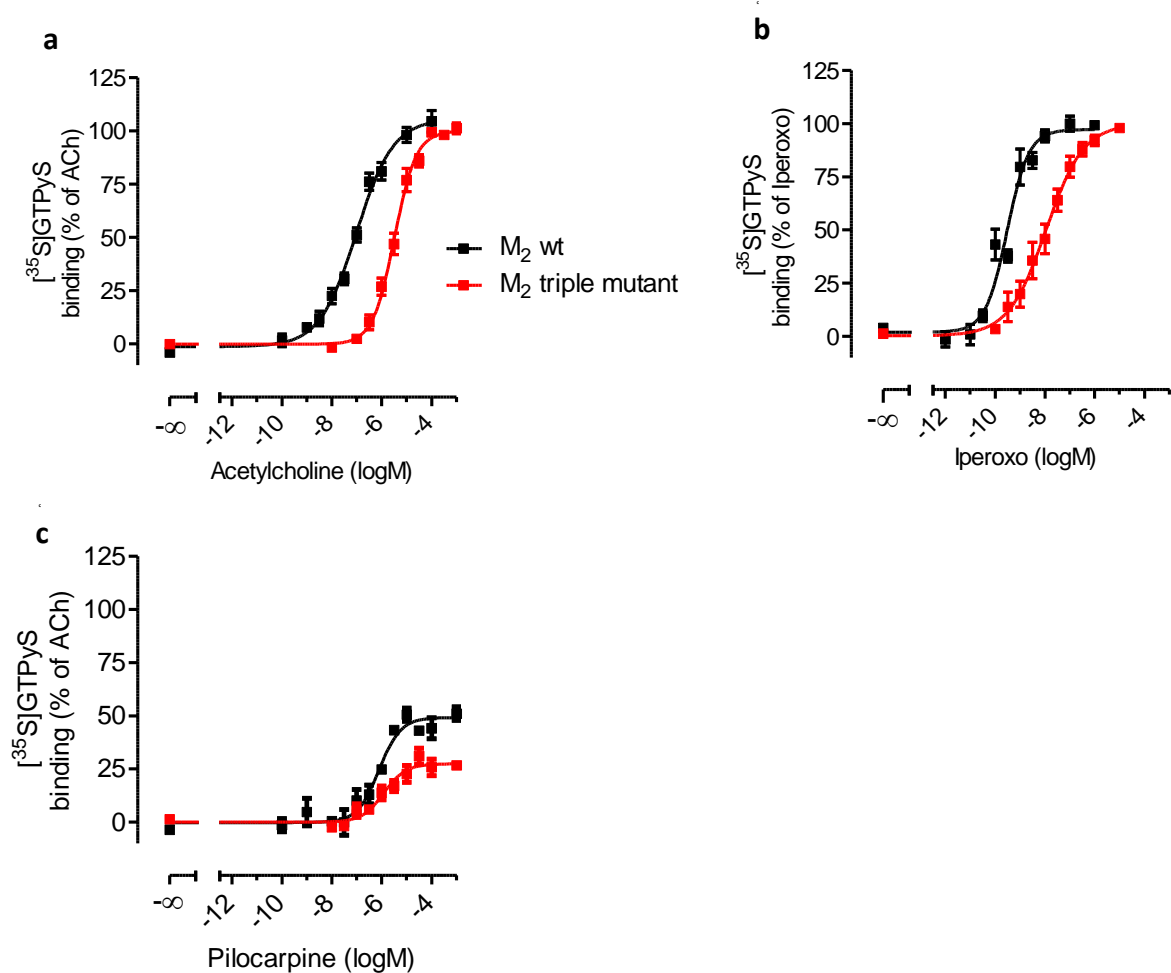


**Figure 3.8 Full agonists lose potency whilst the partial agonist shows a decrease in maximum effect at the M<sub>2</sub> triple mutant.**  $[^{35}\text{S}]\text{GTP}\gamma\text{S}$  binding to membranes of CHO-hM<sub>2</sub> wt and triple mutant cells indicates receptor-mediated G<sub>i/o</sub> protein activation. The maximum  $[^{35}\text{S}]\text{GTP}\gamma\text{S}$  binding induced by ACh separately for M<sub>2</sub> wt and triple mutant was set at 100% and  $[^{35}\text{S}]\text{GTP}\gamma\text{S}$  binding in the absence of ligand was set at 0%. The slope factor ( $n_H$ ) was not significantly different from 1 for each individual curve except for ACh M<sub>2</sub> wt and iperoxo M<sub>2</sub> triple mutant (see **Table 3.6**). Data shown are means  $\pm$  S.E.M of 3-5 experiments performed in triplicates.

ACh = acetylcholine.



<b>[<sup>35</sup>S]GTP<sub>γ</sub>S binding</b>					
	<b>pEC<sub>50</sub> (n<sub>H</sub>)</b>		<b>ΔpEC<sub>50</sub> (Wt-mutant)</b>	<b>%E<sub>max</sub></b>	
	<b>M<sub>2</sub> wt</b>	<b>M<sub>2</sub> triple mutant</b>		<b>M<sub>2</sub> wt</b>	<b>M<sub>2</sub> triple mutant</b>
Acetylcholine	7.07 ± 0.05 (0.59 ± 0.09)	5.49 ± 0.07 <sup>###</sup>	1.59 ± 0.09	100 ± 0.13	100 ± 0.08 <sup>ns</sup>
Iperoxo	9.52 ± 0.09	7.96 ± 0.13 <sup>###</sup> (0.56 ± 0.09)	1.50 ± 0.21	100 ± 0.004	99 ± 1.04 <sup>ns</sup>
Pilocarpine	6.10 ± 0.15	5.91 ± 0.17 <sup>°</sup>	0.19 ± 0.08	49 ± 4	28 ± 3 <sup>**</sup>

**Table 3.6 [<sup>35</sup>S]GTP<sub>γ</sub>S binding to membranes of CHO-hM<sub>2</sub> cells as a measure of G<sub>i/o</sub> signalling.** pEC<sub>50</sub> is the negative logarithm of the ligand concentration required to induce half the maximal activation. ΔpEC<sub>50</sub> is the difference between the pEC<sub>50</sub> values of the M<sub>2</sub> wt and M<sub>2</sub> triple mutant. E<sub>max</sub> shows the maximal activation induced by a ligand relative to acetylcholine. n<sub>H</sub> indicates the slope factor of the regression curve. n<sub>H</sub> is 1 unless when stated in the table (F-test, p<0.05). Data shown are means ± S.E.M of 3-5 experiments performed in triplicates. Statistical analysis performed by One-way Anova, Tukey's Multiple Comparison Test.

% Emax = percentage of Acetylcholine Emax.

<sup>ns</sup> Not significantly different from the Emax at the M<sub>2</sub> wt.

<sup>\*\*</sup> Significantly different from the Emax at M<sub>2</sub> wt (<sup>\*\*</sup> p < 0.05).

<sup>°</sup> Not significantly different from the pEC<sub>50</sub> at the M<sub>2</sub> wt.

<sup>###</sup> Significantly different from the pEC<sub>50</sub> at the M<sub>2</sub> wt (<sup>###</sup> p < 0.05).

### 3.2.2.2 Dynamic mass redistribution (DMR)

#### 3.2.2.2.1 $G_{i/o}$ signaling

The Dynamic Mass Redistribution (DMR) assay is a label-free, non-invasive technique which measures cellular processes which happen as a result of biomolecular relocation within the cell (Schröder *et al.*, 2010 and 2011). DMR was used to investigate the effects of the  $M_2$  triple mutant on the  $G_{i/o}$  signalling pathway in live cells. As in the [ $^{35}$ S]GTP $\gamma$ S binding assay, the endogenous ligand acetylcholine, superagonist iperoxo and the partial agonist pilocarpine were investigated here to probe their maximal activation effects at the  $M_2$  wt (control) and the triple mutant.

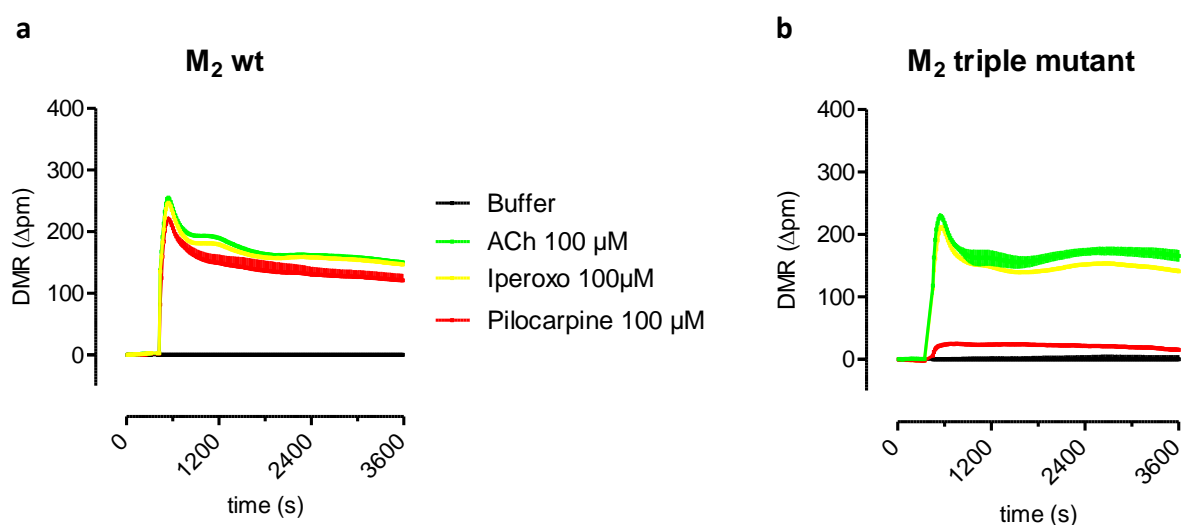


**Figure 3.9 DMR activation by muscarinic agonists shows  $G_{i/o}$  activation.** Dynamic mass redistribution (DMR) responses measured as wavelength shifts ( $\Delta$ pm) were measured over time after addition of acetylcholine (ACh), iperoxo and pilocarpine in CHO-h $M_2$  wild type (a) and triple mutant cells (b). ACh (100 $\mu$ M) was used as a positive control of maximum activation. Positive DMR ( $\Delta$ pm) display  $G_{i/o}$  signalling. Shown are means and S.E.M of baseline-corrected data from one representative of four independent experiments conducted in quadruplicates.

Acetylcholine and Iperoxo did not display a significant reduction in maximum effect ( $E_{max} = 100 \pm 2.3\%$  and  $99 \pm 0.9\%$ , respectively) at the  $M_2$  triple mutant. As expected, pilocarpine displayed its partial agonistic properties at the  $M_2$  wt whereby it produced a maximum effect of ( $E_{max} = 86\% \pm 1.9$ ). Pilocarpine's maximal effect at the given ligand concentration was significantly different compared to acetylcholine and iperoxo at the  $M_2$  wt. However, at the  $M_2$  triple mutant pilocarpine was unable to stimulate a significant DMR activation through the

G<sub>i/o</sub>-pathway. This is reflected by about only 4% activation of the DMR signal which was not significantly different from the buffer signal in the experiments (**Figure 3.9 and Table 3.7**).

DMR- G <sub>i/o</sub> activation		
	M <sub>2</sub> wt	M <sub>2</sub> triple mutant
	E <sub>max</sub> (% of ACh)	
Acetylcholine	100 ± 4	100 ± 2.3 <sup>ns</sup>
Iperoxo	97. ± 0.8	99 ± 0.9 <sup>ns</sup>
Pilocarpine	86 ± 1.9 <sup>ooo</sup>	4.4 ± 0.9 <sup>***</sup>

**Table 3.7 Maximal effect of G<sub>i/o</sub> activation in DMR.** E<sub>max</sub>(%) indicates the maximal amount of G<sub>i</sub>-signalling pathway activation as a percentage of the endogenous acetylcholine (100µM) set at 100%. The superagonist iperoxo and the partial agonist pilocarpine were also used at a concentration of 100µM, respectively. Data represents means of four independents experiments. Statistical analysis was performed by the Student's t-test.

<sup>\*\*\*</sup>Significantly different from the E<sub>max</sub> at M<sub>2</sub> wt (<sup>\*\*\*</sup> p < 0.05).

<sup>ns</sup>Not significantly different from the E<sub>max</sub> at M<sub>2</sub> wt.

<sup>ooo</sup>Significantly different from the E<sub>max</sub> of acetylcholine and iperoxo at M<sub>2</sub> wt (<sup>ooo</sup> p < 0.05)

#### 3.2.2.2.1 G<sub>s</sub> signalling.

##### M<sub>2</sub> triple mutant reduces G<sub>s</sub>-signalling

Although it predominantly signals through the G<sub>i/o</sub>-proteins, the M<sub>2</sub> receptor can also relay downward signaling through the G<sub>s</sub> pathway. This is also termed receptor promiscuous signaling whereby a receptor can engage more than a single signalling pathway (Kenakin, 2003; Kebabian *et al.*, 2009). Here, the investigation focused on finding out the effects of the triple mutation in the allosteric core region of the M<sub>2</sub> receptor on the signalling via the G<sub>s</sub>-pathway. The Dynamic Mass Redistribution (DMR) assay was used to measure the signalling through the G<sub>s</sub>-pathway.

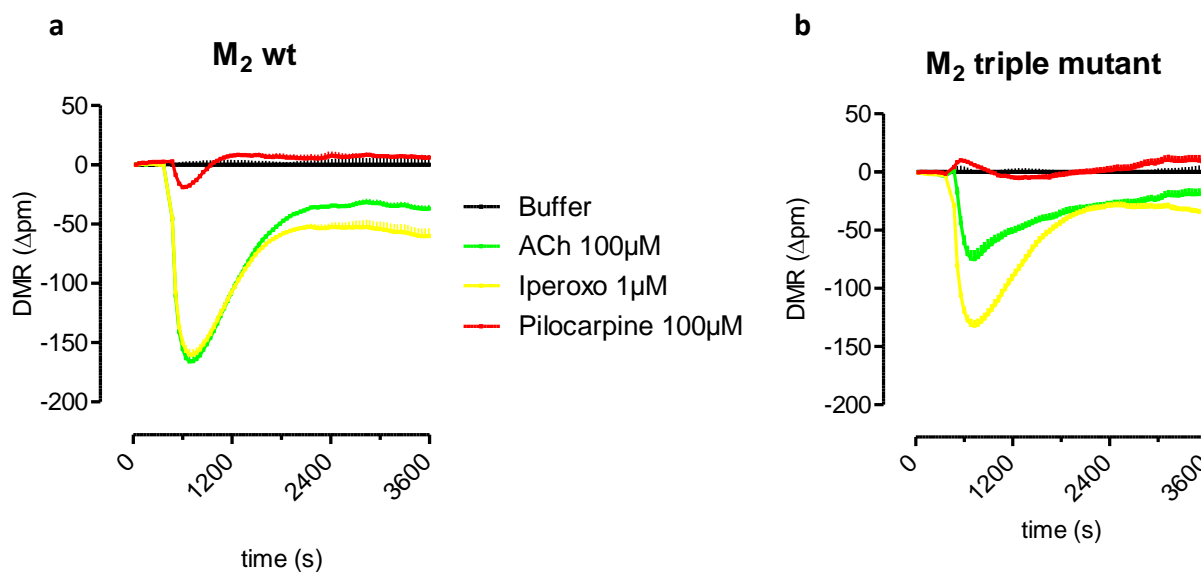


**Figure 3.10 DMR reveals a decrease in  $G_s$ -signalling at the  $M_2$  triple mutant.** Pretreatment of cells stably transfected with the  $M_2$  wt and triple mutant receptor, with the  $G_i$  inhibitor PTX (100ng/ml) for 18-24 h revealed  $G_s$  signalling shown as negative DMR ( $\Delta$ pm). The full agonists acetylcholine (ACh) (100 $\mu$ M), and iperoxo (1 $\mu$ M) induce  $G_s$  signalling. Shown are means and S.E.M of baseline-corrected data from one representative of at least four independent experiments conducted in quadruplicates.

CHO cells stably transfected with the  $M_2$  wt and  $M_2$  triple mutant receptor were pretreated with PTX to inhibit the function of the  $G_{i/o}$ -proteins. PTX is a hexameric protein which irreversibly ADP-ribosylates  $G_{i/o}$  proteins (Kaslow *et al.*, 1987). Hence, the  $G_{i/o}$  protein remains in the inactive GDP-bound state and unable to inhibit adenylyl cyclase activity. The endogenous ligand acetylcholine, superagonist iperoxo and partial agonist pilocarpine were employed to characterise  $G_s$  signalling in DMR assay. The full agonists acetylcholine and iperoxo were both able to maximally stimulate the activation of the  $G_s$  pathway at the  $M_2$  wt as demonstrated by their  $E_{max}$  values of  $100 \pm 4$  and  $98 \pm 3$ , respectively. In contrast, the partial agonist pilocarpine failed to activate the  $G_s$  signalling pathway at the  $M_2$  wt receptor ( $E_{max} = -8 \pm 4$ ) (**Fig 3.10a and Table 3.8**).

Acetylcholine and iperoxo were still able to activate  $G_s$  signalling through DMR at the  $M_2$  triple mutant. However, for acetylcholine there was a marked decrease in  $G_s$  signalling of about 57% at the  $M_2$  triple mutant ( $E_{max} = 43 \pm 5$ ) compared to the  $M_2$  wt. For iperoxo (1 $\mu$ M), there was a decrease in  $G_s$ -mediated signalling of about 19% at the  $M_2$  triple mutant ( $E_{max} = 79 \pm 3$ ) compared to the  $M_2$  wt. The partial agonist pilocarpine, just like in the  $M_2$  wt cells failed to stimulate  $G_s$ -mediated DMR also at the  $M_2$  triple mutant ( $E_{max} = -4 \pm 2$ ) (**Fig 3.10b and Table 3.8**).

DMR- G <sub>s</sub> activation		
	M <sub>2</sub> wt	M <sub>2</sub> triple mutant
		E <sub>max</sub> (% of ACh)
Acetylcholine	100 ± 4	43 ± 5 <sup>**</sup>
Iperoxo	98 ± 3	79 ± 3 <sup>**</sup>
Pilocarpine	-8 ± 4	-4 ± 2 <sup>ns</sup>

**Table 3.8 Maximal efficacies for G<sub>s</sub> activation in DMR.** E<sub>max</sub>(%) indicates the maximal amount of G<sub>s</sub>-signalling pathway activation as a percentage of the endogenous acetylcholine (100µM) set at 100%. The superagonist iperoxo and the partial agonist pilocarpine concentrations used were (1µM) and (100µM), respectively. Data represents means of at least four independent experiments. Statistical analysis was performed by the Student's t-test.

<sup>\*\*</sup>Significantly different from the E<sub>max</sub> at M<sub>2</sub> wt ( <sup>\*\*</sup> p<0.05).

<sup>ns</sup>Not significantly different from the E<sub>max</sub> at M<sub>2</sub> wt.

### 3.2.2.3 cAMP accumulation - G<sub>s</sub> signaling

The cAMP assay was carried out to measure the function of the G<sub>s</sub>-protein by monitoring the amount of cAMP production in the cell cytosol. Cells were pretreated with the G<sub>i/o</sub>-protein inhibitor pertussis toxin (PTX) (100ng/ml) in order to measure solely the effects of G<sub>s</sub>-protein function. The endogenous ligand acetylcholine, the superagonist iperoxo and the partial agonist pilocarpine were again used as ligands of choice. The aim was to find out if the reduction in G<sub>s</sub> signaling observed at the M<sub>2</sub> triple mutant in the DMR real time measurements would be replicated in another functional assay. cAMP production was measured as described in chapter 2.5.2.

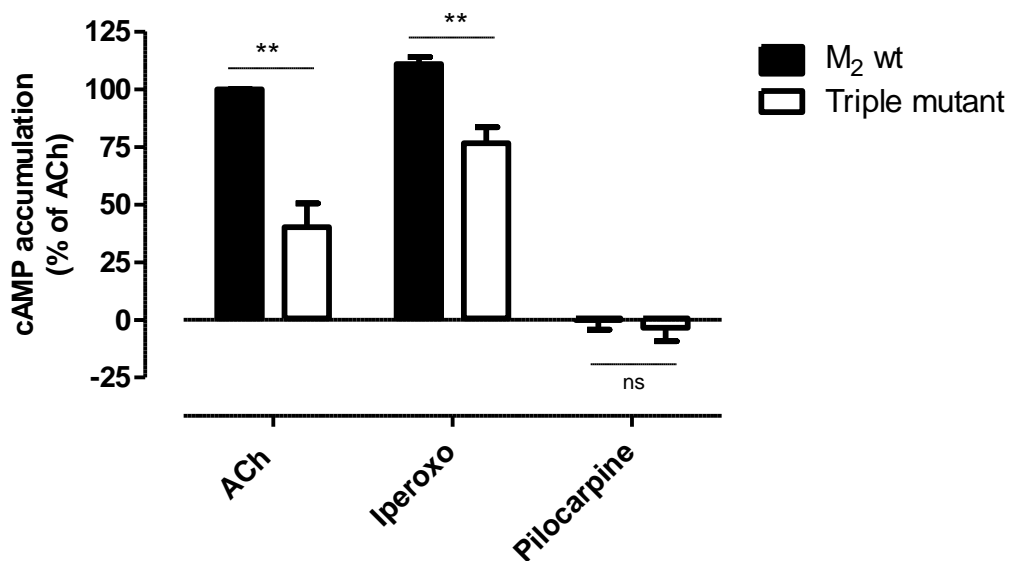


**Figure 3.11 Loss of G<sub>s</sub>-signalling at the M<sub>2</sub> triple mutant.** cAMP accumulation in CHO M<sub>2</sub> wt and M<sub>2</sub> triple mutant cells pretreated with PTX (100ng/ml) as a measure of G<sub>s</sub> signalling. Acetylcholine (ACh) (1mM), Iperoxo (100µM) and Pilocarpine (10mM) were used to stimulate the respective receptors. The maximum activation induced by acetylcholine was set at 100%. Statistical analysis was performed by the Student's t-test.

\*\*Significantly different from maximum cAMP accumulation at the M<sub>2</sub> wt (\*\*p < 0.05)

<sup>ns</sup>Not significantly different from the M<sub>2</sub> wt and also to basal readout

There was a substantial reduction of about 60% in cAMP accumulation at the acetylcholine-stimulated M<sub>2</sub> triple mutant receptor. When the M<sub>2</sub> receptor superagonist iperoxo (100µM) was applied at the M<sub>2</sub> triple mutant, a reduction of about 34% was observed compared to the M<sub>2</sub> wt. Hence, the data show that iperoxo was more potent in stimulating cAMP accumulation at the M<sub>2</sub> triple mutant receptor than the endogenous ligand acetylcholine. Also, iperoxo was more potent than acetylcholine at the M<sub>2</sub> wt receptor even at a ten-fold lower concentration. Iperoxo induced about 10% more cAMP accumulation compared to acetylcholine at the M<sub>2</sub> wt receptor. The partial agonist pilocarpine did not induce cAMP accumulation through the G<sub>s</sub>-protein-mediated signalling either at the M<sub>2</sub> wt or triple mutant receptor (**Figure 3.11 and Table 3.9**). Therefore, both the cAMP accumulation and DMR data appear to be coherent in showing that there is a pronounced loss of G<sub>s</sub> signaling efficacy for the full agonists whilst the partial agonist was unable to induce G<sub>s</sub> activation at the M<sub>2</sub> triple mutant in comparison to the M<sub>2</sub> wt signaling.

cAMP accumulation			
	M <sub>2</sub> wt	M <sub>2</sub> triple mutant E <sub>max</sub> (%)	ΔE <sub>max</sub> (%) (wildtype-mutant)
Acetylcholine	100	40.2 ± 10 <sup>**</sup>	59.8 ± 10
Iperoxo	110.9 ± 3 <sup>°</sup>	76.6 ± 7 <sup>**</sup>	34.3 ± 7.5
Pilocarpine	-0.1 ± 4	-3.4 ± 6 <sup>ns</sup>	-

**Table 3.9 Maximal efficacies for G<sub>s</sub>-mediated cAMP accumulation.** E<sub>max</sub>(%) indicates the maximal amount of cAMP accumulation as a percentage of the endogenous acetylcholine (1mM) set at 100%. ΔE<sub>max</sub>(%) indicates the difference between the efficacy values of the M<sub>2</sub> wt and triple mutant. The superagonist iperoxo and the partial agonist pilocarpine concentrations used were (100μM) and (10mM), respectively.

<sup>\*\*</sup>Significantly different from the E<sub>max</sub> at M<sub>2</sub> wt (\*\* p<0.05)

<sup>ns</sup>Not significantly different from the E<sub>max</sub> at M<sub>2</sub> wt

<sup>°</sup>Significantly different from acetylcholine at M<sub>2</sub> wt (° p<0.05)

Statistical analysis was performed by the Student's t-test.

### 3.3 The allosteric core region of the M<sub>2</sub> receptor: a ‘gate-keeper’ against biogenic amine ligands?

#### 3.3.1 Epinephrine appears to bind and activate the muscarinic M<sub>2</sub> triple mutant receptor

To investigate our hypothesis that opening up the entry channel to the M<sub>2</sub> receptor orthosteric site would allow access to other non-muscarinic biogenic amines, radioligand binding experiments were performed. Radioligand binding experiments focusing on epinephrine were carried out in order to investigate if epinephrine would be able to gain access and bind to the orthosteric binding site of the ‘open’ M<sub>2</sub> triple mutant receptor.

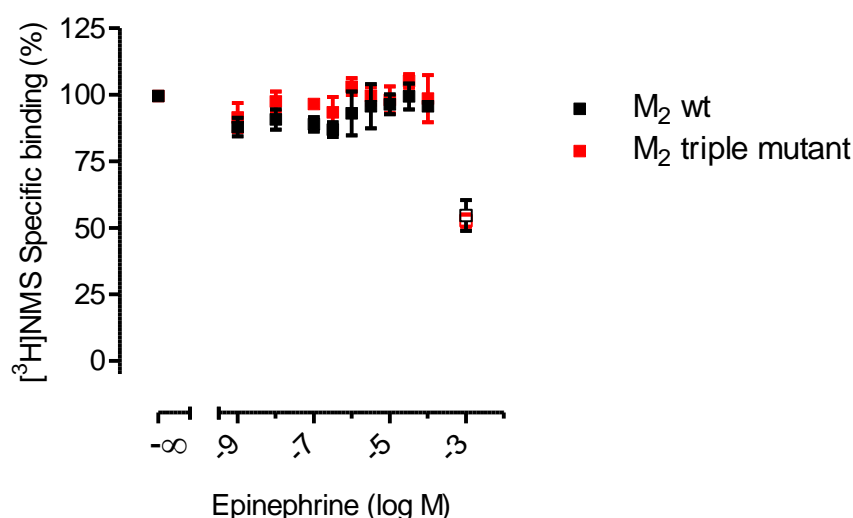


**Figure 3.12 Epinephrine does not exhibit a concentration-dependent displacement of the radioantagonist [<sup>3</sup>H]NMS from the orthosteric binding site of both the M<sub>2</sub> wt and triple mutant receptor.** Equilibrium binding of epinephrine against [<sup>3</sup>H]NMS (0.2nM) in in CHO-hM<sub>2</sub> wild type (black) and triple mutant (red) cell membranes. Epinephrine at moderate concentrations is unable to displace the antagonist [<sup>3</sup>H]NMS at both the M<sub>2</sub> wild type and triple mutant receptors. Non-specific binding was determined by addition of atropine (10μM). The open symbols for M<sub>2</sub> wt (black) and M<sub>2</sub> triple mutant (red) at the concentration of 1 mM epinephrine depict non-specific effects. Shown are the mean values ± S.E.M of four experiments performed in triplicates and analysed by the four parameter logistic function.

[<sup>3</sup>H]NMS equilibrium binding studies were conducted whereby epinephrine would compete with the radio-labelled antagonist [<sup>3</sup>H]NMS for the orthosteric site. From the 1nM to 100μM increase in epinephrine, effects on [<sup>3</sup>H]NMS-binding were not significantly different to the buffer signal. This shows that epinephrine was unable to displace [<sup>3</sup>H]NMS in a concentration-dependent manner at both the M<sub>2</sub> wild type and the M<sub>2</sub> triple mutant receptors. At the highest concentration of epinephrine (1mM) investigated, about 50% of radioligand



displacement was observed. Notably, there was a colour change observed in the experimental setting from clear to orange for epinephrine (1mM) at both the M<sub>2</sub> wild type and triple mutant receptors. Therefore, at epinephrine (1mM) the effects were adjudged to be non-specific (**Figure 3.12**).

Having failed to determine orthosteric binding of epinephrine at the inactive M<sub>2</sub> triple mutant receptor bound to [<sup>3</sup>H]NMS, the recently published and now commercially available high affinity radioagonist [<sup>3</sup>H]Iperoxo (Schrage *et al.*, 2014) was utilised to probe binding of epinephrine. A radioagonist such as [<sup>3</sup>H]Iperoxo would therefore, enable direct probing of activation-related conformational transitions induced by epinephrine at the M<sub>2</sub> triple mutant receptor, which cannot be captured by a radioantagonist [<sup>3</sup>H]NMS. Thus, [<sup>3</sup>H]Iperoxo equilibrium binding studies were carried out in competition with increasing concentrations of epinephrine. Epinephrine was unable to cause any significant displacement of [<sup>3</sup>H]Iperoxo at the M<sub>2</sub> wild type receptor. Interestingly, epinephrine was able to completely displace [<sup>3</sup>H]Iperoxo at the M<sub>2</sub> triple mutant receptor ( $pIC_{50} = 4.24 \pm 0.13$ ) (**Figure 3.13**). Hence, this data suggest that epinephrine is able to gain access into the orthosteric binding site of the active M<sub>2</sub> triple mutant receptor.

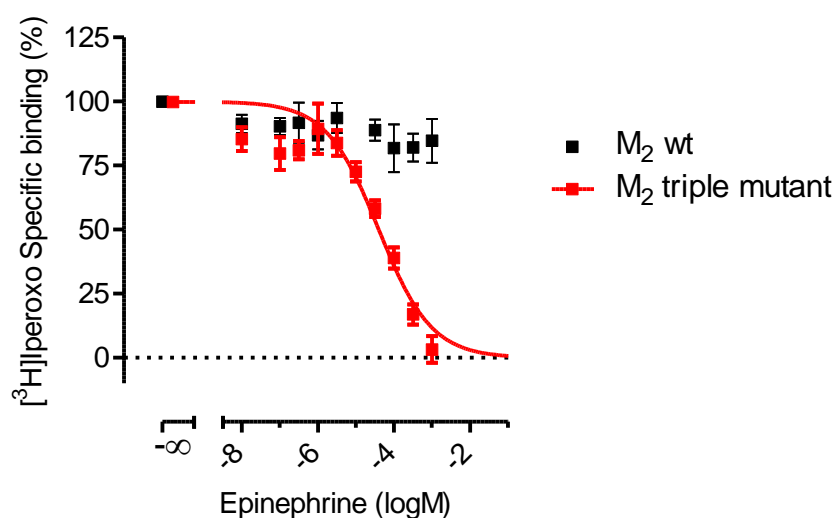


**Figure 3.13 Epinephrine displaces binding of the radioagonist [<sup>3</sup>H]Iperoxo from the orthosteric binding site at the M<sub>2</sub> triple mutant receptor.** Equilibrium binding of epinephrine against [<sup>3</sup>H]Iperoxo (1nM) in CHO-hM<sub>2</sub> wild type (black) and triple mutant (red) cell membranes. Non-specific binding was determined by addition of atropine (10μM). There is no significant difference between the specific binding of [<sup>3</sup>H]Iperoxo at increasing concentrations of epinephrine compared to buffer signal at the M<sub>2</sub> wt receptors (black) (One-way Anova, Dunnett's Multiple Comparison Test).  $pIC_{50}$  of epinephrine at the M<sub>2</sub> triple mutant receptor is  $4.24 \pm 0.13$ . Shown are the mean values  $\pm$  S.E.M 4-5 experiments performed in triplicates and analysed by the four parameter logistic function.

### 3.3.2 Epinephrine partially activates [<sup>35</sup>S]GTPγS binding

After observing the displacement of [<sup>3</sup>H]Iperoxo by epinephrine at the M<sub>2</sub> triple mutant receptor, a functional assay was employed to find out if epinephrine would be able to activate the M<sub>2</sub> triple mutant receptor. The [<sup>35</sup>S]GTPγS binding assay was used to probe the ability of epinephrine in activating the G<sub>i/o</sub> signalling pathway at the M<sub>2</sub> triple mutant receptor. Epinephrine was able to partially activate the M<sub>2</sub> triple mutant receptor. This is shown by a 26% maximum activation of the epinephrine-induced [<sup>35</sup>S]GTPγS binding (**Figure 3.14b and Table 3.10**). Epinephrine mediated [<sup>35</sup>S]GTPγS binding could not be observed at the M<sub>2</sub> wt receptors and in the non-transfected CHO membranes (**Figure 3.14 a and c**). These data suggested that the epinephrine induced signal observed was mediated only through the M<sub>2</sub> triple mutant receptor.

To verify the partial agonism exhibited by epinephrine, an M<sub>2</sub> receptor partial agonist pilocarpine was used as a comparison. The pEC<sub>50</sub> values of  $5.91 \pm 0.17$  and  $5.96 \pm 0.11$  for pilocarpine and epinephrine respectively at the M<sub>2</sub> triple mutant, did not differ significantly. Interestingly, the potency of the endogenous agonist acetylcholine (pEC<sub>50</sub>= $5.49 \pm 0.07$ ) did not differ significantly from potencies of either pilocarpine or epinephrine, at the M<sub>2</sub> triple mutant (**Table 3.10**). Therefore, this data show that epinephrine is able to activate the M<sub>2</sub> triple mutant receptor with similar potency to that displayed by a typical muscarinic partial agonist and also the endogenous ligand acetylcholine at the M<sub>2</sub> wild type receptor.

However, as shown in (chapter 3.2.2.1) pilocarpine lost nearly half of its capability in activating the M<sub>2</sub> wt receptor when applied at the M<sub>2</sub> triple mutant. There was about a 43% decrease in the maximum effect of pilocarpine at the M<sub>2</sub> triple mutant compared to the M<sub>2</sub> wild type receptor. The maximum effect stimulated by both epinephrine and pilocarpine at the M<sub>2</sub> triple mutant (E<sub>max</sub> 26% and 28%, respectively) did not differ significantly (**Figure 3.14b and Table 3.10**). Hence, epinephrine exhibited a similar capability as that of pilocarpine in activating the M<sub>2</sub> triple mutant receptor.

To measure how efficient epinephrine binding is transduced into a G<sub>i/o</sub> mediated response at the M<sub>2</sub> triple mutant, the signalling efficacy which can be measured by the transducer constant ( $\tau$ ) was deduced from the [<sup>35</sup>S]GTPγS binding data. The endogenous full agonist acetylcholine produced very strong positive Log  $\tau$  values of  $1.3 \pm 0.17$  and  $1.7 \pm 0.04$  for the M<sub>2</sub> wt and M<sub>2</sub> triple mutant, respectively. On the other hand, pilocarpine had a lower signalling efficacy (Log  $\tau = -0.007 \pm 0.06$ ) at the M<sub>2</sub> wt. This resembled the signal transduction efficiency induced by a partial agonist. At the M<sub>2</sub> triple mutant, pilocarpine

produced a more negative Log  $\tau$  value of  $-0.4 \pm 0.06$  compared to the M<sub>2</sub> wild type receptor. A more negative Log  $\tau$  value signifies very weak ligand-induced transduction efficiency, consequently making pilocarpine a very weak partial agonist at the M<sub>2</sub> triple mutant. The Log  $\tau$  value for epinephrine at the M<sub>2</sub> triple mutant was  $-0.5 \pm 0.12$ . The signalling efficacy induced by epinephrine was not significantly different from that of pilocarpine at the M<sub>2</sub> triple mutant. Hence, these data reinforce the findings that epinephrine acts as a partial agonists in the activation of the G<sub>i</sub>-proteins via the mutated M<sub>2</sub> receptor (**Figure 3.15 and Table 10**).

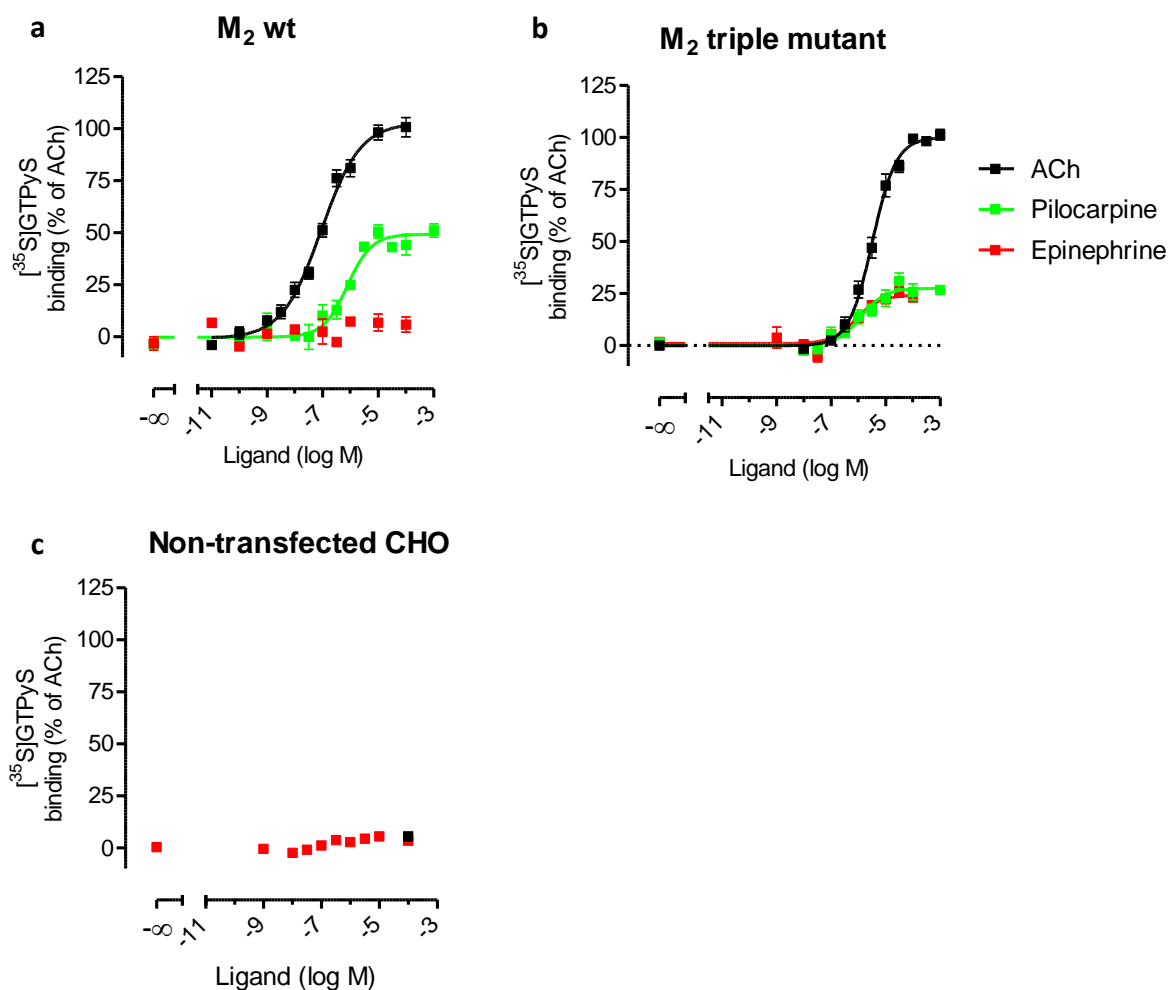


**Figure 3.14 Epinephrine partially activates the M<sub>2</sub> triple mutant receptor.** (a) [<sup>35</sup>S]GTP $\gamma$ S binding to membranes of CHO-hM<sub>2</sub> cells reveals partial activation of G<sub>i/o</sub> signalling mediated by the CHO-hM<sub>2</sub> wt receptor. (b) The partial activation of the G<sub>i/o</sub>-pathway induced by epinephrine (Epi) is comparable to that of a standard hM<sub>2</sub> receptor partial agonist pilocarpine (Pilo) at the M<sub>2</sub> triple mutant receptor. (c) Epinephrine is unable to induce [<sup>35</sup>S]GTP $\gamma$ S activation in non-transfected CHO membranes. The maximum [<sup>35</sup>S]GTP $\gamma$ S binding induced by ACh was set at 100% and the total binding [<sup>35</sup>S]GTP $\gamma$ S binding in the absence of a test-compound was set at 0%. The slope factor ( $n_H$ ) was 1 for each individual curve. Data shown are means  $\pm$  S.E.M of 3-10 experiments performed in triplicates.

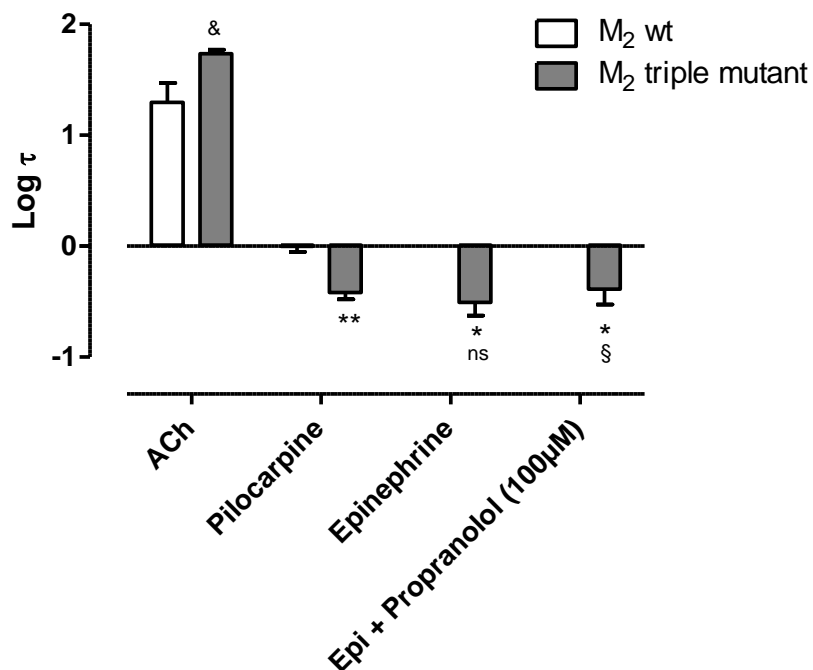


**Figure 3.15 Pilocarpine and epinephrine seems to be very weak partial agonist at the M<sub>2</sub> triple mutant.** Shown are coupling efficiencies (Log τ) of indicated ligands to stimulate [<sup>35</sup>S]GTPγS binding at the M<sub>2</sub> wt and triple mutant receptor. ACh M<sub>2</sub> wt Log τ acts as a control for the full agonist-induced signalling efficacy. Data shown are means ± S.E.M of 3-10 experiments performed in triplicates.

\*\*\*Significantly different from the log τ value of pilocarpine M<sub>2</sub> wild type (\*\*p=0.0035, \*p<0.05)

<sup>ns</sup>Not significantly different from the log τ value of pilocarpine M<sub>2</sub> triple mutant

§Not significantly different from the log τ value of epinephrine triple mutant

&Not significantly different from the log τ value of acetylcholine M<sub>2</sub> wild type

Statistics performed by Student's t-test

<b>[<sup>35</sup>S]GTPγS binding – G<sub>i/o</sub> activation</b>						
<b>Ligand</b>	<b>pEC<sub>50</sub></b> <b>(n<sub>H</sub>)</b>		<b>%E<sub>max</sub></b>		<b>Log τ</b>	
	<b>M<sub>2</sub> wt</b>	<b>M<sub>2</sub> triple mutant</b>	<b>M<sub>2</sub> wt</b>	<b>M<sub>2</sub> triple mutant</b>	<b>M<sub>2</sub> wt</b>	<b>M<sub>2</sub> triple mutant</b>
Acetylcholine	7.07 ± 0.05 (0.59 ± 0.09)	5.49 ± 0.07 <sup>###</sup>	100 ± 0.13	100 ± 0.08	1.3 ± 0.17	1.7 ± 0.04
Iperoxo	9.52 ± 0.09	7.96 ± 0.13 <sup>###</sup> (0.56 ± 0.09)	100 ± 0.004	99 ± 1.04 <sup>ns</sup>	-	-
Pilocarpine	6.10 ± 0.15	5.91 ± 0.17 <sup>§</sup>	49 ± 4	28 ± 3.0	-0.007 ± 0.06	-0.4 ± 0.06
Epinephrine (Control) (n=10)	-	5.96 ± 0.11 <sup>§,°</sup>	-	26 ± 1.0	-	-0.5 ± 0.12
Control for (+Atr 10μM)	-	6.10 ± 0.22	-	24 ± 2.3	-	-
Control for (+ Prop 100μM)	-	6.40 ± 0.15	-	22 ± 1.0	-	-
Control for (+ PTX)	-	5.86 ± 0.14	-	29 ± 1.6	-	-
Epinephrine (+Atropine 10μM)	-	4.20 ± 0.23	-	22 ± 2.0 <sup>ns</sup>	-	-
Epinephrine (+Propranolol 100μM)	-	6.90 ± 0.17 <sup>&amp;</sup>	-	25 ± 1.4 <sup>ns</sup>	-	-0.4 ± .14

**Table 3.10 [<sup>35</sup>S]GTPγS binding as a functional measure of G<sub>i/o</sub> signaling.** pEC<sub>50</sub> is the negative logarithm of the ligand concentration required to induce half the maximal activation. E<sub>max</sub> shows the maximal activation effect induced by a ligand. n<sub>H</sub> indicates the slope factor of the regression curve. n<sub>H</sub> is 1 unless when stated in the table (F-test, p < 0.05). Data shown are means ± S.E.M of 3-10 experiments performed in triplicates. Statistical analysis performed by One-way Anova, Tukey's Multiple Comparison Test.

Atr = atropine and prop =propranolol.

%E<sub>max</sub> = percentage of ACh

<sup>ns</sup>Not significantly different from the E<sub>max</sub> of the respective control at the M<sub>2</sub> triple mutant

<sup>&</sup>Not significantly different from the pEC<sub>50</sub> of control for (+ prop 100μM)

<sup>###</sup> Significantly different from the pEC<sub>50</sub> of epinephrine at the M<sub>2</sub> wt (<sup>###</sup>p < 0.05)

<sup>°</sup> Not significant different from the pEC<sub>50</sub> of pilocarpine at the M<sub>2</sub> triple mutant

<sup>§</sup> Not significantly different from the pEC<sub>50</sub> of acetylcholine at the M<sub>2</sub> triple mutant

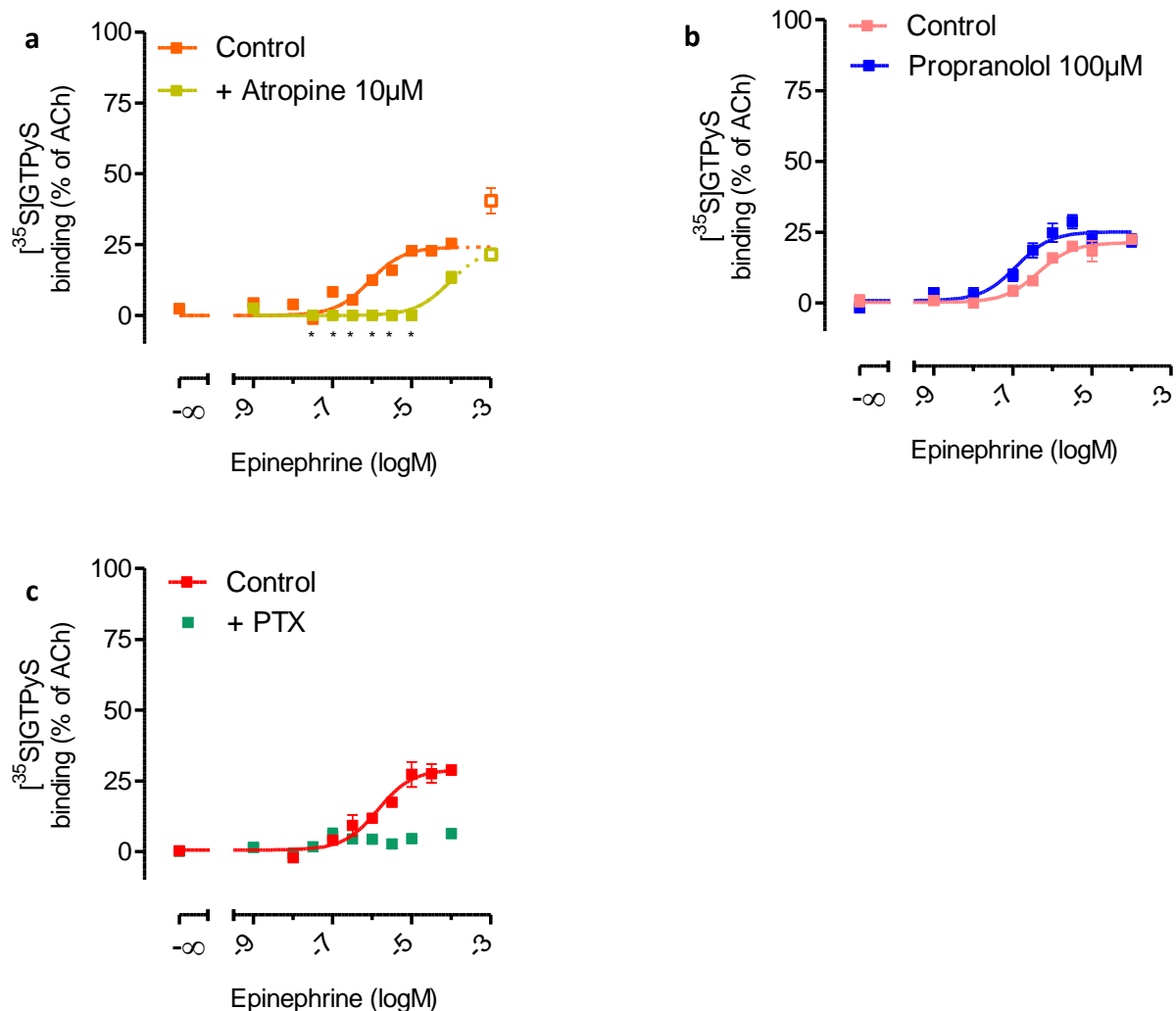


**Figure 3.16 Verification of the  $G_{i/o}$ -activation mediated by epinephrine at the  $M_2$  triple mutant.** (a) Atropine  $10\mu\text{M}$  antagonise epinephrine induced  $[^{35}\text{S}]\text{GTP}\gamma\text{S}$  binding to membranes of CHO-h $M_2$  triple mutant cells. (b) The beta blocker propranolol ( $100\mu\text{M}$ ) is unable to antagonise the epinephrine induced  $[^{35}\text{S}]\text{GTP}\gamma\text{S}$  binding. The  $\text{pEC}_{50}$  in the presence of propranolol ( $100\mu\text{M}$ ) is not significantly different from the control. (c)  $[^{35}\text{S}]\text{GTP}\gamma\text{S}$  binding to membranes of untreated CHO-h $M_2$  triple mutant cells (control) and pre-treated with PTX ( $100\text{ng/ml}$ ) reveal the sensitivity of epinephrine mediated signalling to a  $G_{i/o}$ -protein inhibitor. The maximum  $[^{35}\text{S}]\text{GTP}\gamma\text{S}$  binding induced by ACh was set at 100% and the  $[^{35}\text{S}]\text{GTP}\gamma\text{S}$  binding in the absence of a test-compound was set at 0%. The slope factor ( $n_H$ ) was not different from unity for each individual curve. Data shown are means  $\pm$  S.E.M of 3-10 independent experiments performed in triplicates.

To further verify if the epinephrine mediated  $G_{i/o}$ -signalling at the triple mutant was indeed through a muscarinic receptor, atropine which is a muscarinic receptor inverse agonists was employed. A rightward shift of the agonist curve would signal a competition binding between the agonist (epinephrine) and the inverse agonist or antagonist. Atropine (10  $\mu\text{M}$ ) antagonised the  $G_{i/o}$ -signal mediated by epinephrine. The curve shifted to the right at the highest concentrations studied of 100 $\mu\text{M}$  and 1mM. Concentrations of epinephrine lower than 100 $\mu\text{M}$  were not significantly different from the buffer signal in the presence of atropine and therefore were constrained to zero (buffer). The data points at 1mM epinephrine, though displayed in Figure 16a, were not included in the curve fitting for both the epinephrine control and in the presence of atropine. This was due to the 1mM epinephrine (control) data being out of sync with the rest of the curve data points. The rightward shift in potency of the [ $^{35}\text{S}$ ]GTP $\gamma\text{S}$  binding curve in the presence of atropine therefore suggests that epinephrine was able to activate the  $G_{i/o}$ -proteins through the  $M_2$  triple mutant muscarinic receptor (**Figure 3.16a**).

Propranolol which is a  $\beta$ -adrenoceptor antagonists was applied to the concentration-dependent effect of epinephrine observed in the [ $^{35}\text{S}$ ]GTP $\gamma\text{S}$  binding assay. Propranolol (100  $\mu\text{M}$ ) was used and could not antagonize the epinephrine induced signalling. The control curves (epinephrine only) and in the presence of propranolol did not differ significantly. The maximal efficacy and the potency of epinephrine signaling in both the presence and absence of propranolol (100  $\mu\text{M}$ ) were not significantly different (**Figure 3.16b and Table 3.10**). Hence, these data reflects that propranolol was not able to antagonise the epinephrine induced signal, ruling out any possibilities of the signal being somehow mediated by  $\beta$ -adrenoceptors.

The next step was to move from the receptor protein level and try to confirm the type of the G-protein mediating the epinephrine induced signal at a muscarinic receptor. In order to confirm that the signal produced by epinephrine was a  $G_{i/o}$ -mediated signal, we used membranes of CHO-h $M_2$  triple mutant cells treated with the  $G_{i/o}$ -protein inhibitor PTX (100ng/ml). Epinephrine failed to induce the binding of [ $^{35}\text{S}$ ]GTP $\gamma\text{S}$  in PTX-pretreated  $M_2$  triple mutant membranes (**Figure 3.16c**). This shows that the epinephrine-stimulated signal was indeed a partial activation of the  $G_{i/o}$ -proteins.

### 3.3.3 Epinephrine failed to activate DMR through the M<sub>2</sub> triple mutant receptor

The Dynamic Mass Redistribution (DMR) assay was used to investigate if epinephrine would be able to stimulate global cellular responses in live CHO cells stably transfected with the M<sub>2</sub> triple mutant receptor. In agreement with the hypothesis, epinephrine was unable to stimulate DMR activation in the M<sub>2</sub> wt cells (**Figure 3.17a**). Remarkably, epinephrine was also incapable of activating any significant DMR through G<sub>i/o</sub>-signalling at the M<sub>2</sub> triple mutant receptor in contrast to the G<sub>i</sub>-protein activation observed in the [<sup>35</sup>S]GTPγS binding (**Figure 17b**).

Surprisingly, pilocarpine also failed to activate DMR through the G<sub>i/o</sub> pathway at M<sub>2</sub> triple mutant cells (**Figure 3.17e**). In the M<sub>2</sub> wt cells pilocarpine did activate the G<sub>i/o</sub>-signalling as reflected by the positive DMR peak. In the presence of PTX (100ng/ml) to chemically knockout G<sub>i/o</sub> proteins, insignificant G<sub>s</sub>-signalling could be observed upon receptor stimulation by pilocarpine (**Figure 3.17d**). Therefore, both pilocarpine and epinephrine which displayed a partial agonistic behavior in the [<sup>35</sup>S]GTPγS assay could not activate DMR via the M<sub>2</sub> triple mutant receptor. Epinephrine could not stimulate any DMR in the CHO-non transfected cells lacking the M<sub>2</sub> triple mutant receptor (**Figure 3.17 f**). This provides further evidence for the absence of adrenoceptor-mediated signaling in the cells used to prepare the membranes for the [<sup>35</sup>S]GTPγS binding assay.



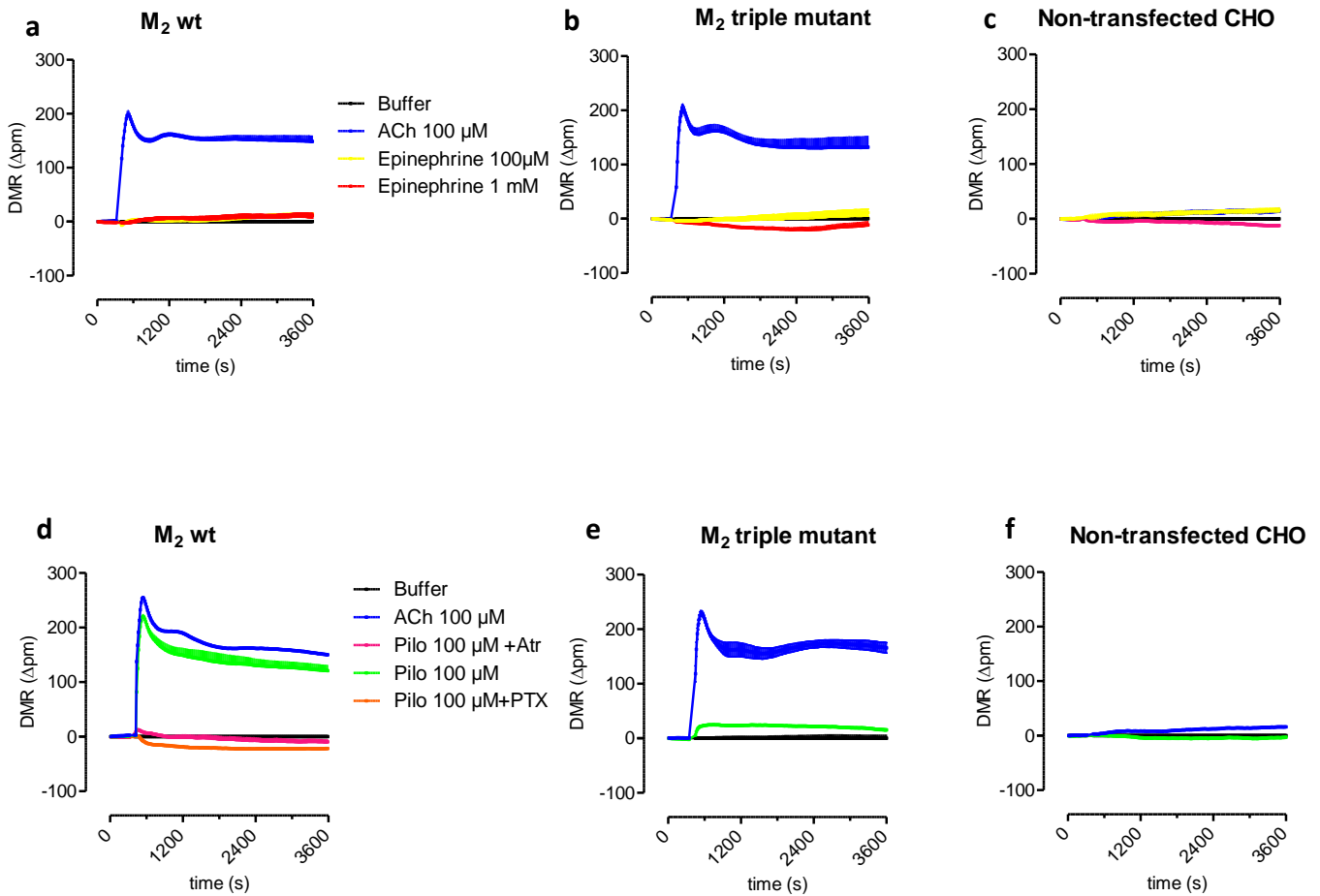


**Figure 3.17 Muscarinic partial agonist pilocarpine and epinephrine lack the ability to activate cellular DMR at the  $M_2$  triple mutant receptor.** (a-f) Baseline-corrected Dynamic mass redistribution (DMR) responses measured as wavelength shifts ( $\Delta$ pm) were measured over time after addition of (a-c) epinephrine and (d-f) pilocarpine in CHO-h $M_2$  wild type, triple mutant and non-transfected CHO cells. ACh (100 $\mu$ M) was used as a positive control of maximum activation. (d) Pretreatment of cells with the  $G_{i/o}$  inhibitor PTX (100ng/ml) for 18-24 hrs revealed  $G_s$  signaling shown as negative DMR ( $\Delta$ pm) and atropine (100 $\mu$ M) determine muscarinic receptor-mediated signaling. Positive and negative DMR ( $\Delta$ pm) display  $G_{i/o}$  and  $G_s$  signaling respectively. Shown are means and S.E.M of baseline-corrected data from one representative of at least four independent experiments conducted in quadruplicates.

### 3.3.4 Epinephrine is unable to bind to the allosteric binding site of the inactive M<sub>2</sub> wt and triple mutant receptor

Epinephrine was unable to cause a concentration-dependent displacement of the radioantagonist [<sup>3</sup>H]NMS from the orthosteric binding site at both the M<sub>2</sub> wt and the triple mutant receptor (**chapter 3.3.1 and Figure 3.12**). Therefore, it was intriguing to investigate if epinephrine would bind to the allosteric binding pocket of either the inactive M<sub>2</sub> wild type or triple mutant receptor. Dissociation binding experiments were carried out, whereby the orthosteric site was pre-occupied by [<sup>3</sup>H]NMS. A delay in the rate of [<sup>3</sup>H]NMS dissociation from the orthosteric binding site in the presence of a modulator, would reveal the allosteric capabilities of that modulator. First, the delay of [<sup>3</sup>H]NMS dissociation in the presence and absence of a concentration-dependent increase of epinephrine was investigated. Epinephrine was not able to cause any significant delay in the dissociation of [<sup>3</sup>H]NMS from the orthosteric site of both the M<sub>2</sub> wild type and triple mutant receptor. In comparison, W84 which is a typical allosteric modulator at the M<sub>2</sub> receptor was able to cause a delay of [<sup>3</sup>H]NMS at both the M<sub>2</sub> wild type and triple mutant receptor ( $pEC_{0.5,diss} = 5.66 \pm 0.03$  and  $3.13 \pm 0.16$  respectively) (**Figure 3.18a and b**).

As shown in chapter 3.1.1 and also from previously published studies (Tränkle *et al.*, 1996) the modes of allosteric interactions in [<sup>3</sup>H]NMS occupied M<sub>2</sub> receptors can be influenced by changes in experimental buffer conditions. Also, allosteric modulators were found to be more potent in low ionic strength buffers (Schröter *et al.*, 2000). Thus, the low ionic strength NaKP<sub>1</sub> buffer was employed to investigate if an M<sub>2</sub> receptor-epinephrine allosteric interaction could be yielded. An increase in the allosteric binding affinity of 1.89 and 1.92 log units for W84 at the M<sub>2</sub> wild type and triple mutant, respectively, was observed in the NaKP<sub>1</sub> buffer compared to the HEPES buffer (**chapter 3.1.1 and Table 3.11**). However, epinephrine was again unable to inhibit the dissociation rate of [<sup>3</sup>H]NMS at either the M<sub>2</sub> wild type or triple mutant even in a low ionic strength buffer (**Figure 3.18b**).

A full time-course [<sup>3</sup>H]NMS dissociation investigation was carried out to further probe if any allosteric effects mediated by epinephrine would be observed compared to only two time points of 5 and 10 minutes in (**Figure 3.18a and b**). Hence, the full time-course dissociation was carried out over a 20-minute dissociation time period in the presence and absence of a high concentration of epinephrine (1mM) at both the M<sub>2</sub> wild type and triple mutant receptor. The half-lives of [<sup>3</sup>H]NMS dissociation in the presence and absence of epinephrine either at

the  $M_2$  wild type or triple mutant did not differ significantly (**Figure 3.18c and Table 3.11**). In support of the 2-time-point kinetics results, epinephrine could not bind to the allosteric site of a [ $^3$ H]NMS occupied receptors even in a 20 min time-course dissociation assay.

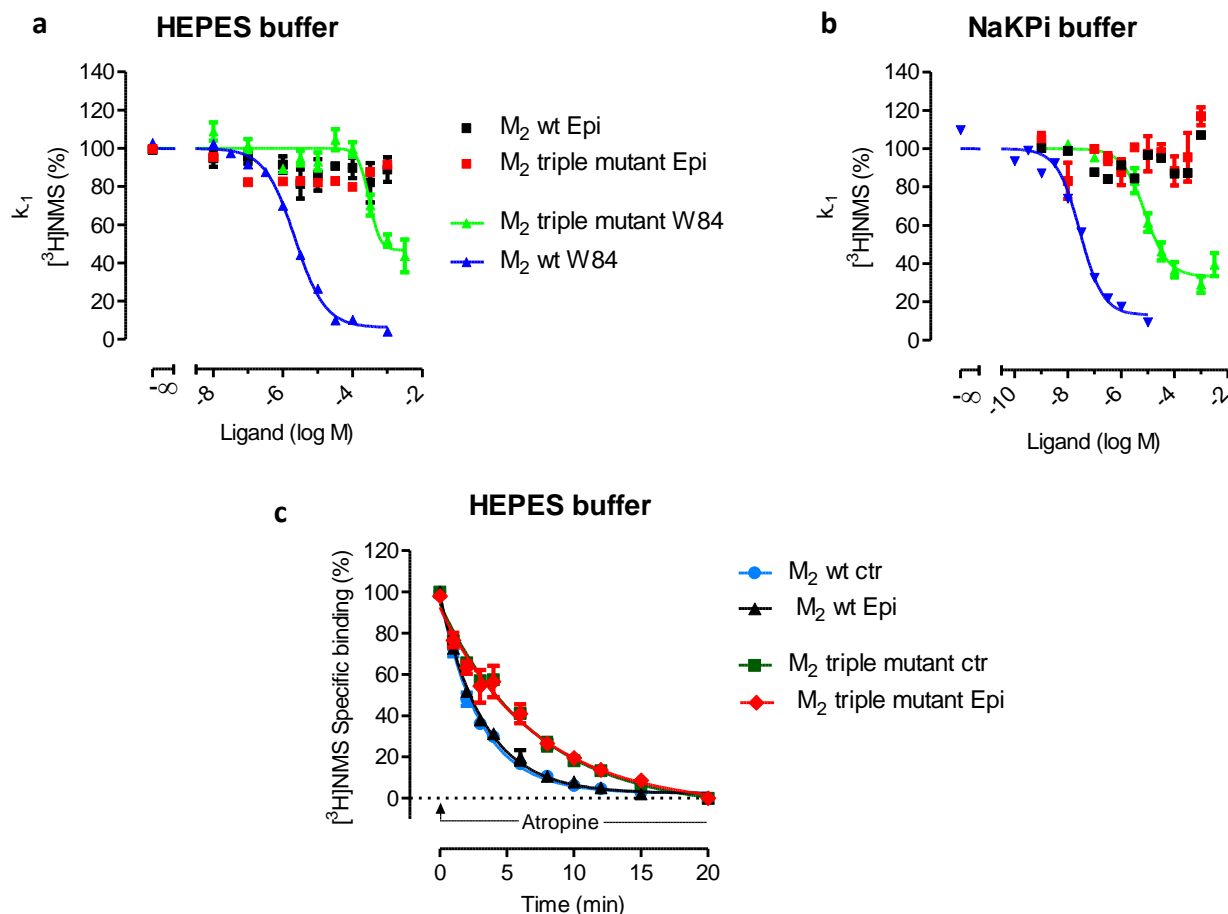


**Figure 3.18 Epinephrine does not retard the dissociation of the orthosteric antagonist [ $^3$ H]NMS from both the  $M_2$  wt and  $M_2$  triple mutant.** (a,b) Membranes of CHO-h $M_2$  cells were pre-labeled with 2nM [ $^3$ H]NMS and the dissociation rate of the labeled ligand was determined in the presence of increasing concentrations of either epinephrine (Epi) or W84. Experiments were conducted in (a) HEPES buffer and (b) NaKPi buffer, respectively. (c) Dissociation rate of the labeled ligand was determined in the presence and absence of Epinephrine (1mM). Atropine (10 $\mu$ M) was applied to prevent radioligand re-association in all experiments. The half-lives ( $t_{1/2}$ ) were derived from one phase exponential decay analysis of single experiments. (a,b) There is a no significant difference between the  $k_{-1}$  values of the  $M_2$  wt Epi and  $M_2$  triple mutant Epi in the presence of epinephrine compared with that of buffer only (One-way Anova analysis, Dunnett's Multiple Comparison Test). Indicated are mean values  $\pm$  S.E.M of 4 experiments performed in triplicates.

Ctr = control

<b>[<sup>3</sup>H]NMS dissociation binding</b>					
	<b>M<sub>2</sub> wt</b>	<b>M<sub>2</sub> triple mutant</b>	<b>ΔpEC<sub>0.5,diss</sub> (wildtype-mutant)</b>	<b>M<sub>2</sub> wt</b>	<b>M<sub>2</sub> triple mutant</b>
	<b>pEC<sub>0.5,diss</sub></b>			<b>t<sub>1/2</sub> (min)</b>	
W84- HEPES buffer	5.66 ± 0.03	3.13 ± 0.16	2.53 ± 0.11	-	-
W84- NaKPi buffer	7.55 ± 0.08 <sup>***</sup>	5.05 ± 0.12 <sup>***</sup>	2.50 ± 0.17	-	-
- Epinephrine (ctr)	-	-	-	2.04 ± 0.12	4.9 ± 0.12
+ Epinephrine (1mM)	-	-	-	2.25 ± 0.15 <sup>ns</sup>	4.98 ± 1.01 <sup>ns</sup>

**Table 3.11 Dissociation binding of [<sup>3</sup>H]NMS in the presence and absence of the allosteric modulator W84 or Epinephrine.** pEC<sub>0.5,diss</sub> indicates the negative logarithm of the concentration which causes half maximal delay of [<sup>3</sup>H]NMS dissociation. ΔpEC<sub>0.5,diss</sub> is the difference between the pEC<sub>0.5,diss</sub> values of the M<sub>2</sub> wt and triple mutant. Data was fitted based on a One phase exponential decay of [<sup>3</sup>H]NMS. Data shown are means ± S.E.M of four experiments performed in triplicates.

<sup>ns</sup>Not significantly different from the t<sub>1/2</sub> (min) of [<sup>3</sup>H]NMS dissociation in the presence of only atropine (-Epinephrine (ctr)). (Student's t-test)

<sup>\*\*\*</sup>Significantly different from the pEC<sub>0.5,diss</sub> obtained in the HEPES buffer (<sup>\*\*\*</sup>p < 0.0001 One-way Anova, Tukey's Multiple Comparison Test)

### 3.3.5 Other biogenic amines

#### 3.3.5.1 [<sup>35</sup>S]GTP $\gamma$ S binding

To probe our hypothesis that non-muscarinic biogenic amines should be able to gain access into the orthosteric site and activate the M<sub>2</sub> triple mutant, other biogenic amines dopamine, serotonin, histamine and norepinephrine were screened by a functional assay. The [<sup>35</sup>S]GTP $\gamma$ S binding assay was used to investigate the capabilities of the biogenic amines in activating the G<sub>i/o</sub> proteins at the M<sub>2</sub> triple mutant.

Histamine and serotonin were unable to activate the G<sub>i/o</sub> proteins at both the M<sub>2</sub> wt and M<sub>2</sub> triple mutant. Norepinephrine was studied at the M<sub>2</sub> triple mutant and in the non-transfected CHO cells lacking the M<sub>2</sub> receptors and a G<sub>i/o</sub> signal could not be observed. Dopamine was only investigated at the M<sub>2</sub> triple mutant and also no activation could be observed. Therefore, in contrast to epinephrine, the other biogenic amines dopamine, serotonin, histamine and norepinephrine failed to show a concentration-dependent activation of the [<sup>35</sup>S]GTP $\gamma$ S binding at the triple mutant receptor (**Figure 3.19**).

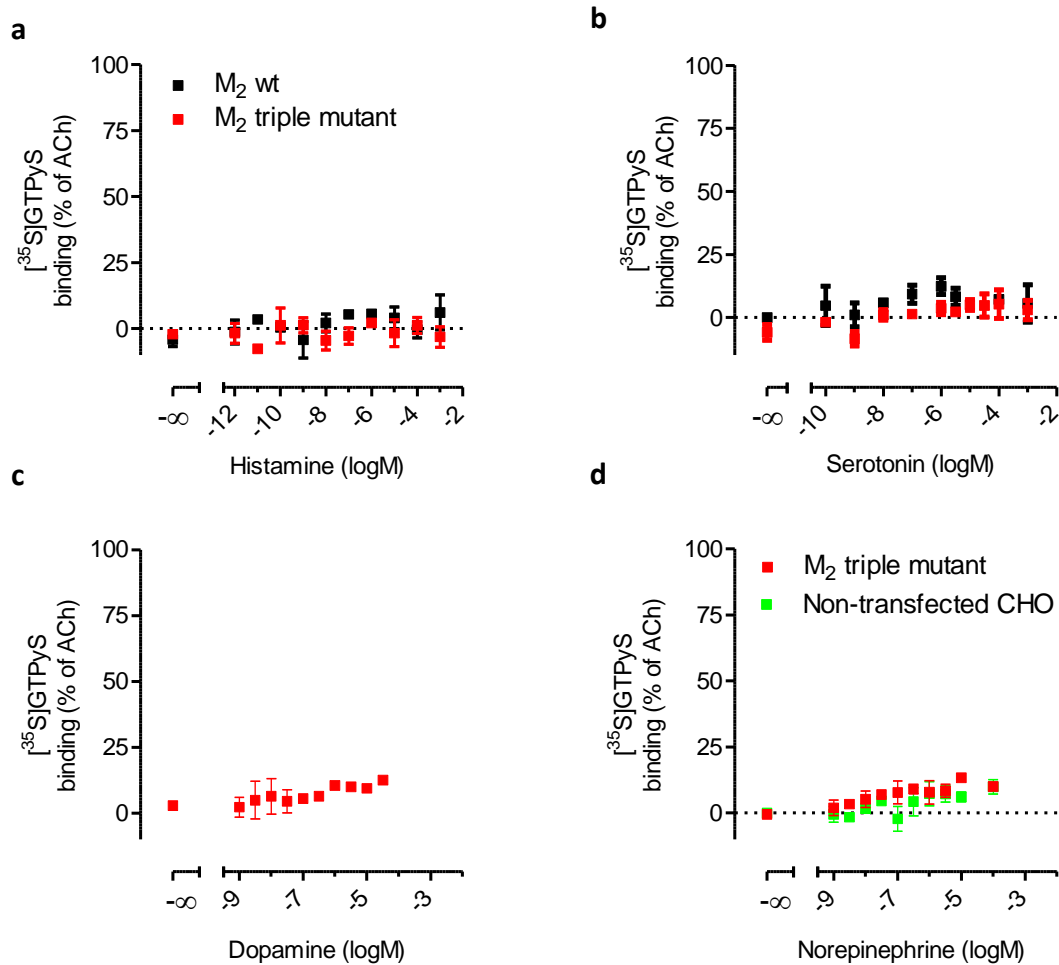


**Figure 3.19 Other biogenic amines appear to be unable to activate the  $\text{G}_{i/o}$  pathway at the  $\text{M}_2$  triple mutant receptor.**  $[^{35}\text{S}]\text{GTP}\gamma\text{S}$  binding to membranes of CHO-h $\text{M}_2$  cells stimulated by the biogenic amines serotonin, histamine, dopamine and norepinephrine does not reveal a concentration-dependent activation of  $\text{G}_{i/o}$  signaling at the  $\text{M}_2$  triple mutant receptor. The maximum  $[^{35}\text{S}]\text{GTP}\gamma\text{S}$  binding induced by ACh was set at 100% and the total binding  $[^{35}\text{S}]\text{GTP}\gamma\text{S}$  binding in the absence of a test-compound was set at 0%. Data shown are means  $\pm$  S.E.M of 2-4 experiments performed in triplicates.

### 3.3.5.2 Dynamic Mass redistribution (DMR)

Having failed to detect  $G_{i/o}$  signaling using the [ $^{35}$ S]GTP $\gamma$ S binding assay, a second functional assay was employed to see if the biogenic amines serotonin, histamine, dopamine and norepinephrine would contradict the results of the [ $^{35}$ S]GTP $\gamma$ S binding assay and produce some signalling at the  $M_2$  triple mutant. Here, the DMR assay was utilised to measure the global response of live CHO  $M_2$  wt and  $M_2$  triple mutant cells. Non-transfected CHO cells which are cells not transfected with both the  $M_2$  wt and the  $M_2$  triple mutant were used here as a negative control.

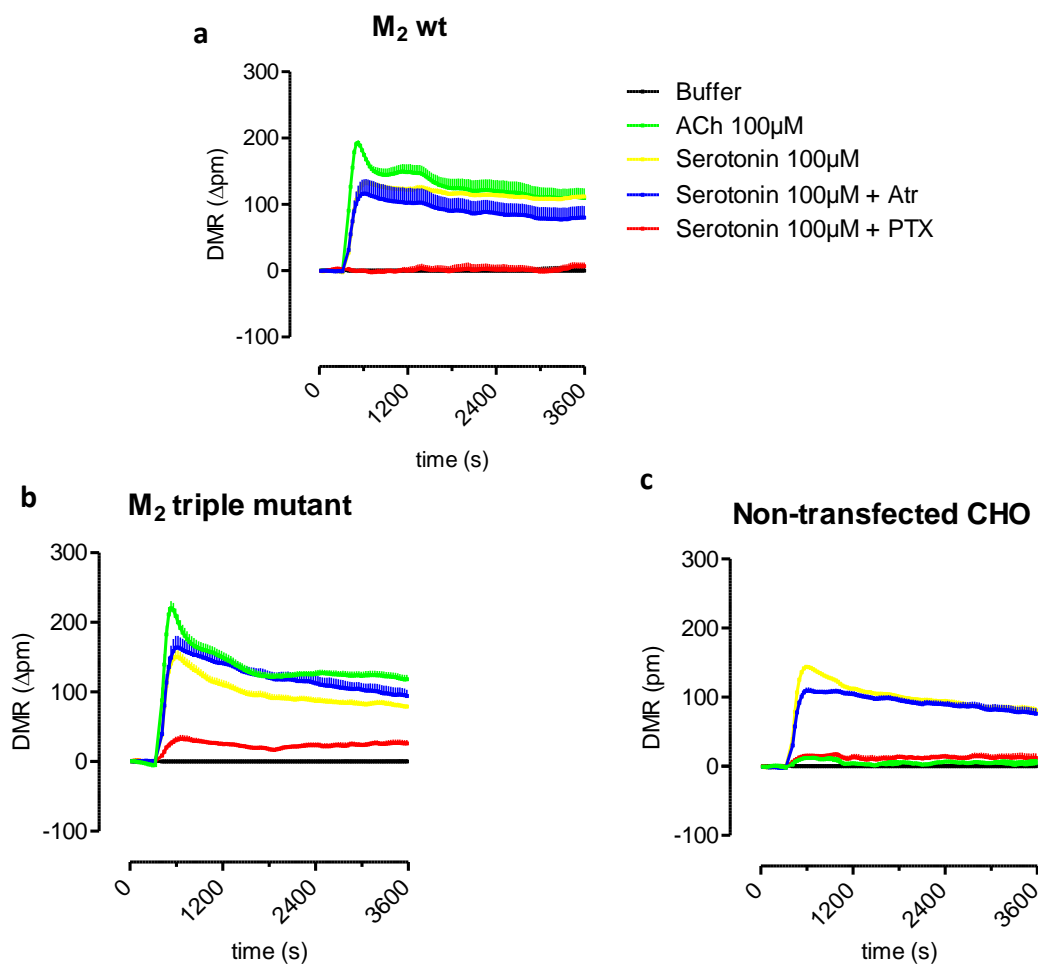


**Figure 3.20** There appears to be some serotonin receptors in the CHO-cells. Baseline-corrected Dynamic mass redistribution (DMR) responses measured as wavelength shifts ( $\Delta$ pm) were measured over time in (a)  $M_2$  wt (b)  $M_2$  triple mutant and (c) non-transfected CHO live cells. Serotonin (100 $\mu$ M) was used to stimulate activation. When indicated atropine 10 $\mu$ M (Atr) was used to block muscarinic mediated signaling. Cells were pretreated with PTX (100ng/ml) for 18-24 hrs to block  $G_{i/o}$  signaling. ACh (100 $\mu$ M) was used as a positive control of maximum activation. Positive DMR ( $\Delta$ pm) reflects  $G_{i/o}$ -signalling. Shown are means and S.E.M of baseline-corrected data from one representative of four independent experiments conducted in quadruplicates.

Serotonin 100 $\mu$ M was observed to be stimulating a DMR response in the M<sub>2</sub> wt cells. The signature of the positive DMR signal mediated by serotonin was characteristic of the M<sub>2</sub> receptor-mediated G<sub>i/o</sub> signalling. M<sub>2</sub> wt cell were pretreated with PTX (100ng/ml) to probe if the serotonin-induced signal was indeed via G<sub>i/o</sub> signalling. PTX blocked the serotonin mediated G<sub>i/o</sub> signal at the M<sub>2</sub> wt. However, G<sub>s</sub> signalling could not be detected in the absence of the G<sub>i/o</sub> signal. To explore if serotonin was signalling through the M<sub>2</sub> wt muscarinic receptor, atropine (10 $\mu$ M) which is a muscarinic receptor inverse agonist was applied. Atropine was unable to block the serotonin G<sub>i/o</sub>-mediated signal. This suggested that the identified G<sub>i/o</sub> signal was being mediated through another receptor other than a muscarinic M<sub>2</sub> wt receptor (**Figure 3.20a**).

In the M<sub>2</sub> triple mutant cells, similar results to those obtained in the M<sub>2</sub> wt cells were obtained. Again the G<sub>i/o</sub> signal in the M<sub>2</sub> triple mutant cells was insensitive to atropine, reflecting that it was not mediated through a muscarinic receptor (**Figure 3.20b**). CHO cells which were not transfected with either the M<sub>2</sub> wt or the triple mutant receptor were utilised to further identify if the G<sub>i/o</sub> signal could still be obtained in the absence of the M<sub>2</sub> wt and triple mutant receptors. The serotonin-mediated signal was indeed still present in the non-transfected CHO cells. The G<sub>i/o</sub> signal was similar in the presence and absence of atropine and could be quenched by the G<sub>i/o</sub> protein inhibitor PTX. Acetylcholine could not produce a signal in the non-transfected CHO cells, thereby confirming the absence of either the M<sub>2</sub> wt or the M<sub>2</sub> triple mutant receptors (**Figure 3.20c**). Hence, the presence of a serotonin induced signal in the non-transfected cells also supported the observation whereby atropine failed to quench the signal, that the G<sub>i/o</sub> signal was mediated by other non-muscarinic receptors present in the CHO cells.

Dopamine was also studied in the DMR assay to probe if it would yield some activation at the M<sub>2</sub> triple mutant in live cells. A significant dopamine-mediated signal was detected at the M<sub>2</sub> wt. This signal was blocked by the G<sub>i/o</sub> inhibitor PTX and also by the muscarinic inverse agonist atropine. This showed that somehow dopamine was producing a partial DMR signal through the M<sub>2</sub> wt receptor. However, this dopamine-stimulated DMR signal was different in shape to the expected characteristic G<sub>i/o</sub> signal produced by the typical muscarinic agonists at the M<sub>2</sub> receptor. It might be due to the fact that only a single concentration was studied here and that this signal might be a point somewhere on the signalling curve. Intriguingly, a dopamine mediated signal could not be observed in both the M<sub>2</sub> triple mutant and the non-transfected CHO cells. Acetylcholine still produced a G<sub>i/o</sub> signal at the M<sub>2</sub> triple mutant



showing that the receptors were still present and functional (**Figure 3.21**). Therefore, the data suggests that the  $G_{i/o}$  signal produced by dopamine in DMR was mediated only through the  $M_2$  wt receptor.

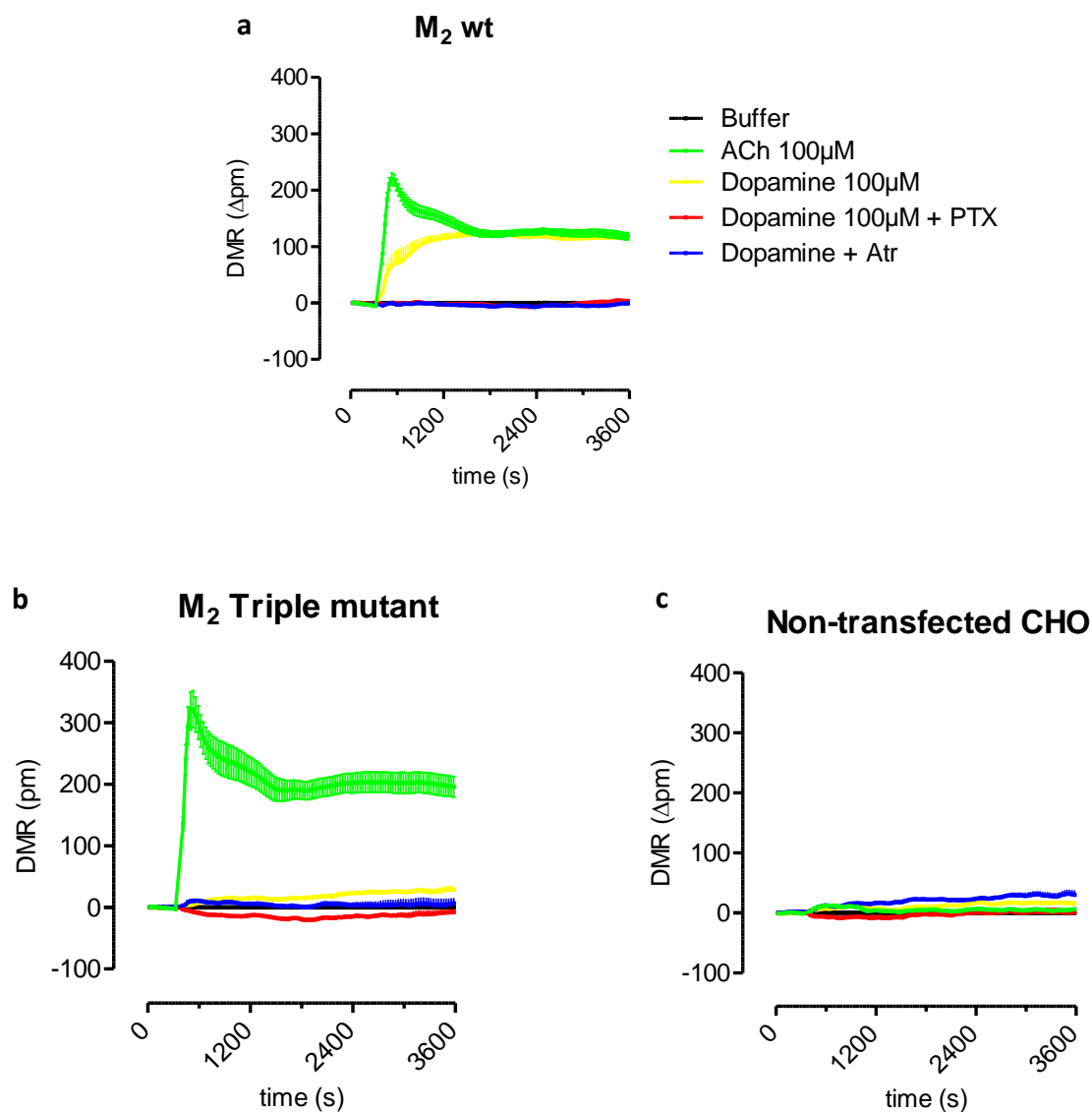


**Figure 3.21 Dopamine seems to stimulate an  $M_2$  wt-mediated  $G_{i/o}$  signal.** Baseline-corrected Dynamic mass redistribution (DMR) responses measured as wavelength shifts ( $\Delta$ pm) were measured over time in (a)  $M_2$  wt (b) triple mutant and (c) non-transfected CHO live cells. Dopamine (100 $\mu$ M) was used to stimulate activation. When indicated atropine 10 $\mu$ M (Atr) was used to block muscarinic mediated signaling. Cells were pretreated with PTX (100ng/ml) for 18-24 hrs to block  $G_{i/o}$  signalling. ACh (100 $\mu$ M) was used as a positive control of maximum activation. Positive DMR ( $\Delta$ pm) reflects  $G_{i/o}$ -signalling. Shown are means and S.E.M of baseline-corrected data from one representative of 4 independent experiments conducted in quadruplicates.

Histamine could not stimulate DMR activation either at the  $M_2$  wt or  $M_2$  triple mutant (**Figure 3.22**).

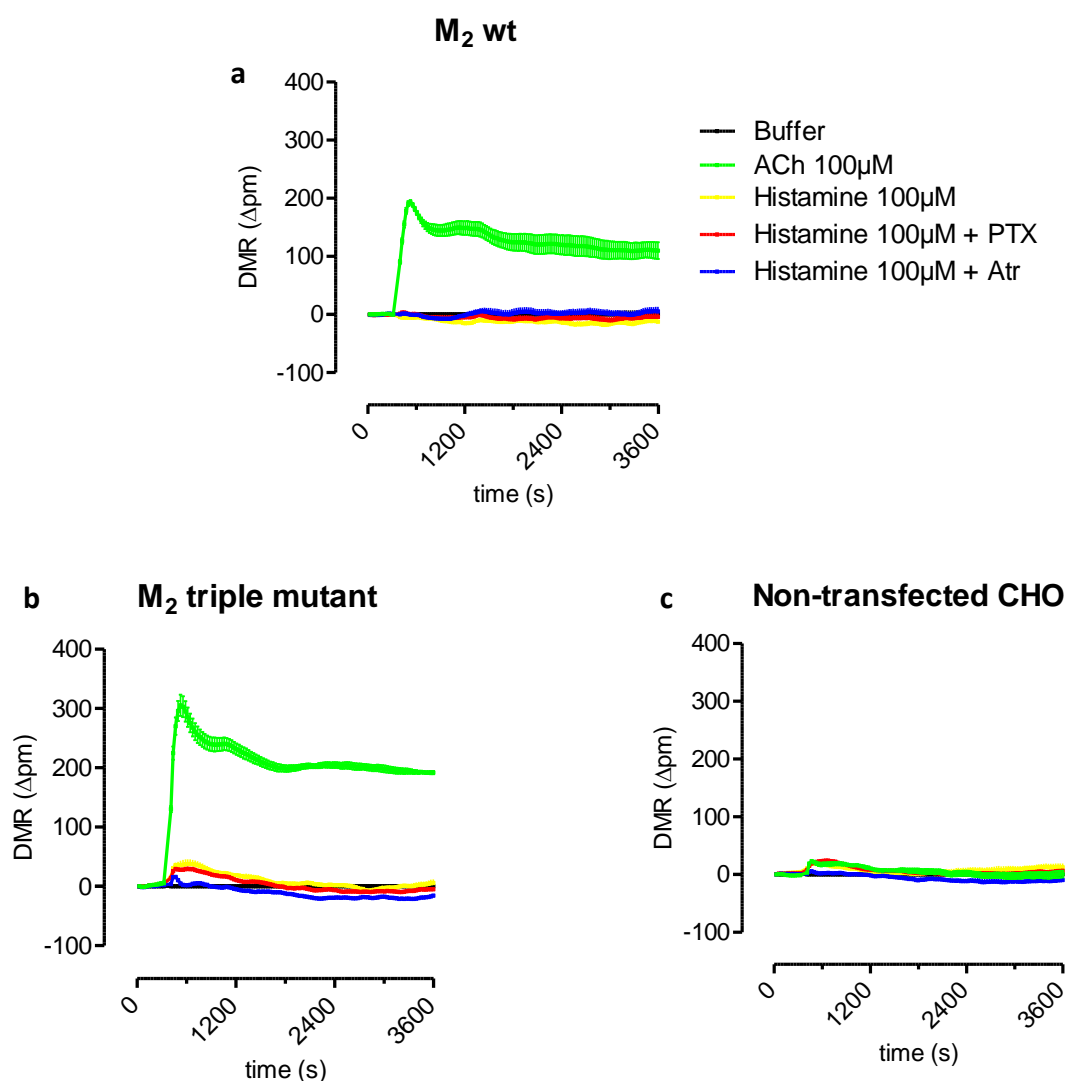


**Figure 3.22 Histamine does not activate DMR at both  $M_2$  wt and  $M_2$  triple mutant.** Baseline-corrected Dynamic mass redistribution (DMR) responses measured as wavelength shifts ( $\Delta$ pm) were measured over time in (a)  $M_2$  wt (b) triple mutant and (c) non-transfected CHO live cells. Histamine (100 $\mu$ M) was used to stimulate activation. Atropine 10 $\mu$ M was used to block muscarinic mediated signaling. Cells were pretreated with PTX (100ng/ml) for 18-24 hrs to block  $G_{i/o}$  signalling. ACh (100 $\mu$ M) was used as a positive control of maximum activation. Positive DMR ( $\Delta$ pm) reflects  $G_{i/o}$ -signalling. Shown are means and S.E.M of baseline-corrected data from one representative of four independent experiments conducted in quadruplicates.

### 3.3.5.3 [<sup>3</sup>H]NMS equilibrium binding against dopamine and histamine

The [<sup>3</sup>H]NMS equilibrium binding assay was conducted to investigate if some of the biogenic amines would interact with the orthosteric binding site of the M<sub>2</sub> triple mutant receptor. Histamine and dopamine although unable to stimulate [<sup>35</sup>S]GTPγS binding (**Figure 3.19**) and DMR activation (**Figure 3.21 and 3.22**) at both the M<sub>2</sub> wt and the M<sub>2</sub> triple mutant, were probed if they could displace [<sup>3</sup>H]NMS from the orthosteric binding site. The objective was to find out if histamine and dopamine were able to bind to the orthosteric binding site of the M<sub>2</sub> triple mutant receptor in CHO live cells regardless of being unable to stimulate receptor activation. A concentration-dependent histamine displacement of [<sup>3</sup>H]NMS could not be observed for both histamine and dopamine (**Figure 3.23 and 3.24**). For dopamine, the highest three concentration appeared to cause [<sup>3</sup>H]NMS displacement (**Figure 3.24**). On the other hand these three concentrations turned from clear in colour to brown in the experimental setting. Therefore, the results observed in these circumstances were deemed to be unspecific effects. Hence, as well as lacking the ability to activate a mutant muscarinic M<sub>2</sub> receptor, histamine and dopamine were also unable to compete with [<sup>3</sup>H]NMS for the orthosteric binding site of either the M<sub>2</sub> wt or the M<sup>2</sup> triple mutant receptor.

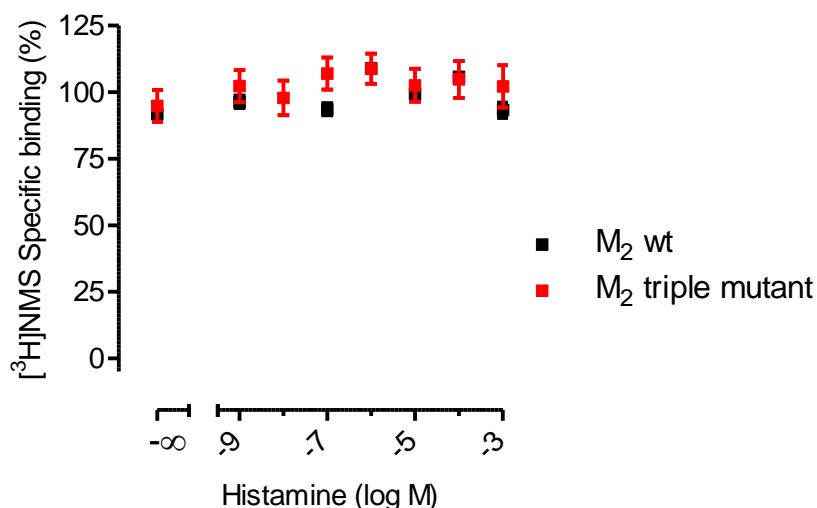


**Figure 3.23 Histamine is unable to bind to the orthosteric binding site of the M<sub>2</sub> wt and triple mutant receptor.** Equilibrium binding of [<sup>3</sup>H]NMS (0.2nM) against the biogenic amine histamine in CHO-hM<sub>2</sub> wild type (black) and triple mutant (red) intact cells. Non-specific binding was determined by addition of atropine (10μM). Shown are the mean values ± S.E.M of three experiments performed in triplicates and analysed by the four parameter logistic function.

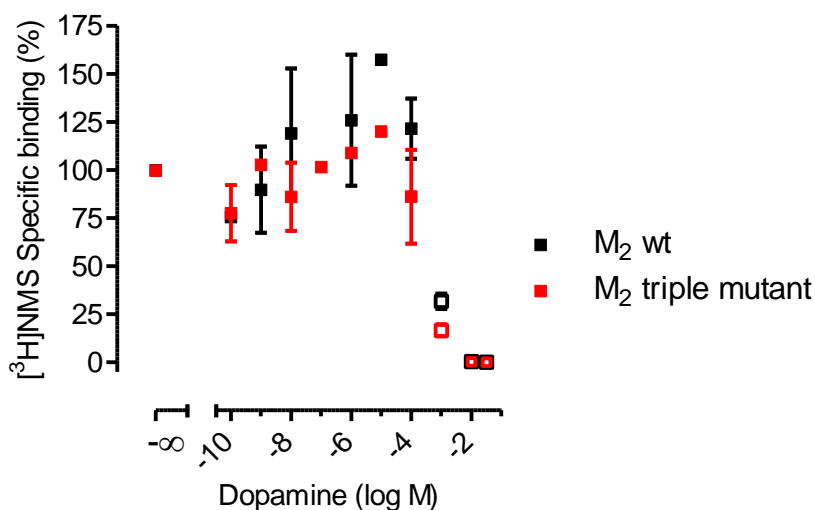


**Figure 3.24 Dopamine is unable to displace  $[^3\text{H}]\text{NMS}$  from the orthosteric site of either the  $\text{M}_2$  wt or  $\text{M}_2$  triple mutant receptor in a concentration-dependent manner.** Equilibrium binding of  $[^3\text{H}]\text{NMS}$  (0.2nM) against the biogenic amine dopamine in CHO-h $\text{M}_2$  wild type (black) and triple mutant (red) intact cells. Non-specific binding was determined by addition of atropine (10 $\mu\text{M}$ ). Open symbols reflect data points which changed colour in the experimental setting from clear solution (normal) to brown. Shown are the mean values  $\pm$  S.E.M of three experiments performed in triplicates and analysed by the four parameter logistic function.

#### 3.3.5.4 $[^3\text{H}]\text{Iperoxo}$ equilibrium binding against norepinephrine

Having obtained the displacement of the radioagonist  $[^3\text{H}]\text{Iperoxo}$  with epinephrine (**chapter 3.3.1 and Figure 3.13**), norepinephrine which only differs with epinephrine by a single methyl group was also probed to find out if it could displace  $[^3\text{H}]\text{Iperoxo}$ . The  $[^3\text{H}]\text{Iperoxo}$  equilibrium binding assay was used to find out if norepinephrine could be able to bind to the orthosteric site of an active  $\text{M}_2$  triple mutant receptor. A concentration-dependent displacement of  $[^3\text{H}]\text{Iperoxo}$  could not be observed at the  $\text{M}_2$  wt receptor. The concentrations of norepinephrine studied from the lowest concentration up to 100 $\mu\text{M}$  were not significantly different to the buffer signal. Only the 1mM concentration did cause a significant radioligand displacement of about 25%. At the  $\text{M}_2$  triple mutant, the 100 $\mu\text{M}$  and the 1mM concentrations caused a significant displacement of  $[^3\text{H}]\text{Iperoxo}$ . Therefore, the data suggests that at high concentrations norepinephrine is able to cause some significant displacement of the radioagonists  $[^3\text{H}]\text{Iperoxo}$  (**Figure 3.25**). On the other hand the displacement of  $[^3\text{H}]\text{Iperoxo}$

by epinephrine at the  $M_2$  triple mutant was incomplete, which can signify a high negative cooperativity between norepinephrine bound to the allosteric site against the orthosteric agonist [ $^3H$ ]Iperoxo.

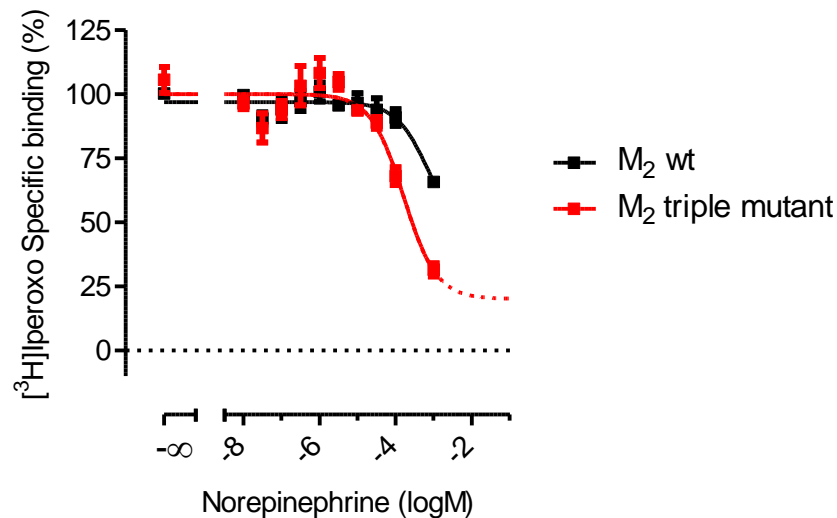


**Figure 3.25 Norepinephrine appears to cause a partial displacement of the agonist [ $^3H$ ]Iperoxo from the  $M_2$  triple mutant orthosteric binding site.** Equilibrium binding of [ $^3H$ ]Iperoxo (1nM) against a concentration-dependent increase of norepinephrine. Experiments were carried out in CHO-h $M_2$  wild type (black) and triple mutant (red) membranes. Non-specific binding was determined by addition of atropine (10 $\mu$ M). Shown are the mean values  $\pm$  S.E.M 4-5 experiments performed in triplicates and analysed by the four parameter logistic function.

### 3.3.5.5 Serotonin and histamine are unable to retard [ $^3H$ ]NMS dissociation

Two-point kinetic dissociation experiments whereby the orthosteric site was pre-occupied by [ $^3H$ ]NMS were carried out against serotonin and histamine. After failing to detect any binding of histamine to the orthosteric binding site, the objective here was to find out if the serotonin and histamine would interact with the allosteric binding site of either the  $M_2$  wt or the  $M_2$  triple mutant. A delay in the rate of [ $^3H$ ]NMS dissociation from the orthosteric binding site in the presence of a modulator would reveal the formation of ternary complexes of the receptor, [ $^3H$ ]NMS and the allosteric modulator. The dissociation experiments were carried out in an allosteric binding favourable NaKPi as shown in chapter 3.1.1. The aim was to enhance the chances of the biogenic amines studied to interact with the allosteric binding site of the muscarinic receptors. However, both serotonin and histamine were still unable to inhibit the dissociation of the radioligand [ $^3H$ ]NMS at either the  $M_2$  wt or the  $M_2$  triple mutant (**Figure 3.26**).

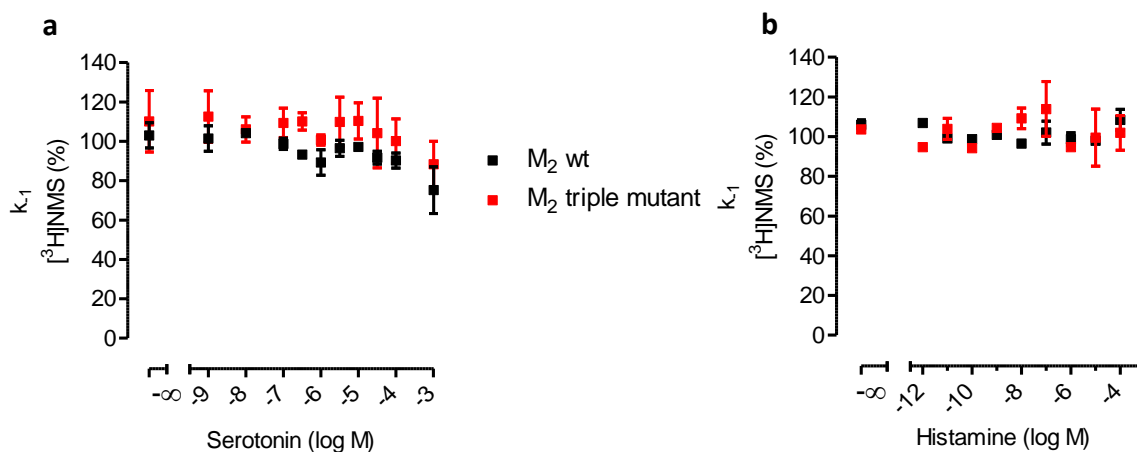


**Figure 3.26 Serotonin and histamine are unable to retard [<sup>3</sup>H]NMS dissociation.** Concentration-effect curves for the allosteric delay of [<sup>3</sup>H]NMS dissociation. CHO-hM<sub>2</sub> wt and triple mutant cell membranes were pre-labeled with [<sup>3</sup>H]NMS and the dissociation rate of the labeled ligand was determined in the presence of different concentrations of the allosteric modulator **(a)** serotonin and **(b)** histamine. Experiments were conducted in NaKPi buffer. Atropine (10μM) was applied to prevent radioligand re-association. The dissociation rate constant ( $k_{-1}$ ) was obtained from one phase exponential decay analysis of single experiments. Indicated are mean values  $\pm$  S.E.M of 4 experiments performed in triplicates.

### 3.4 Role of the M<sub>2</sub> receptor allosteric core region for orthosteric/allosteric binding cooperativity

#### 3.4.1 Allosteric moiety ligands

Dualsteric compounds are ligands which consist of two different pharmacophores (orthosteric and allosteric) linked by a carbon chain. Here, allosteric moieties 6-naph and 6-phth which only interact with the allosteric binding site where studied in radioligand equilibrium binding studies. The aim was to investigate the effects of the triple mutant on the orthosteric/allosteric binding cooperativity ( $\alpha'$ ) between the allosteric moieties of dualsteric ligands and the orthosteric radioligand [<sup>3</sup>H]NMS. Also, allosteric binding affinity (pK<sub>B</sub>) can be determined from [<sup>3</sup>H]NMS equilibrium binding studies.

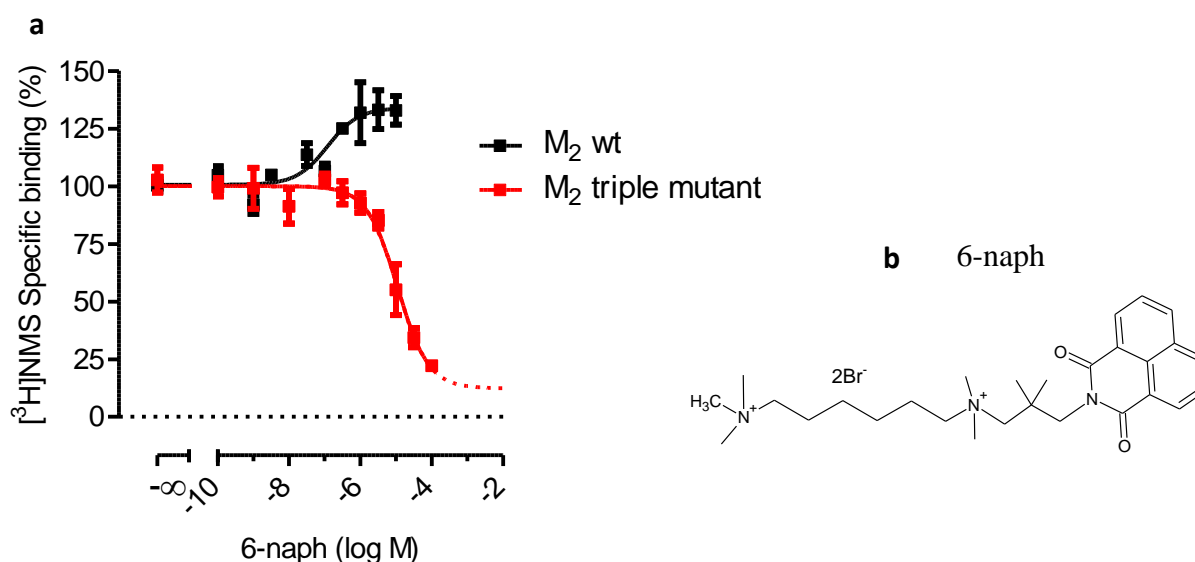


**Figure 3.27 The allosteric moiety 6-naph loses affinity and promotes [<sup>3</sup>H]NMS displacement at the M<sub>2</sub> triple mutant.** (a) Equilibrium binding of [<sup>3</sup>H]NMS (0.2nM) against increasing concentrations of the allosteric fragment 6-naph. Investigation was carried out using the membranes of the CHO M<sub>2</sub> wt and M<sub>2</sub> triple mutant cells. Non-specific binding was determined by atropine (10 $\mu$ M). Shown are the mean values  $\pm$  S.E.M of four experiments performed in triplicates and analysed by the four parameter logistic function. (b) Shows the structure of 6-naph.

The allosteric fragment 6-naph enhanced the binding of the orthosteric ligand [<sup>3</sup>H]NMS at the M<sub>2</sub> wt receptor thereby behaving as a positive allosteric modulator. The cooperativity ( $\alpha'$ ) between 6-naph and [<sup>3</sup>H]NMS at the M<sub>2</sub> wt was  $2.10 \pm 0.14$ . However, the signal was reversed at the M<sub>2</sub> triple mutant receptor whereby 6-naph ( $\alpha' = 0.05 \pm 0.03$ ) promoted [<sup>3</sup>H]NMS displacement from the orthosteric binding site. 6-naph could not cause a complete

[<sup>3</sup>H]NMS displacement at the M<sub>2</sub> triple mutant. About 15% of the radioligand remained bound on the M<sub>2</sub> triple mutant in equilibrium with saturating concentration of 6-naph (100μM) (**Figure 3.27 and Table 3.12**).

On the other hand the allosteric ligand 6-phth displayed negative cooperativity against the equilibrium binding of [<sup>3</sup>H]NMS at both the M<sub>2</sub> wt and triple mutant. At the M<sub>2</sub> triple mutant ( $pK_B = 3.84 \pm 0.07$ ), 6-phth lost 1.23 decades of binding affinity compared to the M<sub>2</sub> wt ( $pK_B = 5.07 \pm 0.03$ ). However, 6-phth displayed similar cooperativity against [<sup>3</sup>H]NMS equilibrium binding at both the M<sub>2</sub> wt ( $\alpha' = 0.06 \pm 0.01$ ) and M<sub>2</sub> triple mutant ( $\alpha' = 0.01 \pm 0.03$ ). Here, also the radioligand displacement binding was not complete at saturating concentrations reflecting that 6-phth functioned as an allosteric ligand at the M<sub>2</sub> triple mutant (**Figure 3.28 and Table 3.12**). It can also be noted that 6-naph is more affine than 6-phth at both the M<sub>2</sub> wt and M<sub>2</sub> triple mutant. 6-naph is about 1.7 and 1.5 log units more affine than 6-phth at the M<sub>2</sub> wt and triple mutant, respectively.

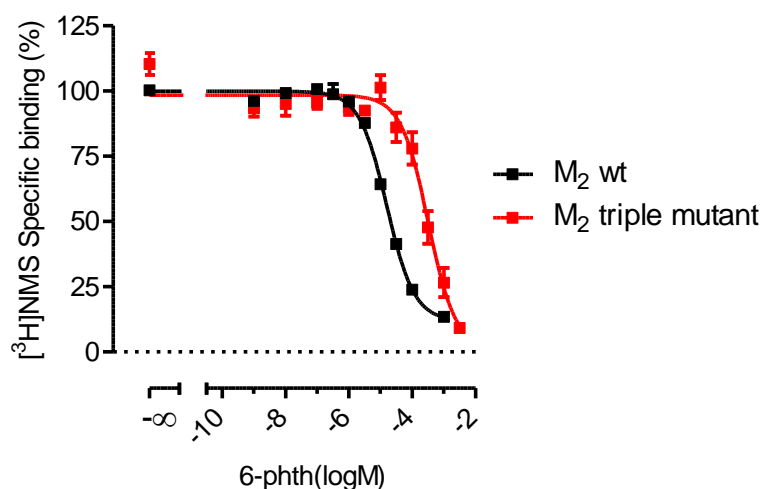


**Figure 3.28 The allosteric moiety 6-phth loses binding affinity at the M<sub>2</sub> triple mutant.** Equilibrium binding of [<sup>3</sup>H]NMS (0.2nM) against increasing concentrations of the allosteric fragment 6-phth. Investigation was carried out using the membranes of the CHO M<sub>2</sub> wt and triple mutant cells. Non-specific binding was determined by atropine (10μM). Shown are the mean values  $\pm$  S.E.M of at least four experiments performed in triplicates and analysed by the four parameter logistic function with a slope factor of -1.



<b>[<sup>3</sup>H]NMS equilibrium binding</b>			
	<b>M<sub>2</sub> wt</b>	<b>M<sub>2</sub> triple mutant</b>	<b>ΔpK<sub>A</sub></b> <b>(wildtype- mutant)</b>
	<b>pK<sub>B</sub> (α')</b>		
6-naph	6.77 ± 0.22 (2.10 ± 0.14)	5.35 ± 0.10 (0.05 ± 0.03)	1.42
6-phth	5.07 ± 0.03 (0.06 ± 0.01)	3.84 ± 0.07 (0.01 ± 0.03) <sup>ns</sup>	1.23

**Table 3.12 Equilibrium binding of the allosteric moieties of dualsteric ligands.** pK<sub>B</sub> represents the negative logarithm of affinity values for respective allosteric ligand at the unoccupied M<sub>2</sub> wt and M<sub>2</sub> triple mutant receptors. ΔpK<sub>B</sub> is the difference between the pK<sub>B</sub> values of the M<sub>2</sub> wt and triple mutant. α' is a measure of cooperativity between the inactive binding of the respective allosteric ligand and the radioligand [<sup>3</sup>H]NMS. Positive cooperativity is reflected by α' > 1. Data are means ± S.E.M of four experiments performed in triplicates.

<sup>ns</sup> Not significantly different from the α' at the M<sub>2</sub> wt (p < 0.05 Student's t-test).

### 3.4.2 Dualsteric ligands

Bock *et al.*, 2014 showed that two functionally distinct populations of the M<sub>2</sub> receptors coexist and can be stabilised by a single dualsteric ligand which exhibit dynamic ligand binding. This means the dualsteric ligand is capable of binding in two opposite orientations and stabilise either the active or inactive receptor conformation (**Figure 3.29**). Here, the aim was to investigate the importance of the allosteric core binding domain in determining the receptor fractional occupancies and preferred binding orientations of the dualsteric ligands. The dualsteric ligands probed were iper-6-phth, iper-6-naph, isox-6-phth and isox-6-naph. Iper-6-phth and iper-6-naph are composed of the muscarinic agonist iperoxo and (phth) part of the allosteric inverse agonist W84 or (naph) naphmethonium, respectively, bridged by a hexamethylene carbon chain linker. The 'isox' dualsteric ligands have isoxazole instead of iperoxo as the orthosteric agonist. [<sup>3</sup>H]NMS equilibrium binding data of these dynamic ligands was analysed by two methods, the Global analysis of 2 curves consisting of dualsteric ligand binding and allosteric moiety binding only and the Global analysis of 4 curves

consisting of the dualsteric ligand binding, allosteric moiety binding, dualsteric ligand [<sup>35</sup>S]GTPγS and acetylcholine [<sup>35</sup>S]GTPγS data. These two methods were used to find the active ( $K_A$ ) and inactive ( $K_B$ ) equilibrium binding constants of the dynamic ligands in order to determine the dualsteric ligand fractional occupancies and binding orientation ( $R_{pose}$ ) ratios.

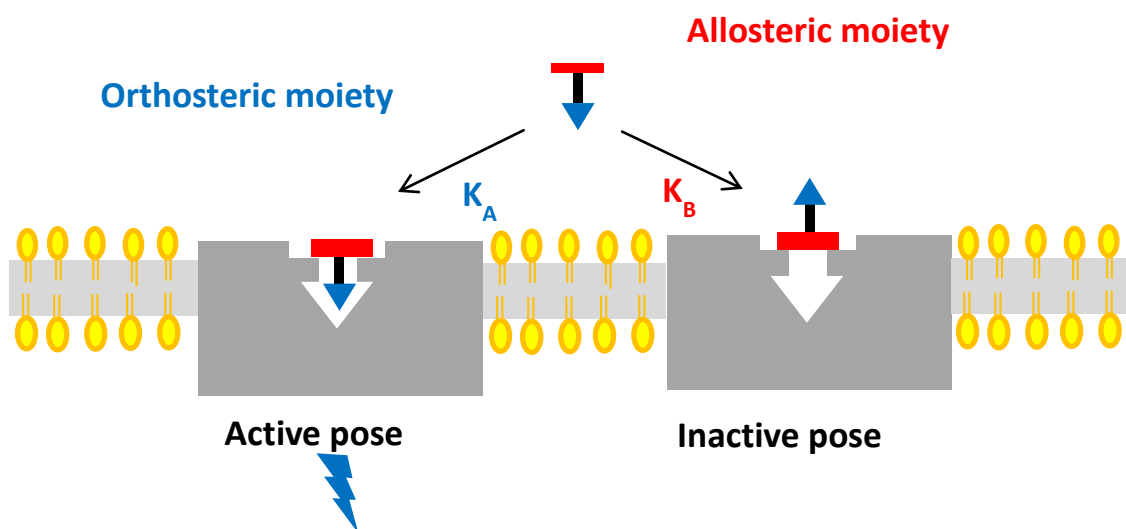


**Figure 3.29 Dualsteric ligands exhibit dynamic ligand binding.** The dualsteric pose stabilises the active receptor state whilst the purely allosteric orientation stabilises the inactive receptor state.  $K_A$  and  $K_B$  are equilibrium dissociation constants for the active and inactive binding poses. A dualsteric ligand consists of an allosteric moiety (red), carbon chain linker (black) and the orthosteric moiety (blue).

#### 3.4.2.1 [<sup>3</sup>H]NMS Equilibrium binding

Global analysis of dualsteric ligand and allosteric moiety binding only (Global analysis of 2 curves)

Iper-6-phth was more affine when binding in the dualsteric orientation ( $pK_A = 6.44 \pm 0.03$ ) than in the purely allosteric inactive pose ( $pK_B = 5.21 \pm 0.03$ ) at the  $M_2$  wt. The trend was also similar for the  $M_2$  triple mutant whereby iper-6-phth had a  $pK_A$  of  $5.50 \pm 0.06$  and  $pK_B$  of  $3.83 \pm 0.07$ . The inactive binding orientation of iper-6-phth displayed similar negative cooperativity with [<sup>3</sup>H]NMS at both the  $M_2$  wt ( $\alpha' = 0.05 \pm 0.03$ ) and  $M_2$  triple mutant ( $\alpha' = 0.01 \pm 0.03$ ) (**Figure 3.30 and Table 3.13**). The  $pK_A$  and  $pK_B$  values were used to calculate the fractional sizes of the active and inactive receptor populations (see **chapter 2.4.3.3** for equations). Results obtained show that the fraction of active receptor populations increased at the  $M_2$  triple mutant (98% active) compared to the  $M_2$  wt (94% active). Consequently, the receptor populations in the inactive pose decreased from 6% at  $M_2$  wt to 2% at the  $M_2$  triple mutant (**Figure 3.30b,d**).

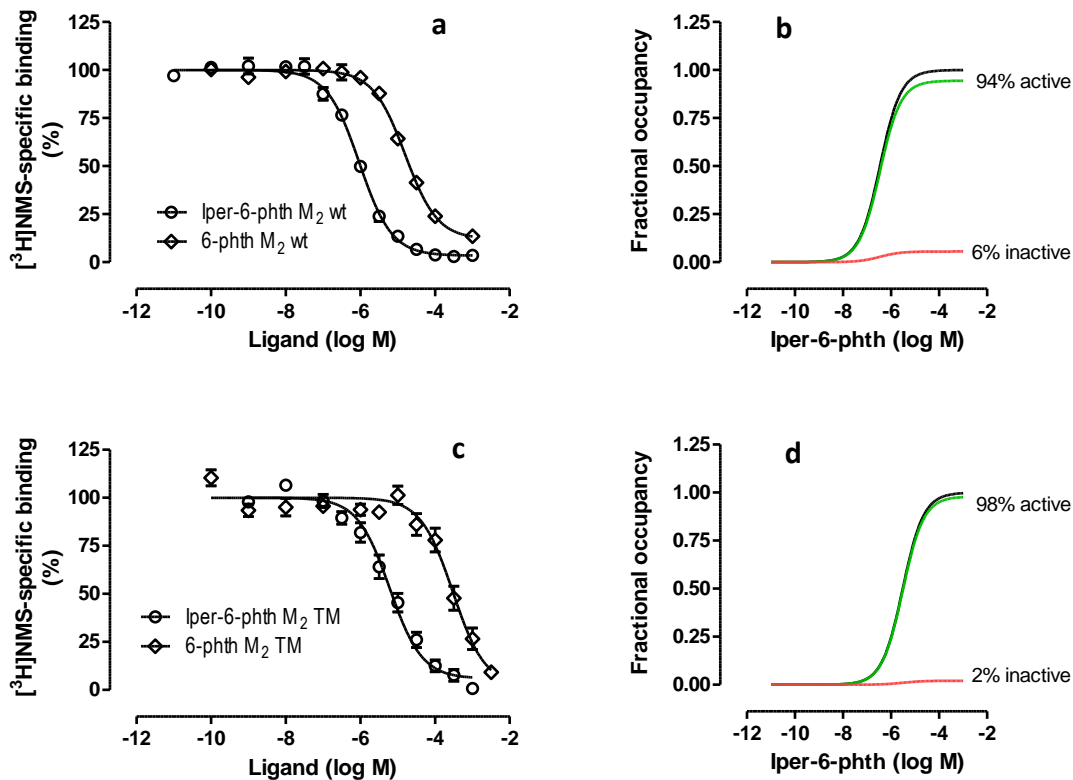


**Figure 3.30 M<sub>2</sub> triple mutant increases the amount of active receptor fractions occupied by iper-6-phth.** (a,c) Equilibrium binding of  $[^3\text{H}]\text{NMS}$  against the increasing concentrations of the allosteric ligand 6-phth and iper-6-phth at the (a) M<sub>2</sub> wt and (c) M<sub>2</sub> triple mutant (M<sub>2</sub> TM) receptors, respectively. (b,d) Fractional binding of the dynamic ligand iper-6-phth at the (b) M<sub>2</sub> wt and (d) M<sub>2</sub> triple mutant receptors, respectively. The total binding, receptor fractional occupancies in the active and inactive poses are shown in black, green and red, respectively. Experiments were conducted using the membranes of the CHO M<sub>2</sub> wt and triple mutant cells. Shown are the mean values  $\pm$  S.E.M of four experiments fitted by the Global analysis of 2 curves.

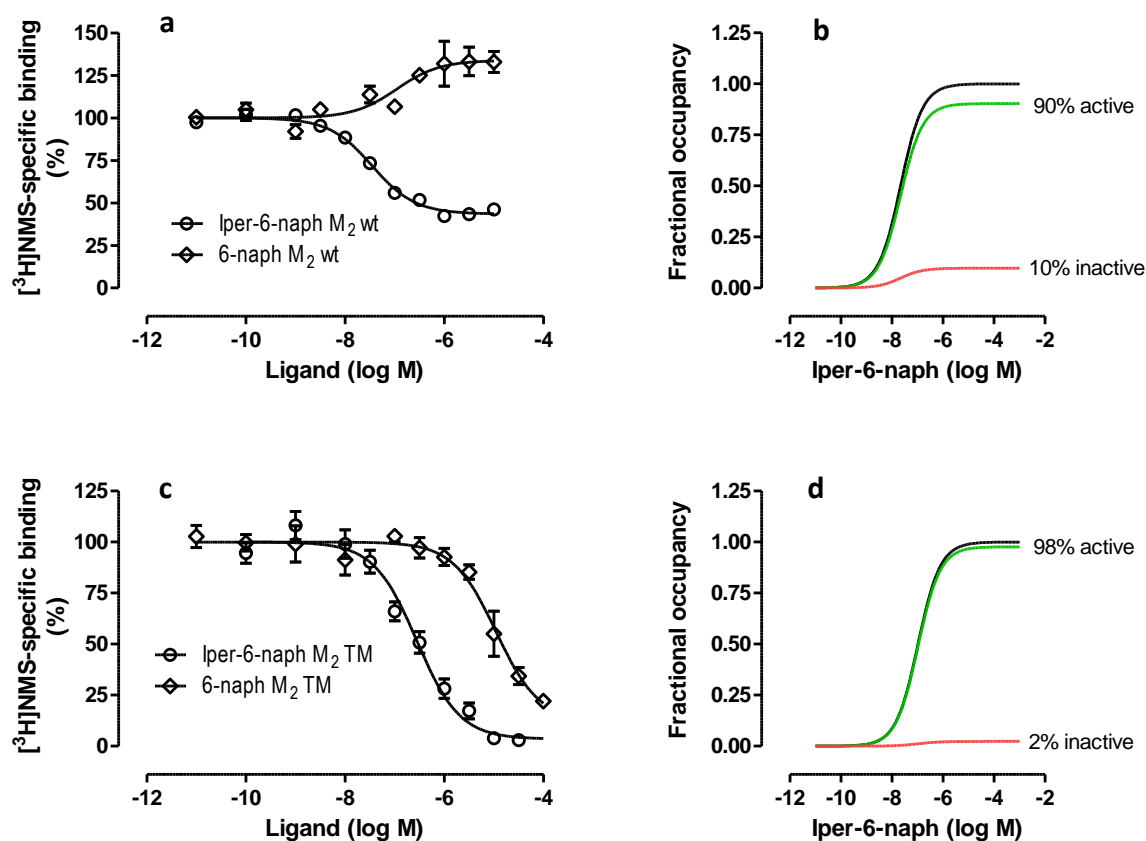


**Figure 3.31 M<sub>2</sub> triple mutant increases the amount of active receptor fractions stabilised by iper-6-naph.** (a,c) Equilibrium binding of  $[^3\text{H}]\text{NMS}$  against the increasing concentrations of the allosteric ligand 6-naph and iper-6-naph at the M<sub>2</sub> wt (a) and M<sub>2</sub> triple mutant (M<sub>2</sub> TM) (c) receptors, respectively. Fractional binding of the dynamic ligand iper-6-naph at the (b) M<sub>2</sub> wt (b) and triple mutant (d) receptors, respectively. The total binding, receptor fractional occupancies in the active and inactive poses are shown in black, green and red, respectively. Experiments were conducted using the membranes of the CHO M<sub>2</sub> wt and triple mutant cells. Non-specific binding was determined by atropine (10 $\mu\text{M}$ ). Shown are the mean values  $\pm$  S.E.M of four experiments performed in triplicates and fitted by the Global analysis of 2 curves.

Iper-6-naph was about 0.83 log units more affine in the dualsteric binding pose ( $\text{pK}_A = 7.60 \pm 0.11$ ) compared to the inactive binding pose ( $\text{pK}_B = 6.77 \pm 0.22$ ) at the M<sub>2</sub> wt. At the M<sub>2</sub> triple mutant there was a loss of about 1.62 log units of affinity of the dynamic ligand binding in the inactive pose ( $\text{pK}_B = 5.35 \pm 0.10$ ) compared to the active binding pose ( $\text{pK}_A = 6.97 \pm 0.06$ ). In contrast to iper-6-phth, the inactive binding orientation ratio of iper-6-naph displays positive cooperativity ( $\alpha' = 2.10 \pm 0.14$ ) with  $[^3\text{H}]\text{NMS}$  at the M<sub>2</sub> wt (**Figure 3.31 and Table 3.13**), just like its allosteric moiety 6-naph. At the M<sub>2</sub> triple mutant, iper-6-naph behaved

exactly the opposite by promoting the displacement of [<sup>3</sup>H]NMS ( $\alpha' = 0.05 \pm 0.03$ ). With iper-6-naph, the fraction of the active receptor populations increased from 90% at the M<sub>2</sub> wt to 98% at the M<sub>2</sub> triple mutant. Consequently, the population of receptors bound in the inactive orientation decreased from 10% at the M<sub>2</sub> wt to 2% at the M<sub>2</sub> triple mutant (**Figure 3.31b,d**).

<b>[<sup>3</sup>H]NMS equilibrium binding</b>				
	<b>M<sub>2</sub> wt</b>		<b>M<sub>2</sub> triple mutant</b>	
	<b>pK<sub>active</sub> (pK<sub>A</sub>)</b>	<b>pK<sub>inactive</sub> (pK<sub>B</sub>) (<math>\alpha'</math>)</b>	<b>pK<sub>active</sub> (pK<sub>A</sub>)</b>	<b>pK<sub>inactive</sub> (pK<sub>B</sub>) (<math>\alpha'</math>)</b>
Iper-6-phth	6.44 ± 0.03	5.21 ± 0.03 (0.05 ± 0.03)	5.50 ± 0.06	3.83 ± 0.07 (0.01 ± 0.03)
Iper-6-naph	7.60 ± 0.11	6.77 ± 0.22 (2.10 ± 0.14)	6.97 ± 0.06	5.35 ± 0.10 (0.05 ± 0.03)

**Table 3.13 Equilibrium binding of iper-6-phth and iper-6-naph ligands.** pK<sub>active</sub> and pK<sub>inactive</sub> represents the negative logarithm of the equilibrium dissociation constants of the active (dualsteric) and inactive (allosteric) binding poses, respectively.  $\alpha'$  is a measure of cooperativity between the inactive binding of the respective dualsteric ligand and the radioligand [<sup>3</sup>H]NMS. Positive cooperativity is reflected by  $\alpha' > 1$ . Data are means  $\pm$  S.E.M of four experiments performed in triplicates.

The dualsteric ligands with the less affine and less potent isoxazole orthosteric moiety in comparison to iperoxo were also probed for their binding properties at the M<sub>2</sub> triple mutant. The binding affinity of isox-6-phth in the active binding pose was observed to be (pK<sub>A</sub> = 5.51 ± 0.04) at the M<sub>2</sub> wt. This was about 0.44 log units more affine than the binding affinity of the inactive orientation (pK<sub>B</sub> = 5.07 ± 0.03) at the M<sub>2</sub> wt. The active binding pose lost about 0.87 log units whilst the inactive pose lost 1.23 log units of binding affinity at the M<sub>2</sub> triple mutant compared to the M<sub>2</sub> wt. The inactive binding orientation of isox-6-phth displayed negative cooperativity with [<sup>3</sup>H]NMS at both the M<sub>2</sub> wt ( $\alpha' = 0.06 \pm 0.01$ ) and M<sub>2</sub> triple mutant ( $\alpha' = 0.01 \pm 0.02$ ) (**Figure 3.32a,c and Table 3.14**). The fraction of the active receptor populations increased from 74% at the M<sub>2</sub> wt to 87% at the M<sub>2</sub> triple mutant. As a result, the fraction of the inactive receptor populations decreased from 26% to 13% at the M<sub>2</sub> wt and M<sub>2</sub> triple mutant, respectively (**Figure 3.32b,d**). This data show that half of the inactive receptor populations turned into active upon the introduction of the M<sub>2</sub> allosteric triple mutation.

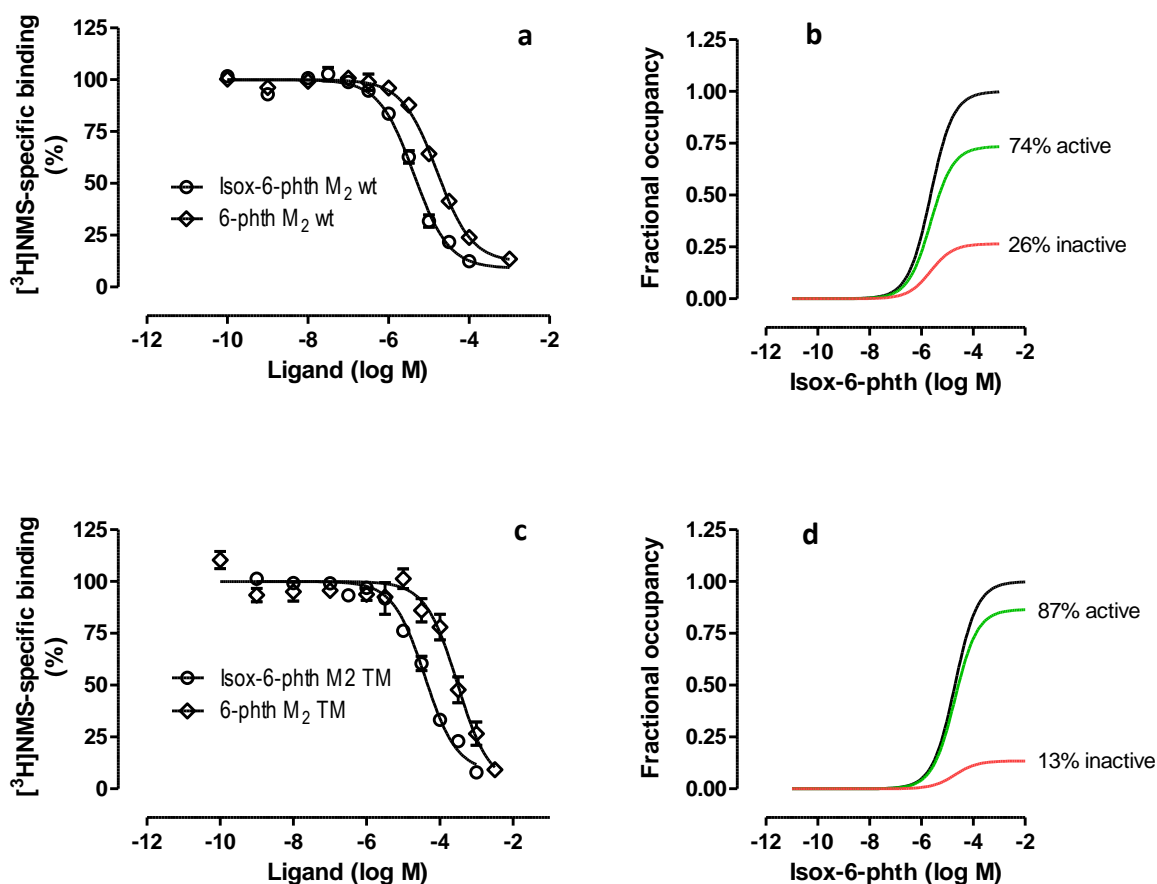


**Figure 3.32 M<sub>2</sub> triple mutant increases the amount of active receptor fractions stabilised by isox-6-phth.** (a,c) Equilibrium binding of [<sup>3</sup>H]NMS against the increasing concentrations of the allosteric ligand 6-phth and isox-6-phth at the (a) M<sub>2</sub> wt and (c) M<sub>2</sub> triple mutant (M<sub>2</sub> TM) receptors, respectively. (b,d) Fractional binding of the dynamic ligand isox-6-phth at the M<sub>2</sub> wt (b) and M<sub>2</sub> triple mutant (d) receptors, respectively. The total binding, receptor fractional occupancies in both the active and inactive poses are shown in black, green and red, respectively. Experiments were conducted using the membranes of the CHO M<sub>2</sub> wt and triple mutant cells. Non-specific binding was determined by atropine (10 μM). Shown are the mean values  $\pm$  S.E.M of at least four experiments performed in triplicates and fitted by the Global analysis of 2 curves.

There was an insignificant difference between the  $pK_A$  ( $6.35 \pm 1.33$ ) and  $pK_B$  ( $6.64 \pm 0.52$ ) of isox-6-naph at the M<sub>2</sub> wt. Therefore, the dynamic ligand could bind to the M<sub>2</sub> wt receptor with similar affinities between the active and inactive binding orientations. When bound in the inactive pose, isox-6-naph enhanced [<sup>3</sup>H]NMS equilibrium binding as reflected by the cooperativity ( $\alpha'$ ) of  $2.02 \pm 0.35$ . On the other hand, isox-6-naph displayed negative cooperativity ( $\alpha' = 0.06 \pm 0.04$ ) with [<sup>3</sup>H]NMS at the M<sub>2</sub> triple mutant (**Figure 3.33a,b and Table 3.14**). The fraction of the active receptor population increased from 34% at the M<sub>2</sub> wt

to 83% at the M<sub>2</sub> triple mutant. Consequently, the inactive receptor populations decreased from 66% at the M<sub>2</sub> wt to 17% at the M<sub>2</sub> triple mutant.

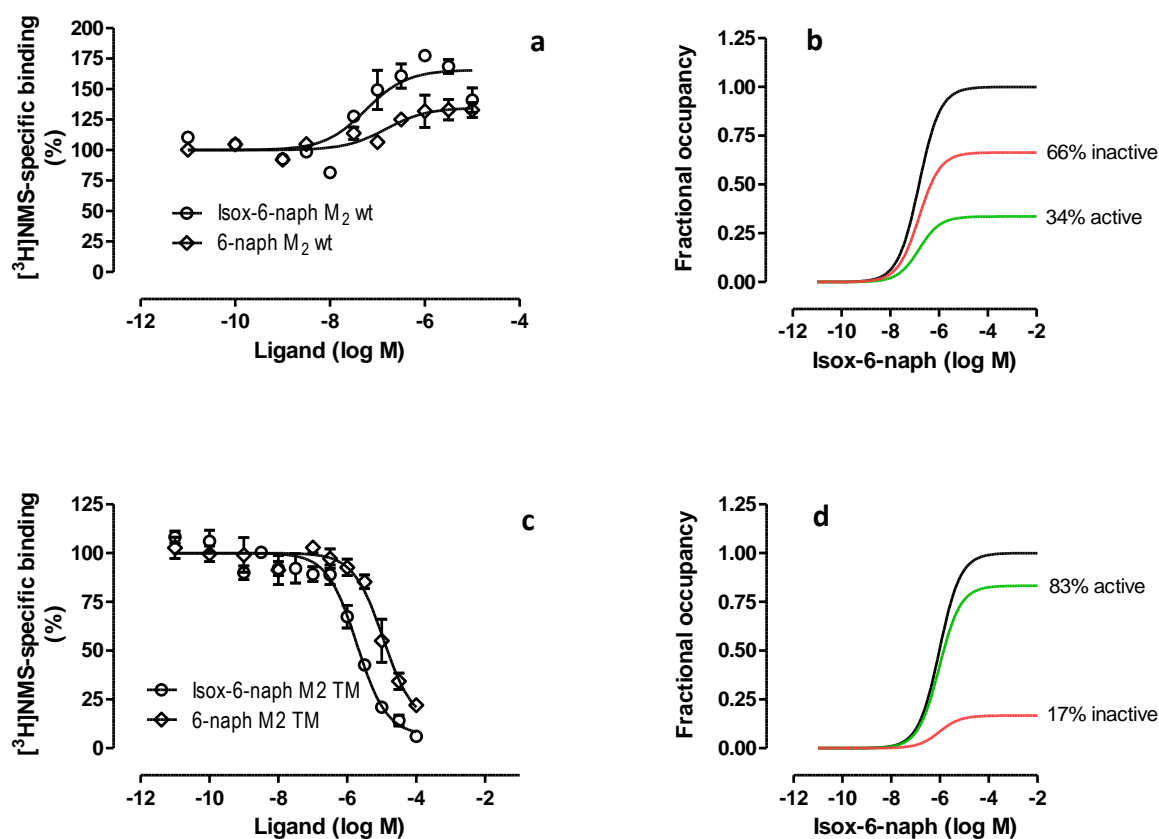


**Figure 3.33 M<sub>2</sub> triple mutant causes a ‘switch’ in isox-6-naph binding from preferentially inactive to active binding orientation (a,c)** Equilibrium binding of [<sup>3</sup>H]NMS against the increasing concentrations of the allosteric ligand 6-naph and isox-6-naph at the (a) M<sub>2</sub> wt and (c) M<sub>2</sub> triple mutant (M<sub>2</sub> TM) receptors, respectively. (b,d) Fractional binding of the dynamic ligand isox-6-naph at the M<sub>2</sub> wt (b) and M<sub>2</sub> triple mutant (d) receptors, respectively. The total binding, receptor fractional occupancies in both the active and inactive poses are shown in black, green and red, respectively. Experiments were conducted using the membranes of the CHO M<sub>2</sub> wt and triple mutant cells. Non-specific binding was determined by atropine (10μM). Shown are the mean values ± S.E.M of four experiments performed in triplicates and fitted by the Global analysis of 2 curves.

<b>[<sup>3</sup>H]NMS equilibrium binding</b>				
	<b>M<sub>2</sub> wt</b>		<b>M<sub>2</sub> triple mutant</b>	
	<b>pK<sub>active</sub> (pK<sub>A</sub>)</b>	<b>pK<sub>inactive</sub> (pK<sub>B</sub>) (α')</b>	<b>pK<sub>active</sub> (pK<sub>A</sub>)</b>	<b>pK<sub>inactive</sub> (pK<sub>B</sub>) (α')</b>
Isox-6-phth	5.51 ± 0.04	5.07 ± 0.03 <sup>***</sup> (0.06 ± 0.01)	4.64 ± 0.11	3.84 ± 0.07 (0.01 ± 0.02)
Isox-6-naph	6.35 ± 1.33	6.64 ± 0.52 <sup>ns</sup> (2.02 ± 0.35)	5.94 ± 0.08	5.25 ± 0.10 (0.06 ± 0.04)

**Table 3.14 Equilibrium binding for isox-6-phth and isox-6-naph ligands.** pK<sub>active</sub> and pK<sub>inactive</sub> represents the negative logarithm of the equilibrium dissociation constants of the active and inactive binding poses, respectively. α' is a measure of cooperativity between the inactive binding of the respective dualsteric ligand and the radioligand [<sup>3</sup>H]NMS. Positive cooperativity is reflected by α' > 1. Data are means ± S.E.M of at four experiments performed in triplicates.

<sup>\*\*\*</sup> Significantly different from the M<sub>2</sub> wt pK<sub>A</sub> (<sup>\*\*\*</sup> p < 0.05 Student's t-test)

<sup>ns</sup> Not significantly different from the M<sub>2</sub> wt pK<sub>A</sub>

Global analysis of 4 curves (dualsteric ligand binding, allosteric moiety binding, dualsteric ligand [<sup>35</sup>S]GTPγS and acetylcholine [<sup>35</sup>S]GTPγS data)

Here, the global nonlinear regression analysis recently published in Chen *et al.*, 2014 was applied in order to determine the estimates of equilibrium dissociation constants for the active (K<sub>A</sub>) and inactive (K<sub>B</sub>) binding poses of the dualsteric ligands at the M<sub>2</sub> wt receptor. The global analysis method simultaneously analyses the dualsteric ligand binding, allosteric moiety binding, dualsteric ligand [<sup>35</sup>S]GTPγS and acetylcholine [<sup>35</sup>S]GTPγS data. The idea of using this method was that combining the binding and functional data would come closer to producing more realistic pK<sub>A</sub> and pK<sub>B</sub> estimates instead of fixing the pK<sub>inactive</sub> and log α' <sub>hybr</sub> in the model using the allosteric moiety [<sup>3</sup>H]NMS equilibrium binding data. Only data at the M<sub>2</sub> wt were analysed by this method for iper-6-naph, isox-6-phth and isox-6-naph.

A set of four curves which comprises [<sup>35</sup>S]GTPγS activation by the endogenous ligand ACh (1) and the dualsteric ligand iper-6-naph-induced [<sup>35</sup>S]GTPγS activation (2), [<sup>3</sup>H]NMS equilibrium displacement by iper-6-naph (3) and the allosteric moiety 6-naph (4), were analysed by the global nonlinear regression analysis (**Figure 3.34**). pK<sub>A</sub> and pK<sub>B</sub> values of 7.75 ± 0.12 and 6.60 ± 0.26, respectively, were obtained for iper-6-naph at the M<sub>2</sub> wt. The values were statistically similar to those obtained by the Global analysis of 2 curves without



the functional data ( $pK_A = 7.60 \pm 0.11$  and  $pK_B$ ) shown in **Table 3.13**. There was also an insignificant difference in the cooperativity ( $\alpha'$ ) values  $2.10 \pm 0.14$  and  $3.47 \pm 2.30$  between the global analysis without and in the presence of dualsteric ligand functional data, respectively. It can be noted that for the cooperativity value in the presence of hybrid functional data, the standard error of mean was significantly high.

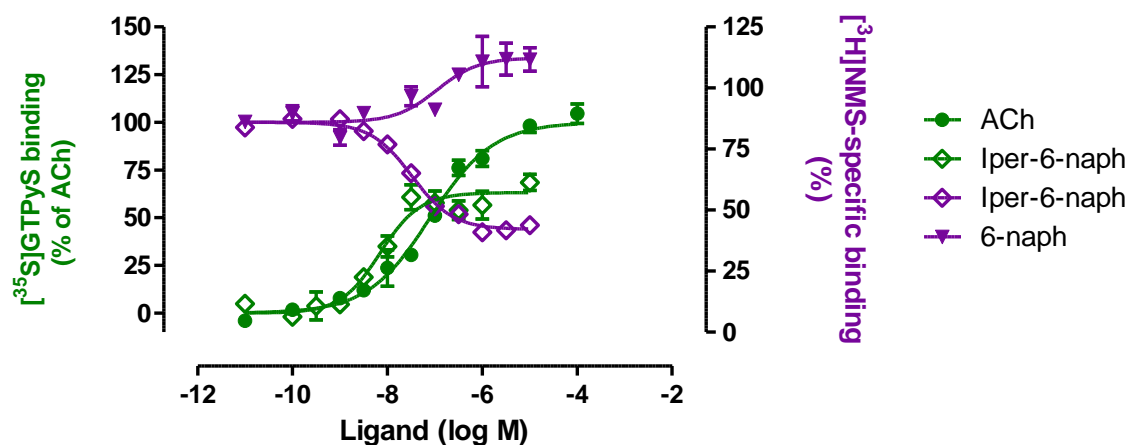


**Figure 3.34** The dualsteric (active) orientation of iper-6-naph promotes  $[^3\text{H}]\text{NMS}$  dissociation and partially activates  $[^{35}\text{S}]\text{GTP}\gamma\text{S}$  binding. Data was obtained using membranes of CHO-hM<sub>2</sub> wt cells. Left ordinate shows the effect of increasing concentrations of acetylcholine (ACh) and the dualsteric ligand isox-6-phth on  $[^{35}\text{S}]\text{GTP}\gamma\text{S}$  binding. Right ordinate shows the equilibrium binding of  $[^3\text{H}]\text{NMS}$  against the dualsteric ligand isox-6-phth and the allosteric moiety 6-phth. Data represent mean values  $\pm$  S.E.M of at least four experiments performed in triplicates analysed by the global curve fitting to sets of four curves.

Isox-6-naph was also subjected the global nonlinear regression analysis in the presence of dualsteric ligand functional data ( $[^{35}\text{S}]\text{GTP}\gamma\text{S}$  binding) (**Figure 3.35**). Changing the orthosteric moiety from iperoxo to isoxazole produced a  $pK_A$  value of  $6.43 \pm 0.82$  for isox-6-naph. This was about 1.32 log units lower than the  $pK_A$  of iper-6-naph. However, the change in the orthosteric fragment from iperoxo to isoxazole had no effect on the  $pK_B$  of isox-6-naph. The binding affinities ( $pK_B$ ) of the inactive populations for both iper-6-naph ( $6.60 \pm 0.26$ ) and isox-6-naph ( $6.64 \pm 0.37$ ) were similar. The  $pK_A$  and  $pK_B$  of  $6.43 \pm 0.82$  and  $6.64 \pm 0.37$  were obtained for isox-6-naph the presence of functional data (**Table 3.15**). These values were similar showing that the active dualsteric and inactive purely allosteric orientations bound to the M<sub>2</sub> wt receptor with equal affinities. The affinity constants were similar to the values obtained with the global analysis of the hybrid and fragment binding data as shown in **Table**

**3.14.** For cooperativity with [<sup>3</sup>H]NMS, isox-6-naph estimate in the presence of functional data was higher ( $\alpha' = 7.03 \pm 6.60$ ) albeit with a very high standard error of mean compared to the data in the absence of the functional data ( $\alpha' = 7.03 \pm 6.60$ ). When compared, the positive cooperativity obtained by these two methods of analysis was not statistically different ( $p > 0.05$ , Student's t-test).

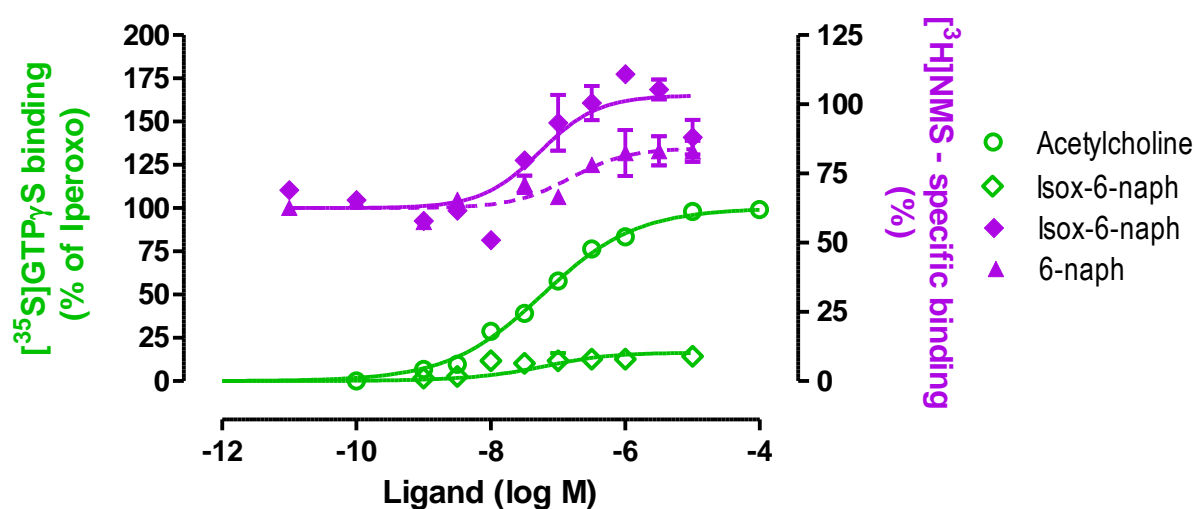


**Figure 3.35 Isox-6-naph preferentially binds in the purely allosteric (inactive) orientation.** Data was obtained using membranes of CHO-hM<sub>2</sub> wt cells. Left ordinate shows the effect of increasing concentrations of acetylcholine (ACh) and the dualsteric ligand isox-6-naph on [<sup>35</sup>S]GTPγS binding. Right ordinate shows the equilibrium binding of [<sup>3</sup>H]NMS against the dualsteric ligand isox-6-naph and the allosteric moiety 6-naph. Data was analysed by the global curve fitting to sets of four curves.

Isox-6-phth exhibited a  $0.46 \pm 0.11$  log units lower  $pK_B$  ( $5.38 \pm 0.07$ ) than the  $pK_A$  ( $5.84 \pm 0.08$ ) (**Figure 3.36**). The  $pK_A$  and  $pK_B$  parameters for isox-6-phth were more affine in the global analysis of binding plus hybrid functional data compared to the analysis of the hybrid and fragment binding only. However the negative cooperativity ( $\alpha' = 0.06 \pm 0.01$ ) of the inactive pose was identical in both sets of analysis. It is notable that the substitution of the allosteric moiety 6-naph with 6-phth produced a hybrid ligand with lower  $pK_A$  and  $pK_B$  binding affinities at the M<sub>2</sub> wt (**Table 3.14 and 3.15**). This can be explained by the weak allosteric binding affinity of 6-phth in comparison to 6-naph as shown in **Table 3.12** and also in Bock *et al.*, 2014a.

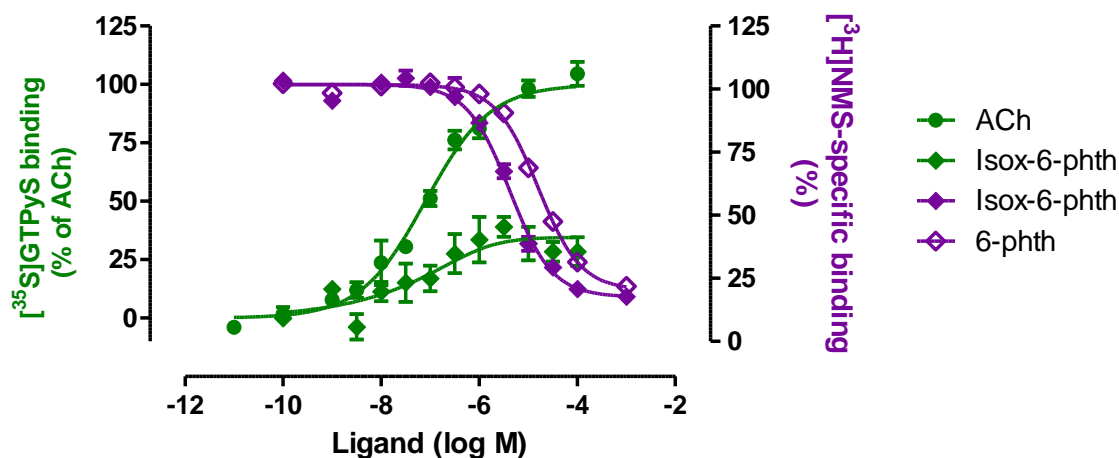


**Figure 3.36** The dualsteric (active) orientation of isox-6-phth promotes [<sup>3</sup>H]NMS displacement. Data was obtained using membranes of CHO-hM<sub>2</sub> wt cells. Left ordinate shows the effect of increasing concentrations of acetylcholine (ACh) and the dualsteric ligand isox-6-phth on [<sup>35</sup>S]GTPγS binding. Right ordinate shows the equilibrium binding of [<sup>3</sup>H]NMS against the dualsteric ligand isox-6-phth and the allosteric moiety 6-phth. Data represent mean values ± S.E.M of at least four experiments performed in triplicates analysed by the global curve fitting to sets of four curves.

<b>[<sup>3</sup>H]NMS equilibrium binding</b>		
	<b>M<sub>2</sub> wt</b>	
	<b>pK<sub>active</sub> (pK<sub>A</sub>)</b>	<b>pK<sub>inactive</sub> (pK<sub>B</sub>) (α')</b>
Iper-6-naph	7.75 ± 0.12	6.60 ± 0.26 <sup>**</sup> (3.47 ± 2.30)
Isox-6-phth	5.84 ± 0.08	5.38 ± 0.07 <sup>***</sup> (0.06 ± 0.01)
Isox-6-naph	6.43 ± 0.82	6.64 ± 0.37 <sup>ns</sup> (7.03 ± 6.60)

**Table 3.15** Binding parameters obtained by the Global analysis of 4 curves. pK<sub>active</sub> and pK<sub>inactive</sub> represents the negative logarithm of the equilibrium dissociation constants of the active and inactive binding poses. α' is a measure of cooperativity between the inactive binding of the respective dualsteric ligand and the radioligand [<sup>3</sup>H]NMS. Positive cooperativity is reflected by α' > 1.

<sup>\*\*</sup>, <sup>\*\*\*</sup> Significantly different from the pK<sub>A</sub> (<sup>\*\*</sup> p < 0.05; <sup>\*\*\*</sup> p < 0.0001 Student's t-test)

<sup>ns</sup> Not significantly different the pK<sub>A</sub>

### 3.5.2.2 [<sup>3</sup>H]NMS dissociation binding

Here, the aim was to investigate the importance of the allosteric core binding region of the M<sub>2</sub> wt receptors on the regulation of the allosteric potency of the dualsteric dynamic ligands and their allosteric fragments. [<sup>3</sup>H]NMS dissociation binding experiments were conducted to probe the effects of the M<sub>2</sub> allosteric triple mutation on the formation of the allosteric ternary complexes including the receptor, radioligand [<sup>3</sup>H]NMS and the test compound. The dualsteric ligands iper-6-phth, iper-6-naph and the allosteric moiety 6-phth were probed for their interaction with the allosteric site at the [<sup>3</sup>H]NMS occupied M<sub>2</sub> wt and triple mutant receptors.

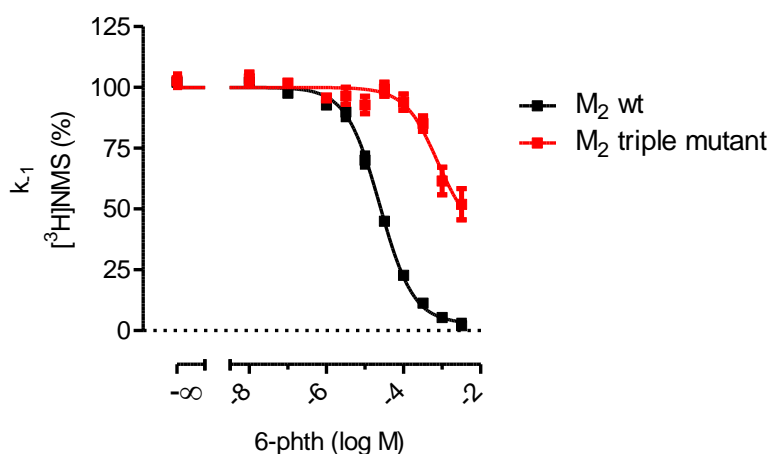


**Figure 3.37 6-phth loses allosteric potency and efficacy to retard [<sup>3</sup>H]NMS dissociation at the M<sub>2</sub> triple mutant.** Membranes of CHO-hM<sub>2</sub> cells were pre-labeled with [<sup>3</sup>H]NMS (2nM) and the dissociation rate of the labeled ligand was determined in the presence of increasing concentrations of the allosteric moiety 6-phth. Atropine (10μM) was used to prevent radioligand re-association. The dissociation rate constant (k<sub>-1</sub>) was derived from one phase exponential decay analysis of single experiments. Indicated are mean values ± S.E.M of 4 experiments performed in triplicates.

The allosteric moiety 6-phth was able to completely block the dissociation of [<sup>3</sup>H]NMS from the orthosteric binding site of the M<sub>2</sub> wt receptor in both cell membranes (**Figure 3.37**) and live cells (**Sup.Figure 3.40**). This can be observed from the M<sub>2</sub> wt curve which levels off at the bottom value (k<sub>-1</sub> = 3 ± 4%) not different from zero (*F*-test, *p*>0.05). The half maximal inhibitory action (pEC<sub>0.5,diss</sub>) of 6-phth at the M<sub>2</sub> wt was 4.62 ± 0.03. The introduction of the triple mutation led to a 1.51 log unit pronounced decrease in allosteric binding affinity observed at the M<sub>2</sub> triple mutant (pEC<sub>0.5,diss</sub> = 3.11 ± 0.14). In contrast to the M<sub>2</sub> wt, the M<sub>2</sub>

triple mutant curve did not level off at zero. The maximum apparent rate constant of dissociation  $k_{-1}$  was reduced to  $52 \pm 7\%$ . This showed that 6-phth was unable to fully retard the dissociation of the radioligand [ $^3\text{H}$ ]NMS from the orthosteric site  $M_2$  triple mutant (Figure 3.37 and Table 3.16).

$[^3\text{H}]$ NMS dissociation binding			
	$M_2$ wt	$M_2$ triple mutant	$\Delta pEC_{0.5,diss}$ (wildtype-mutant)
		$pEC_{0.5,diss}$ (Bottom $k_{-1}$ %)	
6-phth	$4.62 \pm 0.03$ (3 ± 4)	$3.11 \pm 0.14^{***}$ (52 ± 7)	$1.51 \pm 0.15$

**Table 3.16 Retardation of [ $^3\text{H}$ ]NMS dissociation by the allosteric moiety 6-phth.**  $pEC_{0.5,diss}$  indicates the negative logarithm of the concentration which causes half maximal delay of [ $^3\text{H}$ ]NMS dissociation.  $\Delta pEC_{0.5,diss}$  is the difference between the  $pEC_{0.5,diss}$  values of the  $M_2$  wt and triple mutant. Bottom  $k_{-1}$  (%) reflects the apparent rate constant of dissociation at maximal ligand concentrations studied. The slope factor ( $n_H$ ) for both individual curves was not significantly different from -1 (F-test,  $p > 0.05$ ). Data shown are means  $\pm$  S.E.M of 4 experiments performed in triplicates.

\*\*\*Significantly different from the  $pEC_{0.5,diss}$  obtained at the  $M_2$  wt (\*\* $p < 0.0001$  Student's t-test).

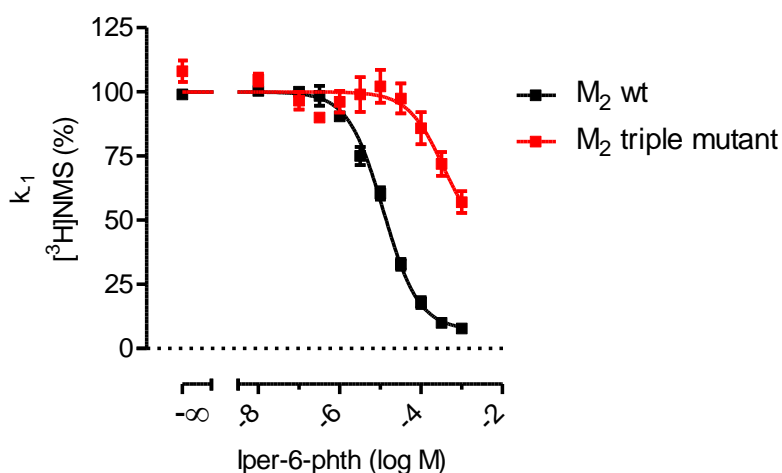


**Figure 3.38 Iper-6-phth loses allosteric potency and efficacy to retard [ $^3\text{H}$ ]NMS dissociation at the  $M_2$  triple mutant.** Membranes of CHO-h $M_2$  cells were pre-labeled with [ $^3\text{H}$ ]NMS (2nM) and the dissociation rate of the labeled ligand was determined in the presence of increasing concentrations of iper-6-phth. Atropine (10 $\mu\text{M}$ ) was applied to prevent radioligand re-association. The dissociation rate constant ( $k_{-1}$ ) was derived from one phase

exponential decay analysis of single experiments. Shown are mean values  $\pm$  S.E.M of 4 experiments performed in triplicates.

The dualsteric ligand iper-6-phth formed allosteric ternary complexes with the M<sub>2</sub> wt receptor and the radioligand [<sup>3</sup>H]NMS. Iper-6-phth was able to completely retard [<sup>3</sup>H]NMS dissociation in both cell membranes and live cells (**Sup. Figure 3.40**) as the M<sub>2</sub> wt curve levels off at a value not significantly different from zero (Bottom  $k_{-1} = 5 \pm 2\%$ ). The allosteric binding affinity ( $pEC_{0.5,diss}$ ) of iper-6-phth was  $4.93 \pm 0.03$  at the M<sub>2</sub> wt type receptor. At the M<sub>2</sub> triple mutant, there was a substantial loss of allosteric binding affinity of 1.47 log units compared to the M<sub>2</sub> wt for iper-6-phth. Also, in contrast to the M<sub>2</sub> wt, iper-6-phth was unable to completely retard the dissociation of [<sup>3</sup>H]NMS at the M<sub>2</sub> triple mutant. The maximum retardation of [<sup>3</sup>H]NMS dissociation which could be achieved at the M<sub>2</sub> triple mutant was (Bottom  $k_{-1} 57 \pm 12\%$ ) (**Figure 3.38 and Table 3.17**).

The pattern was similar for iper-6-naph as that observed for iper-6-naph in terms of the loss of allosteric potency at the M<sub>2</sub> triple mutant. Nevertheless, there was an unequivocal pronounced loss of allosteric potency for iper-6-naph of  $2.93 \pm 0.08$  at the M<sub>2</sub> triple mutant ( $pEC_{0.5,diss} = 4.35 \pm 0.06$ ) compared to the M<sub>2</sub> wt ( $pEC_{0.5,diss}$  of  $7.27 \pm 0.06$ ). However, there was no loss in allosteric efficacy at the M<sub>2</sub> triple mutant compared to the M<sub>2</sub> wt. This is reflected by the dissociation curves of both the M<sub>2</sub> wt (Bottom  $k_{-1} = 19 \pm 2\%$ ) and M<sub>2</sub> triple mutant (Bottom  $k_{-1} = 22 \pm 6\%$ ) which plateaued at a level significantly different from zero but not significantly different from each other (**Figure 3.39 and Table 3.17**).

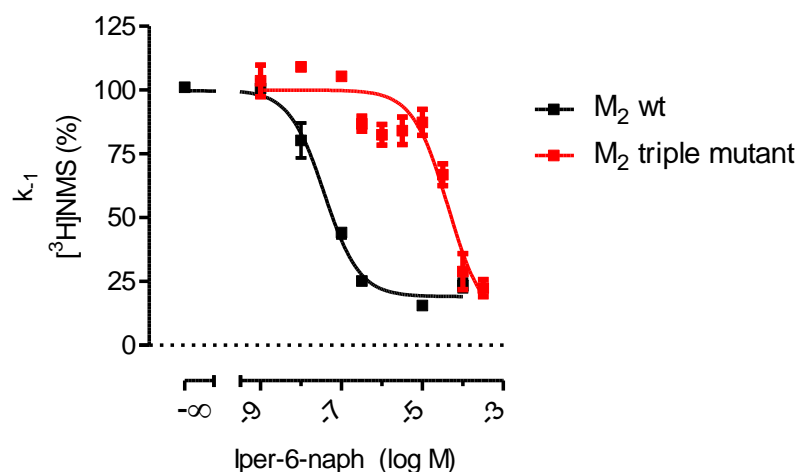


**Figure 3.39 Pronounced loss of allosteric potency for iper-6-naph to retard  $[^3\text{H}]$ NMS dissociation at the  $M_2$  triple mutant.** Membranes of CHO-h $M_2$  cells were pre-labeled with  $[^3\text{H}]$ NMS and the dissociation rate of the labeled ligand was determined in the presence of different concentrations of iper-6-naph. Atropine (10 $\mu\text{M}$ ) was applied to prevent radioligand re-association. The dissociation rate constant ( $k_1$ ) was derived from one phase exponential decay analysis of single experiments. Indicated are mean values  $\pm$  S.E.M of 4 experiments performed in triplicates.

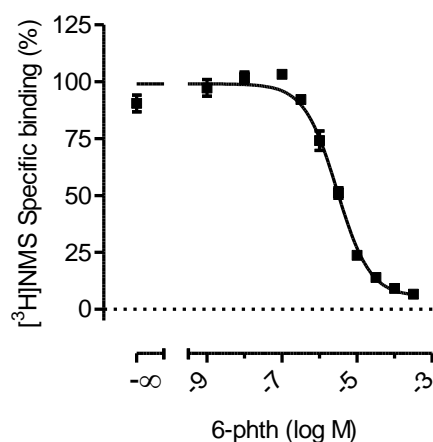
$[^3\text{H}]$ NMS dissociation binding			
	$M_2$ wt	$M_2$ triple mutant	
		$\text{pEC}_{0.5,\text{diss}}$ (Bottom $k_1$ %)	$\Delta\text{pEC}_{0.5,\text{diss}}$ (wildtype-mutant)
<b>Iper-6-phth</b>	$4.93 \pm 0.03$ ( $5 \pm 2$ )	$3.46 \pm 0.23^{***}$ ( $57 \pm 12$ )	$1.47 \pm 0.24$
<b>Iper-6-naph</b>	$7.27 \pm 0.06$ ( $19 \pm 2$ )	$4.35 \pm 0.06^{***}$ ( $22 \pm 6$ )	$2.93 \pm 0.08$

**Table 3.17 Retardation of  $[^3\text{H}]$ NMS dissociation by dualsteric ligands.**  $\text{pEC}_{0.5,\text{diss}}$  indicates the negative logarithm of the concentration which causes half maximal delay of  $[^3\text{H}]$ NMS dissociation.  $\Delta\text{pEC}_{0.5,\text{diss}}$  is the difference between the  $\text{pEC}_{0.5,\text{diss}}$  values of the  $M_2$  wt and  $M_2$  triple mutant. Bottom  $k_1$  (%) reflects the apparent rate constant of dissociation at maximal ligand concentrations studied. The slope factor ( $n_H$ ) for both individual curves was not significantly different from -1 (F-test,  $p > 0.05$ ). Data shown are means  $\pm$  S.E.M of 4 experiments performed in triplicates.

\*\*\* Significantly different from the  $\text{pEC}_{0.5,\text{diss}}$  obtained at the  $M_2$  wt (\*\*\*  $p < 0.05$  Student's t-test).

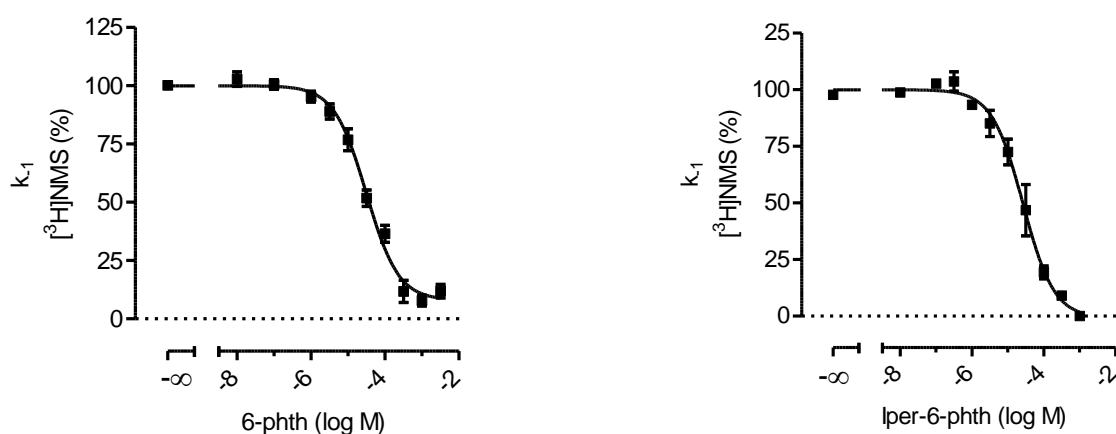
### 3.5.2.3 Supplementary data

#### Equilibrium binding



**Sup. Figure 3.40 [<sup>3</sup>H]NMS displacement in M<sub>2</sub> wt cells.** Equilibrium binding of [<sup>3</sup>H]NMS against the increasing concentrations of the allosteric ligand 6-phth (a) in CHO M<sub>2</sub> wt cells. Non-specific binding was determined by addition of atropine (10μM). Shown are the mean values ± S.E.M of four experiments performed in triplicates and analysed by the four parameter logistic function with a slope factor of -1.

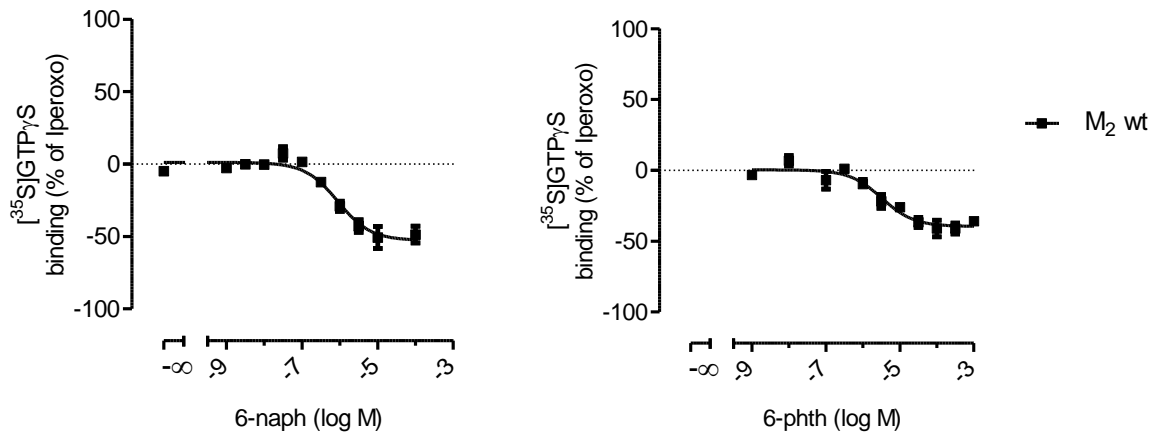
#### Dissociation binding



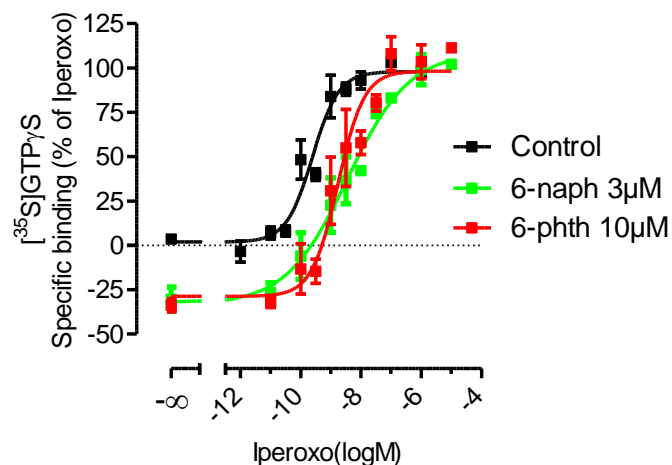
**Sup. Figure 3.41 Retardation of [<sup>3</sup>H]NMS dissociation in the M<sub>2</sub> wt cells.** CHO-hM<sub>2</sub> cells were pre-labeled with 2nM [<sup>3</sup>H]NMS and the dissociation rate of the labeled ligand was determined in the presence of increasing concentrations of the allosteric moiety 6-phth (a) and dualsteric ligand iper-6-phth (b). Atropine (10μM) was applied to prevent radioligand re-association. The dissociation rate constant (k<sub>-1</sub>) was derived from one phase exponential decay analysis of single experiments. Indicated are mean values ± S.E.M of 4 experiments performed in triplicates.



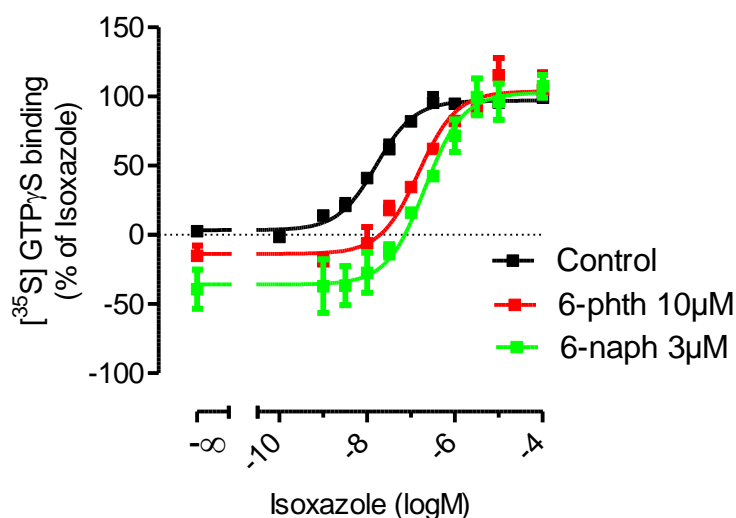
### [<sup>35</sup>S]GTPγS binding



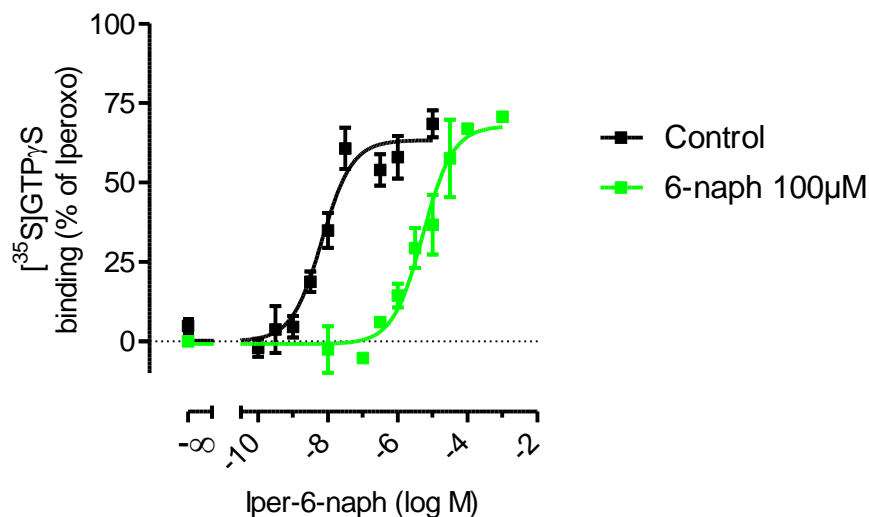
**Sup. Figure 3.42 Allosteric fragments 6-naph and 6-phth are inverse agonists.** [<sup>35</sup>S]GTPγS binding to membranes of CHO-hM<sub>2</sub> wt and triple mutant cells indicates receptor-mediated G<sub>i</sub> protein activation. The maximum [<sup>35</sup>S]GTPγS binding induced by ACh was set at 100% and the total binding [<sup>35</sup>S]GTPγS binding in the absence of ligand was set at 0%. The slope factor (n<sub>H</sub>) was 1 for each individual curve. Data shown are means ± S.E.M of 4 experiments performed in triplicates. ACh = acetylcholine.



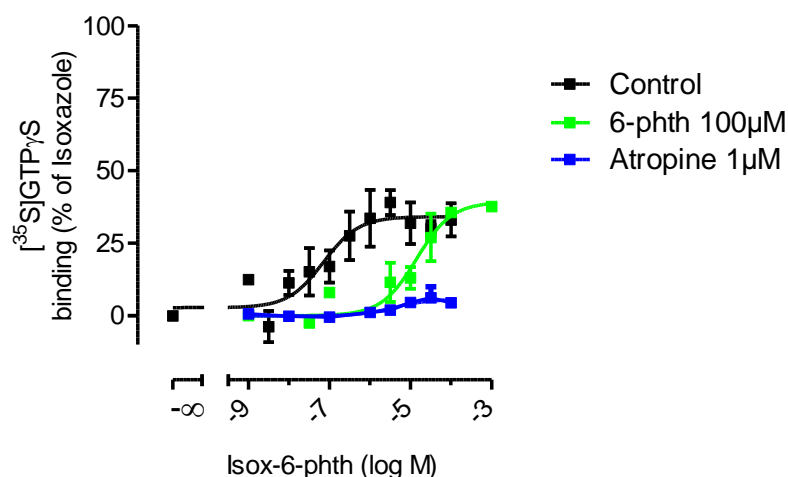
**Sup. Figure 3.43 The superpotent agonist iperoxo curve is shifted rightwards by allosteric moieties 6-naph and 6-phth.** [<sup>35</sup>S]GTPγS binding to membranes of CHO-hM<sub>2</sub> wt and triple mutant cells indicates receptor-mediated G<sub>i/o</sub> protein activation. The maximum [<sup>35</sup>S]GTPγS binding induced by ACh was set at 100% and the total binding [<sup>35</sup>S]GTPγS binding in the absence of ligand was set at 0%. Control is iperoxo-induced concentration effect curve in the absence of any allosteric moiety. Data shown are means ± S.E.M of 3 experiments performed in triplicates. ACh = acetylcholine.



**Sup. Figure 3.44 The allosteric moieties 6-phth and 6-naph reduce the potency of the orthosteric ligand isoxazole.**  $[^{35}\text{S}]\text{GTP}\gamma\text{S}$  binding to membranes of CHO-hM<sub>2</sub> wt cells indicates receptor-mediated G<sub>i/o</sub> protein activation. The maximum  $[^{35}\text{S}]\text{GTP}\gamma\text{S}$  binding induced by ACh was set at 100% and the total binding  $[^{35}\text{S}]\text{GTP}\gamma\text{S}$  binding in the absence of ligand was set at 0%. Control is isoxazole concentration effect curve in the absence of any allosteric moiety. The slope factor ( $n_H$ ) was 1 for each individual curve. Data shown are means  $\pm$  S.E.M of 3-5 experiments performed in triplicates. ACh = acetylcholine.



**Sup. Figure 3.45 Iper-6-naph displays partial agonistic behaviour.**  $[^{35}\text{S}]\text{GTP}\gamma\text{S}$  binding to membranes of CHO-hM<sub>2</sub> wt cells indicates receptor-mediated G<sub>i/o</sub> protein activation. The maximum  $[^{35}\text{S}]\text{GTP}\gamma\text{S}$  binding induced by ACh was set at 100% and the total binding  $[^{35}\text{S}]\text{GTP}\gamma\text{S}$  binding in the absence of ligand was set at 0%. Control is iper-6-naph-induced activation in the absence of the allosteric moiety 6-naph. The slope factor ( $n_H$ ) was 1 for each individual curve. Data shown are means  $\pm$  S.E.M of 4 experiments performed in triplicates. ACh = acetylcholine.



**Sup. Figure 3.46 The dualsteric ligand isox-6-phth displays a partial agonistic behaviour.**  $[^{35}\text{S}]\text{GTP}\gamma\text{S}$  binding to membranes of CHO-hM<sub>2</sub> wt and triple mutant cells indicates receptor-mediated G<sub>i/o</sub> protein activation. The maximum  $[^{35}\text{S}]\text{GTP}\gamma\text{S}$  binding induced by ACh was set at 100% and the total binding  $[^{35}\text{S}]\text{GTP}\gamma\text{S}$  binding in the absence of ligand was set at 0%. Control is isox-6-phth-induced activation in the absence of the allosteric moiety 6-phth or the inverse agonist atropine. The slope factor (n<sub>H</sub>) was 1 for each individual curve except for in the presence of atropine. Data shown are means  $\pm$  S.E.M of 3-4 experiments performed in triplicates.

ACh = acetylcholine.

## 4. DISCUSSION

### 4.1 Pronounced loss of allosteric function at the M<sub>2</sub> triple mutant

#### Loss of allosteric function

Having mutated the three amino acids Y177<sup>ECL2</sup>, W422<sup>7.35</sup> and T423<sup>7.36</sup> previously found to line the core region of the allosteric binding site of the M<sub>2</sub> mAChR (Voigtländer *et al.*, 2003; Prilla *et al.*, 2006; Dror *et al.*, 2013), experiments were carried out to investigate if the common allosteric binding site was still functional. The radioligand dissociation experiments were carried out to find out if the M<sub>2</sub> triple mutant receptor could still form ternary complexes with allosteric and orthosteric ligands. Formation of ternary complexes is a characteristic hallmark of allosteric interactions (Voigtländer *et al.*, 2003; Grossmüller *et al.*, 2006). Results with the flexible alkane-bisammonium allosteric modulator W84 showed that the common allosteric binding site is still present and functional even after the substitution to alanine of the three critical amino acids mentioned above. W84 was still able to retard the dissociation rate of [<sup>3</sup>H]NMS from the orthosteric binding site. The radioligand dissociation kinetic experiment was used here as it allows for the determination of purely allosteric effects (Buller *et al.*, 2002).

W84 was chosen to probe the allosteric effects as it is a flexible compound (Tränkle *et al.*, 1996) and therefore would be an ideal ligand to explore fully the core docking site of the allosteric ligands. The idea was to investigate the importance of simultaneously substituting the critical epitopes and therefore a flexible compound could possibly have been able to switch conformations and interact with other epitopes in the allosteric ligand binding pocket. W84 was still able to bind to the allosteric binding site of the M<sub>2</sub> triple mutant receptor albeit with a remarkably large reduction in potency of 2.53 log units. Also, W84 could only retard the rate of [<sup>3</sup>H]NMS dissociation to about 50% in M<sub>2</sub> triple mutant cells (**chapter 3.1.1 and Table 3.1**). These data support the previously published data observed with single and double mutants of the M<sub>2</sub> receptor which also showed a profound loss in allosteric binding affinity and efficacy.

The M<sub>2</sub> single mutant W422<sup>7.35</sup>A displayed a reduction in W84 allosteric potency by 1.51 log units. However, the M<sub>2</sub> single mutant T423<sup>7.36</sup>A on its own had insignificant effect on the potency of W84 (Voigtländer *et al.*, 2003; Prilla *et al.*, 2006). In this study W84 lost 2.53 log units of potency at the M<sub>2</sub> triple mutant. Therefore, when comparing with the data from

Voigtländer *et al.*, 2003 it appears that the further loss of 1.02 log units of W84 allosteric binding affinity observed at the M<sub>2</sub> triple mutant can be attributed to the Y177<sup>ECL2</sup>A mutation. Even though the T423<sup>7.36</sup>A single mutation was insignificant, it is difficult to judge if the loss of extra 1.02 log units of affinity can be solely attributed to the Y177<sup>ECL2</sup>A or in combination with T423<sup>7.36</sup>A. However, it cannot be ruled out that the T423<sup>7.36</sup>A might contribute to the loss in W84 allosteric binding affinity when mutated simultaneously with other epitopes mentioned.

### **Buffer dependency of allosteric binding**

The binding of W84 to the orthosteric site-occupied M<sub>2</sub> wt and triple mutant receptors was investigated in live CHO cells and in cell membranes. In live cells the HBSS+20mM HEPES buffer was used whilst in cell membranes, the high ionic strength HEPES buffer and the low ionic strength NaKPi buffer were applied. The idea was to explore the effects of the M<sub>2</sub> triple mutation on allosteric binding in different assay settings and buffer conditions. Data showed that the overall affinity of W84 was buffer dependent. This is reflected by increased allosteric potency of W84 to retard [<sup>3</sup>H]NMS dissociation in the low ionic strength buffer compared to the high ionic strength one at both the M<sub>2</sub> wt and triple mutant receptors (**chapter 3.1.1; Table 3.1**).

Nevertheless, the relative gain of W84 allosteric binding affinity in the NaKPi buffer was independent of the M<sub>2</sub> triple mutation as the gain in affinity was observed at both the M<sub>2</sub> wt and triple mutant. In addition, the loss of allosteric potency at the M<sub>2</sub> triple mutant was similar in all three buffer conditions and also when comparing the live cells and cell membranes (**chapter 3.1.1; Table 3.1**). This shows that the buffer dependency of W84 binding in either the live cells or membranes is not regulated by these three amino acids of the core allosteric binding region. Also, the data is consistent with previous findings which showed that allosteric modulators were generally more potent in the low ionic strength NaKPi buffer (Tränkle *et al.*, 1996).

### **Equilibrium binding**

The radioligand [<sup>3</sup>H]NMS equilibrium binding studies against the allosteric ligand W84 were performed to measure the affinity of the allosteric ligand for the orthosteric free receptors. This assay also allows the determination of cooperativity between the allosteric and orthosteric ligand (Ehlert, 1988). W84 displayed a very huge loss in binding affinity of about

2.5 log units at the M<sub>2</sub> triple mutant receptor compared to the M<sub>2</sub> wt in both the high and low ionic strength buffers. Prilla *et al.*, 2006 showed that at the single mutant W422<sup>7.35</sup>A, W84 lost 1.6 log units of affinity at the orthosteric free receptor. Hence, the extra loss in W84 binding affinity of about 1 log unit at the M<sub>2</sub> triple mutant can be attributed to the other two mutations Y177<sup>ECL2</sup>A and T423<sup>7.36</sup>A. However, it is difficult to judge if both Y177A and T423A are necessary for the further 1 log unit loss in affinity. Investigations with Y177A and T423A double M<sub>2</sub> double mutant or the Y177A single mutant receptor would solve this problem.

Similar to the orthosteric-occupied receptors, the overall binding affinity of W84 at the orthosteric-free receptors was sensitive to the buffer conditions. There was an increase in binding affinity at both the M<sub>2</sub> wt and triple mutant in the low ionic strength buffer (**Table 3.2**). This is in line with previous findings which showed that low ionic strength buffers enhance the sensitivity of muscarinic receptors towards allosteric modulation (Ellis *et al.*, 1991; Tränkle *et al.*, 1996). However, the loss of binding affinity at orthosteric-free M<sub>2</sub> triple mutant receptors was not influenced by changes in buffer ionic strength (**Table 3.2**).

In contrast to the binding affinity (pK<sub>A</sub>), the negative cooperativity between W84 and [<sup>3</sup>H]NMS was sensitive to the M<sub>2</sub> triple mutant in the high ionic strength buffer compared to the low ionic strength buffer. The negative cooperativity was enhanced about 3-fold at the M<sub>2</sub> triple mutant in the high ionic strength buffer whilst there was an insignificant change in negative cooperativity in the low ionic strength buffer. Therefore, the increased negative cooperativity observed at the M<sub>2</sub> triple mutant in high ionic strength buffer might be due to the buffer influencing W84 to adopt an orientation which enhances negative cooperativity with the radioligand, at the compromised allosteric docking site. In a low ionic strength buffer W84 seems to adopt a similar binding orientation at both the M<sub>2</sub> wt and triple mutant receptors which result in similar negative binding cooperativities with [<sup>3</sup>H]NMS (**chapter 3.1.2 and Table 3.2**). In other words, the low ionic strength buffer seems to reduce negative cooperativity between the allosteric ligand and orthosteric radioligand [<sup>3</sup>H]NMS at the M<sub>2</sub> triple mutant.

W84 lost the same amount of binding affinity in both the [<sup>3</sup>H]NMS orthosterically occupied ( $\Delta pEC_{50,diss} = 2.53$ ) and unoccupied ( $\Delta pK_A = 2.47$ ) M<sub>2</sub> triple mutant receptors compared to the wild type (**chapter 3**). This reflects that the pronounced loss of W84 allosteric binding

affinity caused by the allosteric triple mutation was independent of the presence or absence of the orthosteric radioligand. The allosteric binding data clearly suggest that there are more important amino acids which form the allosteric core binding domain of the M<sub>2</sub> receptor. This is because allosteric binding could still be observed for the flexible allosteric ligand W84, though with a pronounced loss in binding affinity.

#### **4.2 The M<sub>2</sub> allosteric binding site confers some selectivity to chemically distinct muscarinic agonists orthosteric ligand binding**

In recent years it has been shown that the allosteric binding vestibule contributes to the binding of orthosteric ligands. The flexibility of the M<sub>2</sub> receptor extracellular loop 2 (E2) has been observed to be critical in the binding of both allosteric and orthosteric GPCR ligands (Avlani *et al.*, 2007). It has been shown in previous studies that the conserved allosteric epitope W422<sup>7.35</sup> contributes more than 1 log unit of binding affinity for the endogenous agonist acetylcholine (Jäger *et al.*, 2007). At the M<sub>2</sub> triple mutant, acetylcholine lost about 2 log units of binding affinity which is nearly a log unit more than observed at the W422<sup>7.35</sup> single mutant by Jäger *et al.*, 2007. Hence, these results show that the other two amino acids T423<sup>7.36</sup> and Y177<sup>ECL2</sup> contribute to the extra 1 log unit loss of acetylcholine binding affinity. In line with these previous findings, the data here show that the allosteric core binding domain of the M<sub>2</sub> receptor also plays a critical role in determining the binding of structurally different agonist ligands at the M<sub>2</sub> wild type receptor.

Structurally different M<sub>2</sub> receptor agonists acetylcholine, carbachol, iperoxo McN-A-343, oxotremorine-M and oxotremorine displayed loss of binding affinity at the triple mutant M<sub>2</sub> receptor. However the loss of binding affinity was non-uniform among the full agonists as summarised in **Figure 4.1**. The endogenous ligand acetylcholine displayed the largest loss of affinity of about 2 log units. However, the partial agonist pilocarpine and inverse agonists NMS, atropine and scopolamine were insensitive to the disruption of the allosteric binding site. This is in agreement with previous findings which showed that W422<sup>7.35</sup> is essential for the binding of the full agonist acetylcholine but not for the partial agonist pilocarpine whose binding properties were similar to the inverse agonists (Jäger *et al.*, 2007). Hence, the data here suggest that the M<sub>2</sub> allosteric core binding site located at the entrance to the orthosteric site is able to decipher different pharmacophores of orthosteric ligands and thereby possess a key mediating role in the binding of chemically distinct muscarinic agonist ligands.

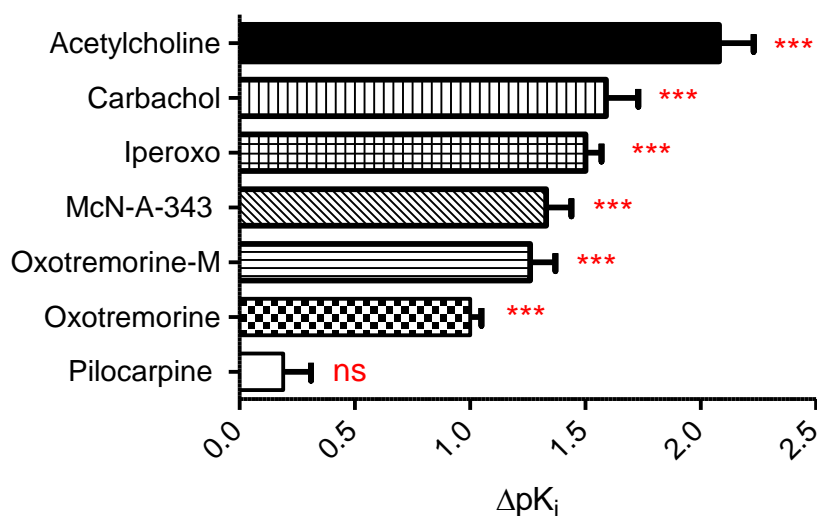


**Figure 4.1 Structurally different muscarinic agonists display a differentiated loss in binding affinity at the M<sub>2</sub> triple mutant compared to M<sub>2</sub> wt.** ΔpK<sub>i</sub> represents the difference between the pK<sub>i</sub> values of the M<sub>2</sub> wt and triple mutant.

\*\*\* The affinity (pK<sub>i</sub>) at the M<sub>2</sub> triple mutant is significantly different from the M<sub>2</sub> wt pK<sub>i</sub> (\*\*\*) p < 0.05)

<sup>ns</sup> The affinity (pK<sub>i</sub>) at the M<sub>2</sub> triple mutant is not significantly different from the M<sub>2</sub> wt pK<sub>i</sub>  
 Statistical analysis was performed by the Student's t-test

### 4.3 The core region of the allosteric binding site regulates M<sub>2</sub> receptor orthosteric activation

#### G<sub>i/o</sub> signalling

The endogenous muscarinic ligand acetylcholine, the superagonist iperoxo and partial agonist pilocarpine were chosen to probe M<sub>2</sub> triple mutant receptor activation. In the [<sup>35</sup>S]GTPγS binding assay the full agonist acetylcholine and iperoxo were able to fully activate the M<sub>2</sub> triple mutant receptor similar to the M<sub>2</sub> wt. However, the potencies of these full agonists were greatly reduced at the M<sub>2</sub> triple mutant compared to the M<sub>2</sub> wt. Acetylcholine and iperoxo showed a decrease of 1.6 and 1.5 log units in potency respectively, at the M<sub>2</sub> triple mutant in comparison to the M<sub>2</sub> wt. These observations correspond with the data from Klause, 2013 whereby both acetylcholine and iperoxo lost 1.5 log units of potency at the single mutant W422<sup>7.35</sup>A. Bock *et al.*, 2012 also reported a 1.5 log unit loss in potency at W422<sup>7.35</sup>A. Hence, the data here suggest that the other two amino acids Y177<sup>ECL2</sup> and T423<sup>7.36</sup> mutated were not essential for the activation of the M<sub>2</sub> receptor by the full agonists iperoxo and acetylcholine. Nevertheless, the loss in potency observed shows that at least the residue W422 is involved in mediating the potency of the agonists acetylcholine and iperoxo. Therefore, the loss in agonist



potency at the M<sub>2</sub> triple mutant can be attributed to the loss in binding affinity shown in **figure 4.1**.

To the contrary, the partial agonist pilocarpine exhibited a decrease in maximum activation at the M<sub>2</sub> triple mutant whilst its potency remained unchanged compared to M<sub>2</sub> wt receptors (**chapter 3.2.2; figure 3.8**). This data, therefore show that the allosteric core binding site is sensitive to agonist-dependent conformational changes in agreement with the single M<sub>2</sub> W422<sup>7.35</sup>A mutation studies (Jäger *et al.*, 2007) which also showed that there was a substantial loss of maximum activation with pilocarpine and not with the full agonist acetylcholine. [<sup>35</sup>S]GTPγS binding studies whereby the M<sub>2</sub> wt allosteric site was occupied by an allosteric ligand to mimic allosteric mutations in the presence of an agonist were performed by Jäger *et al.*, 2007. These also showed that allosteric modulators reduced the potency of full agonists whereas the potency of the partial agonist pilocarpine was not changed. Taken together, the data suggest that full agonists such as acetylcholine and iperoxo are able to stabilise an active receptor conformation without the contribution of the core region of the allosteric site. On the other hand, the allosteric site core region seems to be an important component of the conformational changes required for pilocarpine-induced receptor activation.

However, in the dynamic mass redistribution (DMR) assay, pilocarpine was unable to stimulate DMR activation at the M<sub>2</sub> triple mutant. In DMR there is signal amplification as the signal output is measured downstream of the receptor protein (**Figure 4.2**) (Schröder *et al.*, 2010). In this study, this can also be confirmed by the results of the partial agonist pilocarpine which produced higher maximal effects, closer to the full agonists' efficacy in DMR compared to the [<sup>35</sup>S]GTPγS binding assay at the M<sub>2</sub> wt. Even with signal amplification in DMR, the partial agonist pilocarpine was unable to significantly activate the M<sub>2</sub> triple mutant receptor (**Figure 4.3**).

In order to establish the reasons why the partial agonist pilocarpine is unable to stimulate DMR more experiments need to be carried out (**see chapter 6, outlook**). Nevertheless, the data suggests that pilocarpine is incapable of activating the G<sub>i/o</sub> signalling pathway further downstream of the M<sub>2</sub> triple mutant receptor. The coupling efficiency (τ) of the compounds which is a parameter used to determine the signalling efficacy of compounds, that is how efficient an agonist binding is transduced into a response was utilised to analyse the [<sup>35</sup>S]GTPγS binding data. The full agonist acetylcholine did not lose coupling efficiency whilst pilocarpine lost a significant amount of signalling efficacy at the M<sub>2</sub> triple mutant

compared to the  $M_2$  wt, thereby becoming a very weak partial agonist (**Figure 3.15; Table 3.10**). This might explain why the partial agonist pilocarpine failed to stimulate the global relocation of cellular biomolecules in DMR as the signal transduction capability was severely diminished at the  $M_2$  triple mutant.

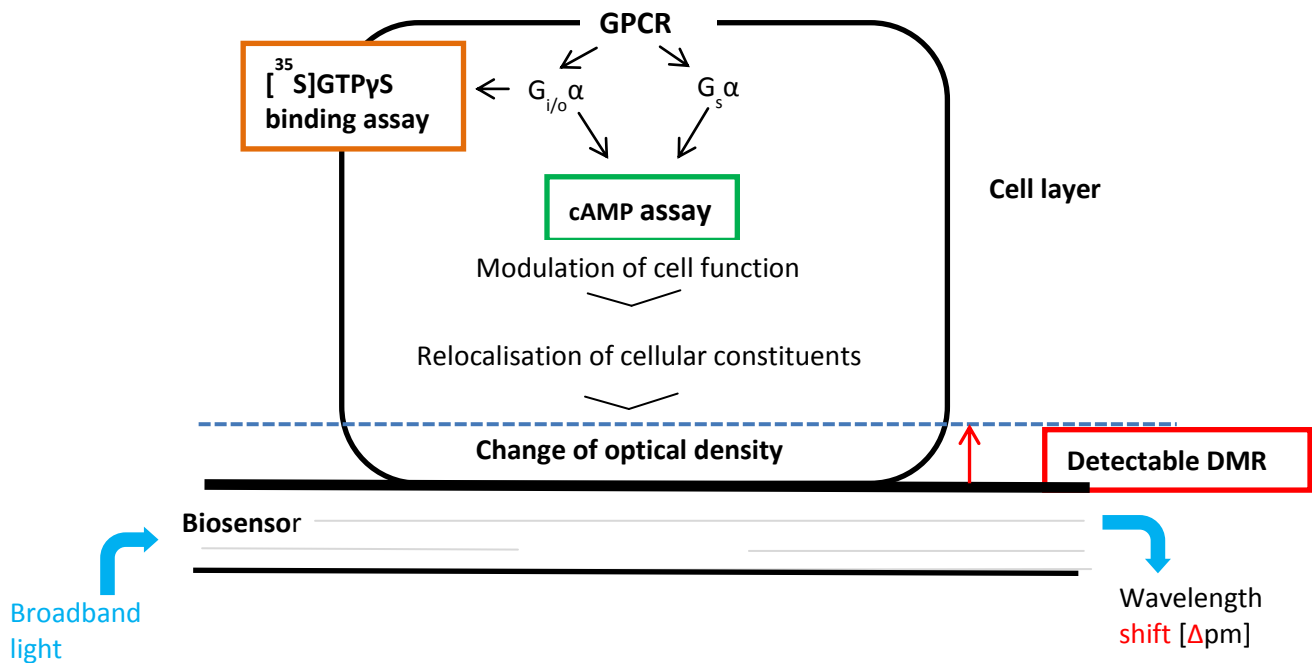


**Figure 4.2 Different levels of detecting signalling pathways.** The [ $^{35}\text{S}$ ]GTP $\gamma$ S binding assay (brown box) enables for the determination of proximal signalling in membrane preparations, measuring the direct consequences of receptor activation. cAMP assay (green box) is a second messenger assay downstream of the G-proteins which measures  $G_{i/o}$  and  $G_s$  signalling. The DMR assay (blue and red) is a non-invasive assay which measures the global relocation of biomolecules and the area of measurement is further downstream of the receptor at the bottom of the cell (150nm range of detectable DMR). Adapted from Kebig *et al.*, 2009 and Schröder *et al.*, 2010).

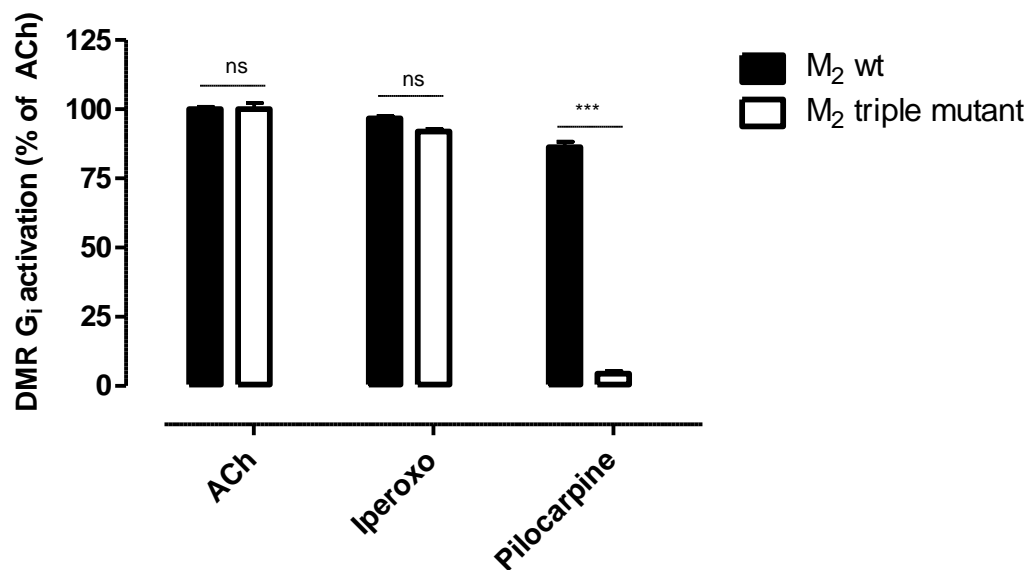


**Figure 4.3 The partial agonist pilocarpine is unable to activate  $G_{i/o}$  signalling in DMR via the  $M_2$  triple mutant.**  $G_{i/o}$  signalling by the full agonists acetylcholine (ACh), and iperoxo and the partial agonist pilocarpine in  $M_2$  wt and triple mutant cells. The maximum  $G_i$  activation induced by acetylcholine was set at 100% and the basal in the absence of ligand as 0%. Statistical analysis was performed by the Student's t-test. Data represents means  $\pm$  S.E.M of four independent experiments.

\*\*\* Significantly different from maximum  $G_{i/o}$  activation at the  $M_2$  wt (\*\* $p < 0.0001$ )

<sup>ns</sup> Not significantly different from the maximum  $G_{i/o}$  activation at the  $M_2$  wt and

### **$G_s$ signalling**

The concept of GPCR promiscuity is now established, whereby a receptor protein is able to interact and signal through different types of G-proteins. The  $M_2$  receptor predominantly signals through the  $G_{i/o}$  proteins (Caulfield and Birdsall, 1998) but can also convey signal transduction through the  $G_s$  proteins. This can be referred to as functional selectivity or ligand induced differential signalling (Kenakin, 2003; Urban *et al.*, 2007). Here, the effects of the  $M_2$  triple mutation on the  $M_2$ - $G_s$  signalling were examined with the second messenger cAMP assay and the DMR assay. The endogenous ligand acetylcholine, the superagonist iperoxo and the partial agonist pilocarpine were chosen to cover the wide spectrum of agonists' effects.

The maximum effect of full agonists acetylcholine and iperoxo was reduced at the  $M_2$  triple mutant in  $G_s$  activation. This was observed in both the cAMP accumulation and DMR assays. However, the superagonist iperoxo displayed a smaller decrease in maximum activation than

acetylcholine in both assays even though the acetylcholine concentration was 10 and 100 fold higher than iperoxo in the cAMP accumulation and DMR, respectively (**Figure 3.11 and Figure 4.4**). As iperoxo is a superagonist and known to display super efficacious traits and extraordinarily high potency at the  $M_2$  receptor (Schrage *et al.*, 2013; Kruse *et al.*, 2014) the data suggests that the allosteric core region of the  $M_2$  receptor also regulates the maximum effect levels mediated by structurally different full agonists in activating the  $G_s$  pathway. This also shows that the allosteric site core region is more sensitive to the endogenous ligand acetylcholine compared to iperoxo in terms of the  $G_s$  activation. On the other hand, the partial agonist pilocarpine was unable to activate  $G_s$  in both assays signalling in both the  $M_2$  wt and triple mutant. It appears that pilocarpine fails to induce receptor confirmation which is able to trigger the activation of the  $G_s$  pathway.

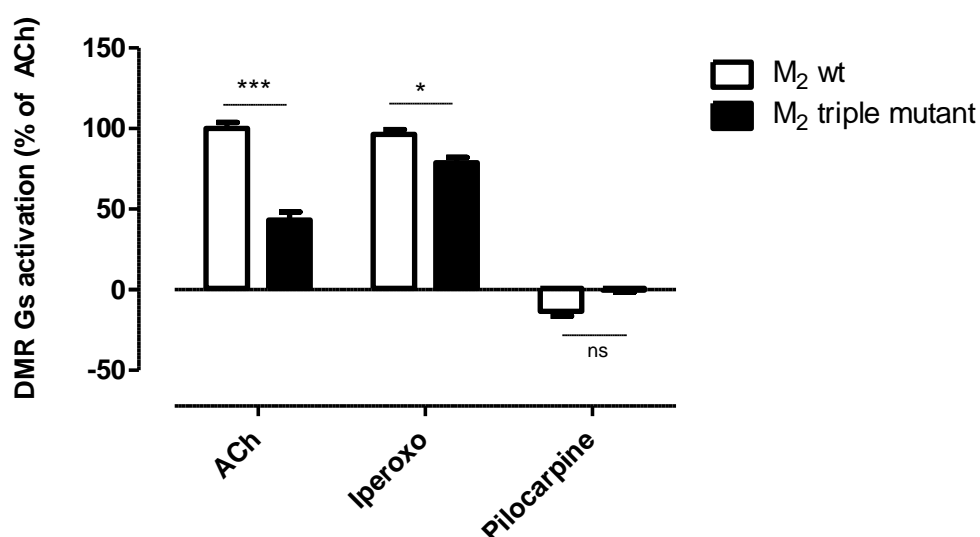


**Figure 4.4 Quantifying the loss of  $G_s$  signalling measured by DMR.**  $G_s$  signalling by the full agonists acetylcholine (ACh) (100 $\mu$ M), and iperoxo (1 $\mu$ M) is significantly reduced at the  $M_2$  triple mutant. Pilocarpine (100  $\mu$ M) could not induce any significant  $G_s$  activation both at the  $M_2$  wt and  $M_2$  triple mutant receptors. The maximum  $G_s$  activation induced by acetylcholine was set at 100% and the basal in the absence of ligand as 0%. Statistical analysis was performed by the Student's t-test. Data represents means of four independent experiments.

\*\*\* Significantly different from maximum  $G_s$  activation at the  $M_2$  wt (\*\* $p < 0.001$ ; \*  $p < 0.05$ )

<sup>ns</sup> Not significantly different from the maximum  $G_s$  activation at the  $M_2$  wt

#### **4.4 The M<sub>2</sub> core allosteric binding site as a selectivity filter against non-muscarinic biogenic amine ligands?**

Even with the recent advancements in crystal structures, some structural features of GPCRs still remain to be elucidated and their physiological functions remain unknown. Here, it seems that the allosteric binding domain of the M<sub>2</sub> receptor also functions as a barrier against epinephrine, a non-muscarinic ligand, at an M<sub>2</sub> receptor which is not locked in the inactive state. The findings suggest that epinephrine is able to gain entrance into the orthosteric binding site and partially activate the G<sub>i/o</sub> signalling when the ‘gate-keeping’ mechanism of the M<sub>2</sub> receptor is compromised.

#### **Epinephrine displaces the binding of the orthosteric agonist [<sup>3</sup>H]Iperoxo at the M<sub>2</sub> triple mutant receptor**

All of the studies investigating the allosteric vestibule as a probable selectivity filter for orthosteric ligand binding have so far been focused mainly on selectivity within respective receptor-family subgroups. This study goes a step further and investigates the M<sub>2</sub> allosteric binding site as a possible barrier or selectivity filter against the non-muscarinic biogenic amine ligand epinephrine. Equilibrium binding studies with the recently produced novel muscarinic radioagonist [<sup>3</sup>H]iperoxo, showed that epinephrine was able to compete with the radioligand for the orthosteric binding pocket of the M<sub>2</sub> triple mutant receptor (**Figure 3.13**). The high affinity and stable radioagonist [<sup>3</sup>H]iperoxo, currently poses as the best tool available for the direct probing of conformational transitions in active muscarinic receptors (Schrage *et al.*, 2014). Therefore, the results suggest that the allosteric core binding site also functions as a critical selective-barrier for epinephrine at an active M<sub>2</sub> receptor.

In the inactive M<sub>2</sub> wild type and triple mutant receptors, epinephrine was unable to gain entry into the orthosteric binding site. This illustrates that only removing the three bulky aromatic epitopes of the allosteric binding site and opening up the narrow passage leading to the orthosteric binding pocket is not enough to allow access of epinephrine into the M<sub>2</sub> binding pocket. A change in receptor conformation from the inactive state alone also seems insufficient to enable the entrance of epinephrine into the binding pocket of the M<sub>2</sub> wild type as epinephrine failed to significantly displace the radioagonist [<sup>3</sup>H]iperoxo from the orthosteric binding pocket. It is only in the active conformation of the receptor lacking the epinephrine barrier (M<sub>2</sub> triple mutant) in which epinephrine is observed to access the orthosteric binding pocket of a muscarinic receptor.

It is well established that the largest differences amongst GPCRs is in the extracellular vestibule (Rasmussen *et al.*, 2007). Hence, it makes sense that a selective-barrier for the M<sub>2</sub> receptor would be located in this extracellular surface to act as a gate-keeper for the orthosteric binding site against non-muscarinic ligands such as epinephrine. The recent crystal structure shows that when activated, the M<sub>2</sub> receptor goes through massive conformational changes in the extracellular surface, leading to a contraction of the extracellular vestibule. Also, in the presence of iperoxo an allosteric agonist LY2119620 forms extensive aromatic staking interactions with the key allosteric epitopes W422<sup>7.35</sup> and Y177<sup>ECL2</sup> (Kruse *et al.*, 2013). Thus, the findings argue that at least two important conditions are necessary to abolish specificity of the M<sub>2</sub> receptor towards muscarinic ligands and allow an adrenoceptor ligand, epinephrine to bind in the orthosteric pocket. Therefore, the data argues that removing the aromatic barrier at the entrance to the orthosteric binding site coupled with the transition of the receptor from the inactive state, creates a receptor conformation whereby the orthosteric site becomes accessible to epinephrine.

### **Epinephrine partially activates the M<sub>2</sub> triple mutant**

The activation mechanism of the M<sub>2</sub> receptor seems to be a dynamic process whereby the receptor goes through several intermediate states from the inactive until it reaches the fully active state (Miao *et al.*, 2013). Data suggests that when the receptor is not locked in an inactive state by a radioantagonists such [<sup>3</sup>H]NMS, epinephrine is able to bind to an M<sub>2</sub> receptor conformation lacking the epinephrine-selective barrier and induce receptor activation. First, the [<sup>35</sup>S]GTPγS binding experiment which exclusively captures the G<sub>i</sub>-signalling pathway (Milligan 2003) proximal to the GPCR was employed. Results from this study show that epinephrine partially activates the G<sub>i/o</sub> pathway but with a very low maximum effect of about 24%. Surprisingly, epinephrine was as potent as the typical muscarinic partial agonist pilocarpine acting on the M<sub>2</sub> wt and triple mutant receptors. Moreover, the potency of epinephrine was also similar to that of the endogenous ligand acetylcholine at the M<sub>2</sub> triple mutant. Epinephrine also displayed similar submaximal efficacy levels as pilocarpine at the M<sub>2</sub> triple mutant receptor (**Figure 3.14; Table 3.10**). Thus, this evidence shows that when the barrier against epinephrine is compromised, epinephrine can behave as a typical partial agonist at an M<sub>2</sub> receptor.

However, the coupling efficiency ( $\tau$ ) of epinephrine and pilocarpine at the M<sub>2</sub> triple mutant were very weak compared to that of pilocarpine at the M<sub>2</sub> wild type receptor in the [<sup>35</sup>S]GTPγS binding assay (**Figure 3.15**). This might explain why we do not observe G<sub>i/o</sub>-

signalling at the M<sub>2</sub> triple mutant for both epinephrine and pilocarpine in the DMR assays. The label free DMR technology measures a cumulative response overlay of signal processes happening in the entire living cells (Kebig *et al.*, 2009), whilst the [<sup>35</sup>S]GTPγS binding assay enables for the determination of proximal signaling in membrane preparations (Akam *et al.*, 2001) (**Figure 4.2**). Results suggest that due to the weak coupling efficiency between the receptor and G-protein at the M<sub>2</sub> triple mutant, partial agonists become very weak partial agonists which are unable to stimulate a global relocalisation of biomolecules which can be measured as either a positive or negative DMR signal.

It is a plausible outcome that an adrenergic ligand would be able to activate a muscarinic receptor if it would manage to gain entry into the orthosteric binding pocket as presented in this study. Amine ligands are all positively charged at physiological pH and interact with a key negatively charged aspartate residue (Asp<sup>3.32</sup>) residue in their respective orthosteric binding sites (Jaakola *et al.*, 2008). M<sub>2</sub> Asp103<sup>3.32</sup> plays a central role in the activation of the M<sub>2</sub> receptor whereby its acidic side chain engages in a charge to charge interaction with the positively charged amine moiety of the ligand (Avlani *et al.*, 2007; Haga *et al.*, 2012; Kruse *et al.*, 2013). This aspartate moiety is conserved across all biogenic amine GPCRs (Ring *et al.*, 2007).

It is critically important to have this selectivity filter in place to prevent non-specific activation of the M<sub>2</sub> receptor by other non-muscarinic biogenic amines as in this case epinephrine. Even though the other biogenic amines serotonin, histamine, norepinephrine and dopamine were unable to yield the activation of the triple mutant receptor (**Figure 3.19**), it does not disprove the hypothesis. It can be speculated that there is a gate keeping mechanism specific for each of the non-muscarinic biogenic amines at the M<sub>2</sub> receptor. For example, norepinephrine here seems to partially displace the radioagonist [<sup>3</sup>H]iperoxo which can signify a high negative cooperativity of norepinephrine bound in the allosteric site against [<sup>3</sup>H]iperoxo bound in the orthosteric pocket (**Figure 3.25**). The disruption of the right combinations of epitopes just outside the entrance to the orthosteric access might result in the M<sub>2</sub> receptor losing its specificity as a muscarinic receptor for the other biogenic amines. On the other hand, it is possible that other biogenic amines might be able to access the binding site of our M<sub>2</sub> triple mutant but are unable to evoke receptor activation as reflected by the norepinephrine data (**Figure 3.19d and 3.25**).

## 4.5 The M<sub>2</sub> triple mutant increases the fraction of active receptor populations

### Equilibrium binding

This part of the thesis dealt with the results of part of the project for the Bock *et al.*, 2014a publication on dualsteric ligand binding. Dualsteric (hybrid) ligands are composed of the orthosteric moieties covalently linked to the allosteric moieties enabling these hybrid ligands to interact with the orthosteric and allosteric binding site, simultaneously (Kebig *et al.*, 2009). The data here helped produce the novel findings that the dualsteric ligands are able to stabilise two receptor populations of the M<sub>2</sub> receptor. The dualsteric ligands are able to achieve this phenomenon by binding in either the active dualsteric or inactive allosteric orientations, termed dynamic ligand binding (**Figure 4.5**) (Bock *et al.*, 2014a). Here, investigations were further carried out with the M<sub>2</sub> triple mutant in radioligand binding experiments to probe the effects of the allosteric triple mutation on the dynamic ligand binding of dualsteric ligands.

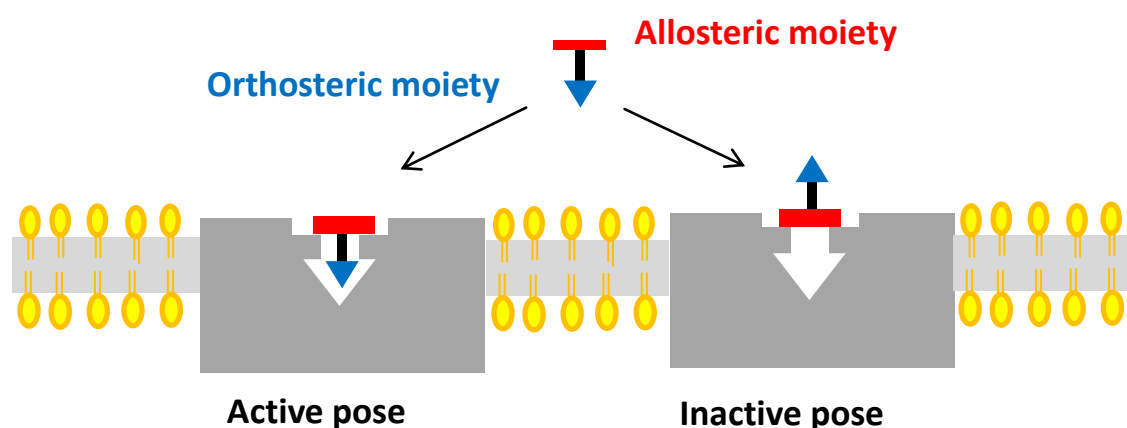


**Figure 4.5** A dualsteric ligand can stabilise an active (dualsteric) pose or a purely allosteric (inactive) pose. A dualsteric ligand consists of an allosteric moiety (red), carbon chain linker (black) and the orthosteric moiety (blue).

### Allosteric moieties

The allosteric moieties 6-naph and 6-phth can be described as inactive at the M<sub>2</sub> wt receptor as they were unable to cause receptor activation, but actually function as inverse agonists (**Sup. Figure 3.42**). Although 6-naph generally displayed higher binding affinities at both the M<sub>2</sub> wt and the M<sub>2</sub> triple mutant than 6-phth, both inactive moieties lost similar amounts of binding affinity at the M<sub>2</sub> triple mutant (**Table 3.12**). This shows that the substitution of the



three amino acids in the allosteric core binding region of the M<sub>2</sub> was not particularly more sensitive to the binding of either allosteric moiety. However, 6-naph switched from promoting orthosteric radioligand binding at the M<sub>2</sub> wt to enhancing the orthosteric radioligand displacement at the M<sub>2</sub> triple mutant (**Figure 3.27; Table 3.12**). This corresponds to the published data (Bock *et al.*, 2014a) which showed that the M<sub>2</sub> W422<sup>7.35</sup>A allosteric loss-of-affinity single mutation enhances the displacement of the orthosteric ligand [<sup>3</sup>H]NMS.

On the other hand the cooperativity of 6-phth with the orthosteric radioligand [<sup>3</sup>H]NMS did not change at the M<sub>2</sub> triple mutant in comparison to the M<sub>2</sub> wt (**Figure 3.28; Table 3.12**). In summary the data suggests that the interaction of 6-naph with the allosteric core region of the M<sub>2</sub> receptor is crucial not only for the binding affinity but also the cooperativity. It seems that although 6-naph loses affinity at the M<sub>2</sub> triple mutant, it somehow adopts a binding orientation within the allosteric binding site which results in an increased negative cooperativity with the orthosteric ligand. In contrast 6-phth displayed negative cooperativity already at the M<sub>2</sub> wt and this cooperativity was unchanged at the M<sub>2</sub> triple mutant. This suggests that the three mutated amino acids seem to be unimportant regarding the cooperativity of 6-phth with [<sup>3</sup>H]NMS binding.

### Dualsteric ligands

Two recently developed methods of data analysis were used to obtain the fractional occupancies and the binding orientation ratios ( $R_{pose}$ ) for the dualsteric ligands. The fractional occupancy (chapter 3.4.2) determines the fractional size of active versus inactive receptor populations. The orientation ration ( $R_{pose}$ ) on the other hand quantifies the equilibrium position between active and inactive receptor ensembles. The first method was the global simultaneous analysis of the dualsteric ligand binding and allosteric moiety binding only (Global analysis of 2 curves). This is a global analysis which combines the Ehlert, 1988 and the May/Antony, 2007 equations. The global analysis share the  $K_B$  (affinity of the purely allosteric inactive pose) value between the two equations given above to enable the model to find numerical estimates which try to meet the demands of both equations. Sharing the  $K_B$ , however, does not mean that  $K_B$  is fixed but that both data sets can contribute or are flexible to find values for parameters such as  $K_A$  (affinity of the dualsteric active pose) and  $\alpha'$  (cooperativity of the hybrid ligand with [<sup>3</sup>H]NMS).

The second method was the global simultaneous analysis of dualsteric ligand binding, allosteric moiety binding, dualsteric ligand [<sup>35</sup>S]GTPγS and acetylcholine [<sup>35</sup>S]GTPγS data (Global analysis of 4 curves). The idea was that both the dualsteric ligand functional and binding data should contribute to the finding of the parameter K<sub>A</sub> of the hybrid ligand without predefining the K<sub>B</sub> or the cooperativity (α') by values obtained from the allosteric moiety of the respective dualsteric ligand (Chen *et al.*, 2014).

The dualsteric ligands with iperoxo as their orthosteric moiety, iper-6-phth and iper-6-naph displaced [<sup>3</sup>H]NMS at both the M<sub>2</sub> wt and triple mutant. This reflected the preferential binding of these hybrids in the active orientation. However, the displacement was incomplete showing that there was a small population of receptors which were occupied by the purely inactive orientation of the hybrid ligands (**Figure 3.30 and 3.31**). This is coherent with the data published by Bock *et al.*, 2014a, which also showed that the iper-6-phth and iper-6-naph bind to the M<sub>2</sub> wt preferentially in the active pose with a small percentage binding in the purely allosteric pose. This also explains at least partially why the dualsteric ligands show partial agonistic behaviour (**Sup. Figure 3.45 and 3.46**) (Bock *et al.*, 2014a).

At the M<sub>2</sub> triple mutant the relative fraction of active versus inactive receptor populations actually increased for both iper-6-naph and iper-6-phth ( $R_{pose} = 1.69 \pm 0.10$  and  $1.61 \pm 0.12$ ), respectively in comparison to the M<sub>2</sub> wt ( $R_{pose} = 1.24 \pm 0.05$  and  $0.83 \pm 0.12$ ) (**Figure 4.6; Table 4.1**). An  $R_{pose}$  value greater than 0 ( $R_{pose} > 0$ ) shows that a dualsteric ligand preferentially binds in the dualsteric active pose (>50%), whilst an  $R_{pose}$  value less than 0 ( $R_{pose} < 0$ ) reflect a preferential binding in the purely allosteric inactive pose. As the allosteric fragments 6-naph and 6-phth lose affinity at the M<sub>2</sub> triple mutant, this results in an increased amount of receptor populations being occupied preferably by the active dualsteric binding poses of these dynamic ligands.

When the orthosteric moiety was changed from iperoxo to isoxazole, which is less affine but equally efficacious with respect to the maximum effect (**Sup. Figure 3.42 and 3.43**), the  $R_{pose}$  ratios decreased compared to the 'iper' dualsteric ligands (**Figure 4.6; Table 4.1**). As the orthosteric 'isox' moiety binds with lower affinity than iperoxo, this result in more of the 'isox' dualsteric ligands binding in the inactive pose compared to the 'iper' dualsteric ligands. At the M<sub>2</sub> triple mutant isox-6-phth and isox-6-naph displayed about 2-fold higher  $R_{pose}$  ratios of  $0.81 \pm 0.14$  and  $0.70 \pm 0.14$ , respectively compared to the M<sub>2</sub> wt.

The  $R_{pose}$  data of isox-6-naph at the M<sub>2</sub> wt is not so clear to clearly state that isox-6-naph preferentially binds in a pure allosteric orientation. The  $R_{pose}$  value obtained at the M<sub>2</sub> wt was -0.3 suggesting that the inactive binding pose is the preferred orientation (**Table 4.1**). However, the standard error of (SEM = ± 1.76) was too big to make a concrete statement on the position of equilibrium ( $R_{pose}$ ) of isox-6-naph. This may show that the operational model of dynamic ligands is unable to properly fit data for ligands such as isox-6-naph which display a higher/equal allosteric binding affinity ( $K_B$ ) than the ( $K_A$ ). The  $R_{pose}$  obtained here for isox-6-naph at the M<sub>2</sub> wt, is in agreement with that shown in the in the Bock *et al.*, 2014a whereby isox-6-naph was also shown to have a slightly negative  $R_{pose}$  ratio. However, there were no error bars given in the publication to compare with the big standard error of mean obtained here.

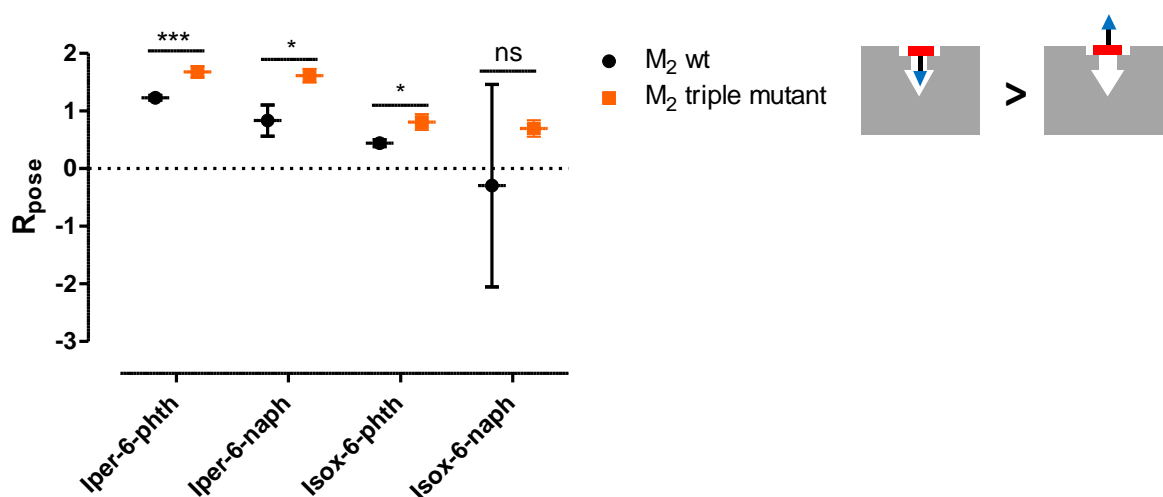


**Figure 4.6 The M<sub>2</sub> triple mutant increases the fractional receptor occupancy of the active dualsteric pose.** The relative fraction of the active versus inactive receptor populations of the dualsteric ligands iper-6-phth, iper-6-naph, isox-6-phth and isox-6-naph at the M<sub>2</sub> wt and M<sub>2</sub> triple mutant.  $R_{pose} = -\log K_{active}/K_{inactive}$ . Indicated are  $R_{pose} \pm SEM$  derived from the global analysis of the hybrid and fragment binding only.

\*\*\*, \*Significantly different from the M<sub>2</sub> wt  $R_{pose}$  (\*\*\*, \* p < 0.05)

<sup>ns</sup>Not significantly different from the M<sub>2</sub> wt  $R_{pose}$

Statistical analysis by Student's t-test

Therefore, looking at the data from the global analysis of dualsteric ligand binding and allosteric moiety binding only, it can be concluded that the binding pose ( $R_{pose}$ ) ratios of dualsteric dynamic ligands iper-6-phth, iper-6-naph and isox-6-phth increase at the M<sub>2</sub> triple mutant (**Figure 4.6**). Given the fact that M<sub>2</sub> allosteric triple mutation leads to a pronounced loss of allosteric binding affinity of the allosteric moieties 6-naph and 6-phth, the dualsteric

pose of the hybrid ligands is preferred at the triple mutant. In other words, this shows that the core allosteric binding domain of the M<sub>2</sub> receptor fine tunes the amount of active and inactive receptor populations and in some cases may lead to a complete ‘switch’ in preferential binding orientation as clearly shown by the isox-6-naph fractional occupancy data (**Figure 3.33**).

The Global fit of 4 curves analysis (Chen *et al.*, 2014) was performed with isox-6-naph in order to try and reduce the standard error of the mean of K<sub>A</sub> by the addition of functional data. However, the error could not be significantly reduced (**Table 4.1**). Hence, the position of equilibrium ( $R_{pose}$ ) of isox-6-naph compound has so far been difficult to analyse and adjustments to the global fit model need to be done in order to solve the problem of a huge K<sub>A</sub> error. One way to achieve this would be to substitute the  $\alpha'$  in the global analysis of four curves by K<sub>B</sub> and the dissociation constant EC<sub>0.5,diss</sub> as another method of calculating the K<sub>active</sub> and K<sub>inactive</sub> using dissociation binding instead of equilibrium binding data. In the end, the ( $R_{pose}$ ) values for the dualsteric ligands iper-6-naph, isox-6-naph and isox-6-phth at the M<sub>2</sub> wt determined by the hybrid binding data only and in the presence of the hybrid functional data were similar (**Table 4.1**).

M <sub>2</sub> wt		
	$R_{pose}$	
	Global analysis (2 curves)	Global analysis (4 curves)
Iper-6-naph	0.83 ± 0.27	1.16 ± 0.30
Isox-6-naph	-0.30 ± 1.76	-0.22 ± 1.12
Isox-6-phth	0.45 ± 0.06	0.46 ± 0.12

**Table 4.1 Comparison of  $R_{pose}$  estimates obtained using binding data only and in the presence of functional data.**  $R_{pose}$  data for the dualsteric ligands iper-6-naph, isox-6-naph and isox-6-phth. Global analysis data are parameter estimates ± SEM derived from the global fits.  $R_{pose} = -\log K_{active}/K_{inactive}$ . Global analysis (2 curves) represents global analysis of hybrid and fragment binding only. Global analysis (4 curves) represents global analysis of dualsteric ligand binding, allosteric moiety binding, dualsteric ligand [<sup>35</sup>S]GTPγS and acetylcholine [<sup>35</sup>S]GTPγS data.

### **The M<sub>2</sub> triple mutant forms ternary complexes with dualsteric ligands and the radioligand [<sup>3</sup>H]NMS**

The two dualsteric ligands iper-6-phth and iper-6-naph were both still able to interact with the [<sup>3</sup>H]NMS-occupied M<sub>2</sub> triple mutant receptor in a purely allosteric manner. Both dynamic ligands could still form allosteric ternary complexes with the mutated M<sub>2</sub> receptor and the radioligand [<sup>3</sup>H]NMS (**Figure 3.38 and 3.39**). However, these two dualsteric ligands exhibited a pronounced loss of allosteric binding affinity at the M<sub>2</sub> triple mutant in comparison to the M<sub>2</sub> wt. These results corresponds to the dissociation data of the allosteric moiety 6-phth (**Figure 3.37; Table 3.16**) which show that 6-phth was still able to interact with the allosteric binding site of the M<sub>2</sub> triple mutant. Nevertheless, iper-6-naph lost a huge 1.46 log units binding affinity more than iper-6-phth at the M<sub>2</sub> triple mutant. It could be that the allosteric 6-naph loses more binding affinity than 6-phth at the triple mutant which results in the hybrid iper-6-naph losing more binding affinity too than iper-6-phth. Unfortunately, 6-naph dissociation binding was not performed in this study to compare with the 6-phth binding affinity.

Iper-6-phth and 6-phth both lost similar amounts of allosteric potency to retard [<sup>3</sup>H]NMS dissociation at the M<sub>2</sub> triple mutant ( $\Delta pEC_{0.5, \text{diss}} = 1.47 \pm 0.24$  and  $1.51 \pm 0.15$ ) respectively, compared to the M<sub>2</sub> wt (**Figure 3.36 and 3.37**). This is also another evidence that the dualsteric compounds are able to bind purely in the inactive allosteric pose as both the hybrid and fragment lose the same amount of binding affinity when the M<sub>2</sub> triple mutant orthosteric site is occupied by the radioligand [<sup>3</sup>H]NMS (**Figure 4.7**). The triple mutation was unable to distinguish between the binding of the allosteric moiety on its own and in the presence of the orthosteric iperoxo moiety. These data show that the allosteric core region is critical in determining the allosteric binding affinity of the allosteric moiety alone and also for the dualsteric ligand bound in the purely allosteric pose.

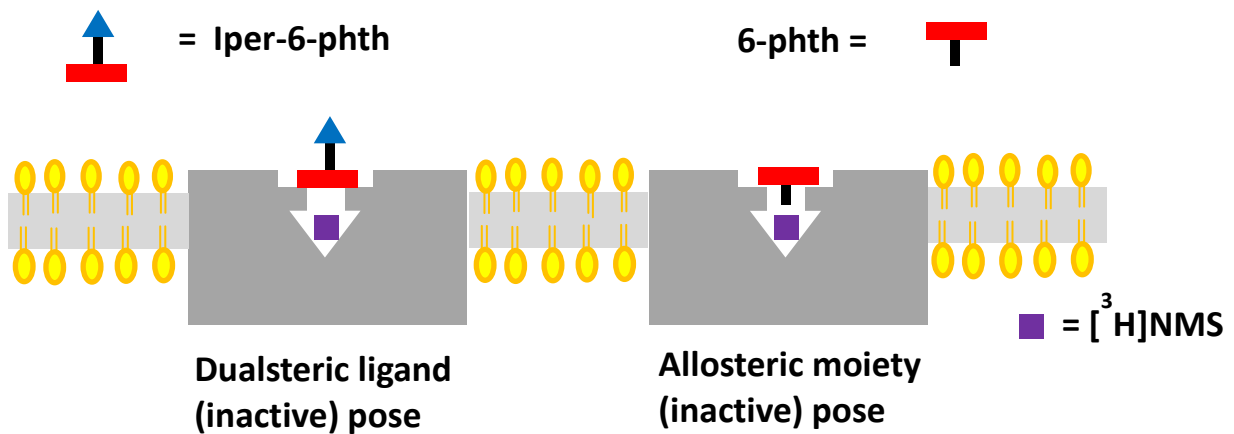


**Figure 4.7** The  $M_2$  triple mutant still forms ternary complexes with dualsteric ligands. Schematic diagram showing the dualsteric ligand iper-6-phth bound in the purely allosteric (inactive) pose and the allosteric moiety 6-phth docked in the allosteric pocket of a [ $^3\text{H}$ ]NMS-occupied  $M_2$  receptor

In contrast to the  $M_2$  wt, iper-6-phth and 6-phth became unable to completely retard the dissociation of the radioligand [ $^3\text{H}$ ]NMS from the orthosteric binding site of the  $M_2$  triple mutant (**Figure 3.36 and 3.37**). This is in agreement with the data for the allosteric ligand W84 which also lost allosteric efficacy to inhibit [ $^3\text{H}$ ]NMS dissociation (**chapter 3.1.1 and Table 3.1**). The data, therefore suggest that the docking of either the allosteric moiety or the dualsteric ligand in the purely inactive pose to an orthosterically-occupied  $M_2$  receptor is affected by triple mutation in the allosteric site core binding region. It might be that triple mutation forces the ligands to bind in a different orientation within the allosteric vestibule in a way which makes them incapable of fully inhibiting [ $^3\text{H}$ ]NMS dissociation from the orthosteric binding site.

## 5. Summary

The present study aimed at investigating the consequences caused by the substitution of the three core amino acids (Y177<sup>ECL2</sup> →Ala, W422<sup>7.35</sup> →Ala and T423<sup>7.36</sup> →Ala) located in the “bottleneck-region”, between the orthosteric and the allosteric part of the ligand binding cavity of the M<sub>2</sub> mAChRs on ligand binding, receptor activation and receptor-ligand selectivity. The flexible alkane-bisammonium allosteric modulator W84 showed that the common allosteric binding site is still present and functional even after the substitution of the three critical amino acids. The M<sub>2</sub> triple mutant receptor was still able to form ternary complexes with allosteric and orthosteric ligands. However, there was a huge loss in allosteric binding potency and efficacy to retard the orthosteric radioligand [<sup>3</sup>H]NMS dissociation. The M<sub>2</sub> triple mutant lost 2.5 log units of binding affinity compared to previously published 1.5 log units with the W422<sup>7.35</sup>A single mutant. Hence, it is clear from this study that at least the other amino acids T423<sup>7.36</sup> and Y177<sup>ECL2</sup> contribute to the 1 log unit extra loss of W84 binding affinity. The loss in allosteric binding affinity was insensitive to changes in experimental buffer conditions and whether it was in live cells or cells membranes.

Radioligand binding experiments with [<sup>3</sup>H]NMS at the M<sub>2</sub> wt and triple mutant receptor showed that the triple mutant strongly reduces the binding affinities of the M<sub>2</sub> muscarinic agonists. Interestingly, the partial agonist pilocarpine’s binding to M<sub>2</sub> receptor was observed to be completely insensitive to the triple mutation. Hence, the M<sub>2</sub> allosteric core binding site located at the entrance to the orthosteric site is able to decipher different pharmacophores of orthosteric ligands and thereby possess a key mediating role in the binding of chemically distinct muscarinic agonist ligands.

The [<sup>35</sup>S]GTPγS binding assay showed that the M<sub>2</sub> muscarinic full agonists acetylcholine and iperoxo lose potency at the triple mutant but their maximum effect remain unchanged compared to M<sub>2</sub> wt receptor in G<sub>i/o</sub> signalling. However, the partial agonist pilocarpine lost about half its ability to induce receptor activation as depicted by the decrease in maximum effect at the triple mutant, but its potency remained unchanged compared to M<sub>2</sub> wt receptors. Therefore, the loss in agonist potency at the M<sub>2</sub> triple mutant can be attributed to the loss in binding affinity. The loss in maximum activation for the partial agonist pilocarpine shows that the core region of the allosteric site is an essential part of the network needed to stabilise receptor activation induced by pilocarpine.

[<sup>3</sup>H]NMS Equilibrium binding and [<sup>35</sup>S]GTPγS binding data of dualsteric ligands iper-6-phth, iper-6-naph and isox-6-phth showed the M<sub>2</sub> triple mutant increases the amount of receptor populations bound in the active (dualsteric) pose compared to the inactive (purely allosteric) pose. This shows that the core allosteric binding domain of the M<sub>2</sub> receptor fine tunes the amount of active and inactive receptor populations and in some cases may lead to a complete ‘switch’ in preferential binding orientation as clearly shown by the isox-6-naph fractional occupancy data.

On the topic regarding receptor-ligand selectivity against biogenic amines, equilibrium binding studies with the recently produced novel muscarinic radioagonist [<sup>3</sup>H]iperoxo, showed that epinephrine was able to compete with the radioligand for the orthosteric binding pocket of the M<sub>2</sub> triple mutant receptor. The [<sup>35</sup>S]GTPγS binding assay showed that epinephrine partially activates the G<sub>i/o</sub> pathway at the M<sub>2</sub> triple mutant. Surprisingly, epinephrine was as potent as the typical muscarinic partial agonist pilocarpine acting on the M<sub>2</sub> wt and triple mutant receptors. The signalling efficacy (τ) of epinephrine and pilocarpine at the M<sub>2</sub> triple mutant was very weak compared to that of pilocarpine at the M<sub>2</sub> wild type receptor in the [<sup>35</sup>S]GTPγS binding assay. This suggests that pilocarpine and epinephrine become very weak partial agonists at the M<sub>2</sub> triple mutant. However, both epinephrine and pilocarpine failed to induce G<sub>i/o</sub> signalling at the M<sub>2</sub> triple mutant in the live-cells using DMR assay. This might be explained by the weak signalling efficacy of transducing receptor activation into a downstream signal at the M<sub>2</sub> triple mutant. Hence, this suggests that epinephrine effects are localize close to the M<sub>2</sub> triple mutant receptor molecule.

Norepinephrine appeared to show a partial displacement of the radioagonist [<sup>3</sup>H]iperoxo at M<sub>2</sub> triple mutant. This suggests that norepinephrine might be bound to the allosteric binding site and exhibiting high negative cooperativity with the orthosteric radioligand. Norepinephrine was unable to induce receptor activation either in the [<sup>35</sup>S]GTPγS binding or DMR assay and this trend was true for the other biogenic amines dopamine, histamine and serotonin. In summary, this study neither concludes that the allosteric core region of the M<sub>2</sub> receptor also functions as a biogenic amine selectivity filter nor disproves the hypothesis. Based on results of epinephrine and norepinephrine it can be speculated that there might be a ‘gate-keeping’ mechanism specific for each of the non-muscarinic biogenic amines at the M<sub>2</sub> receptor and more studies need to be done.



Therefore, taken together all these results show that the narrow passage between the allosteric and orthosteric binding site is more than just a core allosteric ligand docking site. It also mediates orthosteric ligand binding and regulates signalling intensity. In other words it has a key role in receptor function. Ultimately, there are hints that this critical area might also function as a selectivity filter against biogenic amine ligands.

## 6. Outlook

Epinephrine appeared to displace [<sup>3</sup>H]Iperoxo at the M<sub>2</sub> triple mutant in the radioligand equilibrium binding studies. If this result is taken on its own it would appear that epinephrine is competing with the radioligand [<sup>3</sup>H]Iperoxo for the orthosteric binding site. However, as shown previously and also in this thesis, allosteric ligands are also able to show full radioligand displacement in equilibrium binding studies. These allosteric ligands are said to be exhibiting high negative cooperativity with the radioligand. Therefore, it will be necessary to conduct radioligand dissociation experiments with the radioagonist [<sup>3</sup>H]Iperoxo in order to investigate if epinephrine would form ternary complexes with the receptor and the radioagonist. It might be that the effects observed in equilibrium binding studies might be due to epinephrine binding to the allosteric site albeit with a high negative cooperativity against [<sup>3</sup>H]Iperoxo equilibrium binding. This also applies to norepinephrine which showed a partial displacement of [<sup>3</sup>H]Iperoxo in equilibrium binding studies.

On the level of signalling, it was very interesting to see that epinephrine cannot stimulate DMR in whole cells but activates [<sup>35</sup>S]GTPγS binding in cell membranes. This would point to a more localized signalling of epinephrine. However, it might be possible that epinephrine only works in membrane preparations and not in live cells. To rule out this possibility, equilibrium binding studies with [<sup>3</sup>H]Iperoxo need to be performed to show that epinephrine indeed binds to the M<sub>2</sub> triple mutant in living cells. Intramolecular FRET at receptor molecules has been demonstrated at the muscarinic receptors to provide real time receptor activation studies (Hoffmann *et al.*, 2005; Marullo and Bouvier, 2007). Therefore, epinephrine binding can also be probed with an M<sub>2</sub> triple mutant-FRET sensor. This would provide a direct evidence of M<sub>2</sub> receptor binding and activation.

The M<sub>2</sub> receptor predominantly signals through the G<sub>i/o</sub> proteins. The upward positive peak observed in DMR with the M<sub>2</sub> receptor signifies G<sub>i/o</sub> signalling. However, the DMR peaks combine all the signalling pathways possible and the use of toxins to mask certain pathways reveals the individual contributing signalling pathways. As the muscarinic partial agonist pilocarpine and epinephrine both failed to activate DMR, it might be that both ligands also partially activate G<sub>s</sub> signalling in DMR. In that case, the small downwards G<sub>s</sub> and upwards G<sub>i/o</sub> signals can neutralise each other resulting in a nearly zero peak which appears as if there is no activation. Hence, DMR experiments can be carried out at the M<sub>2</sub> triple mutant after treating the cells with the G<sub>s</sub> inhibitor cholera toxin (CTX). CTX irreversibly ADP-ribosylates

the  $G_s\alpha$  subunit leading to a permanent G-protein activation. This masks the signal as further activation cannot be detected (Gill and Meren, 1978). Hence, if the  $G_s$  signal is masked a  $G_{i/o}$  signal might be observed in the DMR assay at the  $M_2$  triple mutant for both epinephrine and pilocarpine. However, this is highly unlikely as the cAMP data showed that pilocarpine was unable to stimulate  $G_s$  through both the  $M_2$  wt and  $M_2$  triple mutant receptors (**chapter 3; Figure 3.11**).

Y177<sup>ECL2</sup>A single mutants and Y177<sup>ECL2</sup>A, T423<sup>7.36</sup>A double mutant receptors can be used to find out the exact contributions of each amino acid in the loss of allosteric binding potency. The single mutant T423A has been shown to have an insignificant effect in the loss of the allosteric binding potency. However, having observed a 1.5 log unit and 2.5 log unit loss in binding potency at the at the W422A  $M_2$  single and  $M_2$  triple mutant, respectively it is intriguing to find out if Y177 solely contributes to the extra 1 log unit loss in affinity or that T423 contributes when mutated simultaneously with other epitopes.

The single and double mutants can also help reveal why full [<sup>3</sup>H]Iperoxo displacement is observed with epinephrine (**Figure 3.13**) and only partial displacement with norepinephrine (**Figure 3.25**). This can also lead to explanations why we see activation in the [<sup>35</sup>S]GTP $\gamma$ S with epinephrine (**Figure 3.14**) but not with norepinephrine (**Figure 3.19**) at the  $M_2$  triple mutant. It is also necessary to carry out equilibrium binding studies with [<sup>3</sup>H]Iperoxo for the other biogenic amines dopamine, histamine and serotonin to find out if they would also displace a radioagonist at the  $M_2$  triple mutant. It might be that they bind to the muscarinic mutant receptor but unable to induce receptor activation.

## 7. Abbreviations

°C:	degrees Celsius
5HT:	5-hydroxytryptamine
ACh:	Acetylcholine
ADP:	Adenosine 5'-disphosphate
ANOVA:	Analysis of variance
ATCM:	Allosteric ternary complex model
Atr:	Atropine
cAMP:	Cyclic adenosine monophosphate
CHO:	Chinese hamster ovary
CHO-hM <sub>2</sub> :	Chinese hamster ovary cells stably transfected with the human M <sub>2</sub> muscarinic acetylcholine receptor
CNS:	Central nervous system
CTX:	Cholera toxin
DAG:	Diacylglycerol
DMEM:	Dulbecco's modified eagle medium
DMR:	Dynamic mass redistribution
DMSO:	Dimethyl sulfoxide
ECL2:	Extracellular loop 2
Epi:	Epinephrine
ER:	Smooth endoplasmic reticulum
FBS:	Fetal bovine serum
FRET:	Fluorescence resonance energy transfer
GDP:	Guanosine 5'- diphosphate
GIRK:	G-protein activated inwardly-rectifying potassium channels
G-protein:	Guanine nucleotide-binding protein
GPCR:	G protein-couple receptor

GTP:	Guanosine 5' - triphosphate
HBSS:	Hank's buffered saline solution
HEPES:	4-(2-Hydroxyethyl)-1-piperazineethane sulfonic acid
IP3:	inositol(1,4,5)triphosphate and
IBMX:	3-isobutyl-1-methylxanthine
mAChR:	Muscarinic acetylcholine receptor
M <sub>2</sub> wt:	M <sub>2</sub> wild type
min:	Minutes
NaKPi:	Sodium potassium phosphate buffer
NMS:	N-methylscopolamine
NO:	Nitric oxide
p:	p-value, probability
PBS:	Phosphate buffered saline
pEC <sub>50</sub> :	Negative logarithm of the ligand concentration required to induce half the maximal activation
Pilo:	Pilocarpine
PIP2:	Phosphatidylinositol(4,5)bisphosphate
PKA:	Protein kinase A
PLCβ:	Phospholipase Cβ
pm:	Picometer
Prop:	Propranolol
PTX:	Pertussis toxin
RGS:	Regulators of G-protein signalling
RWG:	Resonant waveguide grating
S.E.M:	Standard error of mean
TM:	Transmembrane

## 8. References

- Akam, E. C.; Challiss, R. A.; Nahorski, S. R. (2001): G(q/11) and G(i/o) activation profiles in CHO cells expressing human muscarinic acetylcholine receptors: dependence on agonist as well as receptor-subtype. In: *British journal of pharmacology* 132 (4), S. 950–958. DOI: 10.1038/sj.bjp.0703892.
- Al-Gadi, M.; Hill, S. J. (1985): Characterization of histamine receptors mediating the stimulation of cyclic AMP accumulation in rabbit cerebral cortical slices. In: *British journal of pharmacology* 85 (4), S. 877–888.
- Allman, K.; Page, K. M.; Curtis, C. A.; Hulme, E. C. (2000): Scanning mutagenesis identifies amino acid side chains in transmembrane domain 5 of the M(1) muscarinic receptor that participate in binding the acetyl methyl group of acetylcholine. In: *Molecular pharmacology* 58 (1), S. 175–184.
- Almaula, N.; Ebersole, B. J.; Zhang, D.; Weinstein, H.; Sealfon, S. C. (1996): Mapping the binding site pocket of the serotonin 5-Hydroxytryptamine<sub>2A</sub> receptor. Ser3.36(159) provides a second interaction site for the protonated amine of serotonin but not of lysergic acid diethylamide or bufotenin. In: *The Journal of biological chemistry* 271 (25), S. 14672–14675.
- Antony, Johannes; Kellershohn, Kerstin; Mohr-Andrä, Marion; Kebig, Anna; Prilla, Stefanie; Muth, Mathias et al. (2009): Dualsteric GPCR targeting: a novel route to binding and signaling pathway selectivity. In: *FASEB journal : official publication of the Federation of American Societies for Experimental Biology* 23 (2), S. 442–450. DOI: 10.1096/fj.08-114751.
- Avlani, Vimesh A.; Gregory, Karen J.; Morton, Craig J.; Parker, Michael W.; Sexton, Patrick M.; Christopoulos, Arthur (2007): Critical role for the second extracellular loop in the binding of both orthosteric and allosteric G protein-coupled receptor ligands. In: *The Journal of biological chemistry* 282 (35), S. 25677–25686. DOI: 10.1074/jbc.M702311200.
- Barlow, R.; Blake, J. F. (1989): Hill coefficients and the logistic equation. In: *Trends in pharmacological sciences* 10 (11), S. 440–441. DOI: 10.1016/S0165-6147(89)80006-9.
- Barnes, N. M.; Sharp, T. (1999): A review of central 5-HT receptors and their function. In: *Neuropharmacology* 38 (8), S. 1083–1152.
- Beaulieu, Jean-Martin; Gainetdinov, Raul R. (2011): The physiology, signaling, and pharmacology of dopamine receptors. In: *Pharmacological reviews* 63 (1), S. 182–217. DOI: 10.1124/pr.110.002642.
- Berger, Miles; Gray, John A.; Roth, Bryan L. (2009): The expanded biology of serotonin. In: *Annual review of medicine* 60, S. 355–366. DOI: 10.1146/annurev.med.60.042307.110802.
- Birdsall, N J M; Lazareno, S. (2005): Allosterism at muscarinic receptors: ligands and mechanisms. In: *Mini reviews in medicinal chemistry* 5 (6), S. 523–543.
- Black, J. W.; Leff, P. (1983): Operational models of pharmacological agonism. In: *Proceedings of the Royal Society of London. Series B, Biological sciences* 220 (1219), S. 141–162.

- Bock, Andreas; Chirinda, Brian; Krebs, Fabian; Messerer, Regina; Bätz, Julia; Muth, Mathias et al. (2014a): Dynamic ligand binding dictates partial agonism at a G protein-coupled receptor. In: *Nature chemical biology* 10 (1), S. 18–20. DOI: 10.1038/nchembio.1384.
- Bock, Andreas; Kostenis, Evi; Tränkle, Christian; Lohse, Martin J.; Mohr, Klaus (2014b): Pilot the pulse: controlling the multiplicity of receptor dynamics. In: *Trends in pharmacological sciences* 35 (12), S. 630–638. DOI: 10.1016/j.tips.2014.10.002.
- Bock, Andreas; Merten, Nicole; Schrage, Ramona; Dallanoce, Clelia; Bätz, Julia; Klöckner, Jessica et al. (2012): The allosteric vestibule of a seven transmembrane helical receptor controls G-protein coupling. In: *Nature communications* 3, S. 1044. DOI: 10.1038/ncomms2028.
- Bock, Andreas; Mohr, Klaus (2013): Dualsteric GPCR targeting and functional selectivity: the paradigmatic M(2) muscarinic acetylcholine receptor. In: *Drug discovery today. Technologies* 10 (2), S. e245-52. DOI: 10.1016/j.ddtec.2012.12.003.
- Bokoch, G. M.; Katada, T.; Northup, J. K.; Ui, M.; Gilman, A. G. (1984): Purification and properties of the inhibitory guanine nucleotide-binding regulatory component of adenylate cyclase. In: *The Journal of biological chemistry* 259 (6), S. 3560–3567.
- Bonner, T. I.; Buckley, N. J.; Young, A. C.; Brann, M. R. (1987): Identification of a family of muscarinic acetylcholine receptor genes. In: *Science (New York, N.Y.)* 237 (4814), S. 527–532.
- Bruysters, Martijn; Jongejan, Aldo; Gillard, Michel; van de Manakker, Frank; Bakker, Remko A.; Chatelain, Pierre; Leurs, Rob (2005): Pharmacological differences between human and guinea pig histamine H1 receptors: Asn84 (2.61) as key residue within an additional binding pocket in the H1 receptor. In: *Molecular pharmacology* 67 (4), S. 1045–1052. DOI: 10.1124/mol.104.008847.
- Buller, Stefan; Zlotos, Darius Paul; Mohr, Klaus; Ellis, John (2002): Allosteric site on muscarinic acetylcholine receptors: a single amino acid in transmembrane region 7 is critical to the subtype selectivities of caracurine V derivatives and alkane-bisammonium ligands. In: *Molecular pharmacology* 61 (1), S. 160–168.
- Bylund, D. B. (1988): Subtypes of alpha 2-adrenoceptors: pharmacological and molecular biological evidence converge. In: *Trends in pharmacological sciences* 9 (10), S. 356–361.
- Bylund, D. B.; Eikenberg, D. C.; Hieble, J. P.; Langer, S. Z.; Lefkowitz, R. J.; Minneman, K. P. et al. (1994): International Union of Pharmacology nomenclature of adrenoceptors. In: *Pharmacological reviews* 46 (2), S. 121–136.
- Caulfield, M. P. (1993): Muscarinic receptors--characterization, coupling and function. In: *Pharmacology & therapeutics* 58 (3), S. 319–379.
- Caulfield, M. P.; Birdsall, N. J. (1998): International Union of Pharmacology. XVII. Classification of muscarinic acetylcholine receptors. In: *Pharmacological reviews* 50 (2), S. 279–290.

- Cavalli, A.; Fanelli, F.; Taddei, C.; De Benedetti, P G; Cotecchia, S. (1996): Amino acids of the alpha1B-adrenergic receptor involved in agonist binding: differences in docking catecholamines to receptor subtypes. In: *FEBS letters* 399 (1-2), S. 9–13.
- Chen, Xinyu; Klöckner, Jessika; Holze, Janine; Zimmermann, Cornelia; Seemann, Wiebke K.; Schrage, Ramona et al. (2015): Rational design of partial agonists for the muscarinic m1 acetylcholine receptor. In: *Journal of medicinal chemistry* 58 (2), S. 560–576. DOI: 10.1021/jm500860w.
- Chen, Zhong-jian; Minneman, Kenneth P. (2005): Recent progress in alpha1-adrenergic receptor research. In: *Acta pharmacologica Sinica* 26 (11), S. 1281–1287. DOI: 10.1111/j.1745-7254.2005.00224.x.
- Cheng, Y.; Prusoff, W. H. (1973): Relationship between the inhibition constant (K<sub>1</sub>) and the concentration of inhibitor which causes 50 per cent inhibition (I<sub>50</sub>) of an enzymatic reaction. In: *Biochemical pharmacology* 22 (23), S. 3099–3108.
- Cherezov, Vadim; Rosenbaum, Daniel M.; Hanson, Michael A.; Rasmussen, Søren G F; Thian, Foon Sun; Kobilka, Tong Sun et al. (2007): High-resolution crystal structure of an engineered human beta2-adrenergic G protein-coupled receptor. In: *Science (New York, N.Y.)* 318 (5854), S. 1258–1265. DOI: 10.1126/science.1150577.
- Choe, Hui-Woog; Kim, Yong Ju; Park, Jung Hee; Morizumi, Takefumi; Pai, Emil F.; Krauss, Norbert et al. (2011): Crystal structure of metarhodopsin II. In: *Nature* 471 (7340), S. 651–655. DOI: 10.1038/nature09789.
- Christopoulos, A.; Lanzafame, A.; Mitchelson, F. (1998): Allosteric interactions at muscarinic cholinceptors. In: *Clinical and experimental pharmacology & physiology* 25 (3-4), S. 185–194.
- Christopoulos, Arthur (2014): Advances in G protein-coupled receptor allostery: from function to structure. In: *Molecular pharmacology* 86 (5), S. 463–478. DOI: 10.1124/mol.114.094342.
- Christopoulos, Arthur; Kenakin, Terry (2002): G protein-coupled receptor allostery and complexing. In: *Pharmacological reviews* 54 (2), S. 323–374.
- DeBlasi, A.; O'Reilly, K.; Motulsky, H. J. (1989): Calculating receptor number from binding experiments using same compound as radioligand and competitor. In: *Trends in pharmacological sciences* 10 (6), S. 227–229.
- Disingrini, Teresa; Muth, Mathias; Dallanoce, Clelia; Barocelli, Elisabetta; Bertoni, Simona; Kellershohn, Kerstin et al. (2006): Design, synthesis, and action of oxotremorine-related hybrid-type allosteric modulators of muscarinic acetylcholine receptors. In: *Journal of medicinal chemistry* 49 (1), S. 366–372. DOI: 10.1021/jm050769s.
- Dror, Ron O.; Pan, Albert C.; Arlow, Daniel H.; Borhani, David W.; Maragakis, Paul; Shan, Yibing et al. (2011): Pathway and mechanism of drug binding to G-protein-coupled receptors. In: *Proceedings of the National Academy of Sciences of the United States of America* 108 (32), S. 13118–13123. DOI: 10.1073/pnas.1104614108.



- Eglen, R. M.; Hegde, S. S.; Watson, N. (1996): Muscarinic receptor subtypes and smooth muscle function. In: *Pharmacological reviews* 48 (4), S. 531–565.
- Ehlert, F. J. (1988): Estimation of the affinities of allosteric ligands using radioligand binding and pharmacological null methods. In: *Molecular pharmacology* 33 (2), S. 187–194.
- Ellis, J.; Huyler, J.; Brann, M. R. (1991): Allosteric regulation of cloned m1-m5 muscarinic receptor subtypes. In: *Biochemical pharmacology* 42 (10), S. 1927–1932.
- Ellis, J.; Seidenberg, M. (1992): Two allosteric modulators interact at a common site on cardiac muscarinic receptors. In: *Molecular pharmacology* 42 (4), S. 638–641.
- Ellis, J.; Seidenberg, M. (2000): Interactions of alcuronium, TMB-8, and other allosteric ligands with muscarinic acetylcholine receptors: studies with chimeric receptors. In: *Molecular pharmacology* 58 (6), S. 1451–1460.
- Ellis, J.; Seidenberg, M.; Brann, M. R. (1993): Use of chimeric muscarinic receptors to investigate epitopes involved in allosteric interactions. In: *Molecular pharmacology* 44 (3), S. 583–588.
- Evans, Bronwyn A.; Sato, Masaaki; Sarwar, Mohsin; Hutchinson, Dana S.; Summers, Roger J. (2010): Ligand-directed signalling at beta-adrenoceptors. In: *British journal of pharmacology* 159 (5), S. 1022–1038. DOI: 10.1111/j.1476-5381.2009.00602.x.
- Evers, Andreas; Hessler, Gerhard; Matter, Hans; Klabunde, Thomas (2005): Virtual screening of biogenic amine-binding G-protein coupled receptors: comparative evaluation of protein- and ligand-based virtual screening protocols. In: *Journal of medicinal chemistry* 48 (17), S. 5448–5465. DOI: 10.1021/jm050090o.
- Fang, Ye; Ferrie, Ann M. (2007): Optical biosensor differentiates signaling of endogenous PAR1 and PAR2 in A431 cells. In: *BMC cell biology* 8, S. 24. DOI: 10.1186/1471-2121-8-24.
- Feliszek, Monika; Speckmann, Valerie; Schacht, Daniel; Lehe, Marec von; Stark, Holger; Schlicker, Eberhard (2015): A search for functional histamine H4 receptors in the human, guinea pig and mouse brain. In: *Naunyn-Schmiedeberg's archives of pharmacology* 388 (1), S. 11–17. DOI: 10.1007/s00210-014-1053-6.
- Ferrari-Dileo, G.; Davis, E. B.; Anderson, D. R. (1992): Effects of cholinergic and adrenergic agonists on adenylate cyclase activity of retinal microvascular pericytes in culture. In: *Investigative ophthalmology & visual science* 33 (1), S. 42–47.
- Fredriksson, Robert; Lagerström, Malin C.; Lundin, Lars-Gustav; Schiöth, Helgi B. (2003): The G-protein-coupled receptors in the human genome form five main families. Phylogenetic analysis, paralogon groups, and fingerprints. In: *Molecular pharmacology* 63 (6), S. 1256–1272. DOI: 10.1124/mol.63.6.1256.
- Gantz, I.; DelValle, J.; Wang, L. D.; Tashiro, T.; Munzert, G.; Guo, Y. J. et al. (1992): Molecular basis for the interaction of histamine with the histamine H2 receptor. In: *The Journal of biological chemistry* 267 (29), S. 20840–20843.

- Gill, D. M.; Meren, R. (1978): ADP-ribosylation of membrane proteins catalyzed by cholera toxin: basis of the activation of adenylate cyclase. In: *Proceedings of the National Academy of Sciences of the United States of America* 75 (7), S. 3050–3054.
- Gnagey, A. L.; Seidenberg, M.; Ellis, J. (1999): Site-directed mutagenesis reveals two epitopes involved in the subtype selectivity of the allosteric interactions of gallamine at muscarinic acetylcholine receptors. In: *Molecular pharmacology* 56 (6), S. 1245–1253.
- Granier, Sébastien (2012): Structure des récepteurs mu et delta des opiacés. In: *Médecine sciences : M/S* 28 (10), S. 870–875. DOI: 10.1051/medsci/20122810016.
- Granier, Sébastien; Kobilka, Brian (2012): A new era of GPCR structural and chemical biology. In: *Nature chemical biology* 8 (8), S. 670–673. DOI: 10.1038/nchembio.1025.
- Grossmüller, Maren; Antony, Johannes; Tränkle, Christian; Holzgrabe, Ulrike; Mohr, Klaus (2006): Allosteric site in M2 acetylcholine receptors: evidence for a major conformational change upon binding of an orthosteric agonist instead of an antagonist. In: *Naunyn-Schmiedeberg's archives of pharmacology* 372 (4), S. 267–276. DOI: 10.1007/s00210-005-0023-4.
- Gyires, Klára; Zádori, Zoltán S.; Török, Tamás; Mátyus, Péter (2009): alpha(2)-Adrenoceptor subtypes-mediated physiological, pharmacological actions. In: *Neurochemistry international* 55 (7), S. 447–453. DOI: 10.1016/j.neuint.2009.05.014.
- Haga, Kazuko; Kruse, Andrew C.; Asada, Hidetsugu; Yurugi-Kobayashi, Takami; Shiroishi, Mitsunori; Zhang, Cheng et al. (2012): Structure of the human M2 muscarinic acetylcholine receptor bound to an antagonist. In: *Nature* 482 (7386), S. 547–551. DOI: 10.1038/nature10753.
- Hammer, R.; Berrie, C. P.; Birdsall, N. J.; Burgen, A. S.; Hulme, E. C. (1980): Pirenzepine distinguishes between different subclasses of muscarinic receptors. In: *Nature* 283 (5742), S. 90–92.
- Hannon, Jason; Hoyer, Daniel (2008): Molecular biology of 5-HT receptors. In: *Behavioural brain research* 195 (1), S. 198–213. DOI: 10.1016/j.bbr.2008.03.020.
- Heitz, F.; Holzwarth, J. A.; Gies, J. P.; Pruss, R. M.; Trumpp-Kallmeyer, S.; Hibert, M. F.; Guenet, C. (1999): Site-directed mutagenesis of the putative human muscarinic M2 receptor binding site. In: *European journal of pharmacology* 380 (2-3), S. 183–195.
- Hill, S. J.; Ganellin, C. R.; Timmerman, H.; Schwartz, J. C.; Shankley, N. P.; Young, J. M. et al. (1997): International Union of Pharmacology. XIII. Classification of histamine receptors. In: *Pharmacological reviews* 49 (3), S. 253–278.
- Hoffmann, Carsten; Gaietta, Guido; Bünemann, Moritz; Adams, Stephen R.; Oberdorff-Maass, Silke; Behr, Björn et al. (2005): A FIAsh-based FRET approach to determine G protein-coupled receptor activation in living cells. In: *Nature methods* 2 (3), S. 171–176. DOI: 10.1038/nmeth742.
- Holzgrabe, Ulrike; Amici, Marco de; Mohr, Klaus (2006): Allosteric modulators and selective agonists of muscarinic receptors. In: *Journal of molecular neuroscience : MN* 30 (1-2), S. 165–168. DOI: 10.1385/JMN:30:1:165.

- Hoyer, D.; Clarke, D. E.; Fozard, J. R.; Hartig, P. R.; Martin, G. R.; Mylecharane, E. J. et al. (1994): International Union of Pharmacology classification of receptors for 5-hydroxytryptamine (Serotonin). In: *Pharmacological reviews* 46 (2), S. 157–203.
- Hoyer, Daniel; Hannon, Jason P.; Martin, Graeme R. (2002): Molecular, pharmacological and functional diversity of 5-HT receptors. In: *Pharmacology, biochemistry, and behavior* 71 (4), S. 533–554.
- Hulme, E. C. (1990): Muscarinic acetylcholine receptors: typical G-coupled receptors. In: *Symposia of the Society for Experimental Biology* 44, S. 39–54.
- Hulme, E. C.; Birdsall, N. J.; Buckley, N. J. (1990): Muscarinic receptor subtypes. In: *Annual review of pharmacology and toxicology* 30, S. 633–673. DOI: 10.1146/annurev.pa.30.040190.003221.
- Huot, Philippe; Parent, André (2007): Dopaminergic neurons intrinsic to the striatum. In: *Journal of neurochemistry* 101 (6), S. 1441–1447. DOI: 10.1111/j.1471-4159.2006.04430.x.
- Jaakola, Veli-Pekka; Griffith, Mark T.; Hanson, Michael A.; Cherezov, Vadim; Chien, Ellen Y T; Lane, J. Robert et al. (2008): The 2.6 angstrom crystal structure of a human A2A adenosine receptor bound to an antagonist. In: *Science (New York, N.Y.)* 322 (5905), S. 1211–1217. DOI: 10.1126/science.1164772.
- Jäger, Dorothea; Schmalenbach, Caroline; Prilla, Stefanie; Schrobang, Jasmin; Kebig, Anna; Sennwitz, Matthias et al. (2007): Allosteric small molecules unveil a role of an extracellular E2/transmembrane helix 7 junction for G protein-coupled receptor activation. In: *The Journal of biological chemistry* 282 (48), S. 34968–34976. DOI: 10.1074/jbc.M705563200.
- Jensen, Brian C.; O'Connell, Timothy D.; Simpson, Paul C. (2011): Alpha-1-adrenergic receptors: targets for agonist drugs to treat heart failure. In: *Journal of molecular and cellular cardiology* 51 (4), S. 518–528. DOI: 10.1016/j.yjmcc.2010.11.014.
- Kaslow, H. R.; Lim, L. K.; Moss, J.; Lesikar, D. D. (1987): Structure-activity analysis of the activation of pertussis toxin. In: *Biochemistry* 26 (1), S. 123–127.
- Kebig, Anna; Kostenis, Evi; Mohr, Klaus; Mohr-Andrä, Marion (2009): An optical dynamic mass redistribution assay reveals biased signaling of dualsteric GPCR activators. In: *Journal of receptor and signal transduction research* 29 (3-4), S. 140–145. DOI: 10.1080/10799890903047437.
- Kenakin, Terry (2014): What is pharmacological 'affinity'? Relevance to biased agonism and antagonism. In: *Trends in pharmacological sciences* 35 (9), S. 434–441. DOI: 10.1016/j.tips.2014.06.003.
- Kenakin, Terry P. (2003): The secret lives of GPCRs. In: *Drug discovery today* 8 (15), S. 674.
- Kholodenko, Boris N. (2006): Cell-signalling dynamics in time and space. In: *Nature reviews. Molecular cell biology* 7 (3), S. 165–176. DOI: 10.1038/nrm1838.
- Klause, Sophia A. (2013) Bachelor thesis: N-alkylation of the superagonist iperoxo leads to distinct binding and G protein activation at muscarinic M<sub>2</sub> receptors. University of Bonn.

- Kooistra, A. J.; Kuhne, S.; de Esch, I J P; Leurs, R.; Graaf, C. de (2013): A structural chemogenomics analysis of aminergic GPCRs: lessons for histamine receptor ligand design. In: *British journal of pharmacology* 170 (1), S. 101–126. DOI: 10.1111/bph.12248.
- Kostenis, E.; Mohr, K. (1996): Two-point kinetic experiments to quantify allosteric effects on radioligand dissociation. In: *Trends in pharmacological sciences* 17 (8), S. 280–283.
- Kostenis, Evi; Waelbroeck, Magali; Milligan, Graeme (2005): Techniques: promiscuous G $\alpha$  proteins in basic research and drug discovery. In: *Trends in pharmacological sciences* 26 (11), S. 595–602. DOI: 10.1016/j.tips.2005.09.007.
- Kruh, J. (1982): Effects of sodium butyrate, a new pharmacological agent, on cells in culture. In: *Molecular and cellular biochemistry* 42 (2), S. 65–82.
- Kruse, Andrew C.; Hu, Jianxin; Kobilka, Brian K.; Wess, Jürgen (2014): Muscarinic acetylcholine receptor X-ray structures: potential implications for drug development. In: *Current opinion in pharmacology* 16, S. 24–30. DOI: 10.1016/j.coph.2014.02.006.
- Kruse, Andrew C.; Ring, Aaron M.; Manglik, Aashish; Hu, Jianxin; Hu, Kelly; Eitel, Katrin et al. (2013): Activation and allosteric modulation of a muscarinic acetylcholine receptor. In: *Nature* 504 (7478), S. 101–106. DOI: 10.1038/nature12735.
- Lagerström, Malin C.; Schiöth, Helgi B. (2008): Structural diversity of G protein-coupled receptors and significance for drug discovery. In: *Nature reviews. Drug discovery* 7 (4), S. 339–357. DOI: 10.1038/nrd2518.
- Lane, J. Robert; Donthamsetti, Prashant; Shonberg, Jeremy; Draper-Joyce, Christopher J.; Dentry, Samuel; Michino, Mayako et al. (2014): A new mechanism of allostery in a G protein-coupled receptor dimer. In: *Nature chemical biology* 10 (9), S. 745–752. DOI: 10.1038/nchembio.1593.
- Langmead, Christopher J.; Christopoulos, Arthur (2006): Allosteric agonists of 7TM receptors: expanding the pharmacological toolbox. In: *Trends in pharmacological sciences* 27 (9), S. 475–481. DOI: 10.1016/j.tips.2006.07.009.
- Lazareno, S.; Birdsall, N. J. (1995): Detection, quantitation, and verification of allosteric interactions of agents with labeled and unlabeled ligands at G protein-coupled receptors: interactions of strychnine and acetylcholine at muscarinic receptors. In: *Molecular pharmacology* 48 (2), S. 362–378.
- Lee, Paul H.; Gao, Alice; van Staden, Carlo; Ly, Jenny; Salon, John; Xu, Arron et al. (2008): Evaluation of dynamic mass redistribution technology for pharmacological studies of recombinant and endogenously expressed g protein-coupled receptors. In: *Assay and drug development technologies* 6 (1), S. 83–94. DOI: 10.1089/adt.2007.126.
- Leppik, R. A.; Miller, R. C.; Eck, M.; Paquet, J. L. (1994): Role of acidic amino acids in the allosteric modulation by gallamine of antagonist binding at the m2 muscarinic acetylcholine receptor. In: *Molecular pharmacology* 45 (5), S. 983–990.
- Leurs, R.; Smit, M. J.; Timmerman, H. (1995): Molecular pharmacological aspects of histamine receptors. In: *Pharmacology & therapeutics* 66 (3), S. 413–463.

Levey, A. I. (1993): Immunological localization of m1-m5 muscarinic acetylcholine receptors in peripheral tissues and brain. In: *Life sciences* 52 (5-6), S. 441–448.

Levey, A. I.; Edmunds, S. M.; Heilman, C. J.; Desmond, T. J.; Frey, K. A. (1994): Localization of muscarinic m3 receptor protein and M3 receptor binding in rat brain. In: *Neuroscience* 63 (1), S. 207–221.

Levey, A. I.; Kitt, C. A.; Simonds, W. F.; Price, D. L.; Brann, M. R. (1991): Identification and localization of muscarinic acetylcholine receptor proteins in brain with subtype-specific antibodies. In: *The Journal of neuroscience : the official journal of the Society for Neuroscience* 11 (10), S. 3218–3226.

Liapakis, G.; Ballesteros, J. A.; Papachristou, S.; Chan, W. C.; Chen, X.; Javitch, J. A. (2000): The forgotten serine. A critical role for Ser-2035.42 in ligand binding to and activation of the beta 2-adrenergic receptor. In: *The Journal of biological chemistry* 275 (48), S. 37779–37788. DOI: 10.1074/jbc.M002092200.

LOWRY, O. H.; ROSEBROUGH, N. J.; FARR, A. L.; RANDALL, R. J. (1951): Protein measurement with the Folin phenol reagent. In: *The Journal of biological chemistry* 193 (1), S. 265–275.

Marullo, Stefano; Bouvier, Michel (2007): Resonance energy transfer approaches in molecular pharmacology and beyond. In: *Trends in pharmacological sciences* 28 (8), S. 362–365. DOI: 10.1016/j.tips.2007.06.007.

Matsui, H.; Lazareno, S.; Birdsall, N. J. (1995): Probing of the location of the allosteric site on m1 muscarinic receptors by site-directed mutagenesis. In: *Molecular pharmacology* 47 (1), S. 88–98.

May, Lauren T.; Leach, Katie; Sexton, Patrick M.; Christopoulos, Arthur (2007): Allosteric modulation of G protein-coupled receptors. In: *Annual review of pharmacology and toxicology* 47, S. 1–51. DOI: 10.1146/annurev.pharmtox.47.120505.105159.

Miao, Yinglong; Nichols, Sara E.; Gasper, Paul M.; Metzger, Vincent T.; McCammon, J. Andrew (2013): Activation and dynamic network of the M2 muscarinic receptor. In: *Proceedings of the National Academy of Sciences of the United States of America* 110 (27), S. 10982–10987. DOI: 10.1073/pnas.1309755110.

Milligan, Graeme (2003): Principles: extending the utility of [35S]GTP gamma S binding assays. In: *Trends in pharmacological sciences* 24 (2), S. 87–90.

Milligan, Graeme; Kostenis, Evi (2006): Heterotrimeric G-proteins: a short history. In: *British journal of pharmacology* 147 Suppl 1, S. S46-55. DOI: 10.1038/sj.bjp.0706405.

Moguilevsky, N.; Varsalona, F.; Guillaume, J. P.; Noyer, M.; Gillard, M.; Daliers, J. et al. (1995): Pharmacological and functional characterisation of the wild-type and site-directed mutants of the human H1 histamine receptor stably expressed in CHO cells. In: *Journal of receptor and signal transduction research* 15 (1-4), S. 91–102. DOI: 10.3109/10799899509045210.

Mohr, Klaus; Tränkle, Christian; Kostenis, Evi; Barocelli, Elisabetta; Amici, Marco de; Holzgrabe, Ulrike (2010): Rational design of dualsteric GPCR ligands: quests and promise.

In: *British journal of pharmacology* 159 (5), S. 997–1008. DOI: 10.1111/j.1476-5381.2009.00601.x.

Myslivecek, J.; Trojan, S. (2003): Regulation of adrenoceptors and muscarinic receptors in the heart. In: *General physiology and biophysics* 22 (1), S. 3–14.

Neve, Kim A.; Seamans, Jeremy K.; Trantham-Davidson, Heather (2004): Dopamine receptor signaling. In: *Journal of receptor and signal transduction research* 24 (3), S. 165–205.

Nonaka, H.; Otaki, S.; Ohshima, E.; Kono, M.; Kase, H.; Ohta, K. et al. (1998): Unique binding pocket for KW-4679 in the histamine H1 receptor. In: *European journal of pharmacology* 345 (1), S. 111–117.

Nunn, Caroline; Feuerbach, Dominik; Lin, Xinwei; Peter, Richard; Hoyer, Daniel (2002): Pharmacological characterisation of the goldfish somatostatin sst5 receptor. In: *European journal of pharmacology* 436 (3), S. 173–186.

Ohta, K.; Hayashi, H.; Mizuguchi, H.; Kagamiyama, H.; Fujimoto, K.; Fukui, H. (1994): Site-directed mutagenesis of the histamine H1 receptor: roles of aspartic acid107, asparagine198 and threonine194. In: *Biochemical and biophysical research communications* 203 (2), S. 1096–1101. DOI: 10.1006/bbrc.1994.2295.

Oldham, William M.; Hamm, Heidi E. (2008): Heterotrimeric G protein activation by G-protein-coupled receptors. In: *Nature reviews. Molecular cell biology* 9 (1), S. 60–71. DOI: 10.1038/nrm2299.

Passani, Maria Beatrice; Blandina, Patrizio (2011): Histamine receptors in the CNS as targets for therapeutic intervention. In: *Trends in pharmacological sciences* 32 (4), S. 242–249. DOI: 10.1016/j.tips.2011.01.003.

Porritt, Michelle J.; Kingsbury, Ann E.; Hughes, Andrew J.; Howells, David W. (2006): Striatal dopaminergic neurons are lost with Parkinson's disease progression. In: *Movement disorders : official journal of the Movement Disorder Society* 21 (12), S. 2208–2211. DOI: 10.1002/mds.21129.

Prilla, Stefanie; Schrobang, Jasmin; Ellis, John; Hölting, Hans-Dieter; Mohr, Klaus (2006): Allosteric interactions with muscarinic acetylcholine receptors: complex role of the conserved tryptophan M2422Trp in a critical cluster of amino acids for baseline affinity, subtype selectivity, and cooperativity. In: *Molecular pharmacology* 70 (1), S. 181–193. DOI: 10.1124/mol.106.023481.

Rasmussen, Søren G F; Choi, Hee-Jung; Rosenbaum, Daniel M.; Kobilka, Tong Sun; Thian, Foon Sun; Edwards, Patricia C. et al. (2007): Crystal structure of the human beta2 adrenergic G-protein-coupled receptor. In: *Nature* 450 (7168), S. 383–387. DOI: 10.1038/nature06325.

Reinhardt, D.; Ritter, E. (1979): Hypothermia-induced potentiation of histamine H2-receptor-mediated relaxation and cyclic AMP increase in the isolated mesenteric artery of the rabbit. In: *Agents and actions* 9 (1), S. 9–14.

Ring, Aaron M.; Manglik, Aashish; Kruse, Andrew C.; Enos, Michael D.; Weis, William I.; Garcia, K. Christopher; Kobilka, Brian K. (2013): Adrenaline-activated structure of  $\beta$ 2-

adrenoceptor stabilized by an engineered nanobody. In: *Nature* 502 (7472), S. 575–579. DOI: 10.1038/nature12572.

Rosenbaum, Daniel M.; Cherezov, Vadim; Hanson, Michael A.; Rasmussen, Søren G F; Thian, Foon Sun; Kobilka, Tong Sun et al. (2007): GPCR engineering yields high-resolution structural insights into beta2-adrenergic receptor function. In: *Science (New York, N.Y.)* 318 (5854), S. 1266–1273. DOI: 10.1126/science.1150609.

Ross, E. M.; Gilman, A. G. (1980): Biochemical properties of hormone-sensitive adenylate cyclase. In: *Annual review of biochemistry* 49, S. 533–564. DOI: 10.1146/annurev.bi.49.070180.002533.

Schmitz, Jens; van der Mey, Dorina; Bermudez, Marcel; Klöckner, Jessica; Schrage, Ramona; Kostenis, Evi et al. (2014): Dualsteric muscarinic antagonists--orthosteric binding pose controls allosteric subtype selectivity. In: *Journal of medicinal chemistry* 57 (15), S. 6739–6750. DOI: 10.1021/jm500790x.

Schrage, R.; Seemann, W. K.; Klöckner, J.; Dallanoce, C.; Racké, K.; Kostenis, E. et al. (2013): Agonists with supraphysiological efficacy at the muscarinic M2 ACh receptor. In: *British journal of pharmacology* 169 (2), S. 357–370. DOI: 10.1111/bph.12003.

Schrage, Ramona; Holze, Janine; Klöckner, Jessica; Balkow, Aileen; Klause, Anne S.; Schmitz, Anna-Lena et al. (2014): New insight into active muscarinic receptors with the novel radioagonist [<sup>3</sup>H]iperoxo. In: *Biochemical pharmacology* 90 (3), S. 307–319. DOI: 10.1016/j.bcp.2014.05.012.

Schröder, Ralf; Janssen, Nicole; Schmidt, Johannes; Kebig, Anna; Merten, Nicole; Hennen, Stephanie et al. (2010): Deconvolution of complex G protein-coupled receptor signaling in live cells using dynamic mass redistribution measurements. In: *Nature biotechnology* 28 (9), S. 943–949. DOI: 10.1038/nbt.1671.

Schröder, Ralf; Schmidt, Johannes; Blättermann, Stefanie; Peters, Lucas; Janssen, Nicole; Grundmann, Manuel et al. (2011): Applying label-free dynamic mass redistribution technology to frame signaling of G protein-coupled receptors noninvasively in living cells. In: *Nature protocols* 6 (11), S. 1748–1760. DOI: 10.1038/nprot.2011.386.

Schröter, A.; Tränkle, C.; Mohr, K. (2000): Modes of allosteric interactions with free and [3H]N-methylscopolamine-occupied muscarinic M2 receptors as deduced from buffer-dependent potency shifts. In: *Naunyn-Schmiedeberg's archives of pharmacology* 362 (6), S. 512–519.

Scott, Clay W.; Peters, Matthew F. (2010): Label-free whole-cell assays: expanding the scope of GPCR screening. In: *Drug discovery today* 15 (17-18), S. 704–716. DOI: 10.1016/j.drudis.2010.06.008.

Seeman, P.; Van Tol, H H (1994): Dopamine receptor pharmacology. In: *Trends in pharmacological sciences* 15 (7), S. 264–270.

Shi, Lei; Javitch, Jonathan A. (2002): The binding site of aminergic G protein-coupled receptors: the transmembrane segments and second extracellular loop. In: *Annual review of*

*pharmacology and toxicology* 42, S. 437–467. DOI: 10.1146/annurev.pharmtox.42.091101.144224.

Shin, Niu; Coates, Elizabeth; Murgolo, Nicholas J.; Morse, Kelley L.; Bayne, Marvin; Strader, Catherine D.; Monsma, Frederick J. (2002): Molecular modeling and site-specific mutagenesis of the histamine-binding site of the histamine H4 receptor. In: *Molecular pharmacology* 62 (1), S. 38–47.

Simon, M. I.; Strathmann, M. P.; Gautam, N. (1991): Diversity of G proteins in signal transduction. In: *Science (New York, N.Y.)* 252 (5007), S. 802–808.

Snow, B. E.; Hall, R. A.; Krumins, A. M.; Brothers, G. M.; Bouchard, D.; Brothers, C. A. et al. (1998): GTPase activating specificity of RGS12 and binding specificity of an alternatively spliced PDZ (PSD-95/Dlg/ZO-1) domain. In: *The Journal of biological chemistry* 273 (28), S. 17749–17755.

Steinfeld, Tod; Mammen, Mathai; Smith, Jacqueline A M; Wilson, Richard D.; Jasper, Jeffrey R. (2007): A novel multivalent ligand that bridges the allosteric and orthosteric binding sites of the M2 muscarinic receptor. In: *Molecular pharmacology* 72 (2), S. 291–302. DOI: 10.1124/mol.106.033746.

Strader, C. D.; Dixon, R. A.; Cheung, A. H.; Candelore, M. R.; Blake, A. D.; Sigal, I. S. (1987): Mutations that uncouple the beta-adrenergic receptor from Gs and increase agonist affinity. In: *The Journal of biological chemistry* 262 (34), S. 16439–16443.

Tränkle, C.; Kostenis, E.; Burgmer, U.; Mohr, K. (1996): Search for lead structures to develop new allosteric modulators of muscarinic receptors. In: *The Journal of pharmacology and experimental therapeutics* 279 (2), S. 926–933.

Tränkle, C.; Mies-Klomfass, E.; Cid, M. H.; Holzgrabe, U.; Mohr, K. (1998): Identification of a [3H]Ligand for the common allosteric site of muscarinic acetylcholine M2 receptors. In: *Molecular pharmacology* 54 (1), S. 139–145.

Tränkle, C.; Mohr, K. (1997): Divergent modes of action among cationic allosteric modulators of muscarinic M2 receptors. In: *Molecular pharmacology* 51 (4), S. 674–682.

Tränkle, Christian; Weyand, Oliver; Voigtländer, Uta; Mynett, Anita; Lazareno, Sebastian; Birdsall, Nigel J M; Mohr, Klaus (2003): Interactions of orthosteric and allosteric ligands with [3H]dimethyl-W84 at the common allosteric site of muscarinic M2 receptors. In: *Molecular pharmacology* 64 (1), S. 180–190. DOI: 10.1124/mol.64.1.180.

Tubio, Maria Rosario; Fernandez, Natalia; Fitzsimons, Carlos Patricio; Copsel, Sabrina; Santiago, Sergio; Shayo, Carina et al. (2010): Expression of a G protein-coupled receptor (GPCR) leads to attenuation of signaling by other GPCRs: experimental evidence for a spontaneous GPCR constitutive inactive form. In: *The Journal of biological chemistry* 285 (20), S. 14990–14998. DOI: 10.1074/jbc.M109.099689.

Tucek, S.; Proska, J. (1995): Allosteric modulation of muscarinic acetylcholine receptors. In: *Trends in pharmacological sciences* 16 (6), S. 205–212.

Urban, Jonathan D.; Clarke, William P.; Zastrow, Mark von; Nichols, David E.; Kobilka, Brian; Weinstein, Harel et al. (2007): Functional selectivity and classical concepts of



quantitative pharmacology. In: *The Journal of pharmacology and experimental therapeutics* 320 (1), S. 1–13. DOI: 10.1124/jpet.106.104463.

van Rhee, A Michiel; Jacobson, Kenneth A. (1996): Molecular Architecture of G Protein-Coupled Receptors. In: *Drug development research* 37 (1), S. 1–38. DOI: 10.1002/(SICI)1098-2299(199601)37:1<1::AID-DDR1>3.0.CO;2-S.

Vilaró, M. T.; Palacios, J. M.; Mengod, G. (1990): Localization of m5 muscarinic receptor mRNA in rat brain examined by in situ hybridization histochemistry. In: *Neuroscience letters* 114 (2), S. 154–159.

Voigtländer, Uta; Jöhren, Kirstin; Mohr, Marion; Raasch, Alexandra; Tränkle, Christian; Buller, Stefan et al. (2003): Allosteric site on muscarinic acetylcholine receptors: identification of two amino acids in the muscarinic M2 receptor that account entirely for the M2/M5 subtype selectivities of some structurally diverse allosteric ligands in N-methylscopolamine-occupied receptors. In: *Molecular pharmacology* 64 (1), S. 21–31. DOI: 10.1124/mol.64.1.21.

Wang, C. D.; Gallaher, T. K.; Shih, J. C. (1993): Site-directed mutagenesis of the serotonin 5-hydroxytryptamine<sub>2</sub> receptor: identification of amino acids necessary for ligand binding and receptor activation. In: *Molecular pharmacology* 43 (6), S. 931–940.

Weiner, D. M.; Levey, A. I.; Brann, M. R. (1990): Expression of muscarinic acetylcholine and dopamine receptor mRNAs in rat basal ganglia. In: *Proceedings of the National Academy of Sciences of the United States of America* 87 (18), S. 7050–7054.

Wess, J. (1993): Molecular basis of muscarinic acetylcholine receptor function. In: *Trends in pharmacological sciences* 14 (8), S. 308–313.

Wess, J. (1997): G-protein-coupled receptors: molecular mechanisms involved in receptor activation and selectivity of G-protein recognition. In: *FASEB journal : official publication of the Federation of American Societies for Experimental Biology* 11 (5), S. 346–354.

Wess, Jürgen (2004): Muscarinic acetylcholine receptor knockout mice: novel phenotypes and clinical implications. In: *Annual review of pharmacology and toxicology* 44, S. 423–450. DOI: 10.1146/annurev.pharmtox.44.101802.121622.

Wilcox, R. E.; Huang, W. H.; Brusniak, M. Y.; Wilcox, D. M.; Pearlman, R. S.; Teeter, M. M. et al. (2000): CoMFA-based prediction of agonist affinities at recombinant wild type versus serine to alanine point mutated D2 dopamine receptors. In: *Journal of medicinal chemistry* 43 (16), S. 3005–3019.

Woehler, Andrew; Ponimaskin, Evgeni G. (2009): G protein--mediated signaling: same receptor, multiple effectors. In: *Current molecular pharmacology* 2 (3), S. 237–248.

Zahn, Katrin; Eckstein, Niels; Tränkle, Christian; Sadée, Wolfgang; Mohr, Klaus (2002): Allosteric modulation of muscarinic receptor signaling: alcuronium-induced conversion of pilocarpine from an agonist into an antagonist. In: *The Journal of pharmacology and experimental therapeutics* 301 (2), S. 720–728.

Zampeli, E.; Tiligada, E. (2009): The role of histamine H4 receptor in immune and inflammatory disorders. In: *British journal of pharmacology* 157 (1), S. 24–33. DOI: 10.1111/j.1476-5381.2009.00151.x.

## 9. Publications

### Research article

Bock, Andreas; **Chirinda, Brian**; Krebs, Fabian; Messerer, Regina; Bätz, Julia; Muth, Mathias et al. (2014a): Dynamic ligand binding dictates partial agonism at a G protein-coupled receptor. In: *Nature chemical biology* 10 (1), S. 18–20. DOI: 10.1038/nchembio.1384.

### Oral presentation

**Chirinda B.**, Bock A. and Mohr K. (2015)

The allosteric core region of the M<sub>2</sub> muscarinic acetylcholine receptor differentially regulates allosteric, orthosteric and dualsteric ligand activity. *DGPT Congress for Experimental and Clinical Pharmacology and Toxicology* (Kiel, Germany)

### Poster presentation abstract

Krebs F., **Chirinda B.** and Mohr K. (2014)

Buffer conditions affect the binding of dualsteric ligands at the muscarinic M<sub>2</sub> receptor. *Jahrestagung der Deutschen Pharmazeutischen Gesellschaft (DPhG)* (Frankfurt, Germany)

## 10. Curriculum vitae

**Brian Munashe Chirinda**

### **Education**

- March 2012 – present:* PhD student in the working group of Prof. Dr. Klaus Mohr  
Pharmacology and Toxicology section, Institute of Pharmacy,  
**University of Bonn, Germany**
- March 2012 – present:* Member of the North-Rhine Westphalia International Graduate  
Research School-BiotechPharma:  
**University of Bonn, Germany**
- Sept 2010 – Jan 2012:* MSc Cancer Cell and Molecular Biology  
**University of Leicester, UK**
- Sept 2007 – June 2010:* BSc (Hons) Medical Biochemistry  
**University of Leicester, UK**
- Sept 2005 – July 2007:* High School A Levels  
**Handsworth Grammar School, UK**

## 11. Acknowledgements

I would like to express my sincere gratitude to Prof. Dr. K. Mohr for accepting me into his working group to carry out my PhD studies. I thank him very much for the guidance and wonderful support he provided me over the three years. I am really grateful for the expertise, knowledge and all that I acquired under his supervision.

I would also like to thank Prof. Dr. I. von Kügelgen for being the second member of the examining committee for my thesis.

I extend my appreciation to Prof. Dr. A. Lamprecht for being my co-supervisor from the NRW International Graduate Research School BIOTECH-PHARMA throughout my study period and also for being the third member of the examining committee for my thesis.

I would also like to thank Prof. Dr. W. Mader for his participation as the fourth member of the examining committee evaluating this thesis.

Many thanks to PD. Dr. C. Tränkle for the invaluable support he provided to me in my time here in the group of Prof Mohr. I would like to thank him especially for the help he offered regarding data analysis.

My sincere appreciation is extended to Dr. A. Bock for his help and unwavering support from my very first day in the working group of Prof Mohr. I thank him for mentoring me throughout my studies. I would like to also thank Dr. R. Schrage for the constructive discussions and superb advice throughout my thesis. Also, special thanks to my friend Fabian Krebs for being an absolutely wonderful colleague in both my work and outside of the study group. He made my stay in Germany and completion of my PhD easier and comfortable whilst away from home.

I would also like to extend my heartfelt thanks to all my colleagues in the group of Prof Mohr in the Pharmacology and Toxicology department for all the kind contributions they made during my PhD studies. I really appreciate their help, support in and outside the lab, expertise and many happy memories during my studies here in Germany. I will be forever grateful to them.

I would also like to thank my colleagues from the working group of Prof. Dr. E. Kostenis who helped with their brilliant cooperation and support.

I would also like to extend my deepest gratitude to my family for their support, encouragement and their unconditional love. Without them I would not have been able to carry out and complete this work.

In the end I would like to thank NRW International Graduate Research School BIOTECH-PHARMA for the scholarship to undertake my PhD studies here in Germany. I also want to show much appreciation to all the members of the graduate school for their support and constructive ideas towards my work.